

Design of new responsive materials based on functional polymer brushes

DISSERTATION

zur Erlangung des akademischen Grades
Doctor rerum naturalium
(Dr. rer. nat.)

vorgelegt

der Fakultät Mathematik und Naturwissenschaften
der Technischen Universität Dresden

von

Diplom-Physikerin
Eva Bittrich

geboren am 23.12.1982 in Bautzen

Die Dissertation wurde in der Zeit von Februar 2007 bis
August 2010 im Leibniz-Institut für Polymerforschung Dresden e.V. angefertigt.

Gutachter: Prof. Dr. Manfred Stamm
Prof. Dr. Willem Norde

Eingereicht am: 13. August 2010

Tag der Verteidigung: 16. November 2010

Danksagung

An dieser Stelle möchte ich Herrn Prof. Dr. Manfred Stamm für die Möglichkeit die vorliegende Arbeit in seiner Arbeitsgruppe anfertigen zu können, sowie die Begleitung dieser Arbeit durch zahlreiche Diskussionen sehr herzlich danken. Herrn Prof. Dr. Willem Norde bin ich sehr dankbar für die Übernahme des zweiten Gutachtens und seine hilfreichen Kommentare zu verschiedenen Aspekten der Arbeit.

Mein ganz besonderer Dank gilt Frau Dr. Petra Uhlmann und Herrn Dr. Klaus-Jochen Eichhorn für ihr stetes Interesse, ihre vielfältigen motivierenden Hinweise und ihre nützlichen Ratschläge im Korrekturprozess der Arbeit.

Darüber hinaus war es mir eine besondere Freude den Arbeitskreis Ellipsometrie kennenzulernen. Hier sei weiterhin unseren Kooperationspartnern Herrn Dr. Karsten Hinrichs und Herrn Dr. Dennis Aulich aufrichtig für die gute Zusammenarbeit gedankt. Herrn Roland Schulze möchte ich sehr für seine Unterstützung im Umgang mit den Ellipsometern danken.

Es war für mich eine außergewöhnliche Gelegenheit als Gastwissenschaftlerin in der Ellipsometriegruppe der Universität Nebraska-Lincoln Messungen durchführen zu können. Hierfür danke ich der gesamten Arbeitsgruppe für Ihre herzliche Aufnahme während dieser Zeit, besonders Herrn Prof. Dr. Mathias Schubert, Herrn Dr. Tino Hofmann und Herrn Keith Brian Rodenhäusen.

Unseren Projektpartnern Herrn Prof. Dr. Sergiy Minko, Herrn Prof. Dr. Igor Luzinov, Herrn Prof. Dr. Marcus Müller und Herrn Dr. Bogdan Zdyrko möchte ich ebenfalls sehr herzlich für Ihre freundliche Aufnahme bei Besuchen und zahlreiche Diskussionen zu ternären Polymerbürsten danken. Besonderer Dank gilt Herrn Dr. Bogdan Zdyrko für die Bereitstellung des Polyethylenglykols.

Herrn PD Dr. Martin Müller danke ich für die Möglichkeit ATR-FTIR Messungen durchführen zu können und Frau Dr. Cornelia Bellmann für Ihre Unterstützung bei ζ -Potential Messungen. Darüber hinaus danke ich Frau Dr. Sina Burkert für ihre Zusammenarbeit bei Untersuchungen an PNIPAAm Bürsten und Herrn Dipl.-Chem. Marco Kuntzsch für seinen Beitrag zu Proteinadsorptionsmessungen und zur Probenpräparation. Frau Dr. Ulla König danke ich sehr für Ihre Unterstützung bei der Messung von Enzymaktivitäten und hilfreiche Diskussionen zu quantitativen kolorimetrischen Messungen. Herrn Dr. Ulrich Oertel möchte ich sehr herzlich für seine Bereitschaft danken, kinetische Fluoreszenzspektroskopie an immobilisierten Enzymen durchzuführen.

Der gesamten Abteilung Nanostrukturierte Materialien verdanke ich eine freundschaftliche Atmosphäre geprägt von offenherziger und reger gegenseitiger Unterstützung. Darüber hinaus wurde mir von allen Kollegen am Leibniz-Institut für Polymerforschung Dresden e.V. stets unkomplizierte Hilfe und Diskussionsbereitschaft entgegengebracht. Hierfür sei allen sehr herzlich gedankt.

Nicht zuletzt möchte ich meiner Familie für ihren stetigen Zuspruch im Entstehungsprozess dieser Arbeit danken, ganz besonders meinem Mann Lars.

Diese Arbeit wurde von der Deutschen Forschungsgemeinschaft DFG im Rahmen des "Materials World Network" finanziert.

Contents

1. Introduction	1
I. Fundamentals	5
2. Polymer brushes	7
2.1. Preparation of polymer brushes	7
2.2. End-grafted polymer brushes	9
2.2.1. Water soluble polymer brushes: LCST behavior	10
2.2.2. Polyelectrolyte brushes	11
2.3. Guiselin brushes	13
2.4. Mixed polymer brushes	14
3. Adsorption of proteins to surfaces	17
3.1. Physico-chemical properties of proteins in solution	17
3.2. Adsorption process	20
3.2.1. Transport to the surface and deposition	20
3.2.2. Driving forces	20
3.2.3. Adsorption isotherm and reversibility of adsorption	23
3.3. Adsorption at non-swelling surfaces	24
3.4. Adsorption at hydrogels and polymer brushes	25
3.4.1. Polyelectrolyte brushes	26
3.4.2. Protein repelling brushes	27
4. Methods for surface characterization	31
4.1. Survey of AFM, ζ -potential determination and ATR-FTIR spectroscopy	31
4.2. Ellipsometry	34
4.2.1. Theory of ellipsometry	35
4.2.2. Ellipsometric setups	37
4.2.3. Ellipsometry on thin organic films	37
4.3. Dynamic contact angle	39
4.4. Quartz crystal microbalance with dissipation mode (QCM-D)	41

II. Experimental	45
5. Materials, brush preparation and properties of dry brushes	47
5.1. Polymers	47
5.2. Model proteins	48
5.3. Buffer solutions	49
5.4. "Grafting-to" of polymer brushes	50
5.5. Surface homogeneity and roughness after preparation	51
5.6. ζ -potentials	53
5.7. Stability	54
6. Ellipsometric measurements and modeling	55
6.1. Course of in-situ measurements	55
6.2. Modeling of dry polymer brushes	56
6.2.1. Optical box model	56
6.3. Modeling of swollen polymer brushes and protein adsorption	58
6.3.1. Brush profiles	58
6.3.2. Effective medium approach (EMA)	60
6.3.3. Modeling of the layer parameters upon protein adsorption	61
6.3.4. Evaluation of the adsorbed amount of protein	62
6.4. Colorimetric quantification of the protein amount	64
III. Results and discussion	67
7. Poly(N-isopropyl acrylamide) grafting-to brushes	69
7.1. Temperature sensitive swelling	69
7.1.1. Molecular mechanism - ATR-FTIR spectroscopy	70
7.1.2. Surface hydrophobicity - Contact angle	72
7.1.3. Integral brush behavior - Spectroscopic ellipsometry	73
7.2. HSA resistance at isotonic conditions monitored by ellipsometry	78
7.3. Summary	82
8. PAA and PAA-b-PS Guiselin brushes	85
8.1. pH- and salt sensitive swelling behavior	85
8.2. Controlled protein adsorption and release	89
8.2.1. pH sensitivity	91
8.2.2. Dependency on the amount of PAA	96
8.3. Quantification of coupled buffer components: A simultaneous SE - QCM-D study	97
8.3.1. Modeling of combined spectroscopic ellipsometry (SE) and QCM-D data	98
8.3.2. pH- and salt sensitive swelling	99

8.3.3. BSA adsorption below IEP of protein	102
8.3.4. BSA adsorption above IEP of protein	104
8.3.5. Changes in the shear viscosity during the adsorption process	106
8.3.6. Comparison of adsorption in 1 mM and 100 mM buffer solution	108
8.4. Summary	109
9. Temperature and pH sensitive PNIPAAm-PAA binary mixed brushes	113
9.1. Physico-chemical interface properties of dry brushes	113
9.2. Environmental sensitive swelling behaviour	117
9.2.1. Coupled swelling dependent on pH and ionic strength	117
9.2.2. Temperature sensitivity	119
9.3. Protein adsorption and release	121
9.3.1. Adsorption of HSA dependent on pH	121
9.3.2. Temperature sensitive adsorption	123
9.3.3. Adsorption kinetics and protein release	124
9.4. Comparison to ternary PNIPAAm - PAA-b-PS brushes	127
9.5. Summary	130
10. Mixed brushes containing Poly(ethylene glycol) (PEG)	133
10.1. PEG-PAA brushes	134
10.2. Salt dependent swelling of PEG-PAA-b-PS	136
10.3. Summary	137
11. Activity of glucose oxidase immobilized at mono and mixed brushes	139
11.1. Enzyme reaction and quantification of resulting H_2O_2	140
11.2. Homopolymer brushes	140
11.3. Mixed brushes	142
11.4. Summary	144
12. Summary and outlook	145
A. Appendix	149
A.1. Dispersion relations for buffer and salted solutions	149
A.2. Comparison of different models for protein adsorption	149
A.3. Refractive indices of swollen polymer brushes	152
A.4. QCM-D data upon protein adsorption	155
List of abbreviations	157
List of figures	160
Bibliography	164

1. Introduction

For the development of smart surfaces high attention is focused on stimuli-responsive polymers [1]. Since type and rate of response to environmental stimuli can be regulated by chain length, composition, architecture and topology, polymer films offer a variety of opportunities to design such stimuli-responsive surfaces. Here different types of film architectures were developed in the past decades, among them regularly ordered block-copolymer films [2–4], cross-linked hyperbranched polymer networks [5], smart hydrogels [6–10] and polymer brushes [11–14], the latter characterized by unique properties due to the tethering of polymers by one end, thus different stretching behavior of the chains in this confined geometry as compared to the solution.

Polymer brushes were firstly investigated because of their positive influence on the steric stabilization of colloids [14]. But also possible applications, like the formation of chemical gates [15–17], tunable adhesion of biomolecules [18, 19], liquid separation in capillaries [20, 21] or sensor applications with immobilized nanoparticles [22], were discussed in recent years for different compositions of polymer brushes. Furthermore biocompatibility of selected brush architectures could be shown [23–26]. Alongside titanium surfaces [27] and positively charged coatings [28] these brushes are appealing for biomedical applications, e.g. as implant coatings preventing adhesion of biomolecules.

On the path to the development of applications it is of high interest to investigate the unique stimuli-responsive behavior of polymers tethered to interfaces and comprehensive experimental and theoretical studies on homopolymer polyelectrolyte as well as temperature sensitive brushes can be found in the literature [11, 29–34]. Additionally there are reports for a few specific binary and ternary mixed brushes on physico-chemical interface properties, swelling behavior and phase separation [35–38].

Among the field of polyelectrolyte brushes well investigated is the swelling behavior of weak polyanionic brushes, such as poly(acrylic acid) (PAA) [29, 31, 39] or poly(methacrylic acid) (PMAA) [40–42]. These polymers are characterized by their pH dependent deprotonation of *COOH*-groups along the chains to negatively charged *COO*⁻ groups. For a fixed pH a non-monotonic dependence on the ionic strength of the solution governs the swollen layer thickness of these polyanionic brushes with an increase of thickness in the osmotic regime and a decrease in the salted regime, thus leading to a maximum swollen layer thickness for intermediate ionic strength [29, 31]. Here the increase of the ionic strength of the solution is considered to lead

to an increase of counter-ion condensation inside the brush, thus forcing the polymer chains to expand due to the osmotic pressure of the trapped counter-ions [30,41]. With increasing ionic strength in solution the Debye length κ^{-1} decreases, leading to a complete screening of electrostatic interactions in the salted regime and thus the salted brush resembles a neutral surface with collapsed polymer chains.

One of the best studied temperature sensitive polymers, the water soluble poly(N-isopropyl acrylamide) (PNIPAAm), undergoes a phase transition in aqueous solution at its lower critical solution temperature (LCST) of 32 °C [43–45]. Below the LCST the polymer chains are swollen in water, whereas above the solvent quality is decreasing and the chains form a more compact structure due to dehydration [32,33]. Due to this phase transition, grafted PNIPAAm brush surfaces display an increase in hydrophobicity [33] as well as a decreased swollen layer thickness [34] above the LCST. Additionally the temperature range of the phase transition and the absolute change in thickness or contact angle was found to depend on molecular weight and grafting density. Since the LCST of 32 °C is close to physiological temperatures and can be considerably increased by copolymerization [46,47] this polymer is appealing for biomedical applications.

Protein resistance was especially examined for polymer brushes consisting of the water soluble poly (ethylen glycol) (PEG) [14,24–26], whereas these brushes were found to reduce protein adsorption considerably with protein resistance for high grafting densities and intermediate chain lengths [48]. Due to their water solubility and high excluded volume, a repulsive osmotic interaction occurs when these brushes are compressed or penetrated by other macromolecules, therefore these PEG brush represent a steric barrier towards protein adsorption [28]. Theoretical concepts for the protein resistance of water soluble polymer brushes were developed [48,49], stating the formation of a stable water film at the brush solution interface as important for the repelling of proteins.

Next to polymer brushes, research on three-dimensional hydrogel networks is promising for the application approaches discussed above [9,50–53]. Here a variety of gel compositions were investigated, whereas for this work especially interesting are the findings for pH- and temperature sensitive hydrogels often consisting of the pH-sensitive PAA and the temperature sensitive PNIPAAm [6,7,54]. For this type of hydrogel a complex pH and temperature sensitive swelling behavior with suppressed temperature sensitivity at low pH was found [7] and discussed in terms of an interpolymer complexation due to hydrogen bonding between these polymers [55].

Within this work we aimed at the combination of water soluble polymers with different environmental sensitivity in brush systems, thus combining PNIPAAm and PAA to establish a mixed brush with pH- and temperature sensitivity in aqueous solution. We studied environmental sensitive changes in the physico-chemical interface properties, the in-situ swelling

behavior and the protein adsorption affinity of these mixed brushes in Chapter 9, and their corresponding homopolymer brushes in Chapter 7 and Chapter 8. By comparing these mixed brush systems with the homopolymer brushes we obtained information about the influence of brush composition and solution parameters on their stimuli-responsive swelling and hence their interaction behavior with the surrounding solution (Sections 7.1, 8.1, 9.1 and 9.2). With the help of these findings we interpreted protein adsorption experiments and tuned the amount of protein at the surface, switching between adsorption and release in tuning pH, salt concentration, temperature and the brush composition (Sections 7.2, 8.2, 8.3 and 9.3). We also included ternary brushes containing PAA-b-polystyrene (PS) into the investigations, where the PS-block represents a hydrophobic model moiety intended for a permanent immobilization of functional biomolecules, e. g. enzymes by hydrophobic interaction (Section 9.4).

Furthermore PNIPAAm was exchanged for the more hydrophilic PEG, and the influence of this polymer on the swelling and adsorption behavior in mixed brushes with PAA was studied and is presented in Chapter 10.

Finally functional biomolecules, e.g. enzymes, shall be exposed switchable to the brush solution interface to tune the enzyme activity due to the stimuli-responsive behavior of mixed polymer brushes. Here we present first results on the activity of the enzyme glucose oxidase immobilized at mono and mixed brush surfaces and the temperature sensitive switching of its activity in binary PNIPAAm-PAA brushes (Chapter 11) .

Part I.

Fundamentals

2. Polymer brushes

The theory of polymer brushes has been extensively reviewed in the past decades [11, 12, 56] and thus will be introduced very shortly here, whereas only important aspects for the following swelling and adsorption measurements will be discussed.

2.1. Preparation of polymer brushes

The preparation of polymer brushes can be divided, according to the type of interaction of the chains with the surface, into physisorption [57–59] and chemisorption [57, 60, 61]. In the first process polymer chains, often block-copolymers, are attached via physical interaction forces, whereas in the second process polymers are covalently bound to a given substrate. Typical binding energies of covalent bonds range from $250 \frac{kJ}{mol}$ to $390 \frac{kJ}{mol}$ and the bond lengths are in the Ångström regime (e.g. 1.54 \AA for C-C bonds in alkanes). Physical interaction energies are considerably lower, but due to multiple binding points polymers can also be attached irreversibly to a surface [62].

Chemisorption can be performed by the "grafting-from" or the "grafting-to" method. In the "**grafting-from**" process precursor molecules are covalently attached to the substrate and the polymer chains are polymerized directly at the surface from a surrounding monomer solution by e.g. conventional radical polymerization or living polymerization methods [14, 63, 64]. With "grafting-from" high thicknesses and grafting densities can be achieved, but it is rather difficult to control the grafting density. Also the polydispersity index (PDI) of the chains can be very high, ranging for conventional radical polymerization between 1.5 and 3 [64]. Here a decrease of the PDI can be achieved by living polymerization methods, for example by controlled radical polymerization [65]. For binary or ternary mixed brushes polymerization of different types of polymers at the surface is difficult to guide and "grafting-to" methods are preferable to achieve defined brush compositions.

In the "**grafting-to**" process preformed polymer chains with a reactive end-group are grafted to a substrate, whereas grafting in the melt or solvent-assisted grafting leads to higher grafting densities due to screening of excluded volume interactions [66]. Carboxyl or vinyl functionalized chains are used [61, 67], and unbound polymer is usually extracted via a selective solvent for the brush polymer material. In the form of the method used in this thesis firstly polymers or silanes equipped with epoxy groups are reacted with the silanol groups of a silicon substrate to establish an anchoring layer covalently bound via ether bondings to the substrate

for the following attachment of the brush polymers [35, 61]. Secondly COOH - functionalized polymer chains are reacted with remaining epoxy groups of this anchoring layer to form ester bondings. The reaction scheme, the functional groups and the resulting chemical bonds are displayed in Figure 2.1.

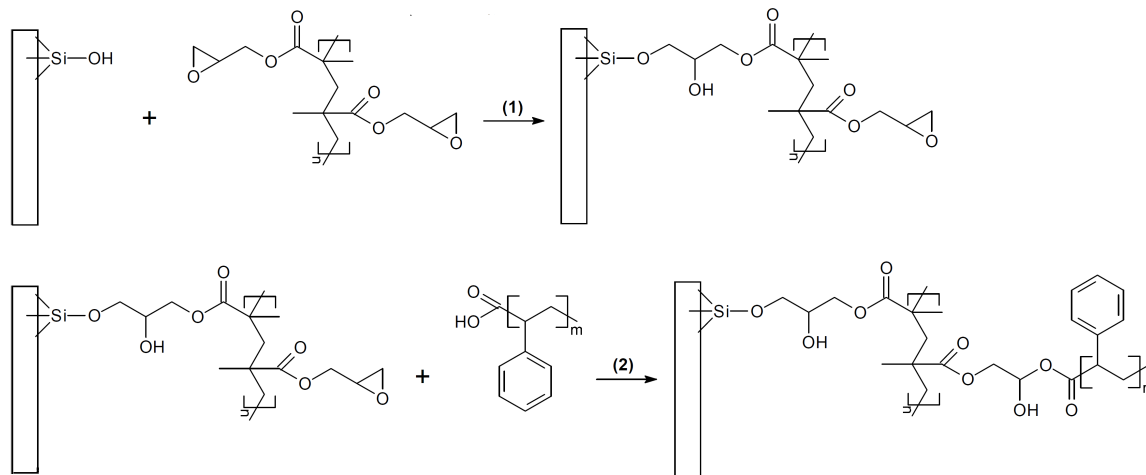


Figure 2.1.: Reaction scheme of the polymer brush formation by "grafting-to" displayed for the example of the grafting of polystyrene chains to a PGMA anchoring layer on a silicon substrate. 1) Grafting of PGMA via ether bonds to the silicon substrate. 2) Grafting of COOH-functionalized polystyrene via ester bonds to the PGMA layer.

With this method the grafting density can be controlled by the annealing time and temperature as well as the thickness of the polymer (melt) layer on top of the anchoring layer, whereas the latter is strongly determined by the concentration of the polymer solution spin-coated onto the anchoring layer. However, the grafting density is limited due to the increasing osmotic pressure of grafted chains against the diffusion of more chains into the brush layer in the ongoing grafting process of the brush polymer chains [12, 14]. Thus often the brush regime cannot be achieved with this method and polymers are grafted in a mushroom conformation. Here the usage of an anchoring layer consisting of reactive polymers (e.g. PGMA) is favorable for achieving considerably high grafting densities. Because of its loop-tail structure these anchoring layers provide an increased amount of epoxy groups for the grafting of brush polymers compared to self-assembled functionalized monolayers (e.g. GPS) [68]. Iyer et al. calculated the initial amount of epoxy groups in a 1 nm thick PGMA film ($M_n = 24,000 \frac{g}{mol}$) to be $4.5 \frac{groups}{nm^2}$ and estimated the amount of active epoxy groups available for the brush preparation to be at least $1.3 \frac{groups}{nm^2}$. They explained the decrease of active epoxy groups in the grafting of the PGMA film with a loss of 60 % due to self-crosslinking and of 15 % – 25 %, the train fraction, due to the reaction with the silicon surface [61, 69]. When grafting the brush polymers, e.g. polystyrene as shown in Figure 2.1, to this anchoring layer a mixing of PGMA loops and brush polymers can occur [69]. The free energy of mixing and the interface thickness can be calculated by the Flory-Huggins equation and for the example of PGMA and PS an interpenetration of up to 1.8 nm was found leading to a fractal interface [69].

2.2. End-grafted polymer brushes

End-functionalized polymers chemically grafted to a surface can be characterized according to the distance between different grafting points and the thickness of the polymer layer.

In [12] the reduced tethered density

$$\Sigma = \sigma \pi R_g^2 \quad (2.1)$$

is introduced, that is proportional to the grafting density

$$\sigma = \frac{d\rho N_A}{M_n} \quad (2.2)$$

and the square of the radius of gyration R_g . Here the grafting density σ can be calculated from the ellipsometrically obtained layer thickness d , the polymer brush density ρ , Avogadro's constant N_A and the number average molecular weight M_n of the polymer chains. Additionally the amount Γ of polymer per unit surface area can be calculated from the polymer brush density ρ and the layer thickness d :

$$\Gamma = \rho \cdot d, \quad (2.3)$$

whereas often the brush density ρ is unknown and the polymer bulk density is taken for the calculations of σ and Γ to obtain approximative results.

With the reduced tethered density Σ , grafted polymers at a surface can be classified into brush, mushroom or pancake regime. Physically Σ is the number of chains within the area that a free non-overlapping chain would occupy at the same environmental conditions [12]. The Σ parameter for the transition between mushroom and brush regime depends on the excluded volume, which varies for different systems. Nevertheless it was found for several brush systems that the brush regime is often present for $\Sigma > 5$ whereas for $1 < \Sigma < 5$ a transition regime occurs followed by mushroom conformations for $\Sigma < 1$ [70–73].

Regarding the swelling behavior of polymer brushes, the first quantitative theoretical investigations led to scaling laws describing the swollen layer thickness of classical neutral brushes in non-polar solvents of different quality (poor, theta or good solvent) dependent on the grafting density and the molecular weight of the polymer chains [11, 74–76]. They were followed by self-consistent mean field calculations and simulation studies, whereas additional informations about e.g. the brush profile as well as the distribution of polymer chain ends could be described [11, 77–79].

Polymers, like polystyrene, as classical neutral brushes can be described by the classical Flory-Huggins model with the Flory-Huggins interaction parameter as the central quantity to describe the polymer-solvent and polymer-polymer interactions [11]. Typically these brushes have an upper critical solution temperature (UCST) below which the solvent changes its quality

from good to poor and the polymer chains deswell. As an example the swelling of end-grafted polystyrene in the good solvent toluol and the near- θ solvent cyclohexane has been investigated [63, 80]. A good agreement with the theoretical brush height predicted by mean-field theory was found for PS brushes at an intermediate grafting density [63], whereas deviations from the scaling laws were demonstrated for very dense PS brushes with grafting densities higher than 1 nm^{-2} [80].

2.2.1. Water soluble polymer brushes: LCST behavior

Water soluble polymer brushes have a more complicated interaction behavior than classical neutral brushes because they induce an ordering in the surrounding polar solvent due to H-bonding. Their effective Flory interaction parameter χ depends on temperature and polymer concentration in contrast to classical neutral brushes, where χ was only changing with temperature [11]. This leads to the phenomenon of a lower critical solution temperature (LCST) where these water soluble polymers exhibit a phase transition from a swollen to a collapsed configuration upon increase of temperature, thus monomer-monomer interactions are more favorable at elevated temperatures than interactions between the monomers and the polar solvent. Typical water soluble polymers showing this phase transition are expressed with their LCST in Table 2.1.

The LCST depends on the molecular weight as well as the environmental conditions (solvent, pressure) and can be shifted by statistic copolymerization [46, 83, 84]. Introduction of more hydrophilic monomers increases the LCST whereas more hydrophobic monomers decrease it. For PNIPAAm-co-PAA in a polyelectrolyte complex with poly(allylamine) a dependency of the LCST on the pH and the concentration of polyelectrolyte complex was found, shifting the LCST in the range of 20 °C to 60 °C [83].

PNIPAAm is one of the best studied water soluble polymers and undergoes a phase transition in aqueous solution at its LCST of 32 °C [43–45]. The phase transition of PNIPAAm brushes in aqueous solution was studied with a variety of methods including neutron reflectometry [34, 85, 86], contact angle measurements [32, 33, 87], surface plasmon resonance [87] and atomic force microscopy [88]. Several aspects of the temperature sensitive phase transition like the increase of the hydrophobicity of the brush surface above the LCST, the collapse of the polymer

Table 2.1.: Lower critical solution temperatures of selected polymers in water.

Polymer	Molecular weight M_n $\frac{g}{mol}$	LCST [°C]	Reference
PNIPAAm	13,200	32	[32]
Poly(2-ethyl-2-oxazoline)	500,000 - 20,000	61-64	[81]
PEG	3,000	173	[82]

chains and changes in the vertical density profile of the brushes could be monitored. Here a distinct transition was found for high molecular weights and intermediate to high grafting densities with all methods, whereas no collapse of the PNIPAAm chains could be concluded from force-distance measurements for low molecular weights and low grafting densities [88].

These results are accompanied by evaluations of the first momentum $\langle z \rangle$ of the brush density profile dependence on temperature obtained by neutron reflectometry [34, 85, 86]. Here the decrease of $\langle z \rangle$ due to a temperature sensitive deswelling was found to occur over a broader temperature range when decreasing molecular weight M_n as well as grafting density σ , and the total changes in $\langle z \rangle$ between 20 °C and 40 °C depended non-monotonically on the ratio M_n / σ with a maximum of thickness change for intermediate σ . Furthermore for high grafting densities a vertical phase separation with a dense and a dilute brush region was observed in the range of the LCST [86].

These changes in the brush density profile with temperature could be connected successfully to self-consistent field simulations [89], and were also proposed on the basis of force-distance measurements [88].

2.2.2. Polyelectrolyte brushes

Polyelectrolyte brushes are characterized by ionizable groups at each monomer unit, thus long-range Coulomb interactions become important in the interaction of these brushes with environmental molecules. In aqueous solution charges can be compensated by oppositely charged counter ions forming electrostatic double layers around charged moieties and at surfaces [90]. The range of the Coulomb interactions is characterized by the Debye screening length κ^{-1} which is strongly dependent on the salt concentration in solution. Typical Debye lengths are displayed in Table 2.2.

Table 2.2.: Typical Debye lengths of monovalent ions in salted solutions [90].

salt concentration [M]	κ^{-1} [nm]
0.0001	30
0.01	3.0
1	0.3

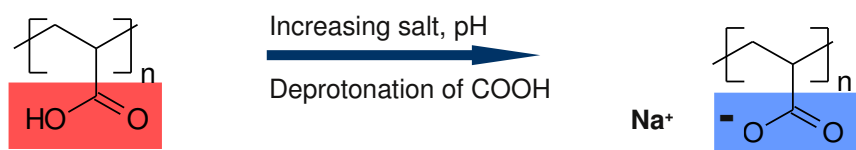


Figure 2.2.: Dissociation scheme of PAA.

According to the fraction of charged monomers polyelectrolyte brushes can be distinguished into quenched brushes (strong polyelectrolytes) with a fixed fraction of charged monomers and annealed brushes (weak polyelectrolytes) with a variable fraction of charged monomers [30]. For quenched brushes the swelling behavior is only dependent on the ionic strength of the solution, whereas for weak polyelectrolytes the degree of dissociation is also a function of the local pH. Thus annealed brushes swell sensitive to both pH and salt concentration in solution. For weak as well as strong polyelectrolyte brushes the swelling is driven by an osmotic pressure, caused by counter-ion localization inside the brush layer, whereas the entropic elasticity of the chains opposes the extension. A representative and well investigated example are brushes consisting of the weak acid poly(acrylic acid) (PAA) (Figure 2.2), which were investigated in the form of Guiselin brushes in this work. Hence the overview of the properties of polyelectrolyte brushes will be restricted to the annealed case and polyanionic brushes in this chapter.

Comprehensive theoretical studies have been done to understand the swelling behavior of polyelectrolyte brushes [91–94]. In his theory for the explanation of colloidal stabilization with grafted polyelectrolytes, Pincus developed a scaling theory for these brushes and found for brushes with no additional ion in solution (thus only dissociated groups with their monovalent counter-ions are present), that the thickness of the swollen layer scales directly with the number of monomers N , the length a of a monomer unit and the square root of the degree of dissociation α (Equation 2.4) [91].

$$d = \alpha^{1/2} N a \quad (2.4)$$

When additional ions, in form of a defined salt concentration c_{salt} , are present in solution, annealed polyelectrolyte brushes can appear in two different regimes. For $c_{salt} \gg c_{H^+}$ (with c_{H^+} the proton concentration in solution given by the pH) the brush is in the salted regime and the concentration of protons inside the brush is approximately the same as in solution [29]. The average degree of dissociation α_b at a fixed pH can be calculated to:

$$\alpha_b = \frac{1}{1 + \frac{c_{H^+}}{K_a}}, \quad (2.5)$$

which is the same as for a monomer (e.g. acrylic acid) in bulk solution. K_a is the monomer dissociation constant. The height of the salted brushes can be calculated with the help of mean-field models [29, 93] to

$$d \cong N a^2 \sigma^{1/3} \left(\frac{\alpha_b^2}{c_{salt}} \right)^{1/3}. \quad (2.6)$$

Here N is the number of monomers in an end-grafted polymer chain and σ the grafting density. For $c_{salt} < c_{H^+}$ and especially in the limit of zero salt concentration the dissociation of protons is hindered because an equal amount of counter-ions for charge neutralization of the negative dissociated groups per monomer is not present, thus $\alpha < \alpha_b$. This regime is called annealed

osmotic brush regime and the degree of dissociation as well as the brush height where derived as [29, 93]:

$$\alpha \cong \left(\frac{\alpha_b}{1 - \alpha_b} a \sigma^{-1} (c_{H^+} + c_{salt}) \right)^{2/3} \quad (2.7)$$

$$d \cong N a^{4/3} \sigma^{-1/3} \left(\frac{\alpha_b}{1 - \alpha_b} (c_{H^+} + c_{salt}) \right)^{1/3} . \quad (2.8)$$

Here α increases with the salt concentration until it reaches α_b and also the thickness is increasing with the salt concentration. However when the brush enters the salted regime d will decrease again according to Equation 2.6, thus a maximum of the swollen layer thickness is expected from theory.

2.3. Guiselin brushes

Guiselin brushes are formed due to the immobilization of polymer chains with more than one grafting point to an attractive surface [62, 95, 96], forming loops and tails of different sizes (Figure 2.3). This polymer layers can be characterized by thickness d , monomer density profile Φ as well as loop and tail size distribution $S(n)$. Here the latter refers to the number of loops and tails per unit surface with more than n monomers.

Theoretical descriptions for the swelling at good and bad solvent conditions exist for Guiselin brushes reversibly and irreversibly physisorbed at a surface, whereas in the latter case the loops are pinned to the surface and no rearrangement is possible [95]. Adsorption was examined either from solution or from the melt. Also chemisorption was discussed and described as non-instantaneous but slow irreversible adsorption leading to the theory of the slowly formed Guiselin brush [96].

Scaling laws for the loop density profile $S(n)$ and for the thickness d of such Guiselin brushes were developed and with the assumption that each loop, consisting of $2n$ monomers, behaves equally to two tails with n monomers, the problem could be converted into describing a very polydisperse end-grafted polymer brush [95]. This assumption is not trivial since loops of $2n$ and tails of n monomers are generally expected to behave energetically differently but at least in the case of reversibly adsorbing chains it could be shown that the layer thickness d as well as the monomer density Φ are independent of the modeling as loops or tails [97].



Figure 2.3.: Scheme of a Guiselin brush where the polymer chains are immobilized via more than one anchoring point along the chain.

Since the pseudo brushes prepared within this work consist of polyanionic PAA the theory of classical neutral Guiselin brushes is only applicable in the case of neutralized PAA chains to describe the scaling behavior of the layer thickness dependent on the number of monomers per chain. The scaling behavior of the brush thickness in a good solvent for irreversibly instantaneous physisorption or non-instantaneous chemisorption is the same, leading to:

$$d = aN^{5/6} \quad (2.9)$$

Here a is the monomer size and N the number of monomers of a single chain, whereas the thickness scales independent of the number n of monomers per tail. Unlike the total thickness, the loop density profile differs for physisorbed and chemisorbed Guiselin brushes. Non-instantaneous chemisorbed brushes swollen in a good solvent have two density regions: A more dense inner region and an outer region with a density profile similar to the physisorbed Guiselin brush.

2.4. Mixed polymer brushes

Since physico-chemical interface properties can be tuned by the grafting of polymer brushes, it is possible to switch these properties between extrema or to enhance the range of sensitivity, e.g. in creating response to different stimuli, when combining differently behaving polymers in mixed brushes. Polymers of one type with a determined mixture of chain lengths as well as chemically different polymers were grafted [67,98]. In the latter case tuning of the wetting behavior after treatment with different solvents was achieved for polystyrene (PS) - poly(2-vinylpyridine) (P2VP) brushes, and a ripple morphology of the brush surface due to phase segregation could be observed [98]. Alongside these experimental findings, theoretical explanations were derived for the phase separation of polymers in binary mixed brushes and diblock copolymer brushes [38,99,100].

Mixed polyelectrolyte brushes

The switching of physico-chemical interface properties by organic solvents prohibits the use of the mixed brush systems mentioned above within biological / physiological environments, hence the investigation of mixed brushes that are sensitive to stimuli adjustable in aqueous solutions has increased lately, and polyelectrolyte brush systems consisting of polyanionic PAA and polycationic P2VP were developed [18,35,37,101]. This mixed brush system was designed to switch the surface charge between positively charged at low pH (P2VP swollen, PAA contracted) and negatively charged at high pH (PAA swollen, P2VP contracted).

As described in Section 2.2.2 these polyelectrolytes change their swelling state sensitive to changes in pH and ionic strength of the solution due to protonation / deprotonation of dissociable groups along the chains. The swelling degree of PAA increases with increasing pH due

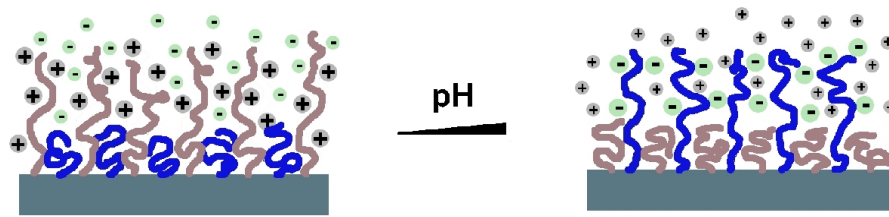


Figure 2.4.: Switching of a PAA-P2VP mixed polyelectrolyte brush with pH.

to the deprotonation of COOH groups, whereas P2VP is in its swollen state at low pH due to the protonation of the nitrogen atom in the pyridine ring.

The complex dissociation behavior of this mixed brush was investigated with several techniques like contact angle and streaming potential measurements [35] or infrared ellipsometry [37] and a charge complexation for intermediate pH could be found, rendering the surface neutral with an isoelectric point of pH 4.9.

3. Adsorption of proteins to surfaces

The adsorption of proteins to surfaces is of great interest in a variety of different fields. On the one hand a number of proteins tend to perform their tasks in-vivo at phase boundaries, e.g. membrane proteins, and the understanding of the influence of these protein-interface-coordination on structure and function of the protein is desirable [102]. On the other hand protein adsorption on artificial surfaces shall be either prevented on medical implant devices [103], or it is desired in a controlled way to create drug delivery systems or biosensors [104,105].

3.1. Physico-chemical properties of proteins in solution

Proteins can be characterized by their molecular weight, shape, state of hydration and their electrochemical behavior [106]. Due to the variation in hydrogen-bonding capacity, hydrophobicity and dissociation behavior of the amino acid residues in the polypeptide chains, proteins are amphiphilic as well as amphoteric. Analytical methods for the determination of properties of proteins are listed in Table 3.1. In changing environmental conditions mostly the ternary structure of the proteins can be affected, leading to denaturation and even unfolding of the protein under extreme conditions.

Protein structure

The primary structure of a protein consists of linear polypeptide chains, where defined sequences of amino acids are covalently linked via peptide bonds, and the sequence of amino acid residues

Table 3.1.: Common methods for the determination of physico-chemical properties of proteins.

Properties	Analytical method
Molecular weight	Ultracentrifugation Sedimentation and gel filtration [107]
Shape	X-ray diffraction of crystallized proteins Sedimentation and gel filtration
Hydration state	High-frequency dielectric spectroscopy Electron microscopy
Electrochemistry	Electrophoresis Electrometric titration

in the chain also determines the secondary and tertiary structure of the protein (Figure 3.1). Proteins can appear as monomers with one polypeptide chain, but also dimers (e.g. human serum albumin, glucose oxidase), trimers (e.g. α -chymotrypsin) or multimers (e.g. fibrinogen), with the respective number of polypeptide chains exist. These subunits are often connected via disulfide bonds and resemble the quaternary structure of a protein complex.

Common secondary structures are β -sheet and α -helix, which are stabilized by H-bonding between the CO- and NH- groups of the peptide backbone and are due to the chirality of their monomers [108]. It was found that within these ordered structures the number of possible conformations was reduced to 25 % compared to the conformations possible in the expanded coil structure [102]. The tertiary structure is determined by the interaction of the amino acid residues (Figure 3.1). Here different interaction forces are present between the residues as well as towards the solvent molecules ranging from disulfide and hydrogen bonding to hydrophobic effects and Coulomb as well as van der Waals forces [109].

The shape of proteins can vary very much with the extrema of globular proteins (closely folded structure) and fibrous proteins (unidimensional threadlike structure). Within this work globular proteins in an aqueous environment were used for adsorption studies. These proteins are almost spherical with packing densities around 75 %, which is in the range of the maximum packing density of hard spheres of equal size (74 %), thus a large fraction of atoms within the protein have to be in van der Waals contact. Hydrophobic side groups are mainly located in the interior of the molecule and charged groups are mostly in the periphery in contact with water [102].

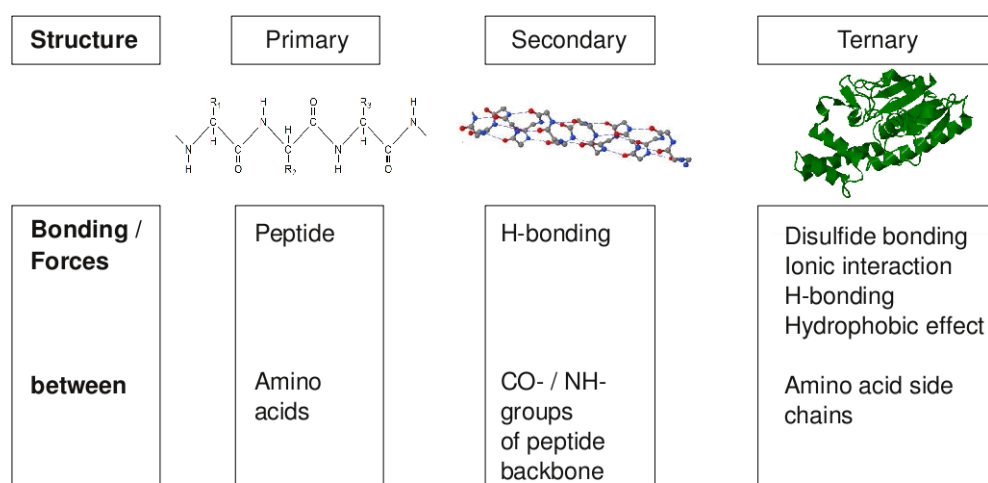


Figure 3.1.: Schematical built up of proteins from amino acids to the compact protein structure. The natural place of protein formation are thereby the ribosomes within cells.

State of hydration

Hydrophilic groups on proteins are present due to dissociated and polar chemical groups on different amino acid residues. Dependent on the pH positively charged groups can be found at lysine, arginine and histidine and negatively charged groups on aspartic and glutamic acid side chains, but hydrogen bonding is also possible with polar groups like amide groups at asparagine and glutamine or OH groups at serine and threonine side chains [106, 110].

The state of hydration is often important for the biological function of proteins, but also for molecular weight or structure determination the knowledge of the amount of hydration is helpful. Often the molecular weight is determined too large due to the bound water, whereas the crystal structure necessary for X-ray diffraction is lost when dehydrating the protein. The water amount bound to one gram of a protein varies with the protein type. For example for the elongated fibrinogen 4g H_2O /g protein was found [111]. The water uptake depends on the pH and is expected to be lower for globular than for fibrous proteins due to their compact structure with an increased amount of hydrophobic groups in the interior.

Furthermore the solubility of proteins in aqueous solutions is affected by their state of hydration and proteins can be precipitated by adding salts like sodium chloride to the solution. Since hydration of the additional ions of the dissolved salt reduces the amount of water molecules available for interaction with polar amino acid side chains of the protein its state of hydration decreases, leading to this salting-out effect.

Charge state

When regarding the charge state of proteins mainly electrometric titration and electrophoresis are used to characterize the amount of positively and negatively charged groups as well as the isoelectric point due to the migration in an electrical field, respectively. As mentioned above anionic and cationic groups are present on amino acid residues, dissociating dependent on the pH.

This results in a buffering effect by the protein at pH 3 to 4 (Reaction of COO^- to $COOH$ at the side chains of aspartic acid and glutamic acid) and pH 9 to 10 (mainly reaction of NH_3^+ to NH_2 at the side chain of lysine) since added acid or base does not change the pH of the solution but leads to a dissociation of the mentioned side chain groups. In the basic region also the loss of protons from hydroxyl groups of the amino acid tyrosine is contributing to the protein buffer capacity noticeably.

In electrophoretic measurements, nowadays mostly zone electrophoresis with the protein placed inside a gel-like material at a defined pH is used and the isoelectric point of the protein can be determined. Since the proteins move towards the negative cathode when positively charged (low pH) and to the positive anode when negatively charged (high pH) the isoelectric point can be determined as the pH when the protein is not moving at all in the electrical field.

3.2. Adsorption process

3.2.1. Transport to the surface and deposition

The process of adsorption is characterized by individual steps including the transport to the surface during adsorption and from the surface in the desorption process, the deposition and relaxation at the surface as well as the detachment process and a restructuring of the desorbed protein in solution [109].

Here the transport to the surface is driven by diffusion but also by convection if the solution above the sorbent surface is in laminar or turbulent flow. In the absence of convection (batch geometry with time $t \gg t_{insert}^{solution}$) a depletion zone next to the sorbent surface occurs, leading to a flux J of protein molecules to the surface of

$$J = (c_b - c_s) \left(\frac{D}{\pi t} \right)^{1/2}. \quad (3.1)$$

Here c_b and c_s are the protein concentrations in the bulk solution and at the surface, and D is the diffusion constant.

If the experiments are performed under steady-state conditions, e.g. in laminar flow, the flux to the surface is determined by the protein concentration difference and the rate constant k_1 which depends on the flow conditions, the geometry and the diffusion constant:

$$J = k_1(c_b - c_s). \quad (3.2)$$

The deposition of protein molecules at the surface is now determined by the rate constant k_2 . This deposition rate constant decreases with increasing c_s until the rate of attachment equals the rate of detachment, leading to:

$$\frac{d\Gamma}{dt} = k_2(c_s - c_{eq}). \quad (3.3)$$

Here the change in the adsorbed amount Γ with time depends on the difference between the protein concentration at the surface c_s and the concentration c_{eq} corresponding to the saturation value of Γ which is determined by the adsorption isotherm (Section 3.2.3). Thus when the protein concentration at the surface equals c_{eq} the adsorption rate becomes zero.

3.2.2. Driving forces

Energetically protein adsorption at constant temperature and pressure takes place if the Gibbs energy G decreases (Equation 3.4) [109]. Here H is the enthalpy, S the entropy and T the absolute temperature in Kelvin.

$$\Delta_{ads}G = \Delta_{ads}H - T\Delta_{ads}S < 0 \quad (3.4)$$

Thereby the adsorption process is mainly governed by structural rearrangements of the protein and its surface polarity, but also by changes in the distribution of charges at the interface and a partial dehydration of the surface. Here different contributions to the change in the Gibbs energy can be assigned to specific interaction processes as listed in Table 3.2 [102].

The strongest driving effect when non-polar surfaces are present in the adsorbing system is dehydration. Although the apolar groups tend to be in the interior of globular proteins, most have still apolar patches near or on the surface. Thus even if the sorbent surface is polar and hydrated, protein adsorption can occur.

Here often structural rearrangements of the protein structure are involved. Since the hydration state in the protein-surface contact area changes, intramolecular hydrophobic interaction becomes less important to maintain the stability of the protein and secondary structures like α -helices or β -sheets can become destabilized. This decrease in structural order increases the conformational entropy of the protein and thus favors the adsorption process. However structural changes are usually small and no unfolding into a loop and tail structure occurs.

Interaction between electrical double layers at the surface and around the protein molecule can also contribute to a negative change in ΔG . An electrical double layer is formed by the charge at a surface and the countercharge present as bound and diffuse counter as well as co-ions around this surface. Often the sorbent surface can be described by the Gouy-Stern model and the protein by a discrete-charge model [112, 113].

A scheme of the electrical double layer with a compact immobile double layer region at the charged surface and a diffuse layer further away from the surface is depicted in Figure 3.2. This double layer model was developed according to the Gouy-Chapman theory with an additional modification of Stern regarding the ions not as point charges but with finite sizes [112]. Here the thickness of the immobile layer is determined by the inner Helmholtz plane with the potential Ψ^{IHP} and the outer Helmholtz plane with Ψ^{OHP} , where the surface potential decreases linearly within this distance from the surface. The potential at the shear plane between compact and diffuse double layer is called ζ -potential and can be determined for

Table 3.2.: Contributions to ΔG_{ads} according to the specific interactions present in a system of one type of protein molecules and a defined sorbent surface in a well-known aqueous environment [102, 109].

	Interaction forces	Contribution to ΔG
ΔG_{disp}	van der Waals dispersion forces	-1 to $-3 \frac{RT}{mol}$ at polymer surface -4 to $-7 \frac{RT}{mol}$ at metal surface
ΔG_{el}	Interaction between electrical double layers	order of $10 \frac{RT}{mol}$
ΔG_{struc}	Rearrangement in structure of protein	order of $10 \frac{RT}{mol}$
ΔG_{hydr}	Dehydration of apolar surfaces	-60 to $-120 \frac{RT}{mol}$

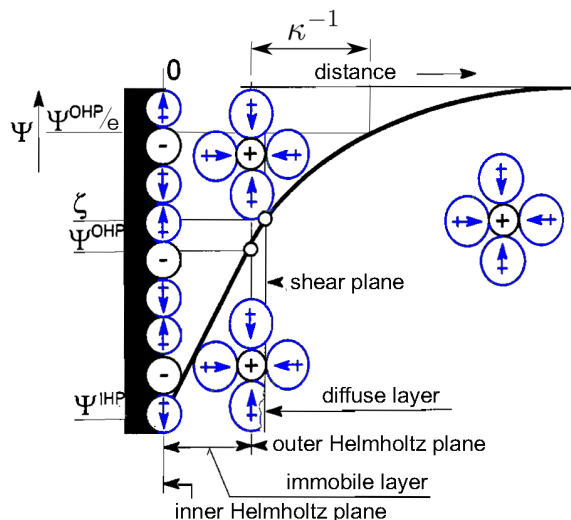


Figure 3.2.: Scheme of the electrical double layer of counter and co-ions as well as water molecules and differently defined planes of potential [114].

planar surfaces from streaming potential measurements [114]. Shear plane and outer Helmholtz plane can differ slightly due to the hydration of surface bound co- and counterions, indicated by the dipole symbols (blue) for water in Figure 3.2. Here the Debye length κ^{-1} is a measure of the thickness of the diffuse double layer, characterizing the distance from the outer Helmholtz plane where the potential Ψ^{OHP} reduces to $\frac{\Psi^{OHP}}{e}$.

If the Debye length is smaller than the thickness of an adsorbed compact protein layer (as in most cases) the net charge density at the protein-sorbent interface is zero because the proteins screen it from further electrostatic interaction with the solution. Also an adjustment of the charges at the sorbent-surface as well as for the protein molecules takes place [115]. To maintain local charge neutrality an incorporation of additional ions at the interface is possible, whereas this process is chemically unfavorable and opposes the adsorption process. Thus the highest adsorbed amount can be found when the charge density on the protein matches that on the surface so no additional ions have to be incorporated [116].

Van der Waals dispersion interactions between the electron orbitals in close vicinity are present as well in the adsorption process. Here the contribution to ΔG for a sphere interacting with a planar surface, where the distance h between surface and sphere is much smaller than the radius a of the sphere, can be approximated to [109]:

$$\Delta G_{disp} = -A_{132} \frac{a}{6h} \quad (3.5)$$

A_{132} is the Hamaker constant for the interaction and can be calculated from the individual constants A_1 , A_2 and A_3 between the molecules of each phase in aqueous solution [117].

If the sorbent-surface is not solid but flexible two opposing tendencies are discussed. Adsorp-

tion is favored in optimizing the contact by adjustment of the surface morphology to the protein shape, but an increased osmotic pressure and a decrease in the conformational entropy of e.g. surface bound polymers when the protein "presses" on the surface opposes the adsorption.

Furthermore at polar surfaces the adsorption of "hard" proteins happens only at electrostatically attractive conditions, whereas "soft" proteins can also adsorb at repulsive conditions due to their structural rearrangements [109].

The relaxation of protein molecules due to structural rearrangements at the sorbent-surface is addressed quantitatively in modeling the protein molecules as tiny core-shell droplets with effective interface tension and "hardness" [108]. The interface tension may change with changes in the protein conformation, whereas adsorption is treated as a droplet spreading. After contact with the surface spreading occurs to increase the contact area. Here the central quantity is the spreading parameter S (derivative of G) and it is expressed in terms of the interface tensions in analogy to a droplet of liquid at a surface. With this model the smaller adsorbed amount Γ of a saturated protein monolayer on a surface with high adsorption affinity compared to a surface with lower adsorption affinity is explained. Here an increased tendency of spreading of the protein due to high adsorption affinity is discussed to lead to a faster saturation of the sorbent-surface with protein molecules.

3.2.3. Adsorption isotherm and reversibility of adsorption

The measurement of Γ at $t \rightarrow \infty$ for different supply rates (concentration of the protein in solution) leads to the adsorption isotherm $\Gamma(c_{eq})$ [109] (Figure 3.3).

For globular proteins usually well defined plateau values can be reached. Here c_{eq} to achieve the plateau region is often in the range of a few tenths of mg/ml . Since the protein molecules undergo relaxation at the sorbent-surface the plateau adsorbed amount depends on the ratio of relaxation rate and supply rate, thus the mode of supply, e.g. undesired convection, affects $\Gamma(c_{eq})$.

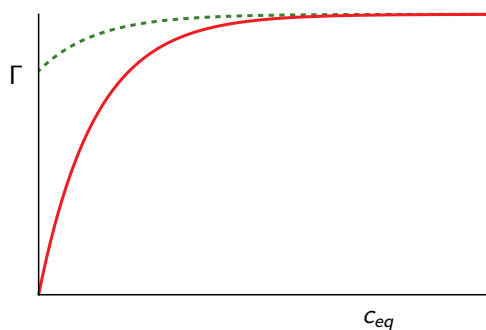


Figure 3.3.: Scheme of $\Gamma(c_{eq})$ of the adsorption (solid line) and the desorption (dashed line). Hysteresis between adsorption and desorption isotherm indicate an irreversible adsorbed amount of protein [109].

If hysteresis between adsorption and desorption as indicated in Figure 3.3 occurs, the adsorption process is not fully reversible. Here reversibility of the process would be given if $\Gamma(c_{eq})_{des}$ would be the same as $\Gamma(c_{eq})_{ads}$ when decreasing again the protein concentration in solution. When hysteresis is observed two metastable states exist, one on adsorption and desorption isotherm respectively, separated by a Gibbs energy barrier. This implies that physical changes, like a structural rearrangement within the protein molecules have occurred in the adsorption process, that are not fully reversed after desorption. Thus the physical structure of the protein molecules is different before adsorption and after desorption, characterizing an irreversible protein adsorption process. As an example for BSA adsorption to silica surfaces at pH 4 a decrease of α -helix structure from 69 % before adsorption to 50 % after desorption could be found [118]. Here the BSA molecules were replaced by surface-active morpholine to analyze a high amount of desorbed protein.

3.3. Adsorption at non-swellaable surfaces

The theoretical concepts for protein adsorption given in Section 3.2 have been developed alongside adsorption experiments at solid surfaces employing techniques like ellipsometry [119–122], total internal reflection fluorescence [119], radio labeling [121] or X-ray reflectivity [123]. Here metal [116, 122] as well as silica surfaces [124, 125], but also hydrophobic polymer surfaces [115, 120] or lipid membranes [126] have been studied.

At a solid or hydrophobic surface it was found that the plateau value of the adsorption isotherm is mostly lower or comparable to a monolayer of closely packed protein molecules with protein layer thicknesses in the range of the dimension of the molecules [109, 127], the latter taken as indication that only comparably small structural rearrangements in the protein molecule take place and no expanded loop and tail structure is formed. Regarding the protein concentration necessary to reach the plateau value of Γ , for example studies of HSA and fibrinogen adsorption have been performed on hydrophobic fluorocarbon polymer films and the plateau value for HSA was found for concentrations starting from $0.15 \frac{mg}{ml}$ [120].

In several studies also competitive adsorption was addressed [119, 128–130]. In a mixed protein solution with equal fractions of different protein types the proteins with the highest diffusion coefficients (smallest molecular weight) are expected to adsorb at first at the sorbent surface but can be replaced by other proteins that have a higher adsorption affinity for the surface.

Regarding the electrochemical situation at the protein-sorbate interface, studies have been performed that demonstrate the charge regulation at the surface as well as on the protein molecules [115, 126]. Furthermore on the one hand adsorption of the protein lysozyme at silica surfaces was found to have a maximum at the isoelectric point (IEP) of the protein [131], ex-

plained by a minimum of electrostatic repulsion between individual protein molecules but also an increased structural stability of the protein at its IEP. Thus closely packed protein layers with a low spreading parameter (high thickness) are forming. On the other hand for the adsorption of lysozyme at a fixed pH at metal surfaces (electrodes) under variation of the applied electrode potential a minimum of the adsorbed amount was found close to the point of zero charge (PZC) of the electrode and an increase of the adsorbed amount around the PZC of the electrode occurred. Since the interface tension of the electrode decreases when it is polarized the adsorption affinity as well as the spreading parameter of the protein decreases leading to a slower saturation of the surface and thus a higher adsorbed amount [108,116].

Biochemical processes have been investigated as well at silica surfaces, for example enzymatic degradation of protein layers [124], complement activation [125] or the activity of chymotrypsin immobilized at a hydrophobic surface [132].

3.4. Adsorption at hydrogels and polymer brushes

Protein adsorption at highly swellable surfaces like hydrogels [9, 50, 133–135] or polyelectrolyte brushes [18, 136–139] was investigated because of their large potential for applications in biological environments, especially in drug release systems [9]. Novel effects of these flexible surfaces like adsorption enhancement due to large water accessible charged surfaces and entropic effects (polyelectrolyte mediated adsorption) [139] as well as protein resistance could be found [25, 28].

Among the field of hydrogels, modulated release systems, that are able to release proteins or drug molecules due to swelling upon external stimuli are most interesting for this work [9]. Here temperature [50, 135] as well as pH-sensitive [134, 140] hydrogels have been developed but also interpenetrating polymer networks, that are sensitive to both stimuli [7, 51]. Adsorption of negatively charged proteins within cationic hydrogels was found to be highly reversible at low ionic strength [134]. Whereas for temperature sensitive PNIPAAm hydrogels (crosslinked with N, N'-methylenebisacrylamide) the release of insulin and albumin was found to be incomplete, with higher amounts of the larger albumin molecules than of the smaller insulin molecules remaining in the gel [135].

The adsorption of particles (including proteins) to polymer brushes has been divided into three different types according to the place of adsorption (Figure 3.4) [14]. In the case of primary adsorption the particle diffuses through the brush and can adsorb directly at the grafting surface, whereas if the particles are too large or the grafting density too high secondary adsorption can occur with the particles adsorbing at the brush-solution interface. Also the case of ternary adsorption may be possible where particles interact directly with the polymer

chains and can adsorb distributed within the brush layer. The type of adsorption is strongly influenced by the particle size but also chain length, distance between grafted chains and types of interactions between particles and polymer chains are of importance.

3.4.1. Polyelectrolyte brushes

Intensive theoretical and experimental studies have been done for polyelectrolyte brushes, including albumin adsorption on PAA brushes in spherical or planar geometries [59,136,141–143].

Here adsorption for likewise negative net charges on brush and protein at the "wrong side" of the IEP of the protein was found, whereas two possible explanations exist for this phenomenon. On the one hand the possibility of charge regulation / reversal on the protein is discussed in terms of an adjustment of the charge of weakly charged amino acids to the local electrostatic potential inside the polyelectrolyte brush. On the other hand due to a charge anisotropy (patchiness) of the protein, positive charged patches exist on the protein that could lead to an entropically favorable replacement of the small counter-ions inside the brush with protein molecules. In reference [143] these effects were discussed to be additive, whereas the process of charge regulation was considered as the dominating driving force for most types of proteins.

Furthermore the penetration of protein molecules inside the brush layer could be demonstrated [136], whereas a homogeneous filling of the brush with albumin molecules was found for adsorption at pH 6.7 with a volume fraction of 7 – 10 % [142] (Scheme 3.5). In this study the adsorbed amount also increased with increasing temperature indicating an entropically driven adsorption mechanism for these experiments [142].

Systematic experimental studies on the influence of polymer length, grafting density, pH and salt concentration have been performed as well [59]. The adsorption maximum was found near the IEP of the protein and a fraction of 30 vol% of BSA content in the brush estimated at the maximum, whereas the adsorbed amount strongly increased with higher grafting density and higher polymer chain length. Almost no effect of the protein concentration in solution on

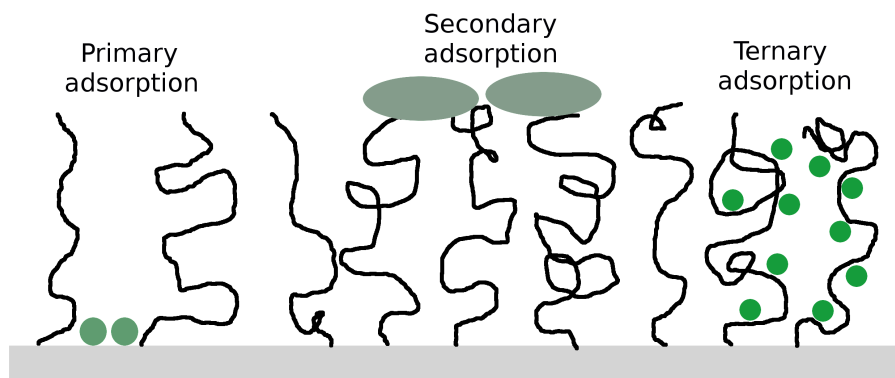


Figure 3.4.: Modes of adsorption on a grafted polymer layer [14].

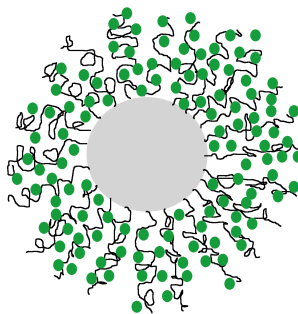


Figure 3.5.: Scheme of the homogeneous distribution of albumin molecules (green) within a spherical polyelectrolyte brush grafted to a polystyrene core particle [136].

the adsorbed amount was observed as expected for this high-affinity system. Furthermore the critical pH above the IEP until which adsorption on the "wrong side" takes place was examined to decrease with increasing ionic strength, and a good agreement of the experimental data with an analytical polyelectrolyte brush model, based on charge regulation and excluded volume interaction, could be found.

Protein adsorption on mixed polyelectrolyte brushes has been studied so far on a binary brush system consisting of the oppositely weak charged polymers PAA and poly(2-vinyl pyridine) (P2VP) [18]. Here the interface charge can be switched from positively charged at low pH to negatively charged at high pH and the influence of pH and ionic strength on the adsorption of α -chymotrypsin (IEP at pH=8.1) and α -lactalbumin (IEP at pH=4.3) was studied. Here polyelectrolyte mediated adsorption at net repulsive conditions could be found for this system at low pH for α -lactalbumin and at high pH for α -chymotrypsin.

Within spherical PAA brushes the activity of immobilized enzymes was tested as well and nearly full activity of the immobilized enzyme could be observed, indicating a large potential of these systems in the field of biosensors [137].

3.4.2. Protein repelling brushes

Further interfaces of great interest for bio-related applications are protein repelling surfaces as well as surfaces allowing controlled biofilm adhesion [28]. Here experimental and theoretical results for highly water soluble polyethylene glycol (PEG) brushes that reduce protein adsorption considerably shall be presented briefly.

PEG chains have high excluded volumes [144]. Thus it is discussed that, if a protein approaches the brush surface and compresses the chains, a repulsive osmotic pressure is induced aiming at the restorage of the initial brush volume [14]. This consideration could be proven experimentally in measuring repulsive interaction forces at the brush surface upon compres-

sion [24].

Further interaction forces that are present in the neutral protein - polymer brush - substrate system are long-range attractive van der Waals forces between protein and substrate as well as a short-range steric repulsion between protein and polymer segments, leading together with the repulsive osmotic pressure to an effective interaction potential (Figure 3.6) [14]. Here dependent on the magnitude of the individual interactions a potential barrier is present. Within this simple model no attractive interaction between the protein molecules and the polymer chains are considered and the proteins are treated as inert particles with sizes much larger than the average distance between grafted polymer chains. Thus for neutral systems (no Coulomb interactions) the brush acts as a steric barrier reducing or even preventing protein adsorption at the brush-solution interface, referred to as secondary adsorption. However, if the distance between grafting sites increases and becomes similar to the dimensions of the adsorbing molecules primary adsorption could occur.

This behavior was found for PEG brushes with high grafting densities and moderate chain length [48, 145, 146]. Here systematic studies of BSA adsorption on PEG brushes showed that for PEG chain lengths of 148 monomers ($M_w = 6,500 \frac{g}{mol}$) the adsorbed amount decreased with increasing grafting density and virtually protein resistance could be found for a grafting density of 0.3 nm^{-2} [48]. However for long PEG chains with more than 445 monomers ($M_w = 19,600 \frac{g}{mol}$) a maximum of the adsorbed amount at low grafting densities (around 0.05 nm^{-2}) was observed and for PEG chains with 700 monomers ($M_w = 23,000 \frac{g}{mol}$) protein adsorption could be found for all grafting densities. This adsorption behavior was discussed in terms of ternary adsorption indicating an additional attractive interaction between the proteins and the PEG monomers [25, 48, 49, 147], that was not accounted for in the model considerations discussed above. Here for self-consistent field calculations an effective segmental adsorption energy per monomer was considered, and the maximum of adsorption at low grafting densities for PEG brushes with long chains theoretically confirmed [48]. The maximum is explained by

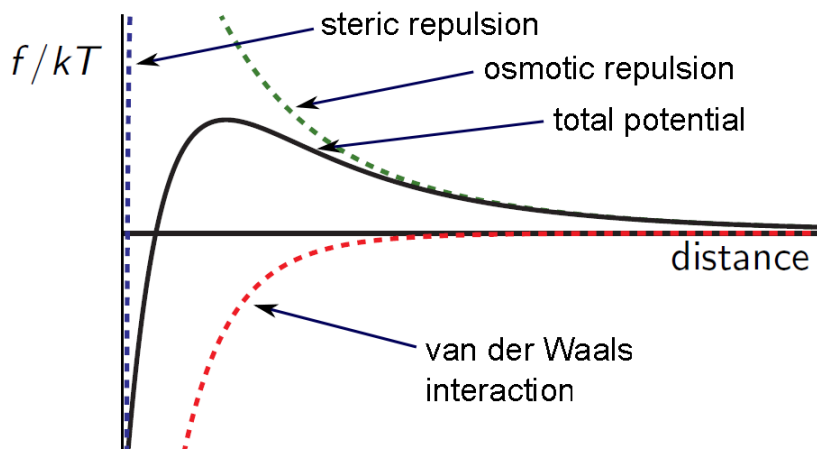


Figure 3.6.: Total force per unit area $\frac{f}{kT}$ acting on a neutral particle approaching a neutral brush (solid line) and individual contributions (dashed lines) [14].

the possibility of protein molecules to diffuse into the PEG brush at low grafting densities and to interact with the monomers [25]. With increasing grafting density on the one hand the number of attractive interaction sites increases leading to a higher adsorbed amount of protein, but on the other hand the fraction of proteins diffusing into the brush decreases, leading eventually to a decrease in the adsorbed protein amount. For short PEG chains the number of adsorption sites along the polymers is too low to increase the adsorbed amount considerably.

4. Methods for surface characterization

Surface characterization methods used within this work are summarized in Table 4.1. Most of the experiments have been performed with in-situ spectroscopic VIS-ellipsometry or single-wavelength null-ellipsometry and a detailed discussion of ellipsometry follows in Section 4.2. Also extensive dynamic contact angle measurements and quartz crystal microbalance experiments have been done and the methods will be presented in Section 4.3 and Section 4.4. Further methods applied for the surface characterization like streaming potential measurements, atomic force microscopy or ATR-FTIR spectroscopy have been used in their standardized way and thus only selected aspects will be mentioned here.

4.1. Survey of AFM, ζ -potential determination and ATR-FTIR spectroscopy

Atomic force microscopy (AFM) in "tapping mode" (Nanoscope IIIa, Dimension 3100, Veeco, USA) operated in air was used to control homogeneity and roughness of the surfaces after preparation and after pretreatment at different pH. Tips of the type BSTap (Budget Sensors, Bulgaria) with a resonance frequency of 300 kHz and a spring constant of 40 N/m were used.

The cantilever oscillates slightly above its resonant frequency, and it contacts the surface for a short period during its oscillation cycle. To overcome adhesion forces between tip and surface as well as the sticking in an adsorbed liquid layer at the surface the amplitude of the cantilever has to be considerably high and is usually in the range of 100 nm. Within the tapping measurement this oscillation amplitude A is maintained constant at $A_{setpoint}$ via a feedback loop and changes in the z -coordinate of the cantilever required to keep A constant are recorded and displayed as a topographic image of the surface. The root mean square (RMS) roughness σ was evaluated with the help of the AFM evaluation program (WSxM [148]), whereas σ_{RMS} is defined as the standard deviation of the height value Z_i of data point i from the average height value Z_{ave} of the image (Equation 4.1).

$$\sigma_{RMS} = \sqrt{\frac{\sum_{i=1}^N (Z_i - Z_{ave})^2}{N}} \quad (4.1)$$

N represents the number of measured data points within the image.

Table 4.1.: Survey of surface characterization methods used in this thesis.

Method	Measurement principle	Measured quantity	Instruments
Ellipsometry	Changes in polarization state of light upon specular reflection	Ellipsometric angles Δ and Ψ	Multiskop, Optrel Berlin, Germany M44 and M2000 J. A. Woollam Co., Inc., Lincoln, NE, USA
AFM (Tapping-mode)	Constant oscillation amplitude secures constant tip-sample interaction	Δz of cantilever to keep Amplitude A at set-point	NanoScope IIIa, Dimension 3100 Veeco, USA
Dynamic contact angle	Wetting of surface by liquid drop	Angle between solid surface and tangent plane to liquid surface	OCA20, DataPhysics Instruments GmbH, Filderstadt, Germany
Streaming potential	Potential at hydrodynamic shear plane	Isoelectric point of charge (IEP) ζ -Potential	ElectroKinetic Analyzer (EKA), Anton Paar GmbH Graz, Austria
QCM-D	Changes in oscillation of acoustic shear wave of quartz crystal	Frequency change Δf and Dissipation change ΔD	Crystal QSX 301 and ellipsometry modul QELM 401 (Q-Sense, Frölunda, Sweden)
ATR-FTIR	IR absorption in evanescent field (sample-reference mode)	Absorbance spectra $A(\nu)$	IFS 55 Equinox FTIR spectrometer (BRUKER-Saxonia, Leipzig) with SBSR mode (OPTISPEC, Zürich, Switzerland)

Streaming potential measurements can be used to derive the ζ -potential at the hydrodynamic shear plane of the diffuse double layer of macroscopic surfaces for example silicon wafers, fibers or membranes (Figure 3.2) [149]. Here the ζ -potential as a function of the pH was measured with the ElectroKinetic Analyzer (EKA, Anton Paar GmbH, Graz, Austria, Figure 4.1). Two silicon surfaces coated with equal polymer brushes are arranged face to face to form a small channel where the electrolyte solution is pumped through in controlled flow. The voltage ΔU corresponding to the streaming potential as a function of the pressure loss Δp in the flow channel is measured by two electrodes.

Here ΔU is connected to the ζ -potential by a relation derived by Helmholtz and Smoluchowski [151].

$$\zeta = \frac{\Delta U}{\Delta p} \cdot \frac{L}{Q} \cdot \frac{\eta}{\epsilon \cdot \epsilon_0} \cdot \frac{1}{R} \quad (4.2)$$

L is the channel length and Q the cross-section area, whereas η , ϵ_0 and ϵ are the viscosity, the absolute and relative dielectric constants of the liquid, respectively. R is the electrical resistance of the system. The pH-value was adjusted with 100 mM KOH and 100 mM HCl.

Attenuated total reflexion Fourier-transform infrared spectroscopy (ATR-FTIR) was operated in-situ to monitor shifts and changes in the shape of characteristical vibration bands of thin polymer brush films upon changes in the environmental conditions. Thin film sensitivity can be achieved with this infrared spectroscopy method due to the utilization of the evanescent wave extending into the brush film. An infrared beam is guided trough a silicon internal reflection element according to Figure 4.2(b) with an angle of incidence that leads to total internal reflection at the silicon-environment interfaces, hence a near-field standing wave, the evanescent field, forms at this interface with an exponential decay of intensity $I(z)$ into the environment. In wavelength regions where an excitation of vibration modes in the thin brush film is possible the evanescent field is attenuated and its altered energy is passed back into the IR beam, thus contributes to the absorption of the IR beam and characteristical vibration bands of the film can be measured.

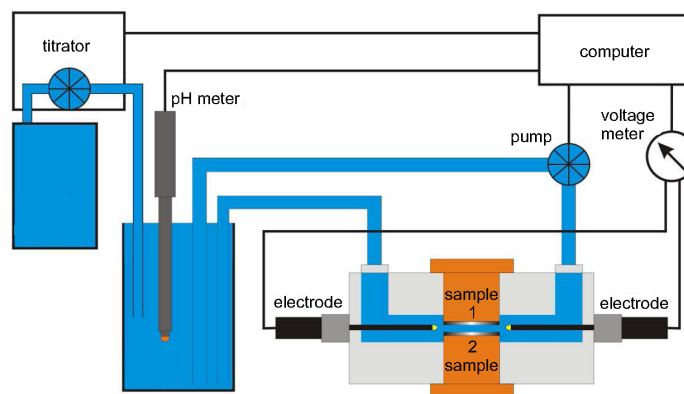


Figure 4.1.: Scheme of a setup (ElectroKinetic Analyzer) for the streaming potential determination in a microslit between two sample surfaces [150].

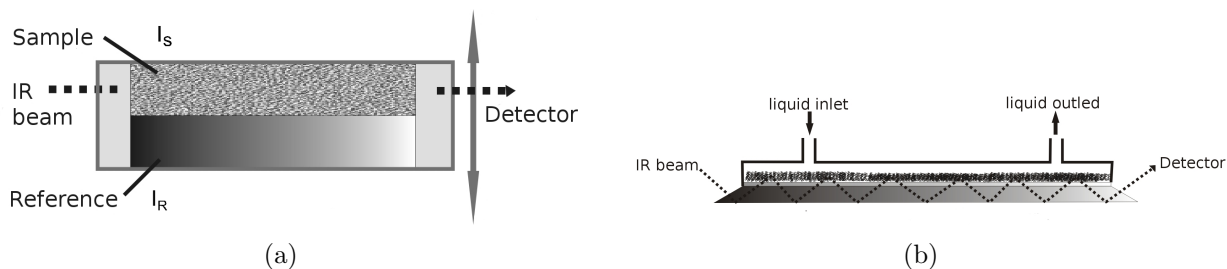


Figure 4.2.: Single-beam-sample-reference concept (a) and scheme of the in-situ cell (b) for ATR-FTIR measurements [152].

A commercial ATR-FTIR attachment in the single-beam-sample-reference (SBSR) mode (OPTISPEC, Zürich, Switzerland) was used [153]. The ATR-FTIR attachment was installed on the IFS 55 Equinox FTIR spectrometer (BRUKER-Saxonia, Leipzig, Germany) equipped with globar source and MCT detector. Trapezoidal silicon internal reflection elements (IRE, $50 \times 20 \times 2 \text{ mm}^3$) from Komlas GmbH, Germany, allowing incident angles of $\theta = 45^\circ$ were used as substrates for the brush films. In-situ measurements were done in a homebuilt in-situ cell (M.Müller, IPF Dresden), which sealed the upper sample (S) half and the lower reference (R) half of the Si-IRE by oval O-rings forming S- and R-compartment, respectively, which both can be filled with various aqueous solutions (Figure 4.2).

The brush layer was located solely on the S half of the Si-IRE and the R half was uncoated. The SBSR concept implies, that single channel spectra $I_{S,R}(\nu)$ were recorded separately of the S and R half of the Si-IRE by guiding one IR beam alternately through these halves. Normalizing the single-channel spectra according to

$$A(\nu) = -\log \frac{I_S(\nu)}{I_R(\nu)} \quad (4.3)$$

resulted in an absorbance spectrum ($A(\nu)$) with proper compensation of the background absorptions due to the SiO_x layer, solvent, water vapor (spectrometer) and ice on the MCT detector window. The temperature of the in-situ cell was controlled by a homebuilt heating jacket, whose temperature could be adjusted via a thermostat water bath. Each measurement was made after an equilibration time of 30 minutes.

4.2. Ellipsometry

Ellipsometry is known as an optical method used in the observation of thin film layer parameters like optical constants (refractive index n , extinction coefficient k) or layer thickness d . Changes in the polarization state of light upon reflection or transmission at a sample are expressed by the ellipsometric angles Δ and Ψ and the experimentally recorded values are compared to theoretical angles calculated from a layer model.

Most often for the monitoring of organic films ellipsometers are operated in the visible range

of light or as single-wavelength ellipsometers but also measurements in the IR range have considerably increased recently [37, 154, 155]. For example spectroscopic VIS ellipsometry was successfully applied to study the structural variation of protein monolayers upon adsorption at hydrophobic surfaces [120].

Within this work solely VIS ellipsometric measurements were performed and basic principles, selected device setups as well as the employment of ellipsometry for the study of thin organic films will be discussed in the following sections.

4.2.1. Theory of ellipsometry

To characterize the reflection of polarized light at a specular surface the electric field is described on the basis of two eigenmodes, the components parallel (E_p) and perpendicular (E_s) to the plane of incidence (Figure 4.3).

Here the state of polarization is described by the amplitude ratio $\frac{E_p}{E_s}$ and the phase difference $\delta_p - \delta_s$, whereas a linear, circular or elliptical polarization is possible for the conditions listed in Table 4.2

Table 4.2.: States of polarizations for the electric field vector E .

Polarization	Amplitudes	Phases
linear	$E_p = E_s$	$\delta_p = \delta_s = 0/180$
circular	$E_p = E_s$	$\delta_p - \delta_s = 90$
elliptical	$E_p \neq E_s$	$\delta_p \neq \delta_s$

Changes in the polarization upon reflection at a specular surface are now described with the change in the relative amplitude ratio $\tan\Psi$ and the relative phase shift Δ according to:

$$\tan\Psi = \frac{E_p^r/E_s^r}{E_p^i/E_s^i} \quad (4.4)$$

$$\Delta = (\delta_p^r - \delta_s^r) - (\delta_p^i - \delta_s^i) \quad (4.5)$$

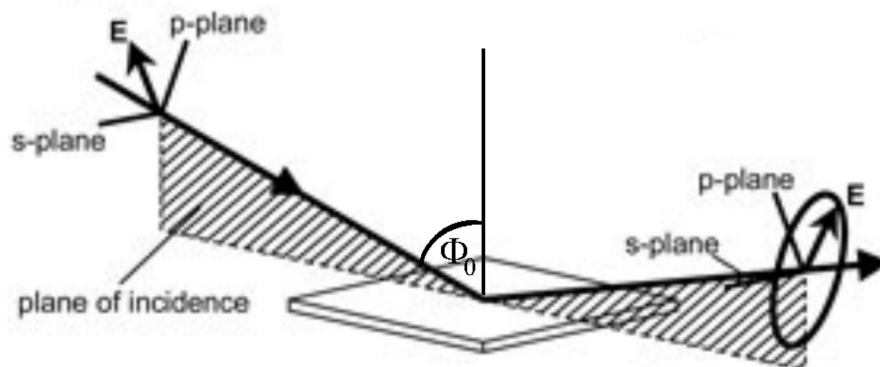


Figure 4.3.: Scheme of the reflection of the electric field vector at a specular surface [156].

Here the indices r and i indicate the reflected and the incident electric field vector respectively. The reflectivity properties of a surface are described by the complex reflection coefficients R_s and R_p :

$$R_p = \frac{E_p^r}{E_p^i} e^{i(\delta_p^r - \delta_p^i)} \quad (4.6)$$

$$R_s = \frac{E_s^r}{E_s^i} e^{i(\delta_s^r - \delta_s^i)} \quad (4.7)$$

leading to the basic equation of ellipsometry:

$$\frac{R_p}{R_s} = \tan\Psi e^{i\Delta} \quad (4.8)$$

R_p and R_s can be derived from the individual reflectances given by the Fresnel coefficients $r_{jm}^{p,s}$ on a phase boundary between two media that are described by the Fresnel equations. r_{jm} depends on the refractive indices N_j, N_m of the media at the phase boundary as well as the angles of propagation Φ_j, Φ_m in the media, whereas for the latter the law of refraction is valid (Figure 4.4).

$$r_{jm} = F(N_j, N_m, \Phi_j, \Phi_m) \quad (4.9)$$

In general the refractive index $n = \sqrt{\epsilon}$ for a material is complex and dependent on the wavelength λ following

$$N(\lambda) = n(\lambda) + ik(\lambda) . \quad (4.10)$$

Here n is the real part of the refractive index, the extinction coefficient k the imaginary part and i the imaginary unit.

For a layer system of two phase boundaries as displayed in Figure 4.4, R_p and R_s can be calculated to:

$$R_p = \frac{r_{01}^p + r_{1s}^p e^{-2\alpha i}}{1 + r_{01}^p r_{1s}^p e^{-2\alpha i}} \quad (4.11)$$

$$R_s = \frac{r_{01}^s + r_{1s}^s e^{-2\alpha i}}{1 + r_{01}^s r_{1s}^s e^{-2\alpha i}} \quad (4.12)$$

$$\alpha = 2\pi \frac{d}{\lambda} N_1 \cos\Phi_1 \quad (4.13)$$

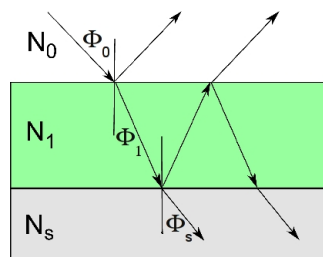


Figure 4.4.: Reflexion in the case of one layer at the substrate surface [157].

whereas d is the thickness of the layer, and r_{01} and r_{1s} are the Fresnel coefficients at the air-layer and the layer-substrate interface respectively. Thus it is comprehensible that the ratio of the reflection coefficients is also a complex function of the wavelength λ , the layer thicknesses d_j of a layer stack and its refractive indices N_j as well as the refractive index N_s of the substrate and the angle of incidence Φ_0 .

$$\frac{R_p}{R_s} = F(\Phi_0, \lambda, N_s, N_j, d_j) \quad (4.14)$$

The basic equation of ellipsometry is valid for homogeneous isotropic systems and the optical constants are evaluated in fitting a model system to the measured ellipsometric data Δ and $\tan \Psi$ by mean-square minimization.

4.2.2. Ellipsometric setups

Basic components of an ellipsometer are light source, polarizer (P), analyzer (A) and detector (D), whereas optional also a compensator (C) can be included into the system. Here different settings were developed either with rotating analyzer, polarizer or compensator, but also settings with phase modulator instead of the compensator (Figure 4.5) [158]. For these setups errors of the rotating elements are the primary source of inaccuracy, because non-idealities in these elements like multiple reflections or a temperature dependent retardance can occur. Thus the accuracy in the ellipsometric angles (Ψ, Δ) is limited to $0.05^\circ - 0.5^\circ$ [159].

A special ellipsometer setup is used in **null-ellipsometry**. Here both analyzer and polarizer are rotating elements and often a compensator is also included but fixed at $\pm 45^\circ$. With this setup the angles of polarizer and analyzer are adjusted to achieve minimum intensity at the detector. Thus the change in polarization introduced by the sample surface is compensated by the combined polarizer - compensator setting leading to linear polarized light upon reflection at the sample surface. With this signal compensation method a very high accuracy within the range of 0.01° to 0.05° for (Ψ, Δ) can be achieved since possible instrumental errors are eliminated due to relative measurements [159]. However since the null-setting of the rotating elements depends on the wavelength, and the iterative adjustment of them is a relatively slow process, single-wavelength ellipsometers are most common when using this setup.

4.2.3. Ellipsometry on thin organic films

Single wavelength ellipsometry was regularly used to study the formation of protein layers on solid surfaces, focusing on the adsorbed amount of protein, but also the increase of refractive index for the single wavelength and the increase thickness in the build up of protein layers was studied [127, 161, 162]. Structural parameters like the fraction of surface coverage of the

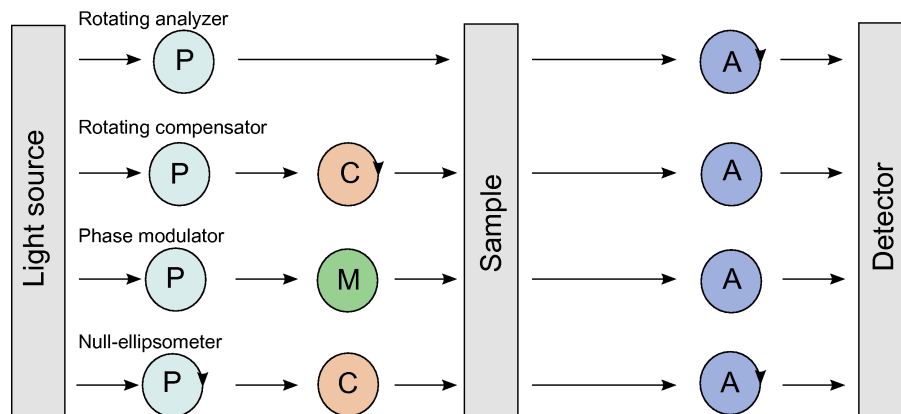


Figure 4.5.: General ellipsometric setups [160].

biomolecule could be derived [161], and the adsorption in monolayers or multilayers could be concluded [127].

Beyond single wavelength measurements spectroscopic ellipsometry (SE) offers the opportunity to derive the dielectric function (the complex refractive index $n(\lambda)$) of thin organic layers over a given wavelength range and to use $n(\lambda)$ for a straight forward determination of its surface concentration in multicomponent surface layers by an effective medium approach. Furthermore microstructural modeling, surface dynamics, molecular orientation, clustering, multilayering and layer density effects can be best addressed by spectroscopic ellipsometry due to an enhanced set of experimental data [163]. Here studies of self assembled monolayers with infrared SE are a prominent example for the determination of molecular orientations due to an analysis of the optical anisotropy of these films [164, 165].

Within this thesis spectroscopic VIS ellipsometry was applied for the measurements of polymer brush films in dry state and in-situ, and to study protein adsorption onto these highly swellable brush films.

Ellipsometric setups with rotating compensator (M2000, J. A. Woollam Co., Inc., Lincoln, NE, USA) and with rotating analyzer plus additional retarder (M44, J. A. Woollam Co.) were used. For the swelling and adsorption measurements the polymer brush samples were fixed in a batch cuvette (TSL Spectrosil, Hellma, Muellheim, Germany) that was closed with a Teflon covering. Dry film measurements were performed at angles of incidence Φ_0 of 65 °, 70 ° and 75 ° in the wavelength range of 371 - 1679 nm, whereas for in-situ ellipsometry Φ_0 was fixed at 68 ° to achieve irradiation of the sample perpendicular to the cuvette sides. The wavelength range for in-situ measurements was reduced to 371 - 800 nm to avoid errors due to absorption in the aqueous buffer solution.

A single wavelength null-ellipsometer was applied solely for protein adsorption studies on PNIPAAm homopolymer brushes, whereas the refractive index $n(\lambda)$ of dry and swollen PNIPAAm brushes was predefined by spectroscopic ellipsometry before. Since the null-ellipsometer provides its pair of ellipsometric angles (Δ and Ψ) with increased accuracy compared to the

rotating analyzer and the rotating compensator setup, we thought it best suitable to study these brush surfaces with very low adsorbed amounts of protein. The same in-situ setup was used as described previously.

4.3. Dynamic contact angle

By studying contact angles of liquids at solid surfaces the phenomenon of wetting can be qualitatively understood [90, 166]. Here the contact line of the liquid drop is formed due to balancing three different forces, that are the interface tensions between liquid and solid (γ_{sl}), between liquid and vapor (γ_{lv}) and between vapor and solid (γ_{sv}) (Figure 4.6).

In the case of smooth, rigid, insoluble and chemically homogeneous surfaces the liquid contact angle is determined as the angle between the solid surface and the tangent plane to the liquid surface, whereas the balance between all interface tensions in the solid surface plane is described by the Young equation (Equation 4.15).

$$\gamma_{sv} = \gamma_{lv} \cos \theta + \gamma_{sl} \quad (4.15)$$

In a non equilibrium drop state, a larger γ_{sv} than the sum of γ_{sl} and the projected part of γ_{lv} leads to a spreading of the drop, whereas when γ_{sv} is smaller the drop would contract. Since γ_{sl} and γ_{sv} are constant at constant experimental conditions (temperature, humidity) for a specific pair of solid and liquid, the force balance is characteristically described by $\cos \theta$ and thus the contact angle θ . However several assumptions are necessary to evaluate interface tensions from contact angle measurements. Firstly, the drop should be rotationally symmetric, which means that the balance between all interface tensions around the contact line is similar. Secondly the equilibrium should instantly form after contact of solid and liquid neglecting inertial effects or the viscosity of the liquid.

According to the equilibrium described by Equation 4.15 three types of wetting regimes can be distinguished. If the contact angle is finite ($\theta > 0$) partial wetting occurs and the corresponding energetic state is characterized by hydrophobicity of the surface. For θ even larger

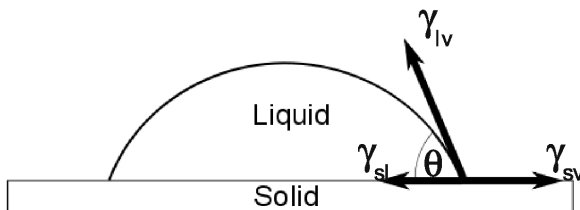


Figure 4.6.: Balance of interface tensions between solid, liquid and vapor determining the liquid contact angle [167].

than 90 ° the surface is defined as non-wetting because the liquid runs easily off the surface and by additionally increasing the surface roughness, e.g. due to structuring, the effect of ultra-hydrophobicity can be introduced [168]. In the opposite case of complete wetting of the surface θ is zero and the surface is defined as hydrophilic.

Furthermore for chemically heterogeneous surfaces, e.g. mixed polymer brushes [], the fraction of each polymer on top of the brushes can be estimated by using the Cassie equation [169]:

$$\cos\theta = f_1\cos\theta_1 + f_2\cos\theta_2 \quad (4.16)$$

where θ_1 and θ_2 are the Young contact angles for the homopolymer brushes and $f_{1,2}$ the fractions for polymer 1 and 2 at the surface [98, 169].

Contact angle measurements within this thesis were carried out as dynamic sessile drop experiments employing an OCA20 (DataPhysics Instruments GmbH, Filderstadt, Germany) at controlled room temperature ($T=23\text{ °C}$) and relative humidity ($\phi_{rel} = 50\%$). Advancing contact angles were evaluated from dynamic dispensing / redispensing measurements with a volume of the sessile drop of 5 μl to 10 μl at a suspension rate of 0.2 $\frac{\mu\text{l}}{\text{s}}$ using the goniometer technique by aligning a tangent at the point of contact between solid surface and sessile drop profile. Low suspension rates were chosen to assure the mechanical equilibrium of all interface tensions between single measurement steps. Receding contact angles could not be measured due to a pinning of the contact line.

For temperature sensitive measurements, a calibrated temperature stage from DataPhysics Instruments GmbH was attached to the contact angle device and the temperature of the dry brushes adjusted to a set-point temperature, whereas the real sample temperature was monitored. Dynamic contact angle measurements were then performed with de-ionized water droplets at room temperature of 23 °C.

In general, polymer brushes, that are swellable in aqueous solution, present non-ideal surfaces for a determination of water contact angles with the goniometer technique. Chemical heterogeneity, swelling in the measurements process, and a possible reorientation of molecular groups at the interface can alter the thermodynamic equilibrium, thus the Young equation can be inapplicable to derive interface tensions [166]. Here the captive bubble method in combination with the Axisymmetric Drop Shape Analysis - Profile (ADSA-P) can be better suited to determine contact angles and interface tensions [166, 170]. With this method contact angles are measured between a captive gas bubble and a swollen surface in a liquid chamber and the shape of the experimental drop is fitted to a theoretical drop profile derived from the Laplace equation of capillarity.

We are aware of the limits of applying the goniometer technique to derive advancing contact angles on swellable polymer brushes. However we obtained all contact angles presented in this thesis reproducibly in the given error limits, and base the presentation of these results on existing literature, where this method for the determination of contact angles, e.g. on PNIPAAm or polyelectrolyte brushes, was applied [33, 35, 84].

4.4. Quartz crystal microbalance with dissipation mode (QCM-D)

In a quartz crystal microbalance, based on the piezo-electric effect, a mechanical oscillation is induced by an applied alternating current [171, 172], and frequency changes Δf are measured upon adsorption of thin films on the crystal. For the dependency of the frequency on an oscillating rigid surface layer with the mass Δm the following equation derived by Sauerbrey is valid [173]:

$$\Delta f = -\frac{2f_0^2}{A\sqrt{\mu_q\rho_q}}\Delta m \quad (4.17)$$

Parameters within this equation are f_0 the resonance frequency of the quartz crystal, A the piezoelectric area, μ_q the shear modulus and ρ_q the density of the crystal. Here the mass has to be coupled under no-slip conditions to the crystal so that the dissipation change $\Delta D = 0$. In the case of measurements in fluids these conditions are no longer valid and dissipation changes have to be taken into account due to the strong damping of the sensor shear wave.

Novel settings also allow the monitoring of these dissipation changes [174], whereas the dissipation of the oscillating mass is inversely proportional to the time constant τ of the damped oscillation:

$$D = \frac{1}{2\pi f\tau} = \frac{E_{dissipated}}{2\pi E_{stored}}. \quad (4.18)$$

Here $E_{dissipated}$ is the energy dissipated in one period of oscillation and E_{stored} the energy stored in the oscillating system. In an experiment the time constant τ of the damped oscillation is measured in periodically disconnecting the crystal from the driving circuit and fitting the decay of the oscillation to an exponentially damped sinusoidal function [175]:

$$A(t) = A_0 e^{-t/\tau} \sin(2\pi ft + \phi) \quad (4.19)$$

A modeling of the dependency of Δf and ΔD on the layer parameters ρ_f , μ_f , η_f and d_f of the film, as they are defined in Table 4.3, was developed mainly by Kanazawa [176] and Voinova [177, 178]. They first introduced the bounding conditions of a Newtonian fluid in describing the frequency change of the crystal with one side immersed in the liquid [176] and secondly the viscoelasticity of adsorbed molecules on the crystal is taken into account in the Voigt-Voinova model [177, 178]. The latter model is based on the Voigt-Kelvin model for

viscoelastic solids [179], whereas the additional pre-assumptions of a uniform film thickness and density have to be valid.

The following model equations are thus used to fit the layer parameters to Δf and ΔD numerically [180]:

$$\Delta f = \frac{Im(\beta)}{2\pi d_q \rho_q} \quad (4.20)$$

$$\Delta D = \frac{-Re(\beta)}{\pi f d_q \rho_q} \quad (4.21)$$

$$\beta = \xi_1 \frac{2\pi f \eta_f - i\mu_f}{2\pi f} \cdot \frac{1 - \alpha e^{2\xi_1 d_f}}{1 + \alpha e^{2\xi_1 d_f}} \quad (4.22)$$

$$\alpha = \frac{\frac{\xi_1}{\xi_2} \cdot \frac{2\pi f \eta_f - i\mu_f}{2\pi f \eta_l} + 1}{\frac{\xi_1}{\xi_2} \cdot \frac{2\pi f \eta_f - i\mu_f}{2\pi f \eta_l} - 1} \quad (4.23)$$

$$\xi_1 = \sqrt{-\frac{(2\pi f)^2 \rho_f}{\mu_f + i2\pi \eta_f}} \quad (4.24)$$

$$\xi_2 = \sqrt{i \frac{2\pi f \rho_l}{\eta_l}} \quad (4.25)$$

Here the allocation of the parameters of layer, liquid and crystal are summarized in Table 4.3.

In this work QCM-D was utilized in a coupled setup with spectroscopic ellipsometry, as displayed in Figure 4.7, in the ellipsometry workgroup of the University Nebraska-Lincoln. An ellipsometric compatible module from Q-Sense was used (QELM 401, Q-Sense, Frölunda, Sweden) and installed on a M2000 (J. A. Woollam Co., Inc., Lincoln, NE, USA). A 0.3 mm thick AT-quartz crystal coated with a 100 nm thick gold layer (QSX 301, Q-Sense) was taken for the measurements. Its resonance frequency is at 4.95 ± 0.05 MHz.

The ellipsometry module consists of Teflon and Titanium and has an angle of incidence of 65° . The liquid volume above the crystal surface is $100 \mu\text{l}$, whereas flow or stagnant liquid measurements are possible. Measurements were either done in flow with a constant flow rate of $0.4 \frac{\text{ml}}{\text{min}}$ or with stagnant solutions. For the exchange of liquids a syringe pump was applied, and a gradient increase of the flow rate was performed when exchanging the solutions.

Table 4.3.: Layer, liquid and crystal parameters (j=q,l,f) important for the evaluation of QCM-D measurements.

Symbol	Description
ρ_j	Density of crystal (q), liquid (l) and film (f)
d_j	Thickness of crystal (q), liquid (l) and film (f)
η_j	Viscosity of liquid (l) and film (f)
μ_j	Shear modulus of liquid (l) and film (f)

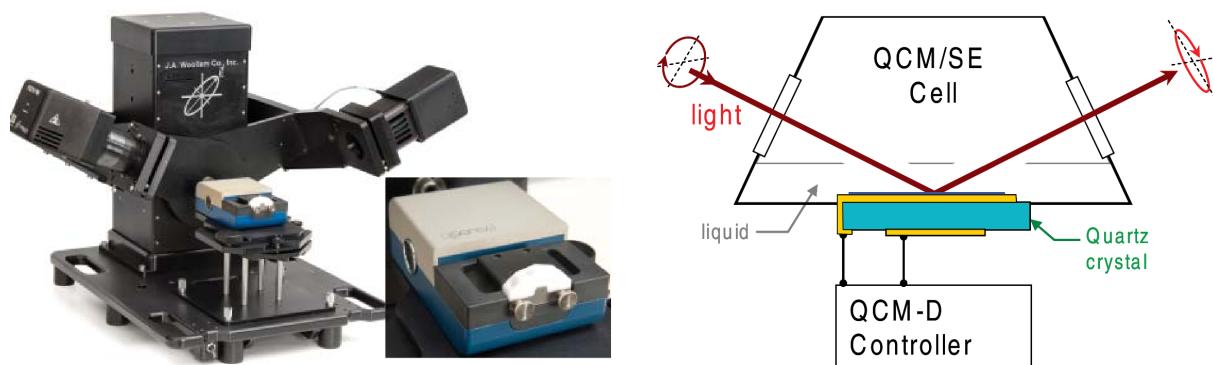


Figure 4.7.: Image and scheme of the combined spectroscopic ellipsometry (SE) - quartz crystal microbalance with dissipation mode (QCM-D) setup [181].

Part II.

Experimental

5. Materials, brush preparation and properties of dry brushes

5.1. Polymers

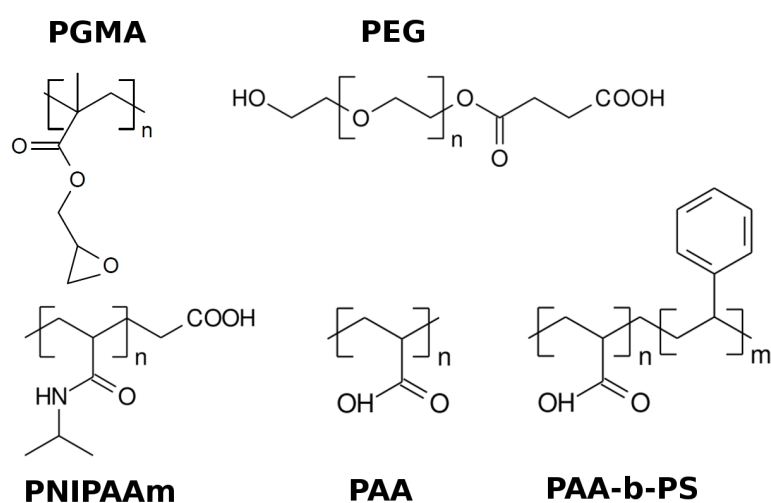


Figure 5.1.: Structural formulas of the polymers used in this thesis.

Polymers used in this thesis for the brush preparation are listed in Table 5.1 and their structure is displayed in Figure 5.1. All polymers, except poly(ethylene glycol) (PEG), were purchased from Polymer Source, Inc. (Montreal, Canada) and used as received. Characteristic data like molecular weight and polydispersity index (PDI) was supplied by the company. Poly(ethylene glycol) (PEG) was kindly provided by B. Zdyrko (Clemson University).

For the calculation of the number of monomers N per chain M_n was divided by the molecular weight of one monomer. The length of a fully stretched chain was calculated according to:

$$d_c = N \cdot \sqrt{i \cdot a^2 (1 - \cos \gamma)} \quad (5.1)$$

with $a = 0.154 \text{ nm}$ the C-C binding length, $\gamma = 109.45^\circ$ the angle of a C-C bond, and i the number of C-C bonds per monomer. The glass transition temperature was determined with differential scanning calorimetry (DSC).

Table 5.1.: Characteristical parameters of polymers used in the brush preparation, including molecular weight M_n , $PDI = \frac{M_w}{M_n}$, number of monomers N , length d_c of a fully stretched chain and glass transition temperature T_g .

Polymer		$M_N[\frac{g}{mol}]$	$\frac{M_w}{M_n}$	N	$d_c[nm]$	$T_g[^\circ C]$
Poly (glycidyl methacrylate)	PGMA	17,500	1.7	—	—	59
Poly (acrylic acid)	PAA	26,500	1.12	368	93	105
Poly (acrylic acid) -b- Poly (styrene)	PAA- b-PS	27,000 1,000	1.26	375 10	94 2	
Poly (N-isopropyl acrylamide)	PNIPAAm					
	PN28k	28,500	1.46	252	63	138
	PN45k	45,000	1.72	398	100	138
	PN47k	47,600	1.22	421	106	
	PN132k	132,000	1.29	1168	294	140
Poly(ethylene glycol)	PEG	5,000	1.5	114	35	-60 [182]

5.2. Model proteins

The globular model proteins α -chymotrypsin and human serum albumin (HSA) as well as the glyco-protein glucose oxidase (GOD) have been chosen for adsorption studies (Table 5.2). Here α -chymotrypsin and glucose oxidase are enzymes, a special class of functional proteins, and the activity of glucose oxidase at different brush surfaces was investigated.

α -chymotrypsin is a digestive enzyme and belongs to the class of serine proteases. It hydrolyzes peptide bonds on the carboxyl end of the bond. The isoelectric point of this functional protein is in the neutral to basic pH regime at pH 8.1 and thus it was chosen here for adsorption

Table 5.2.: Characteristical parameters of model proteins [18, 183–187].

protein	molecular weight [Da]	size [nm ³]	IEP [pH units]	structural details
α -Chymotrypsin	25,200	5.1 x 4 x 4	8.1	11% α -helix 51% β -sheet
HSA (defatted)	66,430	3 x 8 x 8	5.7	55% α -helix 45% random coil
glucose oxidase	160,000	5.5 x 7 x 8	4.2	glyco-protein with 16% carbohydrates

studies of a protein with an IEP at high pH. According to its structure α -chymotrypsin belongs to the globular proteins and has a high β sheet fraction. Here α -chymotrypsin from the bovine pancreas (C4129, Sigma-Aldrich, Inc., St. Louis, MO, USA) Type II in the form of lyophilized powder was used.

HSA is also a globular protein and constitutes about 55% of the human blood plasma. These protein molecules stabilize the colloid osmotic pressure in the blood and serve as carriers of less water-soluble molecules like for example fatty acids. It consists of a single stranded polypeptide and its ternary structure, consisting of two strands is stabilized by 17 disulfide bonds [185]. The protein shape varies with the pH value and it is considered to be a prolate ellipsoid (14.1 x 4.1 nm, N-form) at pH 7, whereas at acidic pH two different forms around pH 4, the F form, and below pH 3, the E form, a molten globule like state, are known [188]. In the transition from N to F the net loss of structure (α -helix) amounts to 8 %, whereas in the transition to the E form only 1 % more of α -helices is destructured. At high pH between pH 7 and pH 9 an expansion of the protein takes place with a loss of 2.5 % of helix structures [189]. The isoelectric point for lipid-bound HSA is at pH 4.7 but increases to pH 5.7 when defatting the protein [190].

Glucose oxidase is an enzyme oxidizing the C1 carbon of glucose, and is present in fungi, e.g. *Aspergillus niger*. The enzyme contains two flavin adenine dinucleotide (FAD) molecules, that function as redox cofactors in the catalytic reaction. Different from HSA and α -chymotrypsin this enzyme contains 16 % carbohydrates and is a glyco-protein. The enzyme reaction will be discussed in more detail in Section 11.1.

5.3. Buffer solutions

Phosphate buffered saline (PBS buffer) was purchased from Sigma-Aldrich, Inc. (St. Louis, MO, USA). This buffer contains 12 mM of the buffer salts disodium hydrogen phosphate and monopotassium phosphate as well as 137 mM sodium chloride and 2.7 mM potassium chloride and has a pH of 7.4. Due to the additional salt content it has the same osmotic pressure, present in human blood and was used here for investigations at isotonic conditions.

For the preparation of buffer solutions with varying pH and cation content, sodium phosphate monobasic dihydrate, sodium phosphate dibasic dihydrate, acetic acid and sodium acetate trihydrate were purchased from Sigma-Aldrich as well. The adjustment of the salt concentration in solution was done with sodium chloride. To secure the pH stability in the pH- and salt dependent swelling experiments the measurements were performed in buffer solutions with a concentration of $c_{Na^+} = 0.01 M$, if the desired ionic strength of the solution was not below 0.01 M, using sodium acetate buffer in the range of pH 4 to pH 5.8 and sodium phosphate buffer between pH 5.9 and 8. For lower ionic strength the pH of the measurement solution was

controlled before and after the experiment and higher ionic strength was adjusted with sodium chloride. Measurements at pH 3 were done solely in sodium chloride solution.

For all buffer solutions the refractive index $n(\lambda)$ was measured with a digital multiple wavelength refractometer DSR-lambda (Schmidt+Haensch GmbH u. Co.) at eight different wavelengths from 435.8 nm to 706.5 nm and in case of PBS buffer also for five different temperatures between 20 °C and 40 °C. Thus dispersion relations for all buffer solutions could be used in the modeling of spectroscopic ellipsometry data. Characteristical dispersion relations of the refractive index $n(\lambda)$ are displayed in the appendix in Figure A.1.

5.4. "Grafting-to" of polymer brushes

(100)-Silicon wafers with a native silicon oxide layer of about 2 nm have been pre-cleaned for 15 minutes in absolute ethanol in an ultrasonic bath to remove fatty acid residues. Afterwards they have been stirred in a solution of ammonium hydroxide, hydrogen peroxide and deionized water in the mixture of 1 : 1 : 5 for 20 minutes at 70 °C. In the last step silica particles at the surface should be removed as well as the silicon oxide layer rebuilt in a smoother way introducing a high amount of OH-groups which leads to a high surface potential and a very hydrophilic interface with an SiO_2 layer thickness of 1.4 ± 0.1 nm.

Onto these cleaned silicon oxide surfaces a PGMA solution of 0.02 wt% in chloroform was spin coated (Spin 150, SPS Coating, The Netherlands) for 10 seconds with a speed of $v = 2000 \frac{u}{min}$ and an acceleration of $a = 1000 \frac{u}{min \cdot s}$. This layer was heated under vacuum at 100 °C for 20 minutes to form ether bonds using epoxy groups of the PGMA and OH-groups of the silicon oxide leading to a thin covalently bound polymer monolayer of 2.3 ± 0.2 nm thickness equipped with remaining epoxy groups for the following grafting-to process [69].

For **PNIPAAm brushes** 1 wt% solution of PNIPAAm-COOH in THF was spin-coated onto the anchoring layer and annealed in a vacuum oven at 150 °C for several time intervals ranging from 5 min to 10 h to obtain grafted brush layers with different grafting densities attached to the PGMA via ester bondings. Non-covalently bonded polymer was removed by Soxhlet extraction for 2.5 h in THF.

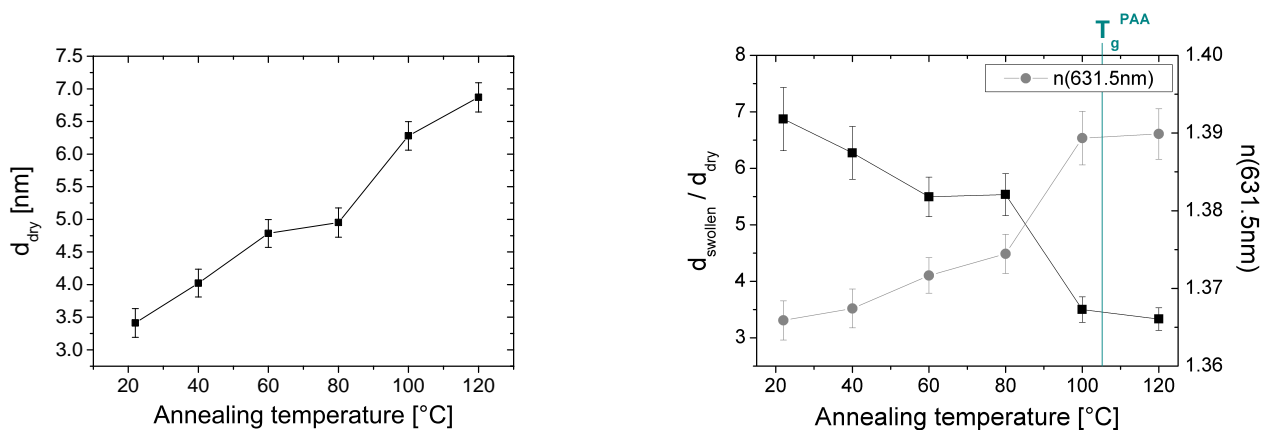
For **PAA Guiselin brushes** 1 wt% solution of PAA in ethanol was spin-coated onto the PGMA layer and annealed at 80 °C in a vacuum oven for 30 min. Ungrafted PAA was removed by extraction in 96 % ethanol. The annealing conditions for these brushes with multiple grafting points were optimized to achieve covalently grafted but still highly swellable polymer layers. According to Figure 5.2 the temperature was chosen at 80 °C, well below the glass transition temperature of 105 °C of this polymer. It could be shown that for annealing temperatures near and above the bulk T_g the swelling degree of the PAA films strongly decreased (Figure 5.2(b)). Since the mobility of the PAA chains increases strongly in the region of the glass transition temperature, more COOH-groups react with the epoxy groups of the PGMA layer

and a higher amount of grafting points is formed, pinning the PAA chains to the surface. Thus the swelling degree in aqueous solution is reduced for PAA Guiselin brushes prepared at elevated temperatures.

The preparation of **PAA-b-PS Guiselin brushes** follows the same steps as described for PAA Guiselin brushes but with Methanol as the solvent for the polymer.

For **PEG brushes** the end-functionalized polymer was grafted from the melt by depositing PEG powder on the surface of a clean glass slide and covering the melting powder with the PGMA coated silicon wafer [191]. Samples were annealed in air at 110 °C for 5 h.

For **PNIPAAm-PAA mixed brushes** first the PNIPAAm brush was formed as discussed above and after extraction of the non-grafted PNIPAAm, PAA was spin-coated, annealed and extracted as described for PAA Guiselin brushes. PNIPAAm-PAA-b-PS, PEG-PAA and PEG-PAA-b-PS mixed brushes were prepared in the same manner.



(a) Dry layer thickness of PAA Guiselin brushes measured with a fixed refractive index at $n = 1.522$.

(b) Degree of swelling and refractive indices of PAA Guiselin brushes upon swelling in 10 mM sodium phosphate buffer solution at pH 7.66.

Figure 5.2.: Layer parameters of PAA Guiselin brushes in the dry state (a) and upon swelling at pH 7.66 (b) after annealing at different temperatures.

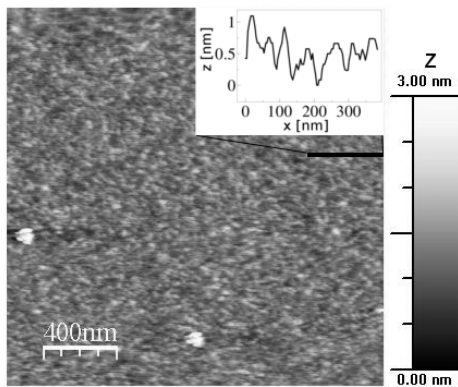
5.5. Surface homogeneity and roughness after preparation

To control surface homogeneity and roughness of the prepared polymer brush films, AFM and dynamic contact angle measurements were performed step by step. AFM images are displayed for the PGMA layer and selected brush layers in Figure 5.3 and contact angle results after preparation and extraction as well as roughnesses σ_{rms} are listed in Table 5.3.

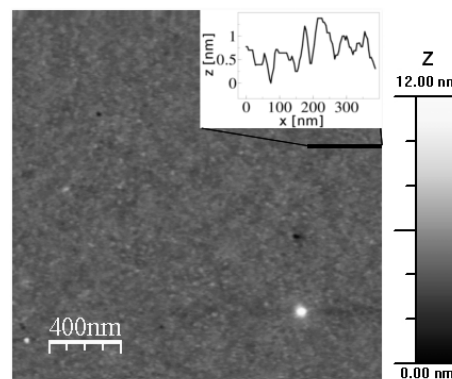
Roughness values for all brushes, except PEG brushes, are below 1 nm and no surface inhomogeneities in the brush layers were observed when the PGMA anchoring layer was homogeneous. PGMA is subject to dewetting on silica surfaces at a relative humidity higher than 10 % and has to be controlled continuously in the preparation process [192].

Table 5.3.: Typical surface roughness values for selected dry brushes after preparation and extraction in the respective solvent and advancing contact angles after immersion in pH 3 solution with 0.1 mM salt concentration. Uncertainties are 0.05 nm for σ_{rms} and 2° for θ_{adv} .

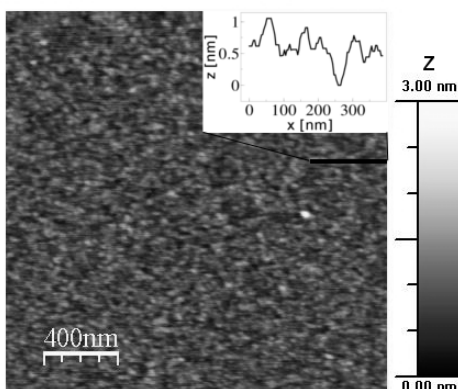
Brush type	Polymers	% polymer 2	σ_{rms} [nm]	θ_{adv} [$^\circ$]
mono	PGMA		0.3	60
mono	PAA		0.4	40
mono	PAA-b-PS		0.8	52
mono	PNIPAAm		0.3	73.5
mono	PEG		1.1	
mix	PN47k-PAA	49	0.6	64
mix	PN47k-PAA-b-PS	32	0.8	
mix	PN47k-PAA-b-PS	49		54.5



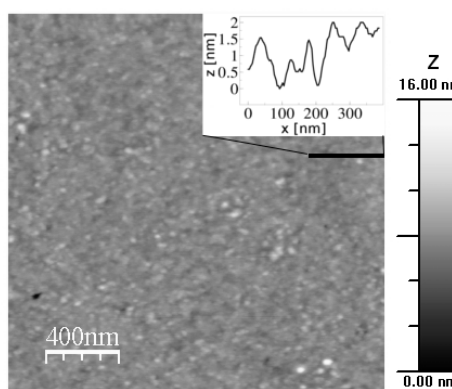
(a) PGMA



(b) PAA Guiselin brush



(c) PNIPAAm brush



(d) (PN47k-PAA mixed brush with 49 % PAA content)

Figure 5.3.: AFM images taken directly after preparation and extraction in the corresponding solvents. Displayed are measurements after applying the simple flattening procedure, subtracting an offset line by line [148]. Additionally the cross-section profile is displayed as an inset in each image for a path of 400 nm marked in black.

Regarding the advancing contact angle, θ_{adv} for PAA Guiselin brushes is 30 ° lower than for PNIPAAm brushes thus indicating a noticeable contrast between these two polymers. For the PAA-b-PS Guiselin brush θ_{adv} is considerably higher than for PAA but still distinguishable from the value for the PNIPAAm brush. The advancing contact angle for the mixed brushes is also considerably lower than for the PNIPAAm brush, thus the second polymer should be present at the surface after immersion of the sample in pH 3 solution at 0.1 mM. Here it is interesting that the smaller contact angle value is achieved for the mixed brush containing PS, which indicates differences in the formation of the binary and ternary mixed brushes. The calculation method for the mixed brush composition will be presented in detail in Section 6.2.

5.6. ζ -potentials

ζ -potentials were calculated from pH-sensitive streaming potential measurements (Figure 5.4). Here the ζ -potential is negative for all brushes in the investigated pH regime. Only the isoelectric point of the PNIPAAm brush could be measured ranging from pH 3.2 (PN28k as displayed in Figure 5.4(a)) to pH 3.8 for PN132k [193]. The trends are similar for all brushes containing PAA and the presence of negative surface charges can be concluded for all investigated samples in the pH-range between pH 4 and pH 8, which is the relevant range for the protein adsorption studies performed here. These charges are either due to the dissociation of COOH to COO^- groups at the PAA chains or due to preferential adsorption of negative ions (e.g. Cl^- , phosphate) on the surface [114].

It is interesting to note, that the ζ -potential for PAA-b-PS Guiselin brushes starts to deviate for $pH > 4$ from the ζ -potential for PAA Guiselin brushes towards higher values, indicating a lower negative charge density at the surface (Figure 5.4(a)). In agreement with these results in Chapter 8 pH-dependent advancing contact angles and HSA adsorption experiments are discussed, that point at an influence of the PS block on the dissociation behavior of PAA at higher pH values for the PAA-b-PS Guiselin brushes.

The pH dependent ζ -potentials for mixed brushes containing PN28k are situated between values for the corresponding homopolymer brushes (Figure 5.4(b)), with higher values between pH 3 and pH 5.1 for (45:55) PN28k-PAA brushes than for (20:80) PN28k-PAA-b-PS brushes due to the higher PAA content in the latter mixed brushes.

Varying the molecular weight of PNIPAAm and the brush composition does not lead to significant changes in the ζ -potential and thus other mixed brushes with their corresponding mono brushes are not presented here. We also refrain from a quantitative discussion since corrections due to the surface conductivity of PAA would be necessary, which are not possible with the EKA device [194]. Also in general the concept of a defined shear plane necessary for the calculation of a ζ -potential has to be regarded critically for highly swellable brush surfaces [195], and thus ζ -potentials for highly swellable PN47k brushes, as presented in Section 7.1.3 will not be discussed.

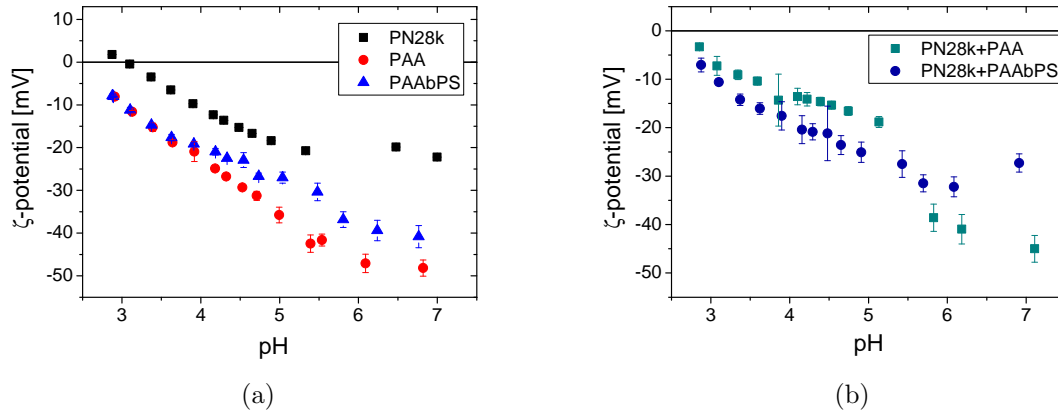


Figure 5.4.: Zeta-potential measurements for homopolymer (a) and mixed brushes (b). Differing from Table 5.3 PN28k and its mixed brushes are displayed [150].

5.7. Stability

The investigation of the stability of homopolymer and binary polymer brushes was considered important because on the one hand the grafting points of the brush polymers are ester bonds and thus can be hydrolyzed at high pH, on the other hand PAA and PNIPAAm chains can interact in the mixed brush, whereas an immobilization of PAA onto the PNIPAAm brush via e. g. hydrogen bonding has to be considered.

In Figure 5.5 the stability of refractive index and swollen layer thickness for three exemplary brushes upon swelling in a 10 mM buffer solution at pH 7 are displayed. At this pH COOH groups along the PAA chains are dissociated and a hydrogen bonding interaction between PNIPAAm and PAA should not be present. As can be seen no significant changes in n and d could be observed for the PNIPAAm brush, the PAA-b-PS Guiselin brush and a PN45k-PAA mixed brush over 12 hours. Stability was also observed when changing the molecular weight of PNIPAAm or the mixed brush composition as well as changing PAA to PAA-b-PS.

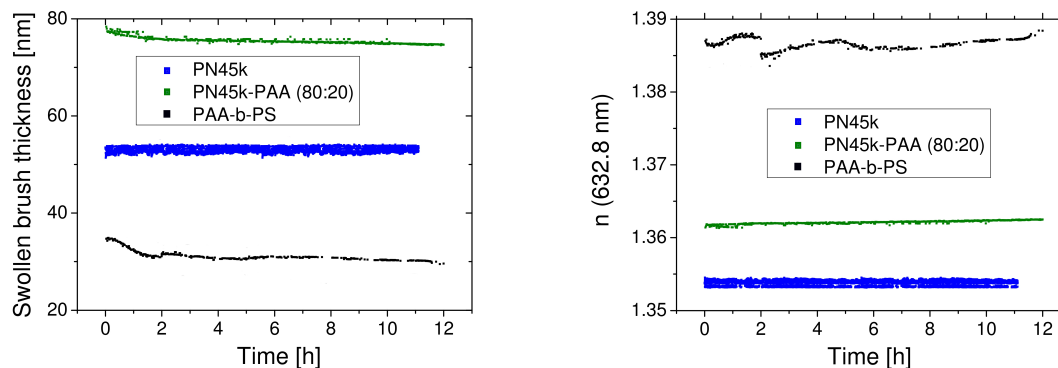


Figure 5.5.: Monitoring of the stability of swollen brush thickness (left) and refractive index n (632.8 nm) (right) swollen over 12 h in 10 mM buffer solution at pH 7 with null-ellipsometry.

6. Ellipsometric measurements and modeling

6.1. Course of in-situ measurements

Most of the in-situ ellipsometric experiments were done in a batch cell. After measurement of the sample in dry state at three different angles of incidence (see Section 4.2.2), the sample was put into the cell. The nominal angle of the cuvette side windows was adjusted to achieve perpendicular irradiation. Erroneous results due to window misalignment were eliminated in controlling the dry sample parameters again in the cell. Here another possibility to determine the window errors is the fitting of a Δ offset upon fixed sample parameters, but was not used here. For both options however the cell has to be thoroughly dry since the samples investigated are highly swellable and already very sensitive to increased humidity, thus the sample parameters change considerably upon changes in the humidity.

After the dry film measurement, the cell is filled with 3 ml buffer solution and the sample equilibrated for at least 10 min. Usually the swelling of these thin films, with a dry layer thickness between 5 - 20 nm was so fast, that the kinetics were not detectable.

After equilibration in the buffer, 0.5 ml of a concentrated protein solution is inserted into the cell to achieve an end-concentration of $0.25 \frac{mg}{ml}$ protein in the solution. Adsorption was allowed for at least 2 h and the increase of the combined layer thickness d_{comb} of polymer brush and protein and the combined refractive index n_{comb} at $\lambda = 631.5nm$ (one-layer model), or the formation of a separate protein layer with distinctive protein layer thickness at a fixed refractive index of $n = 1.375$ (two-layer model), was monitored. After a plateau value in the layer parameters was achieved the protein solution was exchanged to the buffer solution. This was performed in exchanging 2 ml of the solution four times, whereas the brush surface was kept in a rest of 1.5 ml solution at all times to prevent intermediate drying.

Desorption processes were monitored at least for 1 h. The modeling conditions and their range of application are described more closely in Section 6.3.

6.2. Modeling of dry polymer brushes

6.2.1. Optical box model

Thickness d and refractive index n of the investigated polymer brushes have to be modeled using the measured ellipsometric angles Δ and Ψ according to the fundamental equation of ellipsometry (Equation 4.8).

For the modeling a layer-by-layer built up of a box model with sharp interfaces between all layers has been considered appropriate (Figure 6.1(a)) [37, 120, 196].

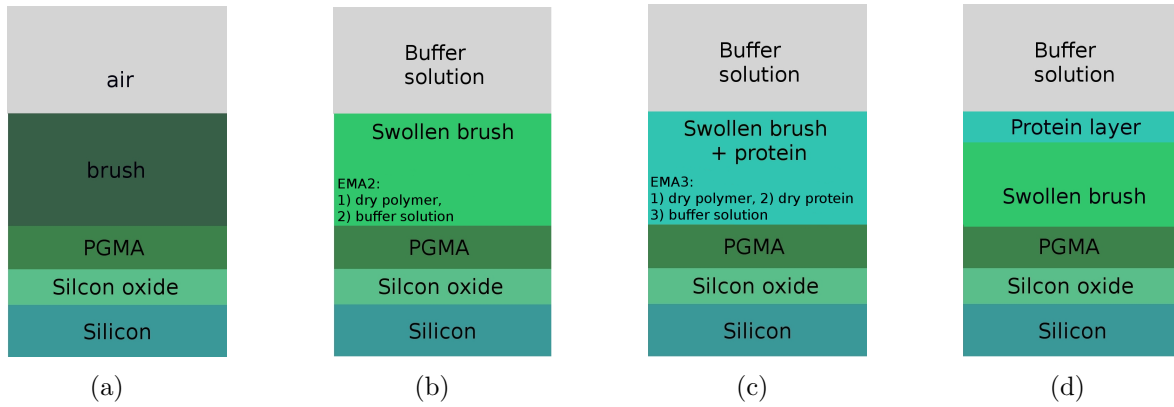


Figure 6.1.: Different box models for modeling of the dry polymer brush (a), the swollen polymer brush (b) and modeling of protein adsorption (c) and (d). The scheme is not in scale and thickness ratios between different layers are arbitrary. For the models (b) and (c) an effective medium approach according to Bruggeman (see Section 6.3.2) was used to model polymer and protein volume fractions.

For the silicon substrate and the SiO_2 layer tabulated refractive indices $n(\lambda)$ were used [120], whereas for the PGMA layer the refractive index was fixed to $n_{PGMA} = 1.525$, evaluated from ellipsometric data of a thick polymer layer. For layer thicknesses higher than ca. 10 nm it was possible to model the dependence of the refractive index of the dry polymer brush according to a Cauchy dispersion (Equation 6.1) with $k = 0$ for transparent layers.

$$n(\lambda) = A + \frac{B}{\lambda^2} \quad (6.1)$$

However for very thin brush layers a separation of thickness d and refractive index n is not possible and then refractive indices determined for thick layers of the corresponding polymers were used to evaluate the brush thickness. Typical refractive indices and thicknesses of dry polymer brush layers are listed in Table 6.1.

Here it is interesting, that for PN47k-PAA-b-PS mixed brushes the total layer thickness as well as the refractive index is higher than for PN47k-PAA brushes. We will discuss differences in these binary and ternary mixed brushes in more detail in Section 9.4.

The composition of mixed brushes was calculated from the ellipsometric thickness data according to Ionov et al. [198], by assuming a similar density of both polymers at the surface.

Table 6.1.: Typical parameters thickness d and refractive index n of dry polymer brushes. The grafting density σ of PNIPAAm brushes was calculated according to Equation 2.2 using the bulk density of PNIPAAm of $\rho = 1.07 \frac{g}{cm^3}$ [197]. For the mixed brushes the volume fraction of polymer 2 was calculated from the ellipsometric thickness data [198]. *Refractive index fixed. The error of n is less than 0.003.

Brush type	Polymers	d [nm]	n (631.5 nm)	σ [nm^{-2}]	% Polymer 2
mono	PAA	5.4 ± 0.2	*1.522	—	
mono	PAA-b-PS	5.7 ± 0.2	*1.522	—	
mono	PN28k	5.0 ± 0.4	*1.448	0.11	
mono	PN45k	7.3 ± 0.3	1.487	0.10	
mono	PN47k	15.1 ± 1	1.474	0.20	
mono	PN132k	12.0 ± 0.4	1.448	0.06	
mix	PN47k-PAA	11.2 ± 0.4	1.477		20
mix	PN47k-PAA	7.4 ± 0.3	*1.474		60
mix	PN47k-PAA-b-PS	14.5 ± 0.2	1.507		17
mix	PN47k-PAA-b-PS	11.3 ± 0.2	1.495		41

The mixed brush ratio can also be calculated directly from the amount Γ_{pol} of the individual polymers at the surface, whereas to derive Γ_{pol} from the ellipsometric thickness data, again the density of the polymers is needed. In the case of PNIPAAm ($\rho_{bulk} = 1.07 \frac{g}{cm^3}$ [197]) and PAA ($\rho_{bulk} = 1.4 \frac{g}{cm^3}$ [199]) in mixed brushes the bulk density of the polymers is considerably different. Thus we compared both calculation methods for the mixed brush composition and found a deviation of less than 5 %. Sydorenko et al. proved the validity of this calculation approach by comparison of the ellipsometrically determined brush composition of 8 nm thick polystyrene - poly(vinyl pyridine) mixed brushes with FTIR spectroscopy results [200].

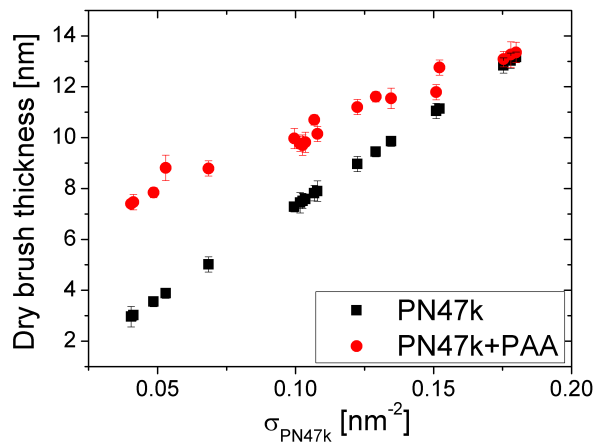


Figure 6.2.: Grafting series for PN47k-PAA mixed brushes.

Thicknesses achieved for a whole grafting series for PN47k-PAA are displayed in Figure 6.2. Here the thickness of the grafted PNIPAAm brushes and the total layer thickness are displayed

as a function of the PNIPAAm grafting density as derived from Equation 2.2. The amount of grafted PAA is decreasing with increasing PNIPAAm grafting density, whereas no second polymer could be grafted for PNIPAAm brushes with a grafting density of 0.18 nm^{-2} . Thus we concluded that PAA is grafted directly to the anchoring layer and is not only immobilized along the PNIPAAm chains by physical interaction.

6.3. Modeling of swollen polymer brushes and protein adsorption

In a first approach the optical box model was also applied to determine n and d for swollen polymer brushes in aqueous solution (Figure 6.1(b)). For the swollen state Cauchy dispersions were applicable to determine n in all cases. Furthermore with the help of an effective medium approach the content of dry polymer within the swollen layer could be determined (Section 6.3.2). Here the approach according to Bruggeman was used.

6.3.1. Brush profiles

Swollen in an aqueous solution, for all brushes investigated in this work a diffuse brush-solution interface rather than a sharp transition has to be considered [11]. With the help of neutron reflectometry measurements especially the brush profile of PNIPAAm brushes was investigated in the literature [11, 34, 86]. Here a continually decreasing PNIPAAm volume fraction with height above the substrate could be found below the LCST and the formation of two different density regimes with a dense region close to the substrate and a dilute region in the outer brush zone was found at the LCST (Figure 6.3). Above the LCST the sharpness of the brush-solution interface was increasing again.

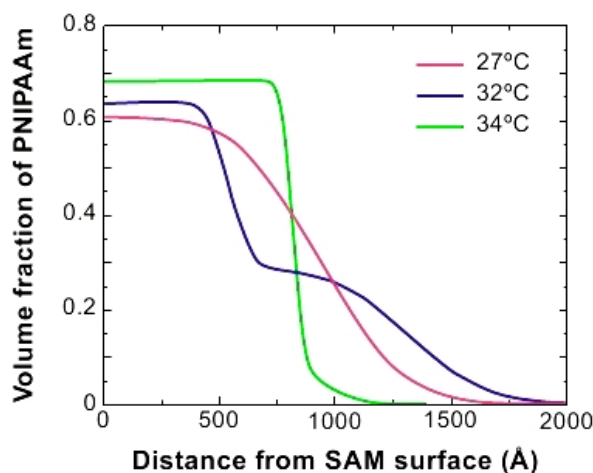


Figure 6.3.: PNIPAAm volume fraction with distance from the grafting sites at three different temperatures determined by neutron reflectometry [11].

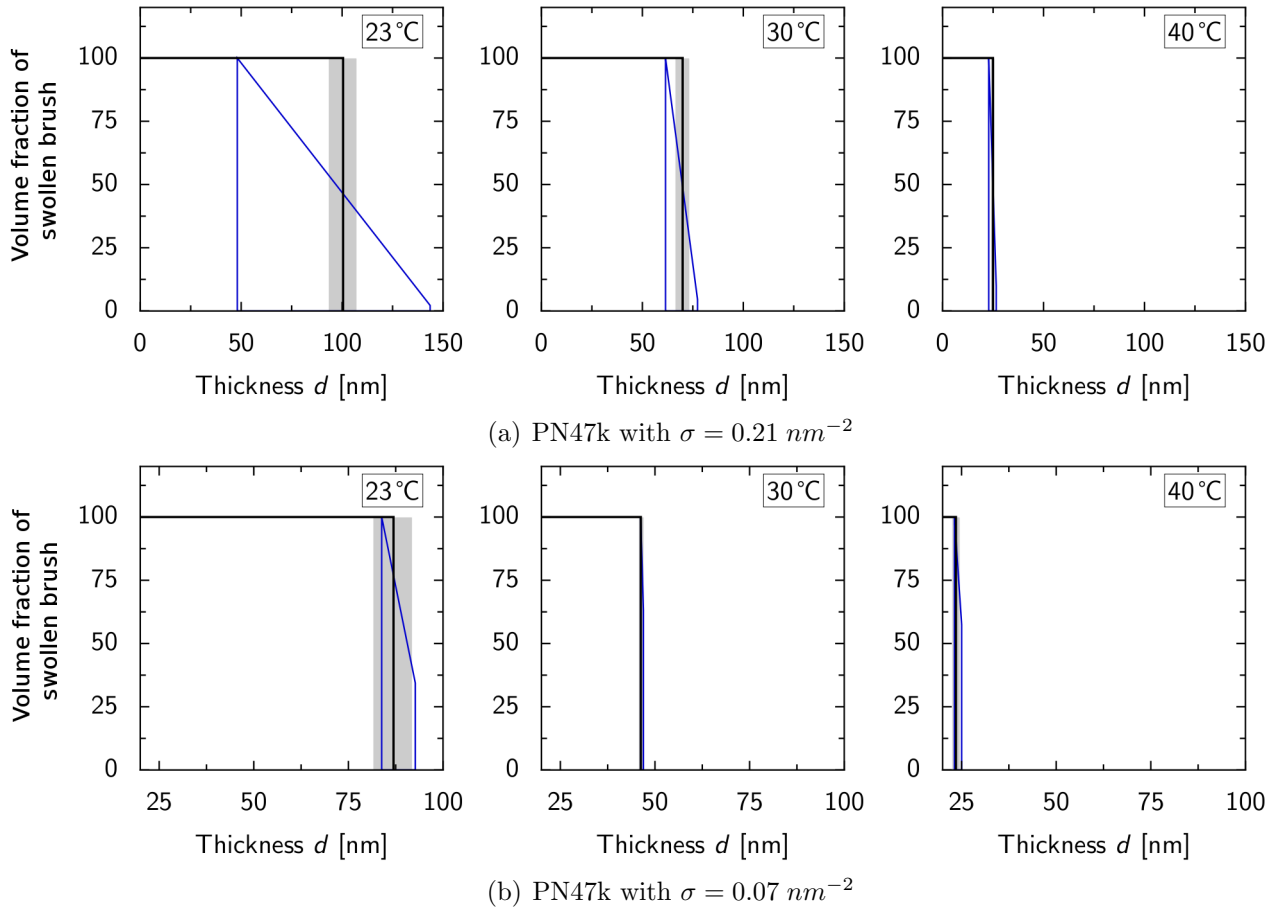


Figure 6.4.: Comparison of a simple optical box model (black solid line) to a box model with additional roughness layer (gray rectangle) and to a box model with graded top layer (blue shaded field). The additional roughness layer was modeled by an EMA layer (see Section 6.3.2) with a volume fraction of buffer and swollen polymer brush of 50 % each. In the graded top layer the volume fraction of the polymer brush is assumed to decrease linear with the distance from the brush surface given by a box model.

Since the swelling of polymer brushes was monitored with ellipsometry in this thesis, an attempt on the modeling of the brush profiles out of ellipsometric data was performed and results are expressed in Figure 6.4 for the swelling of PN47k brushes with two different grafting densities in PBS buffer solution at 23 °C, 30 °C and 40 °C. We compared a simple box model, a box model with additional roughness layer with 50 % buffer content and a box model with linear graded top layer. The dispersion relation of the swollen brush was fixed at the dispersion relation obtained for the simple box model and deviations in the dispersion at the brush-solution interface fitted to the two roughness models. As can be seen in Figure 6.4(a), the deviations from the optical box model decrease with decreasing total layer thickness for a PN47k brush with a grafting density of 0.21 nm^{-2} and reflects the improvement of the sharpness of the brush-solution interface with increasing temperature as monitored with neutron reflectometry in the literature [11]. Here the highest differences in the swollen layer thickness between box model and model with gradient top layer at 23 °C amount to 43 %, with a total thickness of

144 ± 3 nm for the additional gradient layer compared to 101 ± 1 nm for the simple box model. In the case of a PN47k brush with a low grafting density of 0.07 nm⁻² the improvement of the modeling with increasing temperature is less pronounced and even a small increase of the deviations can be observed when comparing the modeling for 30 °C and 40 °C (Figure 6.4(b)).

The dependence of the swelling behavior of PN47k brushes on the grafting density will be discussed more closely in Section 7.1.3, whereas here the possibilities and limits of the box modeling should be expressed. Since the swollen layer thickness determined with the box model, that is obtained along with a defined dispersion relation, is in all subfigures of Figure 6.4 very close to the center of the deviations, we assume that the simplest modeling is sufficient to obtain reliable results on changes in the brush layer thickness upon changes in the environmental conditions.

The dependency of refractive indices $n(\lambda = 631.5 \text{ nm})$ of these PN47k brushes on temperature changes can be found in the Appendix in Figure A.6, whereas $\Delta n(\lambda = 631.5 \text{ nm})$ decreases with decreasing grafting density.

Another method to obtain swollen brush thicknesses, also applied for PNIPAAm brushes, is in-situ AFM [201], whereas to the best of our knowledge so far no combined investigations with both methods are reported.

6.3.2. Effective medium approach (EMA)

To describe the effective dielectric functions of heterogeneous media, effective medium approaches have been developed [202–204]. Here the individual dielectric functions of the components contribute to an effective ϵ according to the underlying model assumptions. Besides a linear combination more advanced approaches were developed leading to the Maxwell-Garnett, the Bruggeman and the Lorentz-Lorenz expression (Table 6.2).

Table 6.2.: Two-component EMA approaches with their model assumptions.

Approach	Assumptions
Lorentz-Lorenz	Mixing of a and b on atomic scale in host medium vacuum
Maxwell-Garnett	b is the host medium and $f_b \gg f_a$
Bruggeman	$f_a \approx f_b$

In this thesis the effective medium approach according to Bruggeman was used, described by the equation [202, 204]:

$$0 = f_a \frac{n_a^2 - n^2}{n_a^2 + 2n^2} + f_b \frac{n_b^2 - n^2}{n_b^2 + 2n^2} \quad (6.2)$$

Here f_a and f_b are the volume fractions of two components a and b and $n_{a,b}$ are the corresponding refractive indices with n the total refractive index of the heterogeneous medium. Typically f_a and f_b are the fitting parameters and refractive indices are given for the components. Also more than two-component effective medium approaches are possible, and a three-component

approach was used to model protein adsorption experiments. However correlations between the volume fractions of the individual components are strongly increasing.

For some situations, e.g. strong swelling of polymer brushes or marginal protein adsorption, the Maxwell-Garnett EMA approach seems more suitable to model the volume fractions correctly because one component, for example the buffer solution, would be the host medium. Both EMA approaches were tested and differences in the modeling results were found to be small enough to be covered by the uncertainties of the modeling.

6.3.3. Modeling of the layer parameters upon protein adsorption

Two-layer model with distinct protein layer

A variety of ellipsometric studies of protein adsorption on surfaces, that are not or very low swellable in aqueous solution, have been performed in recent years [120, 121, 127, 196, 205]. Here a distinct protein layer often with a fixed refractive index of $n_{prot} = 1.375$ was modeled [120], whereas n_{prot} was directly determined from null-ellipsometry data upon adsorption at methylated silica surfaces for several proteins and was found in the range from $n = 1.365 \pm 0.01$ for HSA to $n = 1.380 \pm 0.002$ for lysozyme [127].

For polymer brushes this model approach as depicted in Figure 6.1(d) is applicable if secondary adsorption would be the dominating adsorption process in the system. For highly swellable neutral brushes and polyelectrolyte brushes as presented in this thesis, we observed that this approach is often not successful to describe the protein adsorption. Here ternary adsorption (see Figure 3.4) is expected to dominate the adsorption process for both types of brushes as it was discussed in Section 3.4.1 for polyelectrolyte brushes and in Section 3.4.2 for water soluble PEG brushes with a high number of monomers.

Thus the two-layer model with $n_{prot} = 1.375$ was not applied for the protein adsorption on PAA and mixed brushes containing PAA or PAA-b-PS. However it was used to derive the adsorbed amount on P2VP brushes as a reference of protein monolayer adsorption onto neutral brushes with a very low swelling degree in PBS solution at pH 7.4 in Section 7.2.

One-layer model with a combined polymer-protein layer

Modeling protein adsorption with one layer as depicted in Figure 6.1(c) was done for all experiments where protein adsorption was performed on PAA containing brushes. A Cauchy dispersion was applied to derive the effective refractive index $n_{comb}(\lambda)$, and the effective layer thickness d_{comb} of a combined polymer-protein layer was modeled.

With the help of a three component effective medium approach (EMA3, Section 6.3.2) the protein volume fraction was derived in using the components dry polymer, buffer solution and dry protein. Here the volume fractions of the protein f_{prot} and of the dry polymer f_{pol} in the combined protein-polymer layer can be strongly correlated thus \bar{f}_{pol} was fixed according to the

following equation:

$$\bar{f}_{pol} = f_{pol} \cdot \frac{d_s}{d_{comb}}, \quad (6.3)$$

whereas the volume fraction of the dry polymer f_{pol} in the swollen brush before protein adsorption is weighted with the ratio of swollen layer thickness d_s before adsorption and combined protein-polymer layer thickness d_{comb} after adsorption. For the dry protein a refractive index of $n=1.575$, obtained for BSA adsorption at gold surfaces by H. Arwin [206], was used in the EMA3 approach.

6.3.4. Evaluation of the adsorbed amount of protein

A common approach to evaluate the adsorbed protein amount Γ of a distinct protein layer is the de Feijter approach, originally developed to calculate the adsorbed amount of synthetic and biopolymers on an air-water interface [207]. Here Γ is calculated from the ellipsometrically obtained layer thickness d_{prot} , the layer refractive index n_{prot} , the ambient refractive index n_{amb} and the refractive index increment $\frac{dn}{dc}$ of the protein layer.

$$\Gamma = d_{prot} \cdot \frac{n_{prot} - n_{amb}}{\frac{dn}{dc}} \quad (6.4)$$

This equation is applicable to derive the adsorbed amount at an interface if the refractive index increment is constant up to high concentration values of the adsorbing macromolecules, which was found to be satisfied for several proteins including BSA [207]. Here $\frac{dn}{dc}$ for BSA was calculated from refractive index measurements of protein solutions up to a concentration of $0.27 \frac{g}{ml}$ to $0.187 \pm 0.003 \frac{cm^3}{g}$ [207], whereas the same value of $\frac{dn}{dc}$ was found for HSA [127] and α -chymotrypsin [208].

The validity of the de Feijter approach for the calculation of adsorbed amounts of BSA at solid surfaces was shown by comparison of null-ellipsometry measurements to radio-immunoassays (RIA) in [121], whereas a good agreement between these methods upon adsorption at smooth silicon surfaces with roughnesses below 1 nm was observed. Different adsorbed amounts, however, were derived when adsorbing the protein at etched silicon or proteolytic carbon with roughnesses above 10 nm.

Another method to calculate the adsorbed amount from ellipsometric data was developed by Cuypers et al. [209]. They used a modified Lorentz-Lorenz relation to derive Γ from the layer thickness, the refractive index, the specific refractivity and the partial specific volume of the deposited molecules.

A comparison between the evaluation methods according to Cuypers and de Feijter were done for surfactant adsorption to methylated silica and a general agreement between the derived amounts of surfactat with both methods could be found [210].

In this thesis the adsorbed amount of protein was calculated according to a modified de Feijter approach, via subtraction of the amount of polymer in the swollen brush from the total amount of polymer and protein in a combined composite polymer-protein layer, as displayed in Scheme 6.5 and Equation 6.6. Considering different possibilities to model the adsorbed amount (see Appendix Section A.2), we think that the modeling of a combined polymer-protein layer is the best description of the surface after adsorption of the protein and thus this modified de Feijter approach is applied.

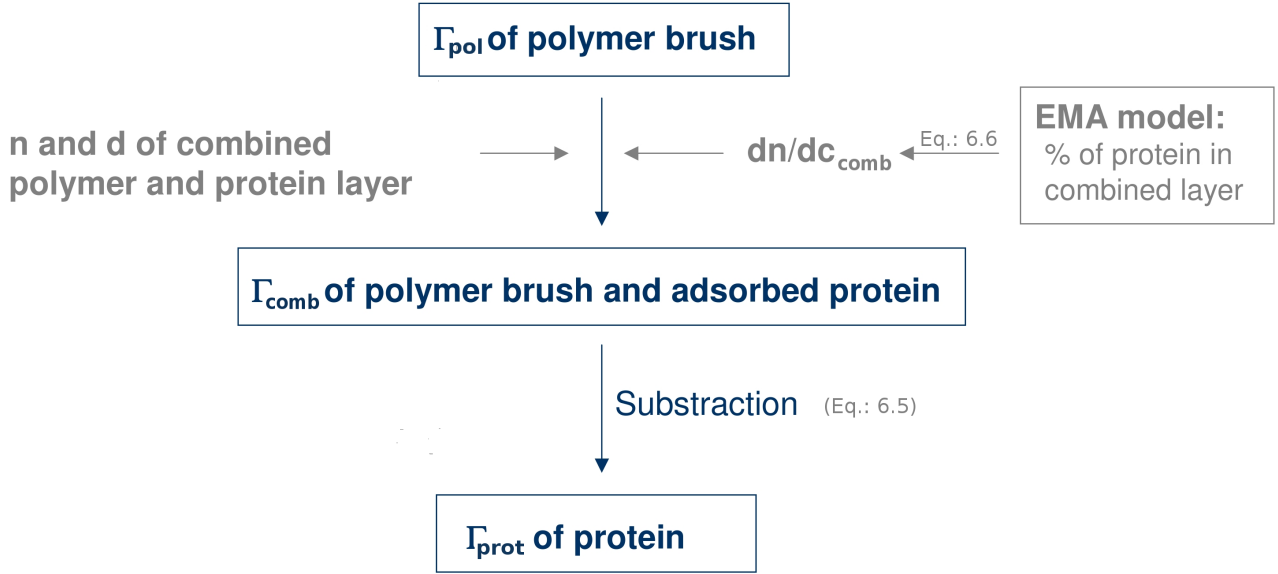


Figure 6.5.: Scheme of the evaluation method applied for the adsorbed amount of protein when using a one-layer model with a combined polymer-protein layer.

$$\Gamma_{prot} = \Gamma_{comb} - \Gamma_{pol} \quad (6.5)$$

$$\begin{aligned}
 &= d_{comb} \cdot \frac{n_{comb} - n_{amb}}{\left(\frac{dn}{dc}\right)_{comb}} - d_s \cdot \frac{n_s - n_{amb}}{\left(\frac{dn}{dc}\right)_{pol}} \\
 \left(\frac{dn}{dc}\right)_{comb} &= \frac{f_{prot} \cdot \left(\frac{dn}{dc}\right)_{prot} + \bar{f}_{pol} \cdot \left(\frac{dn}{dc}\right)_{pol}}{f_{prot} + \bar{f}_{pol}} \quad (6.6)
 \end{aligned}$$

The amount of brush polymer Γ_{pol} at the surface is also calculated by the de Feijter equation, for the swollen polymer brushes before protein adsorption, from the swollen brush layer thickness d_s , refractive index n_s and the refractive index increment of the polymers, whereas the refractive index increment $\left(\frac{dn}{dc}\right)_{pol}$ of the water soluble polymers PNIPAAm and PAA was determined from the measurement of polymer solutions with different concentrations at $\lambda = 589 \text{ nm}$ with a refractometer (Leica AR 600, Leica Microsystems GmbH, Wetzlar, Germany) (Table 6.3.4). For mixed brushes $\frac{dn}{dc}$ was calculated as linear superposition according to the mixed brush ratio, and for PAA-b-PS the refractive index increment of PAA was taken.

The refractive index increment $\left(\frac{dn}{dc}\right)_{comb}$ of the combined polymer-protein layer was derived

from the individual $\frac{dn}{dc}$ values considering the volume fractions of polymer and protein (EMA 3), respectively (Equation 6.6).

Table 6.3.: Refractive index increment in 10 mM salted solution of PNIPAAm and PAA and literature values for P2VP [211], HSA [127], α -chymotrypsin [208], and glucose oxidase [212].

Polymer	$\frac{dn}{dc}$ $\left[\frac{cm^3}{g}\right]$	Protein	$\frac{dn}{dc}$ $\left[\frac{cm^3}{g}\right]$
PNIPAAm	0.169	HSA	0.187
PAA	0.133 (pH 4)	α -chymotrypsin	0.187
	0.138 (pH 8)	glucose oxidase	0.177
P2VP	0.254		

6.4. Colorimetric quantification of the protein amount

A commercial colorimetric assay (Roti-Nanoquant (K880), Carl Roth GmbH, Karlsruhe, Germany) was used to verify the modeling of the adsorbed amount of the protein human serum albumin (A3782, defatted, IEP at pH 5.7, Sigma-Aldrich, Inc.) from ellipsometric data by measuring the absorbances at 450 nm and 590 nm of the desorption solution with an UV-VIS spectrometer.

Adsorption of the protein ($c = 0.25 \frac{mg}{ml}$) to PAA Guiselin brushes was performed at pH 4.8 at 10 mM salt concentration in glass containers for 2h (Step I) with subsequent desorption in the same pure buffer solution for 1h (Step II). A buffer solution prepared from sodium acetate trihydrate and acetic acid was used for these experiments. Finally the protein was desorbed in 10 mM sodium phosphate buffer at pH 7.9 for 1h (Step III) and the solution with desorbed protein of Step III reacted with the colorimetric working solution. The remaining protein amount at pH 7.9 was determined by ellipsometry to $1.0 \pm 0.7 \frac{mg}{m^2}$.

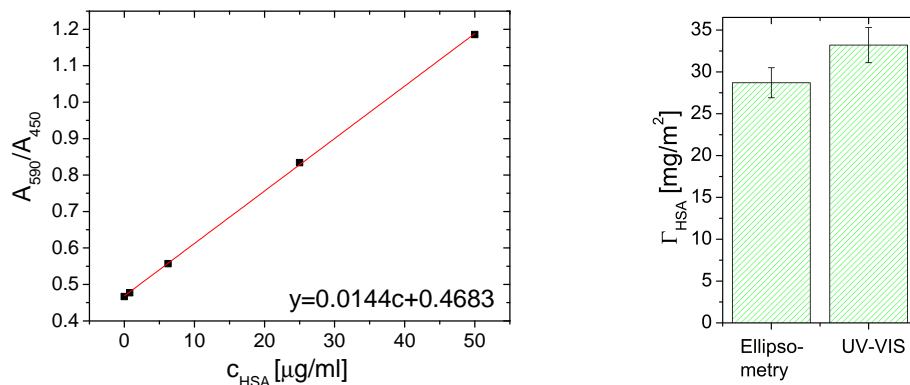
In the colorimetric reaction the protein concentration in solution can be quantified on the basis of the Bradford Coomassie brilliant blue (G-250) assay, where the complexation of G-250 with the protein leads to a shift in the adsorption maximum of the dye [213]. Here it could be shown in the literature that the ratio of the absorbances at 590 nm and 450 nm depends linearly on the protein concentration down to 50 ng of the protein in solution [214].

A calibration curve for the ratio $\frac{A_{590}}{A_{450}}$ for HSA dissolved in 10 mM buffer solution at pH 7.9 is displayed in Figure 6.6(a), and the comparison of the adsorbed amounts Γ_{HSA} determined by ellipsometry and absorbance measurements are presented in Figure 6.6(b).

Here Γ_{HSA} released from the PAA Guiselin brush in Step III as determined by the colorimetric assay is compared to the difference of the ellipsometrically evaluated adsorbed amounts of HSA at pH 4.8 (Step II: $29.7 \pm 1.1 \frac{mg}{m^2}$) and pH 7.9 (Step III: $1.0 \pm 0.7 \frac{mg}{m^2}$).

In the colorimetric assay a protein concentration of $1.9 \pm 0.1 \frac{\mu\text{g}}{\text{ml}}$ was evaluated from absorbance measurements, equivalent to $6.6 \pm 0.4 \mu\text{g}$ of protein in the desorption solution ($V=3.5 \text{ ml}$), which than was referenced to the wafer surface with an area of 2 cm^2 to allow comparison. Laser cutted wafers and micro liter pipettes were used for maximal accuracy, and ellipsometric as well as colorimetric measurements were repeated for five similar PAA Guiselin brush samples. Uncertainties in the evaluated Γ_{HSA} are primarily due to sample variations.

A general agreement of Γ_{HSA} determined by ellipsometry and by the colorimetric assay could be found, whereas adsorbed amounts modeled from ellipsometric data are lower than Γ_{HSA} obtained from absorbance measurements for all investigated samples. We refer this systematic deviation in the ellipsometrically determined Γ_{HSA} to the assumption of a box model as well as the limited contrast at the interface of combined polymer-protein layer and buffer solution. For small adsorbed amounts the sensitivity of the colorimetric assay is too low, and IR-related techniques like ATR-FTIR or IR-ellipsometry will be considered for future experiments to verify the modeling of ellipsometrically determined adsorbed amounts of protein. Nevertheless relative deviations between both methods are less than 15 % for this high amounts of adsorbed proteins.



(a) Calibration curve for the colorimetric assay for HSA in 10 mM buffer solution at pH 7.9.

(b) Comparison of adsorbed amounts derived from ellipsometry and absorbance measurements.

Figure 6.6.: Commercial colorimetric assay to determine the amount of protein desorbed from the PAA brush surface and thus to verify the previously adsorbed amount modeled from ellipsometric data.

Part III.

Results and discussion

7. Poly(N-isopropyl acrylamide) grafting-to brushes

End-grafted PNIPAAm brushes are promising for the creation of responsive surfaces due to their deswelling above a lower critical solution temperature of ~ 32 °C. Some applications for these smart surfaces, like cell adhesion or adsorption of bacteria, depend critically on changes in short range interactions that can be introduced by changes in the hydrophobicity of the surface [215,216]. For other applications the magnitude of conformational change is important, for example in the separation of molecules due to their specific size or the controlled binding of ligands [217,218]. Here few studies exist on the influence of brush parameters, like grafting density σ and molecular weight M_n , of end-grafted PNIPAAm brushes in the intermediate grafting regime on the LCST behavior [32,88]. Whereas these PNIPAAm brushes and their corresponding mixed brushes are especially interesting for the applications mentioned above, due to a high magnitude of changes in the physico-chemical interface properties for intermediate grafting densities.

Thus the LCST behavior of these end-grafted PNIPAAm brushes was investigated more closely in this chapter, and the influence of grafting density as well as molecular weight on the temperature sensitive swelling is reported in Section 7.1, analyzed with three different methods probing different effects of the LCST behavior. Furthermore the protein adsorption affinity was investigated in Section 7.2 at isotonic conditions with in-situ ellipsometry.

7.1. Temperature sensitive swelling

The high sensitivity of the ATR-FTIR technique on changes in molecular vibration bands offers a way to investigate the interaction between molecules, especially the vibrations of the amide and isopropyl groups of the PNIPAAm brush in contact with water molecules. Here changes in the vibration bands for three different molecular weights were investigated below and above the LCST. Dynamic contact angle measurements were done on the same brushes probing changes in the surface wettability upon switching above the LCST. Finally changes in the brush parameters refractive index n and layer thickness d were monitored with in-situ spectroscopic ellipsometry, whereas the highly swellable PN47k was used to monitor changes in the temperature sensitive transition with different grafting densities.

7.1.1. Molecular mechanism - ATR-FTIR spectroscopy

In Figure 7.1 ATR-FTIR spectra of PNIPAAm brushes grafted on a silicon internal reflection element (Si-IRE) are given in the dry state, swollen at $T = 24\text{ }^{\circ}\text{C}$ and swollen at $T = 50\text{ }^{\circ}\text{C}$ for the molecular weights 132,000, 45,000 and 28,000 g/mol. The corresponding layer parameters in the dry state can be found in Table 6.1 in Section 6.2.

Generally, these spectra on thin PNIPAAm brush films agreed with those on PNIPAAm in solution [219], when comparing the position of the intense Amide I band (mainly $\nu(C=O)$) between 1625 and 1650 cm^{-1} and the Amide II (mainly $\delta(NH)$) band between 1535 and 1555 cm^{-1} . These bands form mainly due to the excitation of stretching ($\nu(C=O)$) and bending ($\delta(NH)$) vibrations of the amide groups, but also the stretching vibration of CH bonds in the isopropyl groups between 3000 - 2800 cm^{-1} can be detected. The small peak at 1730 cm^{-1} corresponds to a $\nu(C=O)$ band due to the ester group formed between the COOH group of end-functionalized PNIPAAm and PGMA in the grafting process.

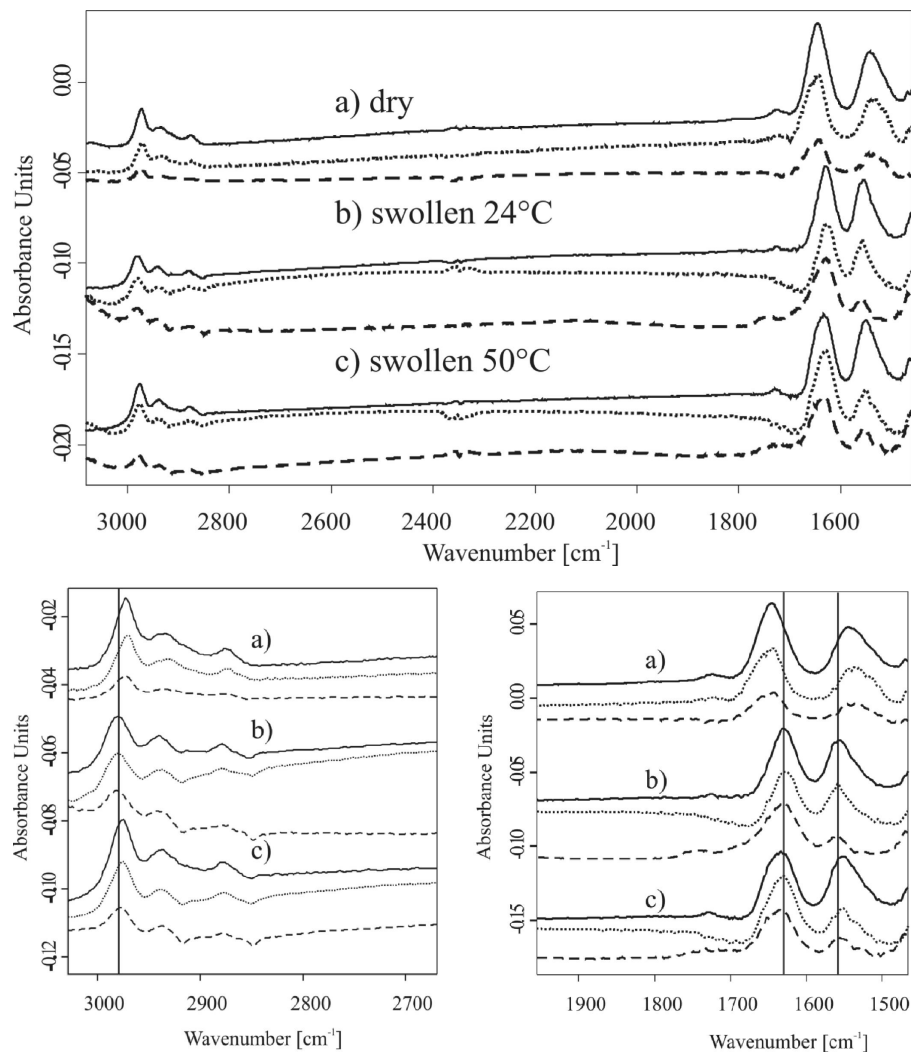


Figure 7.1.: ATR-FTIR spectra of PNIPAAm brushes for three different molecular weights: 132,000 $\frac{\text{g}}{\text{mol}}$ (solid line), 45,000 $\frac{\text{g}}{\text{mol}}$ (broken line) and 28,000 $\frac{\text{g}}{\text{mol}}$ (dotted line) in the dry state (a), swollen in PBS buffer solution at $24\text{ }^{\circ}\text{C}$ (b), and $50\text{ }^{\circ}\text{C}$ (c).

The position peak maxima of Amide I and II of PNIPAAm are highly indicative for type and degree of hydrogen bonding in dependence of the temperature (T) as it was described for PNIPAAm solutions [220, 221]. For $T < LCST = 32\text{ }^\circ\text{C}$, where PNIPAAm is claimed to be in the expanded state, the wavenumber position of the Amide I appears lower and that of the Amide II band higher than for $T > LCST$, where PNIPAAm is claimed to be in the collapsed state. Lowering the Amide I band position can be assigned to hydrogen bond formation between the amide C=O and water ($C = O \cdots H \cdots O - H$) due to weakening the C=O double bond character. The enhancement in the Amide II band position is due to H bond formation between amide N-H and water ($N - H \cdots O - H_2$) restricting the $\delta(NH)$ bending mode and increasing its force constant. Wavenumber positions of the PNIPAAm brush film in dependence of sample state, temperature and molecular weight are given in Table 7.1.

Generally, significant shifts of the Amide bands could be obtained for the different sample states. An upward shift from 1627 (1628) to 1635 cm^{-1} and a downshift from 1558 to 1553 cm^{-1} was obtained for the Amide I and Amide II band, respectively, upon raising the temperature from $T = 25$ to 50 $^\circ\text{C}$. Moreover no significant influence of the molecular weight as well as the grafting density was obtained on that transition behavior. Interestingly, an upward shift to 1647 cm^{-1} and a downshift to 1535 cm^{-1} of the Amide I and Amide II band, respectively, was obtained for the dry PNIPAAm brush compared to the wet state for both $T = 25\text{ }^\circ\text{C}$ and 50 $^\circ\text{C}$. This suggests that the PNIPAAm chains at 50 $^\circ\text{C}$ are still considerably more hydrated than in the dry state. Furthermore, significant shifts of the antisymmetric CH_3 -stretching vibration, denoted as $\nu_{as}(CH_3)$, due to the isopropyl groups could be obtained for the studied samples, which are also given in the Table 7.1. Here the PNIPAAm brush in the wet state showed a downshift from 2981 (2980) cm^{-1} for $T = 25\text{ }^\circ\text{C}$ to 2975 (2976) cm^{-1} for $T = 50\text{ }^\circ\text{C}$ and further to 2970 cm^{-1} for the dry sample, again independently on the molecular weight. An analogous downshift of the $\nu_{as}(CH_3)$ position for PNIPAAm solution upon heating above the LCST was reported by Maeda et al. [220]. They explained this effect, i.e. an upward shift upon cooling below LCST, by contraction of the C-H bond, if water molecules are in the vicinity of the isopropyl group, yet postulating hydrogen bonding between water and C-H bond ($C - H \cdots OH_2$), which is supported by ab-initio calculations [222].

Table 7.1.: Wavenumbers positions of $\nu_{as}(CH_3)$, amide I and II peak of PNIPAAm brushes at the dry and two swollen states at 24 $^\circ\text{C}$ and 50 $^\circ\text{C}$.

peak	Wavenumber position [cm^{-1}]								
	dry state			swollen at 24 $^\circ\text{C}$			swollen at 50 $^\circ\text{C}$		
	PN132k	PN45k	PN28k	PN132k	PN45k	PN28k	PN132k	PN45k	PN28k
$\nu_{as}CH_3$	2970	2970	2971	2981	2980	2980	2976	2976	2975
Amide I	1647	1647	1647	1627	1627	1628	1635	1635	1635
Amide II	1536	1535	1535	1558	1558	1558	1552	1553	1552

7.1.2. Surface hydrophobicity - Contact angle

Contact angle studies for PNIPAAm "grafting-to" and "grafting-from" brushes can be found in the literature [32, 33]. In [33] a dependency of the advancing contact angle on the dry layer thickness could be observed. Here the grafting density was kept constant at $\sigma \approx 0.4 \text{ nm}^{-2}$ and advancing contact angles were measured on polymer brushes with different molecular weight. A sharp phase transition was found for high molecular weights, whereas the highest θ_{adv} measured at 36 °C was 88 ° for a 87.3 nm thick brush and the maximum change in θ_{adv} was ca. 14 °. In [32] for PNIPAAm brushes ($M_n = 13,200 \frac{\text{g}}{\text{mol}}$, PDI=1.06) prepared with "grafting-to", θ_{adv} changed from 51 ° to ca. 89 ° ($\Delta\theta_{adv} = 38$ °) by increasing the temperature to 36 °C, obtained with the dynamic Wilhelmy plate technique.

In this work temperature dependent advancing contact angles for PN28k and PN45k brushes, investigated by ATR in the last section, as well as PN132k brushes with a lower grafting density were measured in steps of 2 °C and are displayed in Figure 7.2(a).

Similar changes towards a more hydrophobic behavior above the LCST like in the literature were monitored, whereas an additional stick-slip behavior was observed for PN45k and PN132k brushes and an example of a dynamic measurement is displayed in Figure 7.2(b). Here the upper limit of the advancing contact angle in the stick-slip pattern was evaluated and is shown in gray in Figure 7.2(a). In [223] stick-slip behavior was discussed due to vapor adsorption in the film as well as due to a surface heterogeneity. We assume these reasons also hold here since penetration of water molecules inside the brush is possible and furthermore the temperature differences between probing drop and surface could lead to surface patches with different surface wettability having lower temperature below the drop than on the contact line thus leading to heterogeneity of the surface. In [223] for a two component surface the upper limit in the stick-

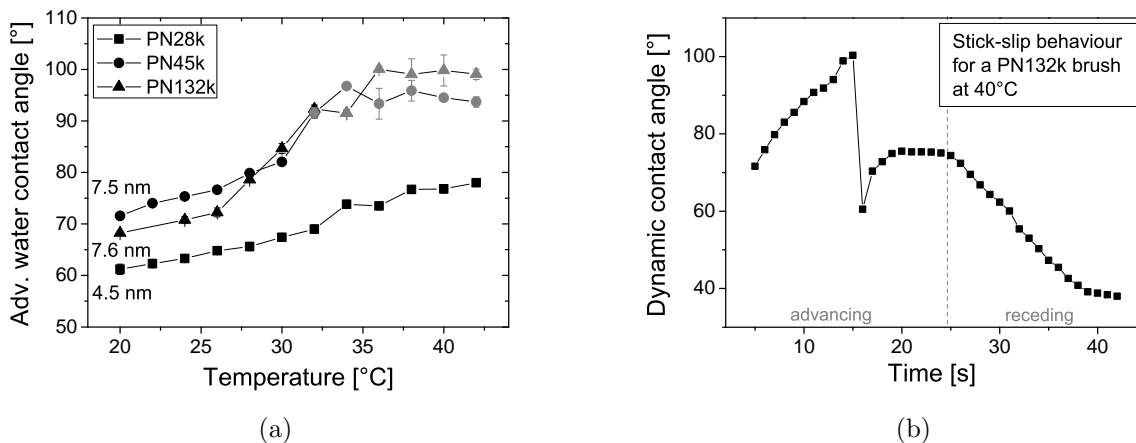


Figure 7.2.: Advancing water contact angles (black) and upper limit of the advancing contact angle in stick-slip pattern (gray) for PNIPAAm brushes with different molecular weight and grafting density (a). Example of a stick-slip behavior (b).

slip pattern was discussed as the advancing contact angle of component one, whereas the lower limit was assigned to the Cassie angle, which is given by the weighted average of the advancing contact angles of the two possible surfaces. Thus here we assigned the upper limit to the advancing contact angle of the PNIPAAm brush at the given substrate temperature, although it is most probable that the situation can not be explained by a two component system ((1) PNIPAAm at substrate temperature, (2) PNIPAAm at water drop temperature of 23 °C) but rather by a gradual change of temperature between water drop and substrate temperature throughout the surface.

The highest difference in θ_{adv} was observed for PN132k brushes with changes from 68 ° at 20 °C to 100 ° at 40 °C. Here it is noteworthy, that for two brush types of PN45k and PN132k with the same dry layer thicknesses but different grafting densities at $\sigma^{45k} = 0.11 \text{ nm}^{-2}$ and $\sigma^{132k} = 0.04 \text{ nm}^{-2}$ the increase in hydrophobicity as well as the total contact angle values are very similar, indicating higher importance of the dry layer thickness / adsorbed amount of polymer at the surface for changes in the surface wettability than molecular weight or grafting density. For PN28k brushes with the shortest polymer chains investigated here, the total increase of the advancing contact angle was considerably lower than for the other two brush types, the transition smoother and no stick-slip behavior occurred. Here θ_{adv} increased about 16 ° compared to 21.5 ° for PN45k and 32 ° for PN132k brushes. Also the influence of the decreased dry layer thickness of 4.5 nm of PN28k brushes on the total advancing contact angle values is visible.

7.1.3. Integral brush behavior - Spectroscopic ellipsometry

Changes in the layer parameters swollen brush thickness and in-situ refractive index upon temperature sensitive deswelling of PNIPAAm brushes were investigated for one molecular weight ($M_n = 47,600 \frac{\text{g}}{\text{mol}}$) dependent on the grafting density. Here dry layer parameters of PN47k brushes are listed in Table 7.2.

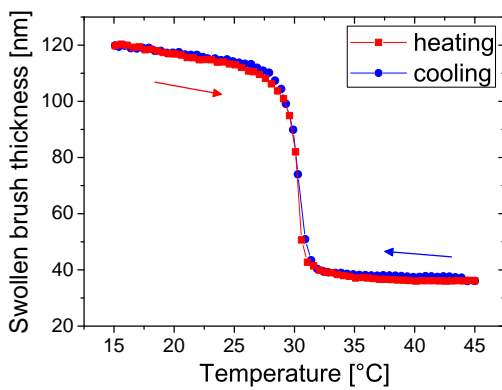
Table 7.2.: Dry brush layer thickness, refractive index and grafting density σ of PN47k brushes examined because of their temperature sensitive swelling behavior. The grafting density was calculated with Equation 2.2 and a bulk density of PNIPAAm of $\rho = 1.07 \frac{\text{g}}{\text{cm}^3}$ [197].

$d_{dry}[\text{nm}]$	$n_{dry}(631.5\text{nm})$	$\sigma[\frac{1}{\text{nm}^2}]$
3.3	1.400*	0.04
5.2	1.465	0.07
7.9	1.462	0.11
15.7	1.468	0.21
24.1	1.478	0.33

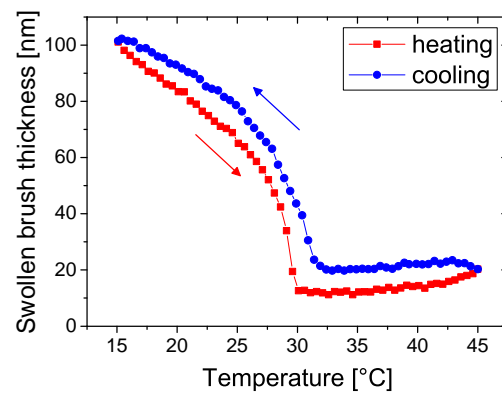
For following EMA evaluations of the swollen state of these brushes it is interesting to note, that the refractive index of the dry layer increases with increasing amount of polymer at the surface.

Swelling was monitored in PBS buffer solution in a heating and cooling cycle with in-situ spectroscopic ellipsometry with a change rate of $0.2 \frac{K}{s}$ of the temperature. Typical changes in the swollen brush thickness upon heating and cooling for a high grafting density at 0.33 nm^{-2} and a low grafting density at 0.07 nm^{-2} are displayed in Figure 7.3.

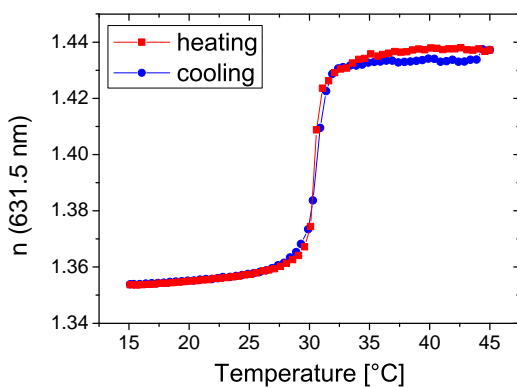
As can be seen a hysteresis between heating and cooling curve of the swollen brush thickness occurs for low grafting density (Figure 7.3(b)) but not for high grafting density (Figure 7.3(a)). At the latter the brush continues to deswell also above the LCST, whereas for low grafting density the brush restarts to swell again above the LCST until the maximum temperature in the experiment.



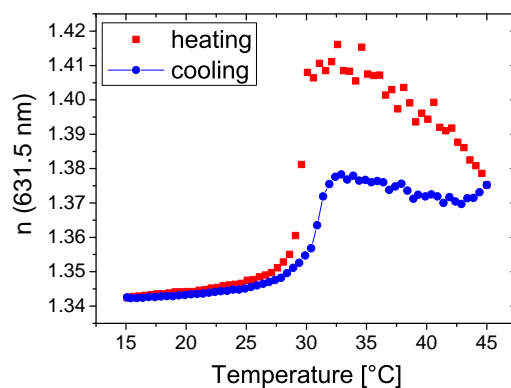
(a) Swollen brush thickness of a PNIPAAm brush with a grafting density of 0.33 nm^{-2}



(b) Swollen brush thickness of a PNIPAAm brush with a grafting density of 0.07 nm^{-2}



(c) Refractive index $n(631.5 \text{ nm})$ for a PNIPAAm brush with a grafting density of 0.33 nm^{-2}



(d) Refractive index $n(631.5 \text{ nm})$ for a PNIPAAm brush with a grafting density of 0.07 nm^{-2}

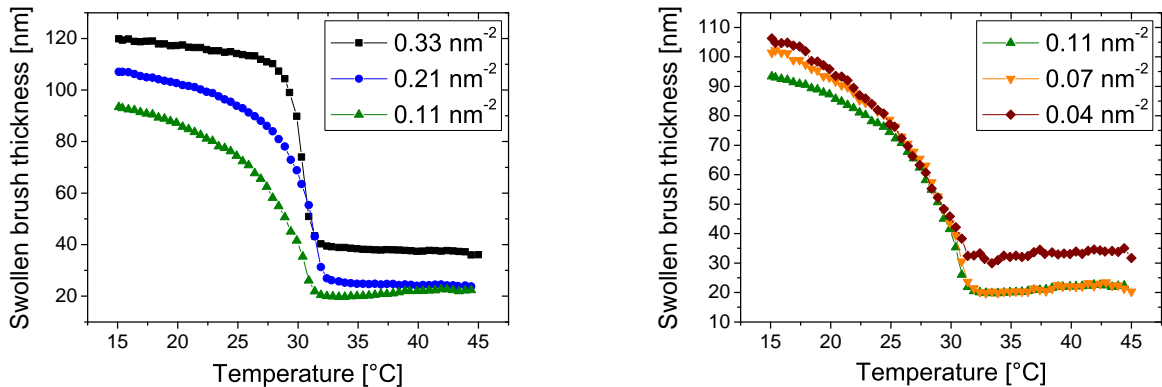
Figure 7.3.: Typical modeled swollen layer thicknesses of PN47k brushes in PBS solution. Heating and cooling experiments for high (a) and low grafting density (b) and corresponding refractive indices (c,d) are displayed.

When cooling the brush surface in both cases the thickness remains at a plateau value until the

point of phase transition were the brush swells again for $T < LCST$. It is also noteworthy that no plateau value of the swollen brush thickness is achieved below the LCST, but the thickness increases with decreasing temperature until the minimum temperature of the experiment.

The increase in the swollen brush thickness below the phase transition temperature is significantly more pronounced for the lower grafting density than for $\sigma = 0.33 \text{ nm}^{-2}$. The changes in the swollen brush thicknesses are also reflected in an inverse behavior of the refractive indices (Figures 7.3(c) and 7.3(d)), with changes of $\Delta n(631.5 \text{ nm}) = 0.09$ for $\sigma = 0.33 \text{ nm}^{-2}$ and $\Delta n(631.5 \text{ nm}) = 0.03$ for $\sigma = 0.07 \text{ nm}^{-2}$. Here the different behavior at high and low grafting density above the LCST and thus the hysteresis between heating and cooling is even more pronounced by a considerably decreasing refractive index between 30 °C and 45 °C in the heating curve of the PN47k brush with 0.07 nm^{-2} (Figure 7.3(d)). Changes in the wavelength-dependent dispersion of $n(\lambda)$ are displayed for the latter PN47k brush as an example in the appendix in Figure A.5(a)

To discuss changes in the temperature sensitive phase transition with varying grafting density more closely the swollen brush thicknesses derived from cooling experiments of several PN47k brushes are presented in Figure 7.4.



(a) Grafting densities from 0.33 nm^{-2} to 0.11 nm^{-2} (b) Grafting densities from 0.11 nm^{-2} to 0.04 nm^{-2}

Figure 7.4.: Typical modeled swollen layer thicknesses of cooling experiments for PN47k brushes swollen in PBS buffer solution for different grafting densities. The corresponding refractive indices can be found in the appendix (Figure A.6).

Here a decrease in the total layer thickness below and above the LCST and a broadening of the transition region can be observed from a grafting density of 0.33 nm^{-2} down to 0.11 nm^{-2} (Figure 7.4(a)), whereas the latter smoother temperature sensitive decrease of swollen brush thickness with decreasing grafting density was also found for the first momentum $\langle z \rangle$ of PNI-PAAm brush density profiles measured with neutron reflectometry [34]. For grafting densities lower than 0.11 nm^{-2} , as can be seen in Figure 7.4(b), changes in the swollen brush thickness are virtually identical between 20 °C and 30 °C whereas the total layer thickness below the LCST increases again with decreasing grafting density.

It is also interesting, that the total layer thickness above the LCST is higher for the boundary cases with a grafting density of 0.33 nm^{-2} and 0.04 nm^{-2} than for brushes with intermediate grafting densities. This aspect can be discussed more closely when regarding temperature sensitive changes in the dry polymer volume fraction inside the swollen PN47k brushes as depicted in Figure 7.5. These volume fractions are calculated by an EMA approach (see Section 6.3.2) from the dispersion relations known for the dry polymer brush, the buffer solution and the swollen polymer brushes, whereas for the latter refractive indices $n(631.5 \text{ nm})$ are presented in the appendix in Figure A.6.

Below the LCST at the beginning temperature of the measurements at $15 \text{ }^\circ\text{C}$ the volume fraction of the dry PNIPAAm brush was $10 \pm 5 \%$, similar for all investigated grafting densities, which indicates highly swollen polymer brushes. Actually the swelling degrees $d_{swollen}/d_{dry}$ at this temperature increased monotonically between $d_{swollen}/d_{dry} = 5$ for a grafting density of 0.33 nm^{-2} and $d_{swollen}/d_{dry} = 30$ for a grafting density of 0.04 nm^{-2} . Although the latter value is very high and has to be considered critically with respect to the box modeling of a diffuse brush-solution interface as described in Section 6.3.1, these results can be discussed when regarding both refractive index and layer thickness of the swollen brushes. Here refractive indices at $15 \text{ }^\circ\text{C}$ differed from $n(631.5 \text{ nm}) = 1.340$ for a grafting density of 0.04 nm^{-2} to $n(631.5 \text{ nm}) = 1.354$ for $\sigma = 0.33 \text{ nm}^{-2}$ (Figure A.6).

Above the LCST a differentiation in the dry polymer volume fraction according to the grafting density is visible in Figure 7.5. Here a general increase in the dry polymer volume fraction can be observed with increasing grafting density, whereas for the two lowest grafting densities the volume fraction is almost identical and for the highest grafting density at 0.33 nm^{-2} it is again decreased about 8% compared to the PN47k brush with 0.21 nm^{-2} . This behavior is reflected in the literature where a maximum of thickness changes for high molecular weight brushes ($75,600 \frac{\text{g}}{\text{mol}} - 230,000 \frac{\text{g}}{\text{mol}}$) was observed for intermediate σ [34].

Finally the temperature of the phase transition was evaluated in determining the temperature ϑ_{half} where either refractive index or swollen layer thickness was decreased / increased by half compared to its starting value at $15 \text{ }^\circ\text{C}$ and its lowest / highest value above the LCST (Figure 7.6). Here also differences due to heating or cooling of the brush surfaces are presented.

As can be seen in Figure 7.6 an increase in the transition temperature ϑ_{half} with increasing grafting density was observed, whereas ϑ_{half} obtained from refractive index measurements was $1\text{-}2 \text{ }^\circ\text{C}$ higher for all grafting densities than ϑ_{half} derived from the swollen layer thicknesses. For the latter ϑ_{half} varied between $26.4 \pm 0.2 \text{ }^\circ\text{C}$ for a grafting density of 0.04 nm^{-2} to 31.2 ± 0.6 for 0.33 nm^{-2} . Here differences upon heating and cooling the brush surface were highest for intermediate grafting densities amounting to $\pm 1 \text{ }^\circ\text{C}$ and indicating a grafting density dependent hysteresis. The dependency of the transition temperature on the grafting density can be fitted linear for the heating curves and to a parabola for the cooling curves leading theoretically to

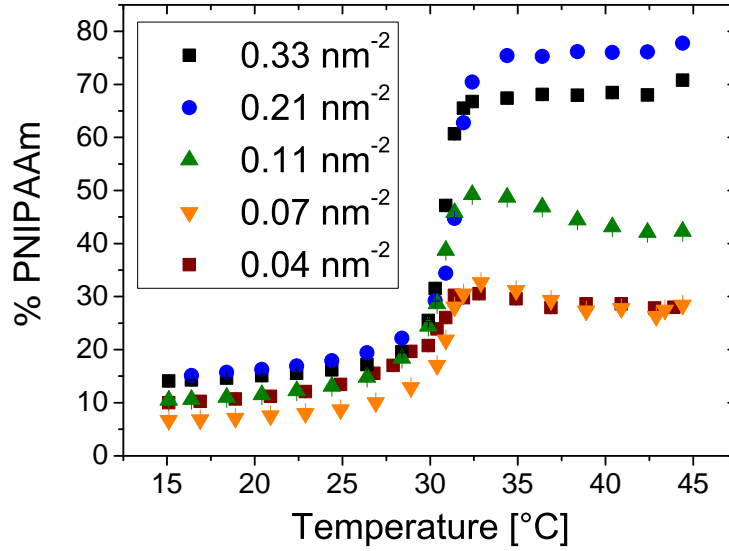


Figure 7.5.: Calculation of the percental amount of PNIPAAm in the swollen brush dependent on temperature and grafting density in PBS buffer, using the dispersion $n(\lambda)$ of the dry PNIPAAm brushes as displayed in the appendix in Figure A.4 and listed in Table 7.2.

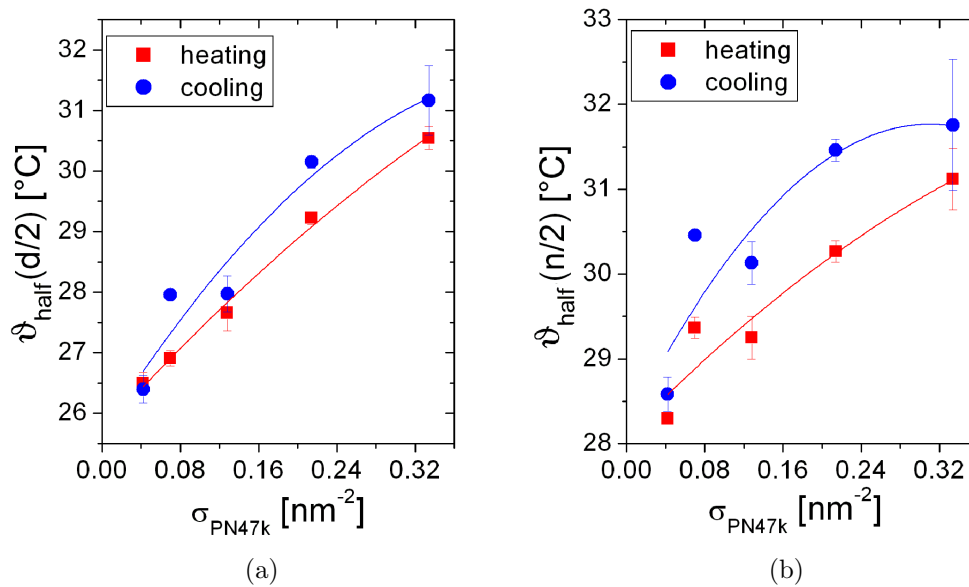


Figure 7.6.: Comparison of the phase transition temperature evaluated from thickness (a) and refractive index data (b) in PBS buffer solution dependent on the grafting density of PN47k brushes.

two intersections, however a physical explanation for these dependencies cannot be provided at the moment.

For PNIPAAm chains in PBS buffer solution with its salt content of ≈ 200 mM a decrease in the phase transition temperature compared to an LCST of 32 °C in water could be found, ranging from $25 - 27$ °C in the literature [215, 224, 225]. Thus it is interesting to note that ϑ_{half} values for the end-grafted PN47k brushes are starting for 0.04 nm^{-2} at 26.4 ± 0.2 °C in the range of the LCST value for PNIPAAm chains in the corresponding solution. In [226] a salting out effect was described for PNIPAAm chains in salted solutions leading to a decrease in the LCST, whereas the presence of cations as well as anions in the solution is discussed to change the water structure, the polymer hydration sheath and thus the polymer interaction with the solvent [227]. Since ϑ_{half} is increasing with increasing grafting density for the PNIPAAm "grafting-to" brushes presented here, less influence of the ions in solution on the hydration sheath of individual polymer chains could be concluded most probably due to increased inter-chain interactions.

7.2. HSA resistance at isotonic conditions monitored by ellipsometry

Controlled protein adsorption is desirable in a variety of possible application like drug delivery systems [228], biosensors or in-vitro serological tests [229]. But also the complete resistance of surfaces to protein adsorption, thus forming biocompatible interfaces, is appealing for application. Here protein adsorption has been found to initiate for example non-desirable thrombosis development in cardiovascular implants, blood coagulation or complement activation [230–233].

The resistance of polymer brushes towards protein adsorption was experimentally and theoretically investigated on the example of PEG brushes [14, 28, 48, 146], leading to a theoretical prediction of suitable brush parameters for neutral water soluble polymer brushes to gain protein resistivity, whereas the formation of a stable water film on top of the brushes is considered important for protein resistant brush surfaces [49, 147].

Before the adsorption experiments the swelling of PNIPAAm brushes in PBS buffer solution was monitored with in-situ spectroscopic ellipsometry below and above the LCST dependent on the molecular weight of PNIPAAm, to connect the adsorbed amount with the swelling behavior of the brushes (Figure 7.7) [193].

The highest swelling degree and thus the largest relative amount of buffer solution inside the brush was obtained for PN47k with a swollen layer thickness 6.3 times higher than the dry thickness and a percentage buffer content of 82 %. For temperatures above the LCST this PNIPAAm brush deswells to 1.5 times of the dry thickness and the buffer content is reduced to 16 %. The high swelling degree below the LCST of PNIPAAm can be explained by the formation of hydrogen bonds between the amide moieties and the ambient water molecules

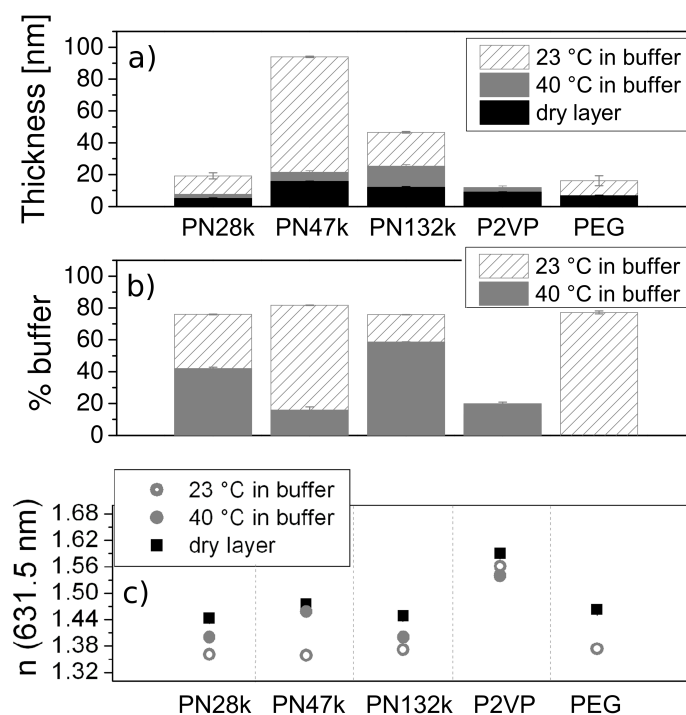


Figure 7.7.: In-situ spectroscopic ellipsometric swelling measurements of PN28k, PN47k, PN132k, P2VP and PEG brushes at 23 °C and 40 °C. Displayed are the fitted swollen layer thicknesses (a) and the percentage amount of buffer solution (b) within the brush layers as well as the refractive indices $n(\lambda = 631.5 \text{ nm})$ (c) of the swollen brushes.

leading to the water solubility of PNIPAAm at 23 °C and its possible suitability as protein resistant surface coating in the brush conformation [49]. Since the polymer brush is less soluble above the LCST more protein adsorption at 40 °C could be expected.

Comparing PN132k and PN28k with the results for PN47k brushes a similar swelling behavior is visible though less pronounced. For the PN28k brushes the swollen layer thicknesses are considerably reduced due to the low molecular weight of the chains of 28,500 g/mol leading to a very thin brush layer above the LCST, whereas the percentage buffer content is equal to the content in PN47k brushes below the LCST and is increased above the LCST. For the PN132k brushes less deswelling above the LCST with a higher remaining buffer content can be seen than for PN28k and PN47k brushes. For P2VP brushes virtually no swelling could be observed at 23 °C and 40 °C as expected, because the nitrogen atom in the pyridine ring is deprotonated and thus the brush is in its neutral, collapsed state at pH 7.4.

Refractive indices increased as expected at 40 °C for all brushes that showed deswelling behavior above the LCST of PNIPAAm (Figure 7.7 (c)). For PN28k brushes swollen layer thickness and refractive index could not be determined separately at 40 °C, thus a refractive index of $n = 1.4$ that is similar to measured values for PN47k and PN132k was used to model a layer thickness for the deswollen brush.

As can be seen in Figure 7.8 virtually no albumin adsorption from 1 mg/ml HSA in PBS buffer solution on all three PNIPAAm brushes could be evaluated for 23 °C and 40 °C. Only for the shortest brushes with $M_n = 28,500$ g/mol a marginal adsorbed amount of less than $0.2 \frac{mg}{m^2}$ was calculated at 40 °C [193].

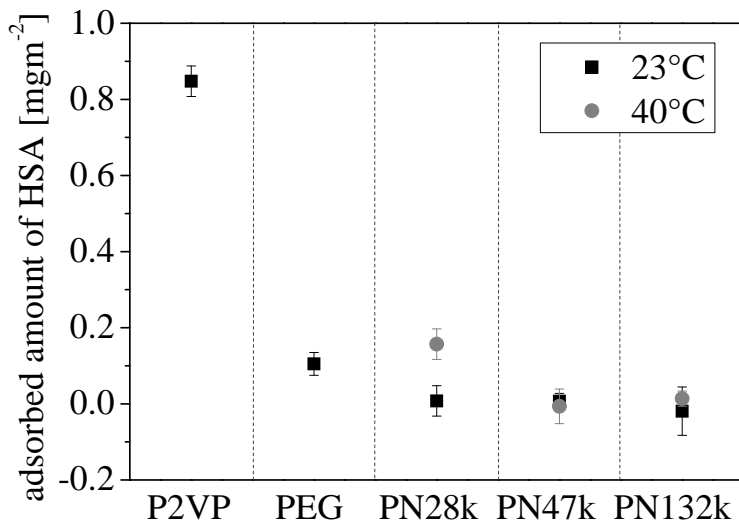


Figure 7.8.: Adsorbed amount of HSA at PN28k, PN47k and PN132k brushes at 23 °C and 40 °C compared to the adsorbed amount at a P2VP and a PEG brush at 23 °C in 0.01M PBS buffer solution at pH 7.4 with a protein concentration of 1 mg/ml. The error of the adsorbed amount was calculated to be maximal 5 % of the absolute value. Only for PN28k brushes at 40 °C an adsorbed amount of HSA could be calculated.

Here the adsorption of HSA onto the PNIPAAm brushes was modeled according to the one-layer approach described in Section 6.3.3 and the adsorbed amount of HSA evaluated in subtracting the amount of polymer from a total amount of macromolecules on the silicon-PGMA surface (Section 6.3.4). We also evaluated the adsorption experiments with a two layer model, with one layer as the swollen polymer brush and an additional protein top layer, where very similar results were obtained as depicted in the appendix in Figure A.3.

A similar adsorbed amount like for PN28k brushes at 40 °C was obtained for the investigated PEG brushes at 23 °C. Also contrary to PN47k and PN132k the swollen brush thicknesses for these protein adsorbing brushes are in the same range below 20 nm, whereas the relative buffer content is higher than for PN47k brushes. Here it is interesting, that the total swollen layer thickness seems to be important for the resistance of the brushes, whereas an influence of the relative amount of buffer inside the polymer layer is not evident for the presented examples of PNIPAAm brushes. This behavior could indicate secondary adsorption of HSA at the brush-solution interface at PN28k and PEG brushes with low swollen brush thicknesses.

However at the moment we do not have an explanation why the PNIPAAm brushes, presented in this thesis, are also highly protein repellent in their collapsed state above the LCST in PBS buffer solution, although contact angle measurements as presented in Figure 7.2(a) point to a considerable increase in the surface hydrophobicity. We assume this special behavior is due to the unique brush structure as well as the brush-solution interface properties in-situ, but also an influence of the salt concentration seems likely when comparing the results with HSA adsorption in less salted buffer solutions (see Figure 9.10(a)). Here further investigations with in-situ AFM, in-situ ATR-FTIR or QCM-D could increase the insight into the adsorption mechanisms on these PNIPAAm brushes. A reference to first cell adhesion studies at similar PNIPAAm brushes will be discussed at the end of this section.

For comparison protein adsorption on P2VP brushes at this environmental conditions was evident. We chose the P2VP brush to demonstrate the sensitivity of the ellipsometric measurements of adsorbed protein layer thicknesses. This brush is chemically neutral at the investigated pH of 7.4 and by using the relatively high salted PBS buffer virtually all remaining charges can be screened. Thus assuming a neutral brush surface we only expect adsorption to take place via the hydrophobic effect resulting in a maximal adsorbed amount of $\approx 0.8 \frac{mg}{m^2}$, that represents a monolayer of HSA [127]. When HSA was adsorbed to the PGMA anchoring layer an adsorbed amount of $0.75 \pm 0.05 \frac{mg}{m^2}$ was observed at 23 °C in PBS buffer solution, indicating similarly monolayer adsorption.

Since these results for protein resistance of PNIPAAm brushes depend on the chosen modeling, the differences in the ellipsometric angles Δ and Ψ for the swollen brushes and after adsorption are presented additionally in Figure 7.9. Here a pronounced increase in Δ and Ψ for the adsorption at PN28k brushes at 40 °C is visible, whereas for PN47k and PN132k the differences in Δ and Ψ are close to zero, indicating virtually no changes in the swollen brush parameters (refractive index and thickness) and thus resistance towards HSA adsorption at the present environmental conditions can be concluded for the latter molecular weights.

Null-ellipsometry is capable of detecting differences in Δ and Ψ as small as 0.01 °, leading to a surface layer sensitivity in the sub-Ångström regime and thus to a very high sensitivity towards adsorption of macromolecules at a surface. In further experiments we plan to recheck these findings on protein resistance in PBS buffer solution with activity measurements on immobilized enzymes, like glucose oxidase.

For buffer solutions with lower salt content so far no consistent results, whether these brushes are resistant, could be obtained but adsorbed amounts were below $0.6 \frac{mg}{m^2}$ in all investigations. Here more detailed studies would be necessary to identify the influence of pH, temperature, polymer chain length and brush grafting density. Due to the dipolar character of the amide groups at the PNIPAAm chains, we expect a less repelling behavior of these brushes for low salt content, since the screening of dipoles would be less effective and van der Waals interac-

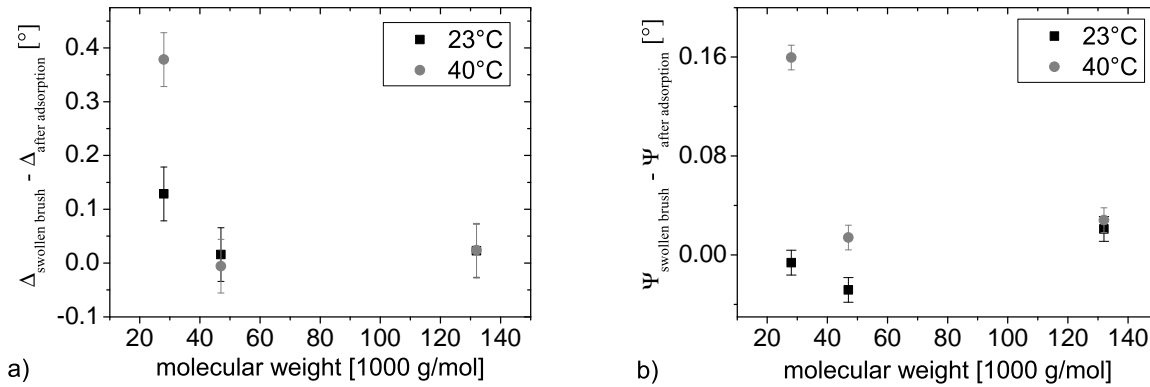


Figure 7.9.: Differences in the ellipsometric angles Δ (a) and Ψ (b) between the values for the swollen brush in 0.01 M PBS buffer solution and after adsorption of HSA from a $1 \frac{mg}{ml}$ protein solution for PN28k, PN47k and PN132k.

tions (dipoles on amide groups - permanent charges on protein molecules) have to be considered.

When comparing these findings to cell adhesion studies on PNIPAAm-g-PEG hydrogel films [234, 235], and on PNIPAAm "grafting-to" brushes with a molecular weight of $66,000 \frac{g}{mol}$ [152, 236]¹, an influence of the brush structure on its protein repelling effect could be concluded. In adhesion studies of L929 mouse fibroblast cells on PNIPAAm brushes low cell adhesion and no proliferation could be observed above and below the LCST of PNIPAAm, whereas at PNIPAAm-g-PEG hydrogel films good adhesion / proliferation was monitored above the phase transition temperature. Below the LCST of the hydrogel film detachment of the cell layer took place. Most interestingly the swelling degree of $\frac{d_{swell}}{d_{dry}} \approx 2$ of the brushes and the hydrogel films above the LCST is comparable, thus the hydration state is not considered as the main effect for the different cell adhesion affinities of these polymer surfaces. An influence of the brush structure above the LCST on its adsorption / adhesion affinity could be possible, because of a potentially more ordered structure in the brushes than in the hydrogels due to inter-chain interactions below and above the LCST as well as the excluded volume effect in these end-grafted brushes. But also the presence of PEG in the hydrogel and the cross-linking of the gel by a low-pressure argon plasma could be factors for the different behavior of brush and hydrogel.

7.3. Summary

Temperature sensitivity as well as protein adsorption affinity at isotonic conditions was presented for end-grafted PNIPAAm brushes with intermediate grafting densities, whereas these

¹Microscopy images of cell adhesion studies at 23 °C and 37 °C on PN66k-brushes made by Dr. Burkert can be found in her PhD-thesis at p. 89. Dr. Burkerts thesis is also available online at <http://nbn-resolving.de/urn:nbn:de:bsz:14-qucosa-26105>

brushes are appealing for applications in drug release systems, as substrates for cell growth and harvest or in other fields where a precise actuation of physico-chemical interface properties like hydrophobicity and layer density is necessary.

Temperature sensitive swelling was investigated with three different methods, probing changes in vibration bands of amide and isopropyl groups with in-situ ATR-FTIR, changes in the surface hydrophobicity with dynamic contact angle measurements and changes in the brush layer parameters thickness and refractive index as well as the temperature of transition and the fraction of buffer inside the brush with in-situ spectroscopic ellipsometry.

The amide I and amide II bands were found to shift with temperature reflecting the decrease of water-polymer hydrogen-bonding above the LCST, whereas at 50 °C the brushes were still considerably hydrated compared to the position of vibration bands in the dry state. No dependency of the band position at 24 °C and 50 °C on molecular weight and grafting density could be observed, indicating a similar state of hydration of the individual polymer chains in the brush for all three PNIPAAm brushes (PN28k: $\sigma = 0.11 \text{ nm}^{-2}$, PN45k: $\sigma = 0.10 \text{ nm}^{-2}$, PN132k: $\sigma = 0.06 \text{ nm}^{-2}$) for each temperature respectively. The absolute intensity of the vibration bands increased with increasing molecular weight and thus with the amount of polymer at the surface.

The surface hydrophobicity was found to increase with increasing temperature, but with significantly higher changes in the advancing contact angle than reported in the literature for PNIPAAm brushes with high grafting density ($\sigma = 0.4 \text{ nm}^{-2}$). Again a dependency on the amount of polymer on the surface was observed with increasing amplitude of change in θ_{adv} for higher amounts at the surface alongside with lower grafting densities. Stick-slip behavior could be observed, that was not reported in the literature for equivalent contact angle measurements. Here a connection between the occurrence of stick-slip and these very high changes in the surface hydrophobicity can be assumed.

For the investigation of changes in the brush layer parameters swollen brush thickness d , refractive index $n(631.5 \text{ nm})$ and polymer content, we focused on the influence of the grafting density σ . Here for all $\sigma < 0.33 \text{ nm}^{-2}$ the polymer content above the LCST was found to increase with increasing grafting density, thus a densification of the brush layer above the LCST with σ could be concluded. The temperature ϑ_{half} , determined by a decrease in n or d about half their starting value, increased with increasing grafting density starting for the lowest grafting density at $\vartheta_{half}(d/2) = 26.4 \text{ °C}$, close to the LCST observed for PNIPAAm chains in PBS buffer solution in the literature. Thus inter-chain interactions between polymers were found to increase with increasing grafting density, reducing the salting out effect in PBS buffer solution. Hysteresis in n and d between heating and cooling the brush surface could be found for low but not for high grafting densities.

Protein adsorption at isotonic conditions was monitored by HSA adsorbing experiments at

23 °C, below the LCST and at 40 °C, above the LCST, at PNIPAAm brushes with different molecular weight in comparison to PEG and P2VP reference brushes. Adsorption of HSA at PNIPAAm brushes could only be found at 40 °C for the shortest PN28k brushes, also indicated by significant changes in the ellipsometric angles Δ and Ψ . The total swollen brush thickness of HSA adsorbing brushes was below 20 nm, whereas for HSA repelling brushes the swollen brush thickness was higher than 20 nm below and above the LCST. Thus the swollen brush thickness was concluded to be more important for a protein repelling behavior than the relative buffer volume fraction inside the brushes for the presented brush examples. Also the unique brush structure with end-grafted chains, that stretch away from the surface, could be a possible reason for the dramatic reduction of adsorbed protein, when regarding the literature on cell adhesion studies at end-grafted PNIPAAm brushes and PNIPAAm-g-PEG hydrogel films.

8. PAA and PAA-b-PS Guiselin brushes

In this chapter we focus on polymer Guiselin-brushes consisting of the weak polyelectrolyte poly(acrylic acid) (PAA) with an isoelectric point of 2.1 [195] and the block-copolymer PAA-b-PS. Here the polymers are grafted with multiple grafting points to a substrate via the carboxy groups along the chains [12, 95]. Above the IEP the remaining free COOH - groups start to dissociate increasing the amount of negative charges in the brush layer [42, 237]. The corresponding pH-sensitive swelling behavior was investigated with in-situ spectroscopic ellipsometry in Section 8.1. This swelling behavior is also influenced by the ionic strength of the buffer solution [29, 238], whereas the transition from the annealed osmotic brush regime to the salted regime was monitored as well [29].

Furthermore the pH-sensitive adsorption / desorption behavior towards human serum albumin (HSA) and α -chymotrypsin was investigated (Section 8.2). Here dominating driving forces are assumed to be electrostatic interaction between the polymers and proteins, including charge regulation on the protein, but also entropic driving forces [59, 109, 143], whereas a penetration of the protein into the brush layer was observed for similar experiments on spherical PAA brushes [136]. The thickness and the refractive index of a combined polymer-protein layer were modeled from in-situ VIS - ellipsometry measurements and the adsorbed amount was evaluated. Finally in Section 8.3 we used a coupled quartz crystal microbalance - ellipsometry setup to monitor changes in the optical layer parameters and the amount of viscoelastically coupled buffer (water) molecules as well as changes in the shear viscosity upon swelling of the Guiselin brushes and adsorption of protein.

8.1. pH- and salt sensitive swelling behavior

The first section of this chapter is aimed at the understanding of the pH- and salt sensitive swelling behavior of PAA Guiselin brushes and the investigation of the influence of a small PS block (6 % of average number of monomers per chain). Experiments on the swelling behavior of these PAA Guiselin brushes were done in cooperation with the ISAS - Institute for Analytical Sciences, Berlin, Germany [239].

The sensitivity of end-grafted PAA brushes with pH and salt content is well investigated in the literature and a short survey was given in Section 2.2.2. Here we present results on the changes in swollen brush thickness and refractive index with pH for PAA Guiselin brushes in Figure 8.1(a), whereas the corresponding dispersions of $n(\lambda)$ can be found in the appendix

(Figure A.5(b)).

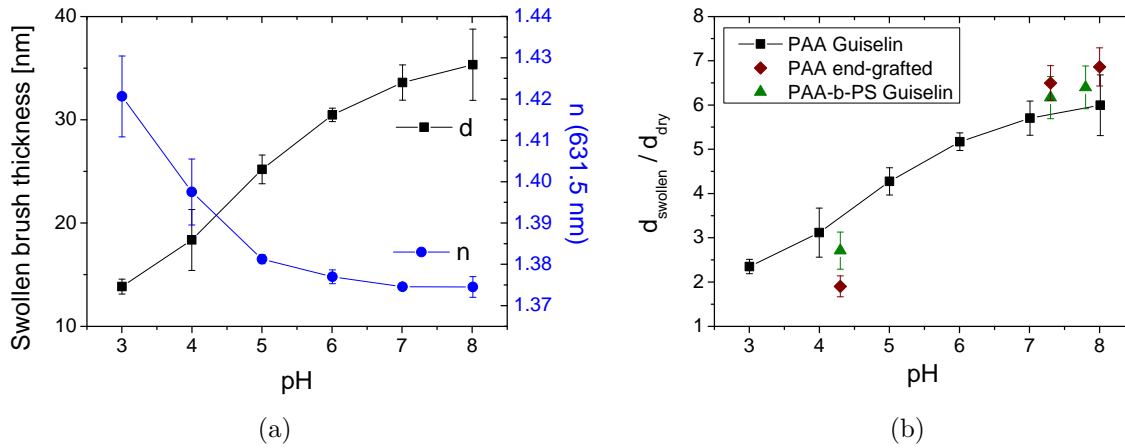


Figure 8.1.: Swollen brush thickness and refractive index at $\lambda = 631.5 \text{ nm}$ (a) as well as degree of swelling (b) of PAA and PAA-b-PS Guiselin brushes upon swelling in 10 mM buffer solutions.

A characteristic increase in the swollen brush thickness with increasing pH value could be monitored accompanied with a decrease in the refractive index. Comparing these results for PAA Guiselin brushes ($M_n = 26,500 \frac{\text{g}}{\text{mol}}$) with swelling experiments on end-grafted PAA brushes with a molecular weight of $23,600 \frac{\text{g}}{\text{mol}}$ and a grafting density of 0.1 nm^{-2} , a comparable degree of swelling $d_{\text{swollen}}/d_{\text{dry}}$ can be observed for both brush systems (Figure 8.1(b)). Here the end-grafted PAA brushes were prepared as reference via hydrolysis of poly(*tert.*-butyl acrylate) end-grafted brushes [18,167].

Also the swelling of PAA-b-PS Guiselin brushes was monitored for selected pH values and no significant differences compared to the pH-sensitivity of PAA Guiselin brushes in the swelling degree could be found. Here it has to be noted, that the swelling measurements were performed starting at low pH and exchanging the buffer solutions in the liquid cell towards increasing pH. Since the concentration of Na^+ at 10 mM, chosen for the pH-sensitive swelling, is below the counter-ion concentration where all COOH groups that can dissociate at the given pH are actually dissociated, the degree of dissociation of each pH step is expected to be lower than the degree of dissociation of PAA chains in solution at the same environmental conditions. Thus the total value of the parameters for n and d as well as the degree of swelling depend on the history of the sample.

To quantify the effect of the counter-ion concentration on the swelling behavior of the Guiselin brushes, salt dependent swelling experiments in NaCl solutions were performed at pH 3, where the amount of dissociated COOH groups on PAA chains in solution is very low, and at pH 8, where for PAA chains in solution the COOH groups are expected to be dissociated to a very high degree. Results for both Guiselin brushes are presented in Figure 8.2.

The swollen brush thickness increases for both Guiselin brushes with increasing salt concen-

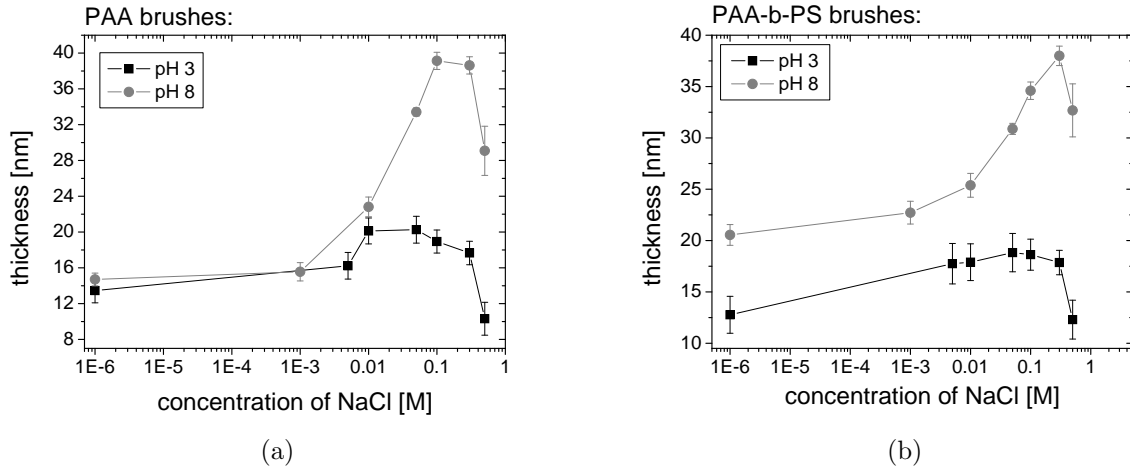


Figure 8.2.: Salt dependent swelling of PAA (a) and PAA-b-PS (b) Guiselin brushes in NaCl solutions at pH 3 and pH 8. The corresponding refractive indices can be found in the Appendix in Figure A.7.

tration until the dissociation fraction $f_{bulk}(pH)$ of the investigated pH value is achieved and decreases again in the salted brush regime. The salt concentration for maximal swelling is comparable for PAA and PAA-b-PS Guiselin brushes at both pH and lies in the range of 0.1-0.2 M for pH 8. It was found in the same region for end-grafted PAA brushes in the literature either assembled from PS-PAA block copolymers or "grafting-from" of the precursor polymer PtBA and subsequent hydrolysis [29, 238].

Differences between PAA and PAA-b-PS Guiselin brushes can be seen in comparing the measurements for pH 3 and pH 8 at salt concentrations below 0.01 M. Here a sensitivity of the swollen brush thickness on the pH could be observed for the PAA-b-PS copolymer Guiselin brushes that was not present for PAA.

For end-grafted PAA brushes Dong et al. found, that the effective bulk pKa value, the logarithmic value of the acid dissociation constant inside the brush, was at pH 6.5 - 6.6, whereas the pKa of the surface differed from the bulk value and was determined at pH 4.4 close to the pKa value found for PAA in solution at pH 4.3 [42, 237]. Thus they proved the presence of a dissociation gradient inside an end-grafted PAA brush with increased charge fraction at higher distances from the substrate surface. As possible reasons for this gradient minimization of the systems free energy [240], an inhomogeneous polymer volume fraction [241], or the formation of a double layer at the brush-solution interface, reducing the ion transport into the brush layer [241], are discussed. Hence we assume, that an influence of the PS-block on volume fraction or free energy minimum is most likely, which could possibly lead to a pH-dependent influence on the dissociation behavior of PAA in the PAA-b-PS copolymer Guiselin brushes. It would be interesting to e.g. correlate titration measurements of these brushes with a quantification of intra-polymer and polymer-solvent H-bonding to get more indices for a correct explanation of this differing swelling behavior.

To estimate the number of grafting-points per chain in these Guiselin brushes the theory of Pincus can be applied, modeling the swelling of the PAA brush with full dissociation ($f_{bulk}(pH)$) but in the absence of additional charges in solution [91] (Section 2.2.2). At the counter ion concentration of maximum swelling, the degree of dissociation in the PAA Guiselin brush was calculated according to Equation 2.5 and the average number of freely swelling monomers N_{free} per chain calculated from the swollen brush thickness (Equation 2.4). The condition of no additional charges is not fully satisfied since Cl^- co-ions are also present in solution, thus the calculation of the average number of grafting points of a PAA chain in the Guiselin brush out of the ratio $\frac{N}{N_{free}}$ remains a coarse estimation (Table 8.1). Here the PAA-b-PS chains were treated like PAA chains neglecting the small PS block.

As can be seen in Table 8.1 the values for the average grafting points per chain differ considerably between pH 3 and pH 8 due to the poor applicability of the estimation according to Equation 2.4 and a possible deviation of the dissociation constant from the value of PAA in solution [42]. However important for this work is the fraction of 1-3 COOH-groups per chain forming grafting points with the PGMA surface. Thus a nominal grafting density of $0.30 \pm 0.15 \text{ nm}^{-2}$ can be assigned to these PAA Guiselin brushes, and their swelling behavior compared to end-grafted brushes. Here the grafting density was calculated by Equation 2.2 from the dry Guiselin brush thickness of 5.4 nm, the bulk density of PAA of $1.4 \frac{\text{g}}{\text{cm}^3}$ [199], and a nominal molecular weight of $M_n/2 = 13,250 \frac{\text{g}}{\text{mol}}$, considering an average number of two grafting points per chain.

Next to the effect of pH-sensitive swelling at very low salt concentrations in solution another influence of the PS block on the Guiselin brush behavior was observed in monitoring the advancing water contact angle θ_{adv} after pretreatment of the brushes in solutions with a counter-ion concentration of $c_{Na^+} = 0.1 \text{ mM}$ at several pH (Figure 8.3).

On the one hand for a small fraction of dissociated COOH-groups at low pH θ_{adv} is 12° higher for PAA-b-PS than for PAA Guiselin brushes at pH 3, whereas a surface fraction of

Table 8.1.: Estimation of the average number of grafting points from the number of freely swelling monomers N_{free} along a PAA chain in a Guiselin brush. For the calculation of the degree of dissociation the dissociation constant for PAA in solution of $pK_a = 4.3$ was used [237], and the monomer length was calculated according to Equation 5.1.

Polymer	N	pH	α_b	d_{max} [nm]	N_{free}	grafting points per chain
PAA	386	3	0.0477	20	364	1.1
		8	0.9998	39	155	2.5
PAA-b-PS	375	3	0.0477	18.5	337	1.1
		8	0.9998	38	151	2.5

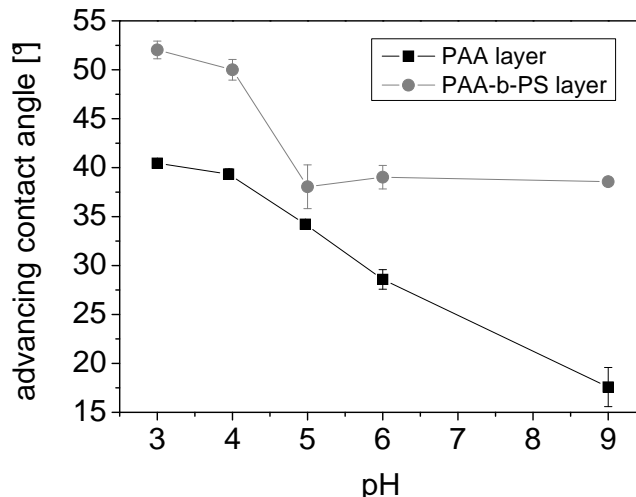


Figure 8.3.: Advancing water contact angles after pH treatment in 0.1 mM NaCl solutions compared for PAA and PAA-b-PS Guiselin brushes.

PS of 20 ± 3 % can be estimated with the help of the Cassie equation (Equation 4.16) and an advancing contact angle for PS-brushes of $\theta_{adv}^{PS} = 90^\circ$ [98]. On the other hand for $pH > 5$ a plateau value at $\theta_{adv} = 38 \pm 2^\circ$ is observed, with a PS surface fraction of 11 % after treatment at pH 6 and 17 % after treatment at pH 9, whereas for the PAA Guiselin brushes θ_{adv} decreases continually with increasing pH until a value of $\theta_{adv} = 17.5 \pm 1.5^\circ$ is achieved at pH 9.

The roughness of these brushes after treatment in 0.1 mM solutions with different pH was controlled with AFM and was below 1 nm, thus the contact angle results should not be influenced critically by the surface roughness. Since contact angle measurements probe the chemical composition of the brush in an interface region of 1-2 nm, this contact angle measurements can be taken as indication that a fraction of PS can be found in the outer region of the PAA-b-PS brush-air interface after swelling in these 0.1 mM solutions and subsequent gentle drying in nitrogen flux. Here the PAA-b-PS Guiselin brush has a total dry layer thickness of 5.7 ± 0.2 nm. Thus a concentration of the PS at the PGMA surface, as in PAA brushes, that are physisorbed by PS-blocks to a PS-surface, seems not likely. We assume for the ellipsometric modeling, that the PS-blocks are evenly distributed throughout the PAA-b-PS Guiselin brush layer.

8.2. Controlled protein adsorption and release

Since polyelectrolyte brushes or networks are promising for controlled drug delivery and the immobilization of functional biomolecules like enzymes [9, 59, 137, 140], in this chapter investigations on the protein adsorption affinity of PAA and PAA-b-PS Guiselin brushes are presented. A scheme of the electrostatic conditions in the brush-protein system below and above the isoelectric point (IEP) of the protein but always above the IEP of an acidic polymer surface can be seen in Figure 8.4.

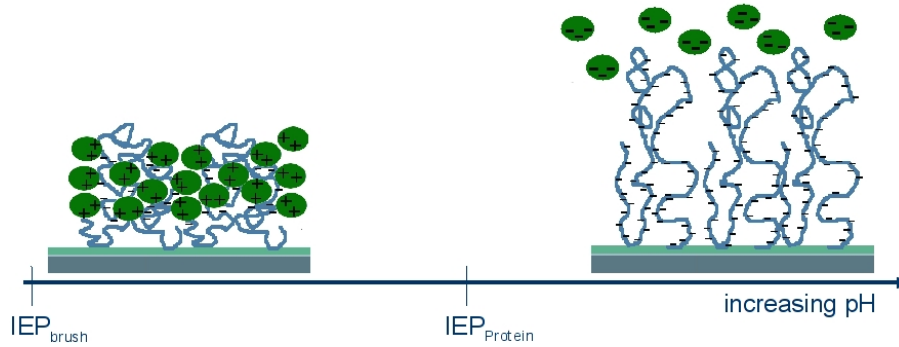


Figure 8.4.: Scheme of the electrostatic attractive conditions below the IEP of the protein and of electrostatic repulsive conditions above the IEP of the protein, not considering counter- and co-ions that are also present in the system.

The mechanism of protein adsorption on negatively charged polyelectrolyte brushes especially at the "wrong side" of the IEP of the protein was discussed in Section 3.4.1. Two theoretical concepts exist for protein adsorption at electrostatic repulsive conditions [143]. On the one hand adsorption can take place due to charge regulation on the protein molecules: Weak amino acids adopt their charged state to the environment, resulting in a charge reversal when penetrating a polyelectrolyte brush that is likewise charged as the protein in solution. On the other hand proteins are expected to replace counter-ions along the charged polymer chains. Although their net-charge would prevent adsorption onto a likewise charged surface, protein surfaces are characterized by a patchiness with a non-homogeneously charge distribution. Thus a replacement of e.g. positive counter-ions like Na^+ on a negatively charged PAA brush could be possible by positively charged patches on the adsorbing protein. This would lead to an increase of the entropy of the system, due to the release of small mobile counter-ions from the surface and immobilization of less mobile large molecules. In [143] both effects were discussed to contribute to the adsorption, whereas charge reversal is considered the dominating effect.

In the literature one comprehensive experimental and theoretical study on the adsorption of BSA onto end-grafted PAA brushes immobilized via a PS-b-PAA block copolymer can be found [59]. Here the influence of parameters like pH, chain length and grafting density as well as the salt concentration in solution was monitored with fixed-angle optical reflectometry. At 10 mM salt concentration de Vos et al. observed a maximum of adsorbed protein amount at pH 5 and a width at half maximum of approximately 2 pH values for a brush with 270 monomers per chain and a grafting density of 0.1 nm^{-2} , whereas the maximum of adsorption varies only slightly with the salt concentration and could be found for $c = 1 \text{ mM}$ to $c = 100 \text{ mM}$ in the vicinity of the isoelectric point of the investigated BSA at pH 5.4. With increasing grafting density the amount of adsorbed BSA was observed to increase from $15 \frac{\text{mg}}{\text{m}^2}$ at $\sigma = 0.05 \text{ nm}^{-2}$ to $30 \frac{\text{mg}}{\text{m}^2}$ at $\sigma = 0.30 \text{ nm}^{-2}$ measured in a 10 mM salted solution with $0.1 \frac{\text{mg}}{\text{ml}}$ BSA concentration.

8.2.1. pH sensitivity

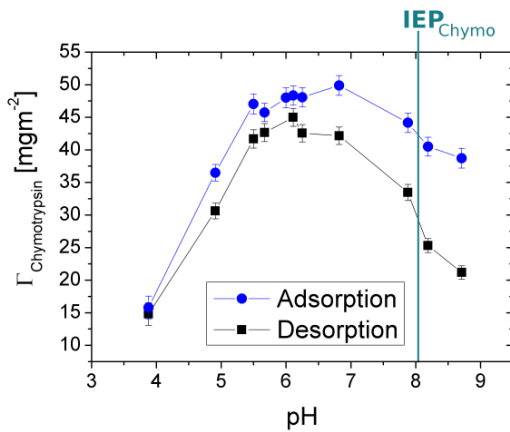
We investigated the pH-sensitive adsorption of α -chymotrypsin and human serum albumin (HSA) onto PAA Guiselin brushes and results for the adsorption in 0.25 $\frac{mg}{ml}$ concentrated protein solution (blue) and the desorption after exchanging the protein-buffer solution again to 10 mM pure buffer solution (black) are presented in Figure 8.5. HSA was also adsorbed onto PAA-b-PS Guiselin brushes to retrieve the influence of the PS-block on the adsorption of this globular protein (Figure 8.7).

Adsorption of HSA onto PAA Guiselin brushes

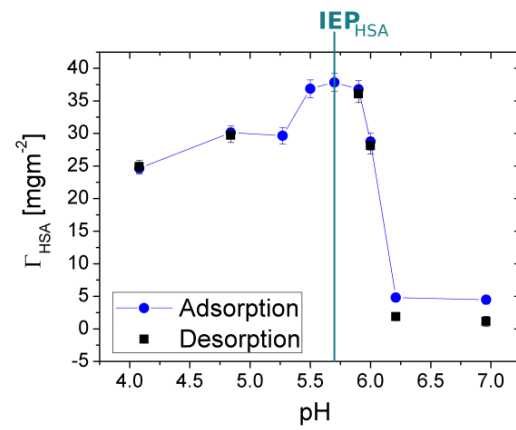
Individual adsorption measurements for fixed pH values on PAA Guiselin brushes are depicted in the Figures 8.5(b), 8.5(d) and 8.5(f). Here the qualitative dependence of the adsorbed amount on the pH for serum albumin found by de Vos et al. [59] could be reproduced with very high adsorbed amounts, presented in Figure 8.5(b), that are increasing until a maximum at the isoelectric point of the protein (pH_{IEP} at 5.7 for defatted HSA) is achieved. The width of the maximum here is approximately 1 pH value and thus smaller than for end-grafted brushes. For the latter it is discussed, that the pH inside the brush is lower than the pH at the brush-solution interface leading to a shift of the pK_a in the interior to $pK_a^{bulk} = 6.5 - 6.6$ [42]. Thus this dissociation gradient in the polyelectrolyte brush could be a possible explanation for a broad protein adsorption maximum when regarding the additional adjustment parameters of charge regulation and charge-patchiness on the protein molecules. Since for the PAA Guiselin brushes presented here the width of the maximum is considerably smaller than for end-grafted brushes this could indicate a more homogeneous dissociation behavior possibly due to a more fractal brush-solution interface as it would be expected when considering these Guiselin brushes as equivalent to a highly polydisperse end-grafted brush.

We could also model the refractive index and the layer thickness of a combined layer of protein and polymer. Here the thickness (Figure 8.5(d)) increases until pH 5.7 and the refractive index (Figure 8.5(f)) decreases. Since the overall adsorbed amount of HSA is increasing with pH this results for n and d indicate a stretching of the combined layer for higher pH values, most probably due to the increase of negative charges on the polymer chains and the protein, whereas the latter should also lead to an increase of counter-ions inside the polymer layer, thus stretching due to the increased osmotic ion pressure is also likely.

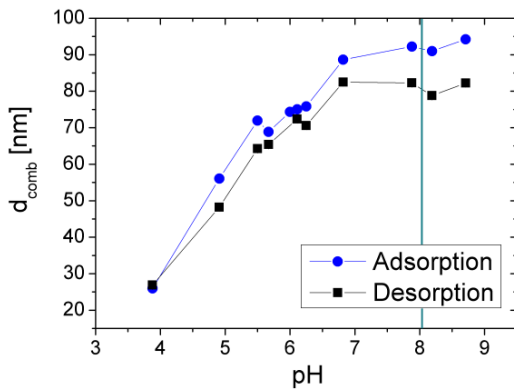
At pH values higher than the IEP of the protein the adsorbed amount starts to decrease and so does the refractive index of the combined layer. Nevertheless the thickness of this layer remains virtually constant and is more than two times higher than that of a PAA brush without adsorbed HSA at similar environmental conditions (see Figure 8.1). Here large changes in the combined protein-polymer thickness can be observed for the adsorption and the desorption



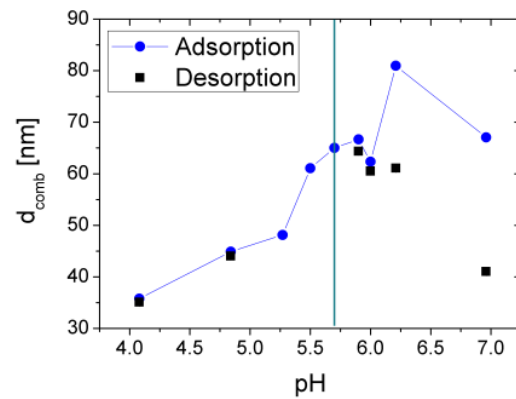
(a) Comparison of the adsorbed amount of α -chymotrypsin after adsorption and after exchange of solution



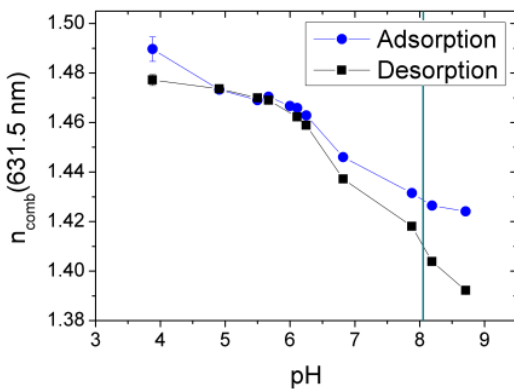
(b) Comparison of the adsorbed amount of HSA after adsorption and after exchange of solution



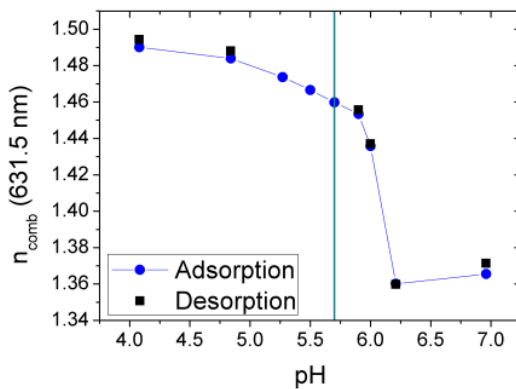
(c) Thickness for α -chymotrypsin



(d) Thickness for HSA



(e) Refractive index for α -chymotrypsin



(f) Refractive index for HSA

Figure 8.5.: pH-sensitive adsorption experiments of α -chymotrypsin and HSA onto PAA Guiselin brushes. Displayed are the adsorbed amount and the combined layer parameters upon adsorption and after exchange of the protein solution to pure buffer again.

process with a difference of 26 nm upon adsorption at pH 7. Above the $IEP_{protein}$ also the adsorbed amount differs between adsorption and desorption, indicating an increased effect of diffusion of protein molecules, due to a concentration gradient between protein solution and protein-brush surface, on the adsorption at the "wrong side" of the IEP.

A very sharp decrease of adsorption capacity can be found in comparing the values of Γ for pH 6 and 6.2. Here the adsorbed amount decreases about 93 % when considering Γ after desorption. It is also interesting, that the refractive index of the combined polymer-protein layer undergoes a minimum around pH 6.2 that is lower than the corresponding refractive index of the PAA brush at this pH, whereas for pH 7 the refractive index n_{comb} is increased again. Here the latter points to a higher stretching of the PAA chains in the presence of HSA molecules than in the corresponding swollen PAA Guiselin brush.

Finally the volume fraction of HSA in the combined polymer-protein layer was derived and is displayed in Figure 8.6(b). Here a volume fraction of 45 % could be monitored at pH 5.7 where Γ_{max} was obtained. No distinction is made between protein inside the brush and adsorbed on the brush-solution interface and especially at the IEP of the protein, multilayer adsorption is possible [242]. In [59] a BSA volume fraction of 30 % at the maximum adsorbed amount was estimated in assuming a PAA brush height equal to the PAA chain contour length. Since the swollen brush thickness and refractive index as well as changes in these parameters upon protein adsorption cannot be measured with optical reflectometry, in-situ spectroscopic ellipsometry provides additional data on the surface layer composition before and after adsorption.

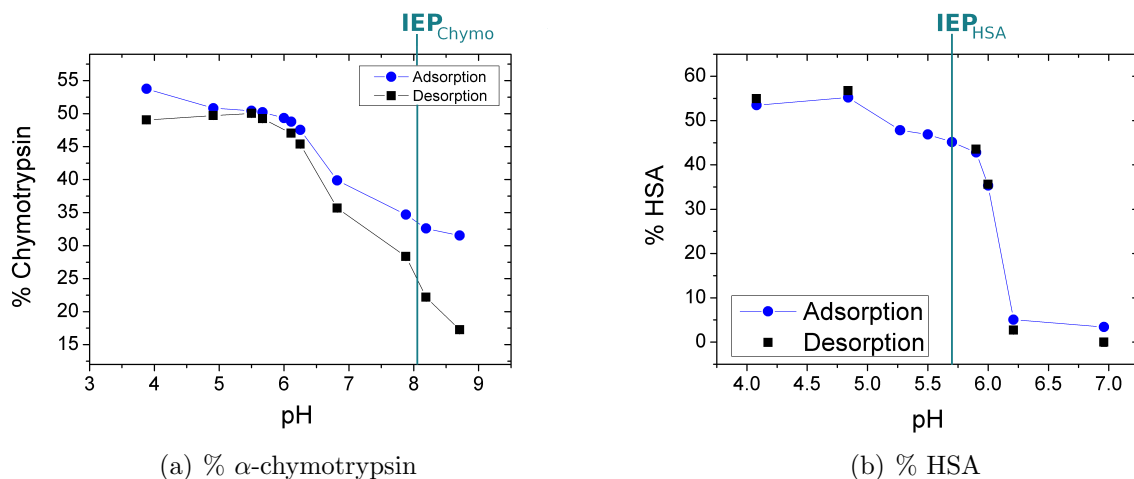


Figure 8.6.: Protein volume fractions of α -chymotrypsin and HSA.

Protein volume fractions of α -chymotrypsin and HSA in a combined polymer-protein layer at different pH.

Adsorption of α -chymotrypsin onto PAA Guiselin brushes

The pH-sensitive adsorption behavior of α -chymotrypsin ($pH_{IEP}^{chymo} = 8.1$) was monitored to retrieve the influence of the IEP of the protein upon adsorption on these PAA brushes. Results for the adsorption of this protein can be found in Figure 8.5(a), 8.5(c) and 8.5(e). Contrary to the adsorption of HSA the maximal adsorbed amount Γ_{max} is not in the region of the pH_{IEP}^{chymo} but can be found in the range of pH 6. Here a distinctive difference between adsorption and desorption is present. For the experimental part of adsorption, Γ_{max} can be found broadly centered around pH 7, whereas after desorption in pure buffer solution Γ_{max} is centered around pH 6 and differences in Γ between adsorption and desorption increase with increasing pH.

This behavior can be qualitatively understood when regarding the pH-dependent charge situation of α -chymotrypsin in solution. Dissociation constants (pK) for $COOH$ and NH_3^+ containing side chains in the protein can be found in the region of pH 3-4 and pH 9-10, respectively, whereas environmental conditions, like other charges in vicinity or hydrophilic / hydrophobic neighboring groups affect the pK-value. Thus at low pH this protein contains a large amount of positive NH_3^+ groups and is positively charged, adsorbing via electrostatic attraction at the PAA brush surface. When increasing the pH $COOH$ -groups start to dissociate, leading to negatively charged groups and the amount of positive charges decreases until at the IEP of this protein the amount of positive and negative charges is equal. Additionally the amount of negative charges at the brush surface, also due to dissociation of $COOH$ groups, increases. The maximum of α -chymotrypsin adsorption at intermediate pH could now be understood as a consequence of equal densities of negative charges at the brush surface and positive charges at the protein molecules plus a diffusion (thus protein concentration) controlled effect that accounts for the differences between Γ after adsorption and desorption. The decrease of Γ towards higher pH would be due to a strong decrease in positive charges ($NH_3^+ \rightarrow NH_2$), whereas the amount of COO^- groups is expected to increase only marginally at $pH > 6$.

Unlike the adsorption of HSA at this PAA brushes, where Γ_{max} could be found at the isoelectric point of the protein, here for α -chymotrypsin Γ_{max} seems to be determined by equal densities of opposite charges on the brush surface and on the protein molecules, where supposedly the incorporation of additional ions to remain charge neutrality, is minimized [109]. Here detailed information on the charge density at the surface and on the protein molecules in solution would be necessary to discuss the adsorption behavior comprehensively.

Although Γ decreases above pH 6 - 7, the combined polymer-protein layer thickness after adsorption increases over the whole pH range, spanning a difference of 68 nm between pH 3.8 and pH 8.7. Interestingly d_{comb} stays constant at 82 nm after desorption for all investigated pH values above pH 6.8, which could be due to a completed dissociation of $COOH$ -groups along the PAA chains, thus the density of possible adsorbing sites at the surface is constant above this pH. Refractive indices and the protein volume fraction decrease over the whole pH range, whereas two regimes are visible, the first one with only marginal decrease until pH 6 and

the second with more changes above pH 6. Together with the plateau in the combined layer thickness above pH 6.8 after desorption, a decrease in the adsorbed amount between pH 6.8 and pH 8.7 is reflected in the thickness and refractive index data. Differences in the protein volume fraction after adsorption and desorption increase above pH 6 in accordance to the results for Γ with a difference of 2.2 % at pH 6.25 and 14.3 % at pH 8.7.

Adsorption of HSA to PAA-b-PS Guiselin brushes

To conclude this section HSA was adsorbed on PAA-b-PS Guiselin brushes to retrieve the influence of the PS block on the adsorption behavior of this protein (Figure 8.7).

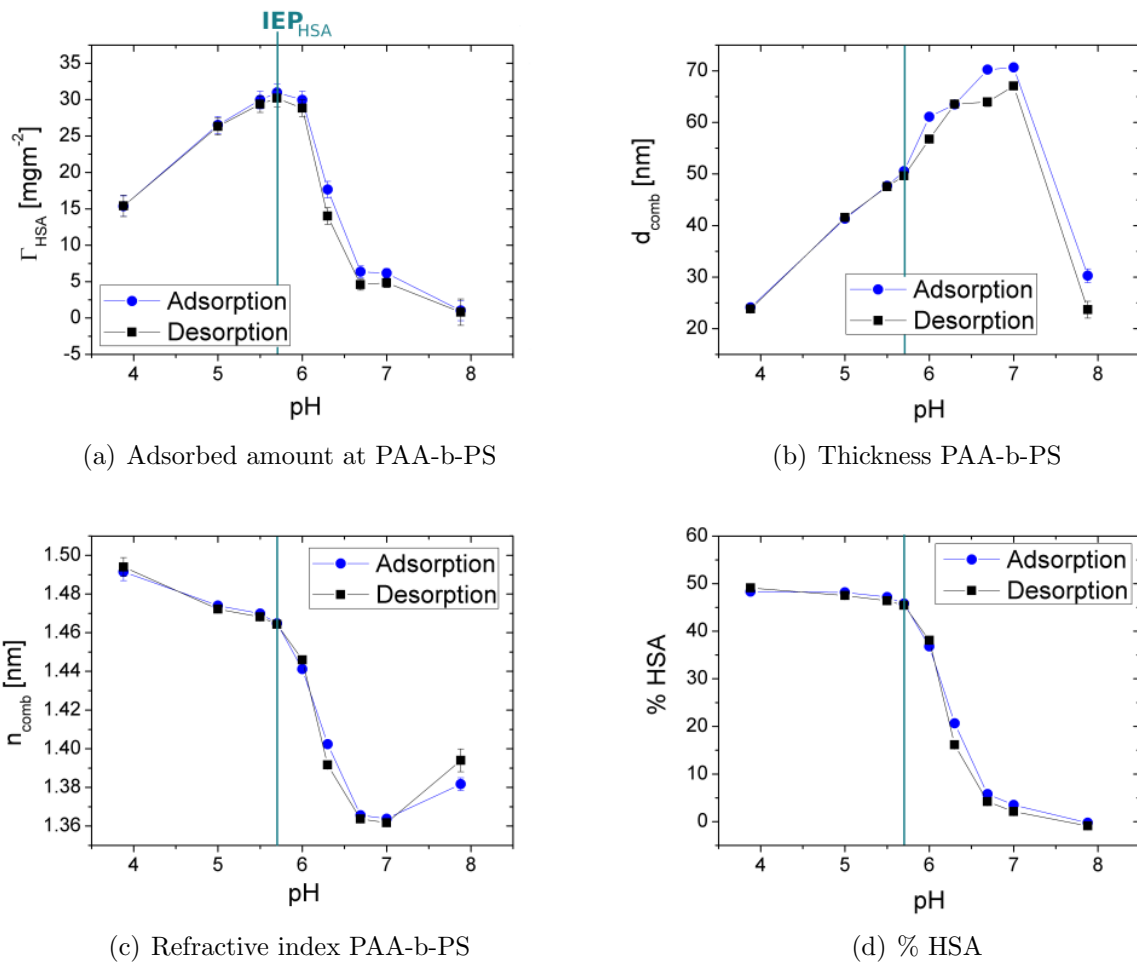


Figure 8.7.: HSA adsorption at PAA-b-PS Guiselin brushes in 10 mM buffer solutions monitoring the adsorbed amount of protein (a), layer parameters (b,c) and layer composition (d) after adsorption of HSA from a $0.25 \frac{mg}{ml}$ protein solution in 10 mM buffer and after exchanging the solution to pure buffer and subsequent desorption.

A similar pH-dependency as for the adsorption on PAA Guiselin brushes is observed. However total Γ -values are slightly smaller and the width of Γ_{max} is larger. Also there is no significant difference between Γ after adsorption and desorption, whereas at pH 7 a slightly higher remaining amount of $4.8 \pm 0.5 \frac{mg}{m^2}$ could be detected after desorption compared to HSA on PAA

Guiselin brushes where the HSA amount was reduced to $1.1 \pm 0.5 \frac{mg}{m^2}$ at this pH after exchanging the protein solution to pure buffer.

A larger difference in Γ of $13.0 \pm 1 \frac{mg}{m^2}$ can be found at pH 6.2 when comparing the adsorbed amount after the adsorption process at both brushes. Here the small PS-block could lead to a shift in the critical pH, where no adsorption at the "wrong side" of the IEP of the protein takes place, to higher pH. This behavior is also reflected in an increasing combined layer thickness up to pH 7 both after adsorption and desorption, whereas for PAA Guiselin brushes d_{comb} after desorption dropped considerably starting at pH 6.

Finally a decrease in Γ comparable to the protein amount at pH 7 at PAA Guiselin brushes can be found at pH 8, accompanied by a pronounced decrease in the combined layer thickness and an increase in the refractive index. For the latter a minimum could be found around pH 7 with $n_{comb}(631.5nm) = 1.363$, again smaller than observed for swollen PAA-b-PS Guiselin brushes without protein (Figure 8.1).

8.2.2. Dependency on the amount of PAA

Since we are interested in the adsorption behavior of mixed brushes with different polymer ratios, the dependency of the adsorbed amount of HSA on the amount of PAA in a Guiselin brush shall be discussed briefly in this section. In Figure 8.8(a) the increase of Γ_{HSA} with the PAA amount at the surface is displayed upon adsorption at pH 6 for Guiselin brushes with $\Gamma_{PAA} = 3 \frac{mg}{m^2}$ to $\Gamma_{PAA} = 9.8 \frac{mg}{m^2}$.

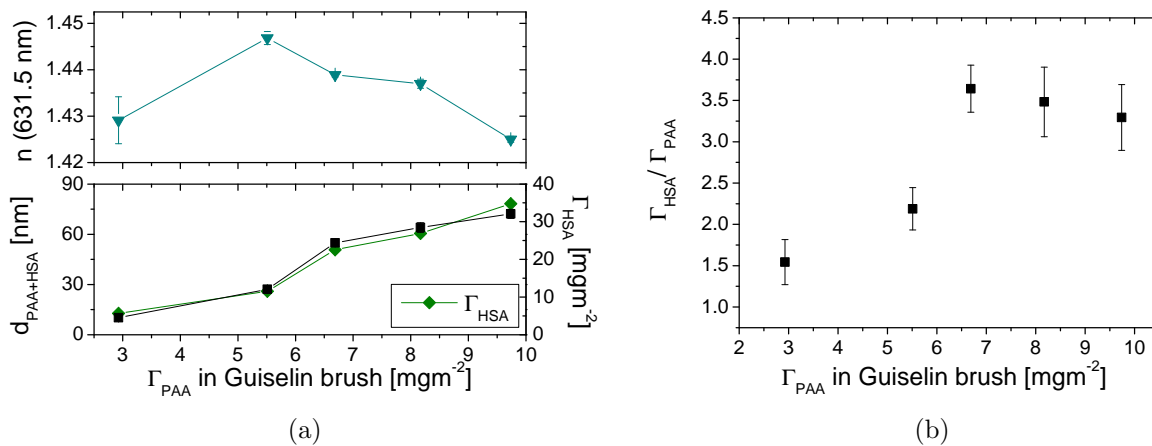


Figure 8.8.: Adsorbed amount of HSA and layer parameters n and d dependent on the PAA amount grafted to the surface (a) and specific adsorbed amount $\frac{\Gamma_{HSA}}{\Gamma_{PAA}}$ (b).

Here the combined polymer-protein layer thickness increased almost linear, whereas the refractive index $n_{comb}(631.5nm)$ varied between 1.425 and 1.446. The specific adsorbed amount as displayed in Figure 8.8(b) is in the range between 1 and 4, with a constant binding capacity of HSA of $\frac{\Gamma_{HSA}}{\Gamma_{PAA}} = 3.5 \pm 0.3$ at high Γ_{PAA} in the given error region. The decrease in $\frac{\Gamma_{HSA}}{\Gamma_{PAA}}$ with decreasing amount of PAA could be due to different effects in the grafting process of these very

thin PAA films. The amount of PAA grafted to the surface was controlled via the concentration of the solution spin-coated beforehand, thus different PAA concentrations in the grafting process could lead to an increased amount of grafting points for small Γ_{PAA} . PAA films with smaller amounts could not be prepared as homogeneous layers and an increasing influence of the surface and the PGMA anchoring layer on HSA adsorption would have to be considered, disturbing the dependency of Γ_{HSA} on Γ_{PAA} .

8.3. Quantification of coupled buffer components: A simultaneous SE - QCM-D study

Coupled spectroscopic ellipsometry (SE) and quartz crystal microbalance measurements with dissipation mode (QCM-D) were performed to obtain kinetic informations about changes in the amount of buffer components (water molecules and counter- as well as co-ions) coupled to the PAA brushes upon salt and pH dependent swelling and adsorption of the protein bovine serum albumin (BSA). The work was done in cooperation with the ellipsometry group of the Department of Electrical Engineering at the University of Nebraska-Lincoln, USA [243].

In the literature combined SE-QCM-D measurements were, for example, used to derive the amount of water molecules coupled to polyelectrolyte multilayers [244], to investigate the swelling of polystyrene brushes in cyclohexane [245], and to quantify changes in the water content of a protein layer upon cross-linking [180].

Also changes in the shear viscosity can be evaluated from the dissipation measurements and thus can be discussed together with changes in the swollen brush thickness and refractive index here, combining the monitoring of optical and mechanical response.

PAA Guiselin brushes were prepared on quartz crystals coated with a 100 nm thick gold layer in firstly spin-coating and crosslinking PGMA on the crystal with a thickness of $d = 2 \pm 0.5 \text{ nm}$ and secondly spin-coating and grafting the PAA chains according to the procedure described in Section 5.4 with subsequent extraction of non-grafted polymers and a PAA layer thickness of $5.3 \pm 0.5 \text{ nm}$. For the adsorption studies bovine serum albumin (BSA) rather than HSA from the human body was taken due to the high amount of protein that is needed in flow experiments. Here BSA is expected to adsorbed similar to HSA onto PAA Guiselin brushes, because of its similar structure and physico-chemical interface properties.

Course of experiments

Adsorption was performed at 1 mM (100 mM) salt concentration below the IEP of BSA ($pH_{IEP} = 5.6$, defatted BSA [246]) at pH 5.2 and above the IEP of the protein at pH 6. Protein adsorption was monitored for overall electrostatic attractive and repulsive conditions, respectively. Experiments were carried out by starting with the PAA brush in water, then

exchanging the solution in constant flow at $(0.4 \frac{ml}{min})$ to 1 mM (100 mM) salted solution. Afterwards, the solution was stagnant for 20 min and exchanged to $0.1 \frac{mg}{ml}$ protein solution by increasing the flow gradually until a constant flow $(0.4 \frac{ml}{min})$ was reached again, and the solution in the measurement chamber was exchanged after approximately 8 min. A volume of more than 10 ml protein solution was pumped through the cell with laminar flow above the brush-solution interface, and adsorption was monitored for at least 25 min. When changes in the layer thickness d_{SE} grew smaller than $1 \frac{nm}{min}$ the protein solution was exchanged again to the pure buffer solution and changes in the combined polymer-protein layer were monitored in the absence of protein in the salted solution. Finally desorption was performed at pH 7.6 at increased electrostatic repulsive conditions.

8.3.1. Modeling of combined spectroscopic ellipsometry (SE) and QCM-D data

Spectroscopic ellipsometry data

For the PAA Guiselin brush modeling of Δ and $\tan \Psi$ was done according to an optical box model consisting of the gold substrate, a PGMA and a PAA layer. The dispersion of the gold substrate was fitted to a B-spline function and Δ -offsets of the windows determined before coating the crystal with PGMA and PAA [181]. The thicknesses of the PGMA layer and the dry PAA layer (see above) were fitted using dispersion relations measured for thick bulk layers, with $n_{PGMA}(631.5nm) = 1.525$ and $n_{PAA}(631.5nm) = 1.522$. For the swollen PAA layer both thickness and refractive index could be modeled using a two parameter Cauchy relation for $n(\lambda)$.

The amount Γ_{SE}^b of buffer solution in the swollen PAA layer was evaluated to

$$\Gamma_{SE}^b = f_b \cdot \rho_b \cdot d_{PAA} . \quad (8.1)$$

Here f_b is the buffer fraction in the swollen PAA layer with a thickness d_{PAA} modeled by a two component effective medium approach according to Bruggeman, using the dispersion relation for dry PAA (component one) and for the buffer solution (component two). The density of the buffer solution ρ_b was set to $1 \frac{g}{cm^3}$ due to the usage of low salted aqueous solutions. To allow comparison with the QCM-D data, changes $\Delta\Gamma_{SE}^b = \Gamma_{SE}^b - \Gamma_{SE}^w$ will be discussed, with Γ_{SE}^w the amount of water inside the box layer for the brush already swollen in water, calculated in the same manner as Γ_{SE}^b (Equation 8.1).

For the in-situ protein adsorption the box model was maintained, whereas instead of the PAA layer, thickness d_{comb} and refractive index n_{comb} of a combined PAA-BSA layer were modeled, because protein can be assumed to penetrate into the PAA brush [136]. The adsorbed amount of protein Γ_{SE}^{BSA} was evaluated with the modified de Feijter approach as presented in Section

6.3.4, whereas Γ_{SE}^{BSA} is obtained by subtracting the amount of the brush polymer Γ_{PAA} from the amount of the combined polymer-protein layer after adsorption.

Quartz crystal microbalance data

Frequency and dissipation shifts for the odd overtones $m = 3, 5, \dots, 11$ were measured with reference to the PAA brush already swollen in water. Δf_m and ΔD_m for the above overtones were fitted to a Voigt-Voinova model of one viscoelastic layer [177, 178, 180], using the software QTools (Q-Sense, Frölunda, Sweden). In the Voigt-Voinova model the combined polymer-protein film is described as a viscoelastic layer with uniform density and a complex shear modulus as described in Section 4.4. Thus an additional energy dissipation and a frequency (overtone)-dependent response of this viscoelastic layer can be utilized to model viscoelastic thickness d_{visc} , viscosity η and shear modulus $\Delta\mu$ individually.

Since we started with the PAA Guiselin brush already swollen in water, changes in the viscoelastic thickness Δd_{visc} were evaluated for a fixed layer density ρ_l of $1 \frac{g}{cm^3}$, reflecting changes in the viscoelastically coupled amount $\Delta\Gamma_{QCMD}$ with respect to the brush in water ¹:

$$\Delta\Gamma_{QCMD} = \rho_l \cdot \Delta d_{visc} . \quad (8.2)$$

For the evaluation of protein experiments $\Delta\Gamma_{QCMD}^{ads} = \Delta\Gamma_{QCMD} - \Delta\Gamma_{QCMD}^b$ was introduced, subtracting changes in the coupled buffer amount $\Delta\Gamma_{QCMD}^b$ due to the initial swelling in the buffer solution from the total amount of coupled molecules $\Delta\Gamma_{QCMD}$ upon protein adsorption. Thus a direct comparison of changes in the viscoelastically coupled amount (buffer and protein molecules) in the adsorption process to the adsorbed amount of protein Γ_{SE}^{BSA} is possible, leading to quantitative information on the changes in coupled buffer molecules $\Delta\Gamma_{buffer}^{ads} = \Delta\Gamma_{QCMD}^{ads} - \Gamma_{SE}^{BSA}$ in adsorption and desorption of protein. Density and viscosity of the buffer solutions were set to the values known for water. Additionally, for the protein adsorption experiments, changes in the shear viscosity of the film were evaluated.

8.3.2. pH- and salt sensitive swelling

Swelling of PAA Guiselin brushes will be discussed for two pH values and two salt concentrations. First the measured parameters in QCM-D, frequency shift Δf and dissipation shift ΔD for the measured overtones are displayed in Figure 8.9(a) and 8.9(b) for the swelling in 1 mM buffer solution at pH 5.2; Δf shifts are normalized by the overtone number m , respectively.

Large changes in both parameters indicate considerably increase of the viscoelastically coupled amount to the brush surface and that modeling of the layer thickness by a viscoelastic model is appropriate [178].

¹We found no differences when modeling Δd_{visc} or the total viscoelastic thickness d_{visc} , whereas since all kinetic measurements were started with the brush in water ($\Delta f^{start} = \Delta D^{start} = 0$), for the modeling of total values (starting point: gold surface) high offsets have to be added to Δf and ΔD , leading to very high fitting errors.

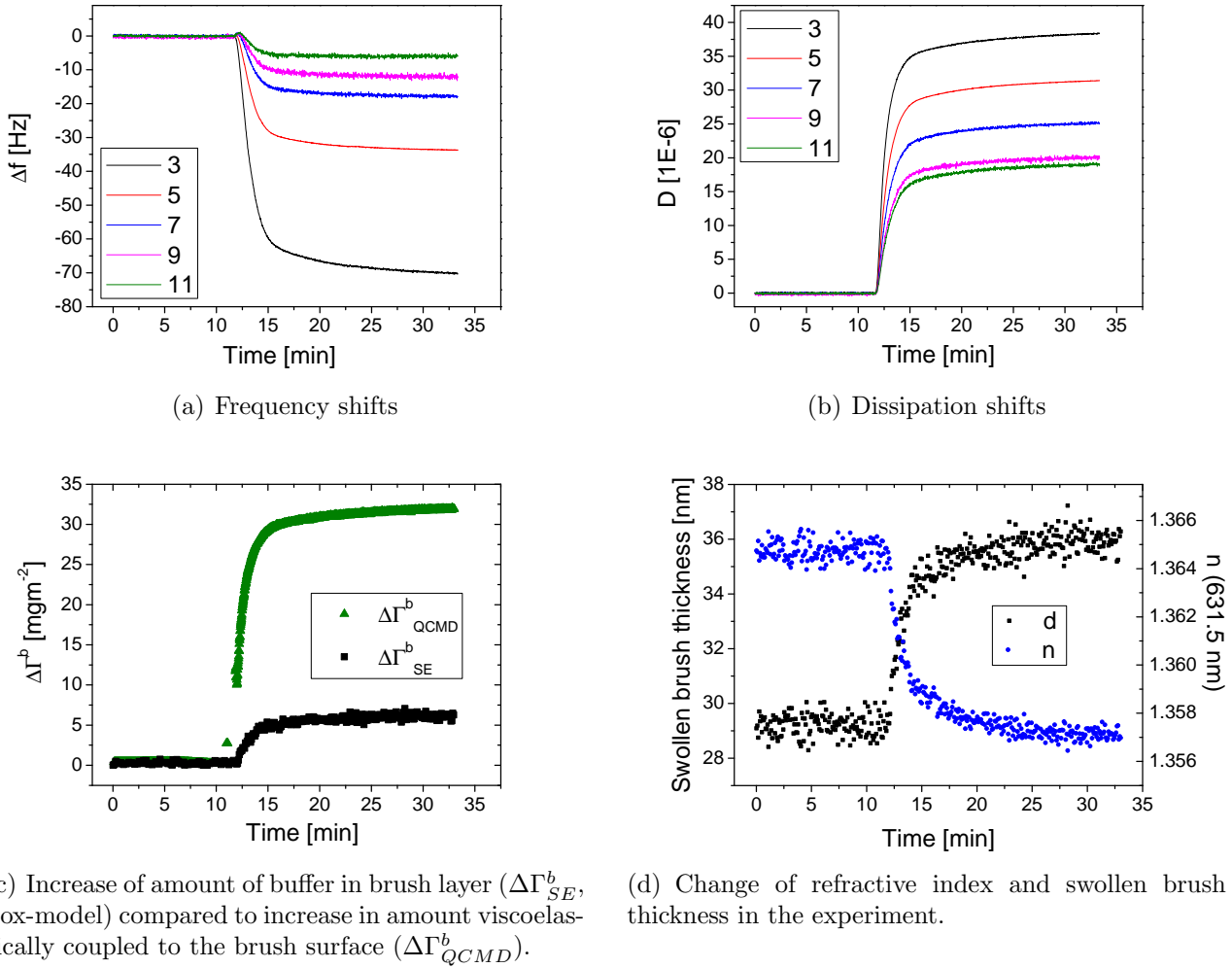
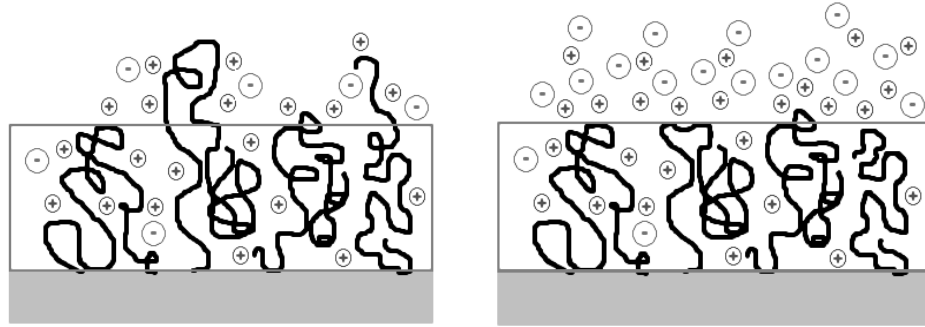


Figure 8.9.: Example of a combined in-situ swelling experiment of salt dependent swelling upon change from water to 1mM buffer solution at pH 5.2.

The change in viscoelastically coupled amount $\Delta\Gamma_{QCMD}^b$ is plotted together with the increase in the amount of buffer inside the modeled box layer from SE measurements in Figure 8.9(c). A large difference between the amount $\Delta\Gamma_{SE}^b$ inside the SE-box layer and $\Delta\Gamma_{QCMD}^b$ is visible. One explanation for this behavior could be the increased contrast of the acoustic QCM-D method [245]. Single PAA chains are suspected to protrude into the buffer solution to a higher extent than indicated by the thickness of the swollen brush modeled from SE measurements and QCM was discussed to be sensitive to these dilute regions of the polymer segment density profile (Figure 8.10(a)) [245]. Another reason could be changes in the electrical double layer due to an increased dissociation of COOH-groups as well as a different counter- and co-ion density at the brush-solution interface in 1 mM salted solution compared to water (Figure 8.10(b)).

Additionally the modeling of $\Delta\Gamma_{SE}^b$, and thus the difference $\Delta\Gamma_{QCMD}^b - \Delta\Gamma_{SE}^b$, provides information of the increase in the amount of buffer molecules that are coupled to the brush-solution interface, in contrast to the amount inside the brush, as given by the SE box model.



(a) Higher $\Delta\Gamma_{QCMD}^b$ due to protruding PAA chains.

(b) Higher $\Delta\Gamma_{QCMD}^b$ due to dimensions of electrical double layer.

Figure 8.10.: Schemes of possible states of the brush surface, leading to differences in $\Delta\Gamma_{SE}^b$ and $\Delta\Gamma_{QCMD}^b$. Displayed are the PAA chains with dissociated groups (black), whereas COO^- groups are not separately marked, and counter- as well as co-ions (gray). For these Guiselin brushes 1-3 grafting points could be concluded from salt-dependent swelling experiments in Section 8.1.

The amount of PAA at the surface is in our case $7.6 \frac{mg}{m^2}$.

This salt sensitive swelling in 1 mM solution is reflected in 8.9(d) by an increase in the brush thickness d_{SE} from 29 nm to 36 nm and a decrease in the refractive index $n(631.5 \text{ nm})$ from 1.365 to 1.357. Interestingly the total values for d_{SE} both in water and in 1 mM salted solution are noticeably higher than they would be expected from the salt sensitive measurements displayed in Figure 8.2. We refer this phenomenon to the usage of a gold substrate here and measurements in flow rather than in stagnant solution.

Changes in the viscoelastically coupled amount as well as the buffer amount in the box-layer were also evaluated for swelling in 100 mM solution and at pH 6. In Figure 8.11 the results for both pH and salt concentrations are displayed.

Here a decrease in $\Delta\Gamma_{QCMD}^b$ is observed in 100 mM salted solution compared to swelling in 1 mM for both pH, although the swollen brush thickness d_{SE} is higher at 100 mM and thus the amount of buffer inside this box-layer is increased compared to swelling in 1 mM. This observation favors an influence of the electrical double layer on the difference between $\Delta\Gamma_{QCMD}^b$ and $\Delta\Gamma_{SE}^b$ since the extension of the electrical double layer decreases with increasing salt content. The roughness or diffuse transition of the swollen brush layer-solution interface on the other hand is expected to increase with increasing swollen brush thickness because of a decreasing refractive index and thus a lower contrast between brush layer and aqueous solution. If dangling polymers would contribute significantly to the differences between $\Delta\Gamma_{QCMD}^b$ and $\Delta\Gamma_{SE}^b$, an increase of $\Delta\Gamma_{QCMD}^b - \Delta\Gamma_{SE}^b$ would be expected, contrary to the observed results.

However the Debye length κ^{-1} , which is characteristic for the extension of an electrical double layer above a surface, is roughly one order of magnitude smaller than the observed changes in the viscoelastic thickness Δd_{visc} (the viscoelastically coupled amount $\Delta\Gamma_{QCMD}^b$).

The total values for $\Delta\Gamma_{QCMD}^b$ and $\Delta\Gamma_{SE}^b$ are higher upon swelling at pH 6 than at pH

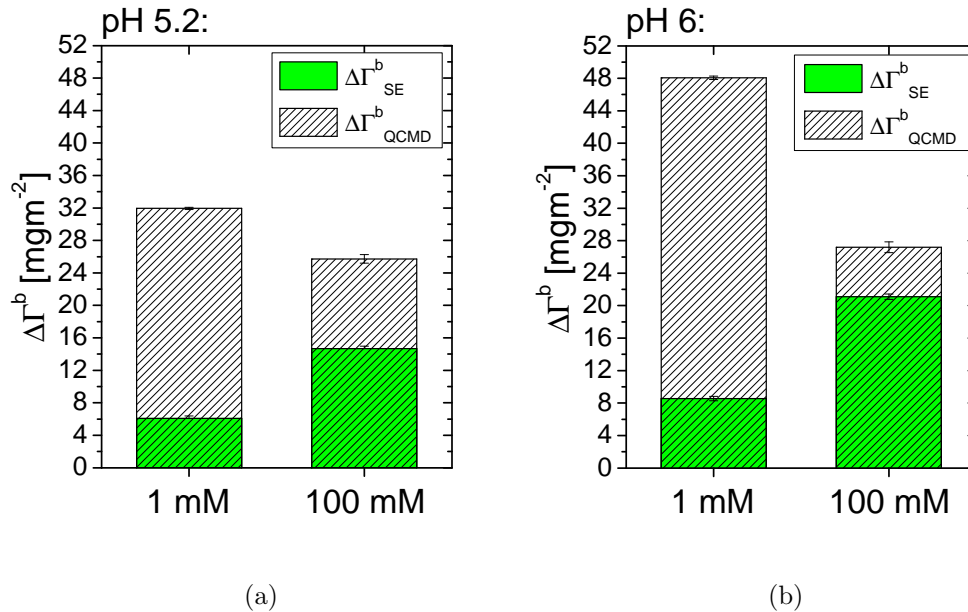


Figure 8.11.: Increase in the viscoelastically coupled amount derived from QCM-D and in the buffer amount inside the brush derived from SE for swelling at pH 5.2 (a) and pH 6 (b) in 1 mM and 100 mM buffer solutions. All values are referenced to the brush already swollen in water.

5.2 as could be expected due to a higher degree of dissociation of the COOH groups on the brush polymers. Interestingly the difference in $\Delta\Gamma^b_{QCMD}$ is increased as well, pointing to the importance of surface charges on this salt dependent swelling effect.

8.3.3. BSA adsorption below IEP of protein

In Figure 8.12 the adsorbed amount of protein Γ_{SE}^{BSA} derived from SE-measurements, changes in the amount of protein and buffer molecules $\Delta\Gamma_{QCMD}^{ads}$ viscoelastically coupled to the brush surface, and changes in the coupled buffer amount $\Delta\Gamma_{buffer}^{ads}$ are displayed, starting with adsorption in 0.1 $\frac{\text{mg}}{\text{ml}}$ protein solution (I), desorption in the corresponding buffer solution at pH 5.2 (II) and desorption in 1 mM buffer solution at pH 7.6 (III). Since $\Delta\Gamma_{QCMD}^{ads}$ is referenced to the brush swollen in the buffer, negative $\Delta\Gamma_{QCMD}^{ads}$ imply a reduction of the viscoelastically coupled amount compared to the brush in 1 mM salted solution.

In Field I of Figure 8.12 a different rate of increase for Γ_{SE}^{BSA} and $\Delta\Gamma_{QCMD}^{ads}$ can be observed. In fact $\Delta\Gamma_{QCMD}^{ads}$ first decreases before it increases again considerably faster than Γ_{SE}^{BSA} . Since the SE data is evaluated according to de Feijter, solely the increase of the adsorbed amount of protein is monitored, making the observation highly interesting. In $\Delta\Gamma_{QCMD}^{ads}$ both the increase of the coupled amount of protein and changes in the coupled amount of buffer components are reflected. Thus to the best of our knowledge differences between $\Delta\Gamma_{QCMD}^{ads}$ and Γ_{SE}^{BSA} reflect changes in the viscoelastically coupled amount of counter- and co-ions as well as water

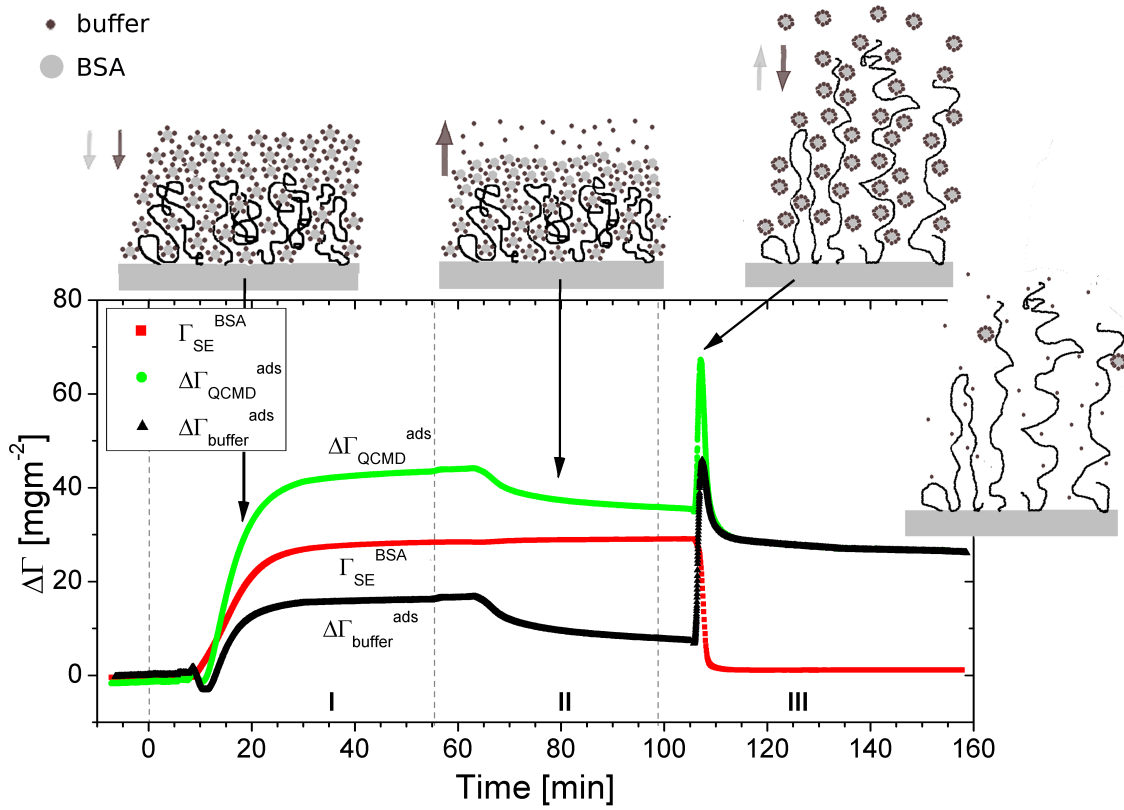


Figure 8.12.: Adsorbed amount of protein Γ_{SE}^{BSA} , changes in the amount viscoelastically coupled to the brush surface $\Delta\Gamma_{QCMD}^{ads}$ and changes in the amount of coupled buffer components $\Delta\Gamma_{buffer}^{ads}$. Measurements are referenced for clearer presentation to the brush surface in buffer solution, displaying (I) adsorption in $0.1 \frac{mg}{ml}$ protein solution, (II) desorption in 1 mM buffer solution at pH 5.2 and (III) desorption in 1 mM buffer solution at pH 7.6. Dotted lines indicate starting times of the pump for the exchange of solution, whereas the new solution reaches the brush surface delayed about 8 min due to the tubing and the gradual increase of flow. Corresponding frequency shifts and dissipation values can be found in the appendix in Figure A.10.

molecules. Here a small increase of $\Delta\Gamma_{buffer}^{ads}$ between 7.5 and 9 min followed by a noticeable decrease from 9 to 11 min is visible. We refer this feature to the exchange of solution in the measurement chamber. However the decrease in $\Delta\Gamma_{buffer}^{ads}$ from 9 to 11 min indicates a removing of viscoelastically coupled molecules from the surface, possibly due to the exchange of coupled buffer components to protein molecules. The subsequent increase in $\Delta\Gamma_{QCMD}^{ads}$ with a higher rate than observed for Γ_{SE}^{BSA} can be well understood considering the absorption of hydrated protein molecules with a surrounding electrical double layer to the brush surface. Here the additional contribution due to ions and water molecules amounts to $16 \pm 1 \frac{mg}{m^2}$ compared to the pure brush in 1 mM solution.

Interestingly when exchanging the solution to 1 mM salted solution again (Field II), although the amount of protein at the surface (Γ_{SE}^{BSA}) stays constant, $\Delta\Gamma_{QCMD}^{ads}$ decreases. Thus ions and

water molecules are released from the surface.

The decrease in $\Delta\Gamma_{buffer}^{ads}$ is accompanied by an increase in the total refractive index and a decrease in the combined polymer-protein layer thickness (Figure 8.13), indicating a contraction of this polymer-protein layer within this box-model picture. But also a sharpening of the polymer-protein - solution interface could possibly lead to this results for n and d .

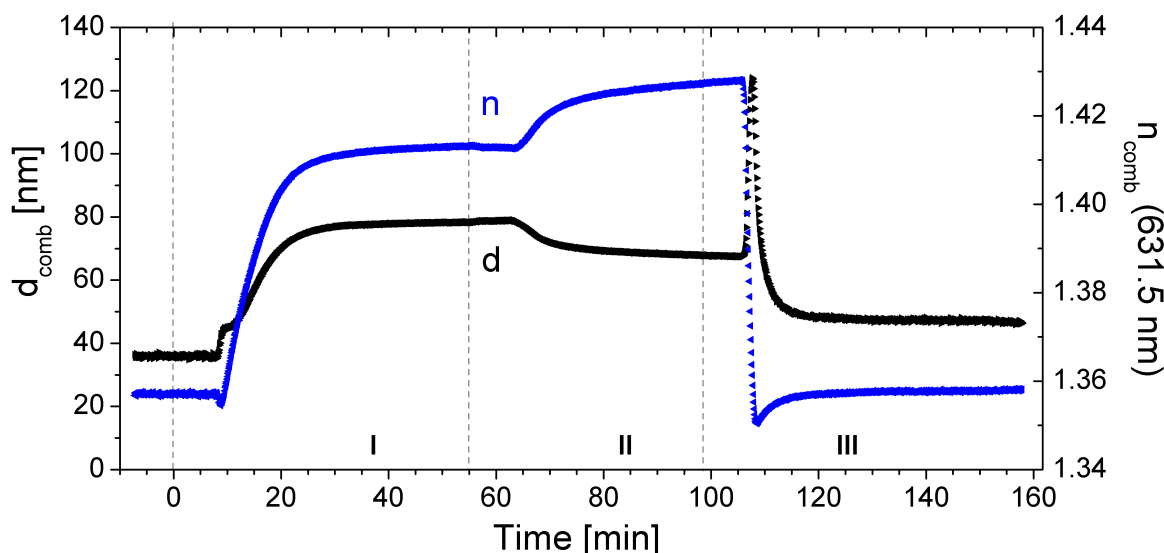


Figure 8.13.: Total refractive index $n_{comb}(\lambda = 631.5 \text{ nm})$ and combined polymer-protein layer thickness d_{comb} , corresponding to the measurements presented in Figure 8.12.

Finally BSA is desorbed in exchanging the 1mM solution at pH 5.2 to a 1 mM solution at pH 7.6 (Field III). The desorption process can be monitored, where upon the decrease in Γ_{SE}^{BSA} first a significant increase in $\Delta\Gamma_{QCMD}^{ads}$ and thus in $\Delta\Gamma_{buffer}^{ads}$ occurs. This behavior can be explained in an additional coupling of buffer molecules in the desorption process due to a temporarily strong stretching of the polymer-protein layer before protein molecules start to desorb. This stretching can also be found from the sharp increase in d_{comb} that accompanies the increase in $\Delta\Gamma_{QCMD}^{ads}$. It is also to be noted that after desorption of the protein, $\Delta\Gamma_{QCMD}^{ads}$ remains at a relatively high value at $26.4 \frac{mg}{m^2}$, stating the difference in viscoelastically coupled amount of buffer between pH 5.2 and pH 7.6 due to an increase of dissociated COO^- groups along the PAA chains.

8.3.4. BSA adsorption above IEP of protein

The adsorption experiment was repeated in the same way at pH 6 to determine changes in the amount of coupled buffer components upon adsorption at the "wrong side" of the IEP of BSA (pH 5.6), and in Figure 8.14 changes in Γ_{SE}^{BSA} , $\Delta\Gamma_{QCMD}^{ads}$ and $\Delta\Gamma_{buffer}^{ads}$ are displayed.

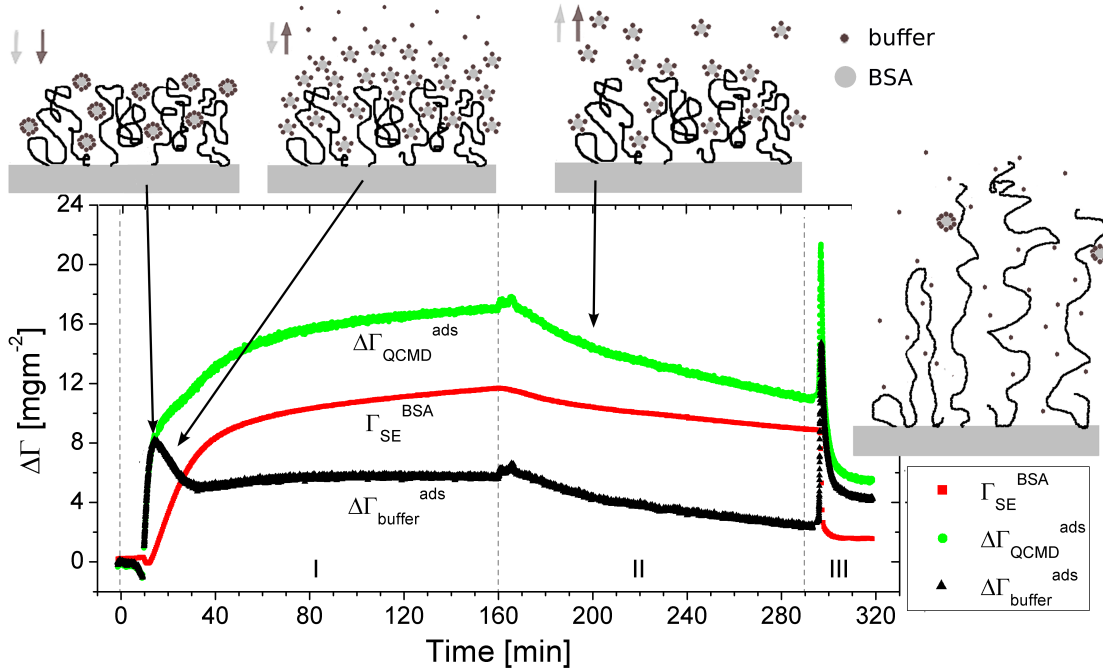


Figure 8.14.: Adsorbed amount of protein Γ_{SE}^{BSA} , changes in the amount viscoelastically coupled to the brush surface $\Delta\Gamma_{QCMD}^{ads}$ and changes in the amount of coupled buffer components $\Delta\Gamma_{buffer}^{ads}$. Measurements are referenced for clearer presentation to the brush surface in buffer solution, displaying (I) adsorption in 0.1 $\frac{mg}{ml}$ protein solution, (II) desorption in 1 mM buffer solution at pH 6 and (III) desorption in 1 mM buffer solution at pH 7.6. Corresponding frequency shifts and dissipation values can be found in the appendix in Figure A.11

In Field I $\Delta\Gamma_{QCMD}^{ads}$ again increases more rapidly than Γ_{SE}^{BSA} . Here over a range of 5 min an increase in $\Delta\Gamma_{buffer}^{ads}$ up to $8 \pm 1 \frac{mg}{m^2}$ can be observed that decreases again to $5.5 \pm 0.4 \frac{mg}{m^2}$ and stays constant in the adsorption process. Thus an excess amount of buffer components is coupled to the brush surface at the beginning of protein adsorption at the "wrong-side" of the IEP, which equilibrates during the adsorption process. Here the peak in $\Delta\Gamma_{buffer}^{ads}$ at 14 min is reflected as negative peak in the refractive index $n_{comb}(631.5nm)$, whereas the combined polymer-protein layer thickness d_{comb} is still increasing (Figure 8.15). After 40 min d_{comb} stays virtually constant but $n_{comb}(631.5nm)$ is further increasing until the end of the adsorption experiment and exchange of the protein solution to pure buffer solution. These findings can be interpreted as a densification of the combined protein-polymer layer in the ongoing adsorption process, thus protein is continuously incorporated into the combined layer.

After exchange of the buffer both $\Delta\Gamma_{QCMD}^{ads}$ and Γ_{SE}^{BSA} decrease in Field II and protein desorption takes place, whereas the decrease in $\Delta\Gamma_{QCMD}^{ads}$ is faster, indicating desorption of buffer components alongside the protein, as it is expected when the hydration shell of protein molecules is taken into account. The desorption process in pure 1 mM buffer at pH 6 is accompanied by a decrease both in thickness d_{comb} and refractive index n_{comb} in 8.15. At this pH desorption of protein begins with starting the pump for the exchange of solution at 158 min of the experi-

ment, indicating a high sensitivity of the combined polymer-protein surface on shear forces / flow for this pH at the "wrong side" of the IEP of BSA.

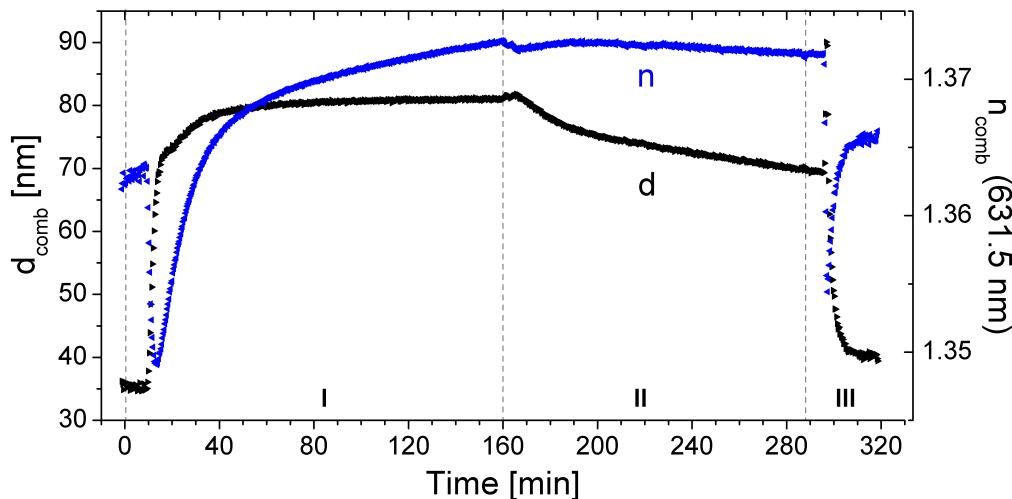


Figure 8.15.: Total refractive index $n_{comb}(\lambda = 631.5 \text{ nm})$ and combined polymer-protein layer thickness d_{comb} , corresponding to the measurements presented in Figure 8.14.

When exchanging the buffer to 1 mM at pH 7.6 the same desorption features as observed in the adsorption experiment at pH 5.2 (8.12) are visible, but less pronounced. Also a temporarily stretching of the layer, indicated by a change in the combined layer thickness d_{comb} from 69 nm to 90 nm, takes place, whereas the increase is also smaller than at pH 5.2, where a stretching from 68 nm to 124 nm could be observed. These differences are due to less protein adsorbed at pH 6 than at pH 5.2. Therefore, fewer charged protein molecules contribute to the incorporation of additional buffer components and thus the stretching of the layer in the desorption process.

The decreased adsorbed amount of protein at pH 6 compared to pH 5.2 was not expected from the nominal IEP of the protein BSA at pH 5.6 and the pH-sensitive adsorption results obtained for HSA on comparable PAA Guiselin brushes grafted onto silicon wafers (Figure 8.5(b)). Here detailed pH-sensitive studies on the BSA adsorption would have to be done to clarify if this effect is caused by the electrochemical properties of the protein, by the different electrochemical properties of the gold substrate compared to silicon or by the different adsorption conditions in stagnant solution and flow.

8.3.5. Changes in the shear viscosity during the adsorption process

Changes in the shear viscosity $\Delta\eta_l$ upon BSA adsorption in 1 mM buffer solution are displayed in Figure 8.16 for adsorption at pH 5.2 (a) and at pH 6 (b) as discussed in the previous two subsections.

Here for adsorption at pH 5.2 an increase in $\Delta\eta_l$ over one order of magnitude occurs upon

adsorption (Field I). Thus the internal friction in the combined polymer-protein layer is considerably higher than for the bare brush surface. When exchanging the protein solution to 1 mM buffer solution again, a further increase in the shear viscosity is monitored (Field II), which is interesting because the amount of ions and water molecules was shown to decrease in Figure 8.12. Thus a less hydrated protein-brush layer would have a higher viscosity at the present environmental conditions than a more hydrated protein-brush layer in equilibrium with $0.1 \frac{mg}{ml}$ protein concentration in the same 1 mM salted solution. With desorption of the protein in Field III at pH 7.6, $\Delta\eta_l$ decreases to values comparable with the pure brush surface, underlining the importance of the protein on the surface for a high shear viscosity.

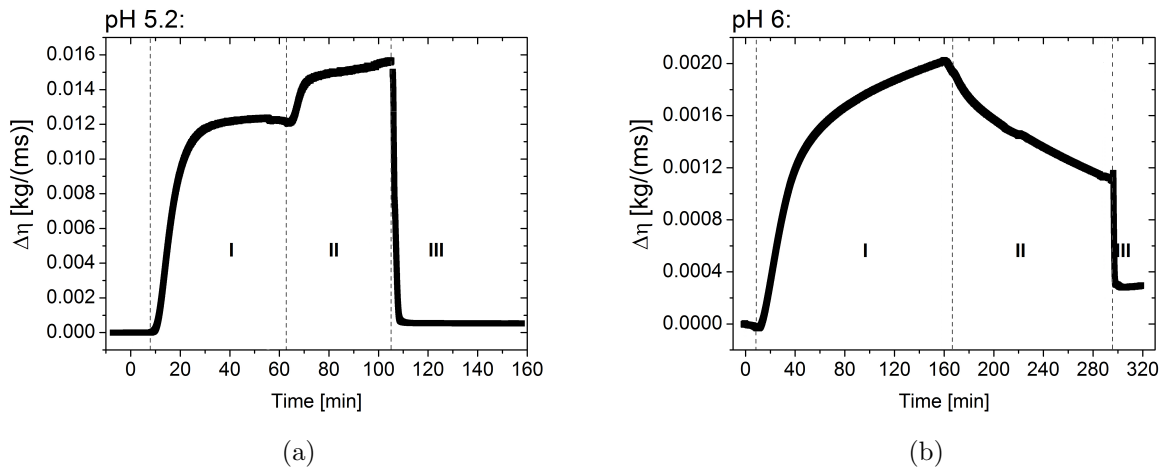


Figure 8.16.: Changes in the viscosity $\Delta\eta_l$ upon BSA adsorption in 1 mM salted solution at pH 5.2 and pH 6. Measurements are referenced for clearer presentation to the brush surface in buffer solution, displaying (I) adsorption in $0.1 \frac{mg}{ml}$ protein solution, (II) desorption in 1 mM buffer solution and (III) desorption in 1 mM buffer solution at pH 7.6.

At pH 6 the change in the shear viscosity upon protein adsorption is relatively small, only $0.002 \frac{kg}{ms}$ (Field I), compared to the changes observed at pH 5.2. Here at the latter pH a 6 times higher $\Delta\eta_l$ was observed, whereas the adsorbed amount of protein at pH 5.2 was 2.3 times higher than at pH 6. The desorption of protein upon exchange to the buffer solution at pH 6 is reflected again in $\Delta\eta_l$, which is decreasing with decreasing amount of protein at the brush surface (Field II). Finally after desorption at pH 7.6 the remaining changes in the shear viscosity are similar to $\Delta\eta_l$ after the adsorption experiment at pH 5.2 (Field III). Thus similar brush states are achieved after adsorption experiments at overall electrostatic attractive and repulsive conditions at this low salt content in solution, considering thickness d_{comb} , remaining amount Γ_{SE}^{BSA} , viscoelastically coupled amount $\Delta\Gamma_{QCMD}^{ads}$ and remaining change in the shear viscosity $\Delta\eta_l$.

8.3.6. Comparison of adsorption in 1 mM and 100 mM buffer solution

In Figure 8.17 plateau values for the amounts Γ_{SE}^{BSA} and $\Delta\Gamma_{QCMD}^{ads}$ are compared after adsorption and desorption in the corresponding buffer solutions for 1 mM and 100 mM salt content at pH 5.2 (a) and pH 6 (b).

After adsorption at pH 5.2, $\Delta\Gamma_{QCMD}$ is similar for both salt concentrations, whereas a decrease in the adsorbed amount of protein from $28 \pm 1 \frac{mg}{m^2}$ at 1 mM to $24.0 \pm 0.4 \frac{mg}{m^2}$ at 100 mM can be found. Furthermore when exchanging protein to buffer solution, desorption of protein takes place at 100 mM, which could not be observed in 1 mM salted solution. At this high salt content the difference between $\Delta\Gamma_{QCMD}^{ads}$ and Γ_{SE}^{BSA} stays virtually constant upon desorption, indicating a constant amount of water and ion molecules viscoelastically coupled to the surface after adsorption in protein solution and desorption in the pure buffer solution.

At pH 6 the adsorbed amount of protein is strongly decreased at 100 mM compared to adsorption in 1 mM solution as it is expected from the literature since the critical pH for adsorption at the "wrong side" of the $IEP_{protein}$ decreases with increasing salt content [59]. In the literature the critical pH was found to decrease from pH 6.75 at 1 mM to pH 5.15 at 100 mM for adsorption of HSA onto end-grafted PAA brushes.

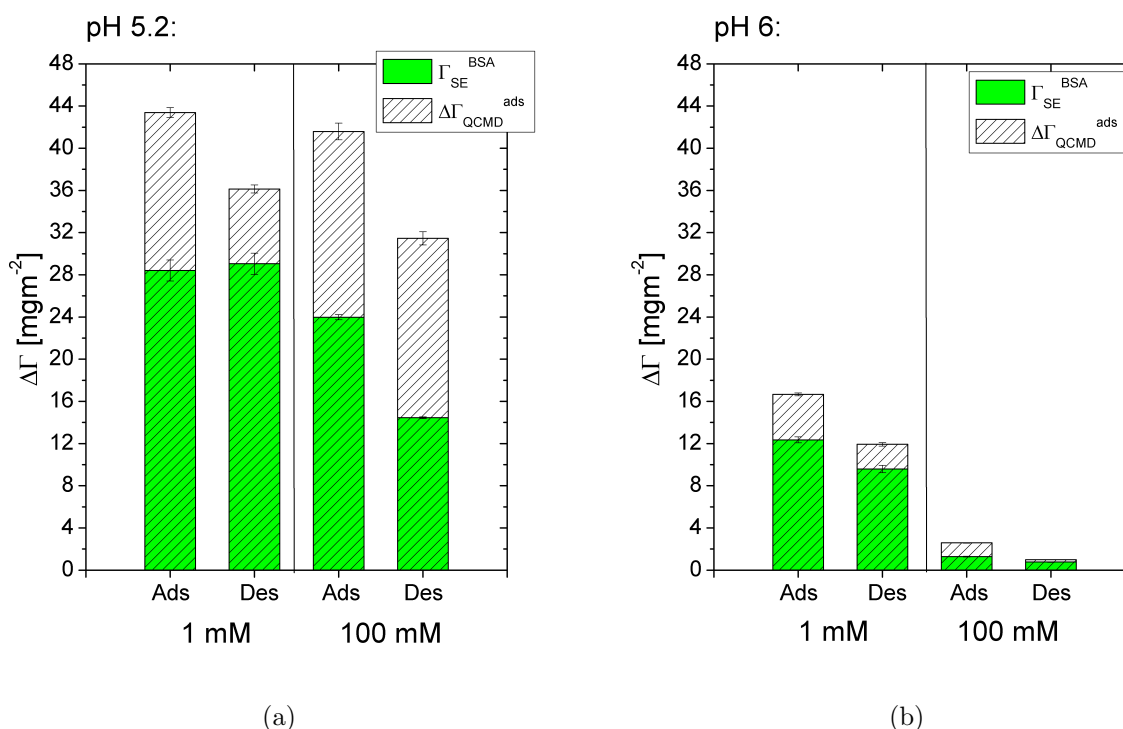


Figure 8.17.: Adsorption and desorption of BSA for 1 mM and 100 mM salt content in pH 5.2 (a) and pH 6 (b) buffer solutions.

8.4. Summary

Swelling of PAA and PAA-b-PS Guiselin brushes was investigated dependent on pH and salt concentration and protein adsorption of defatted HSA with its IEP at pH 5.7 and α -chymotrypsin with its IEP at pH 8.1 monitored pH-sensitive. In coupled ellipsometry - quartz crystal microbalance studies changes in the amount of buffer molecules coupled to the surface in the swelling process as well as in adsorption experiments were observed and changes in the shear viscosity of the surface layer monitored upon protein adsorption.

These highly swellable polyelectrolyte layers are very interesting in drug release applications, where the amount of released protein has to be precisely controlled, although pH and salt content are restricting environmental parameters for this system. Especially at the "wrong side" of the isoelectric point of macromolecules immobilized in these Guiselin brushes (e.g. enzymes) it can be expected that they preserve their structure and thus their function, leading to applications for functionalized surfaces or sensors. Also a very high sensitivity to changes in combined polymer-protein layer parameters upon changes in environmental conditions around the IEP of immobilized proteins makes these surface coatings suitable for accurate sensor applications.

In detail pH- and salt sensitive swelling of PAA Guiselin brushes was found to be comparable to the swelling of end-grafted brushes and 1-3 grafting points per chain could be estimated. An additional small PS block increased the pH-sensitivity at very low salt contents, and led to an increased surface hydrophobicity of the dry PAA-b-PS Guiselin brushes for all pH after pretreatment in 0.1 mM NaCl solutions. Thus an influence of the PS-block on physico-chemical interface properties of PAA Guiselin brushes could be demonstrated.

Upon adsorption of HSA, very high adsorbed amounts could be found centered around the IEP of the protein, comparable to results for end-grafted PAA brushes in the literature. Additionally combined polymer-protein layer parameters were monitored and a stretching of this combined layer with increasing pH, thus increasing negative charges at the surface could be concluded. A very high sensitivity to pH changes was found between pH 6 and 6.2, whereas the combined layer parameters pass through a minimum (refractive index) and a maximum (layer thickness) upon adsorption at the "wrong side" of the protein. Thereby the total values of n_{comb} and d_{comb} indicate a higher stretching of the PAA Guiselin brush in the presence of adsorbed HSA molecules compared to the pure brush at the same environmental conditions.

Adsorption of α -chymotrypsin led to a maximum of adsorbed amount around pH 6 as well and not at the IEP of the protein, accompanied by a continually increasing combined layer thickness and a decreasing refractive index. Thus for this relatively small and "hard" protein the adsorption mechanism was found to be considerably different compared to HSA adsorption.

The PS block in PAA-b-PS Guiselin brushes was found to increase the critical pH until adsorption of HSA at the "wrong side" takes place and the amount of protein irreversible

bound to the brush for individual pH values was also increased. For this block-copolymer brush the minimum in the refractive index $n(631.5 \text{ nm})$ for the combined polymer-protein layer is even more pronounced than observed for PAA Guiselin brushes.

The specific adsorbed amount $\frac{\Gamma_{HSA}}{\Gamma_{PAA}}$ for the adsorption of HSA at PAA Guiselin brushes at pH 6 was found to increase monotonically with increasing PAA content and an amount of HSA of 3.5 ± 0.3 times higher than the amount of PAA at the surface could be adsorbed for PAA Guiselin brushes with a nominal grafting density of $0.30 \pm 0.15 \text{ nm}^{-2}$. Smaller specific amounts of HSA could be adsorbed at the corresponding PAA-b-PS Guiselin brushes.

In simultaneous SE-QCM-D studies changes in the amount of coupled buffer in swelling and protein adsorption experiments could be obtained quantitatively. A considerable increase in the amount of viscoelastically coupled buffer components could be observed upon swelling of PAA Guiselin brushes in electrolyte solutions. Compared to the buffer content inside the swollen brush layer as given by a SE-box model, a high amount can be coupled to the brush-solution interface. Here the decrease of coupled buffer amount with increasing salt content indicates high influence of the electric double layer on the difference between optically (SE) and acoustically (QCM-D) determined buffer amount at the brush surface.

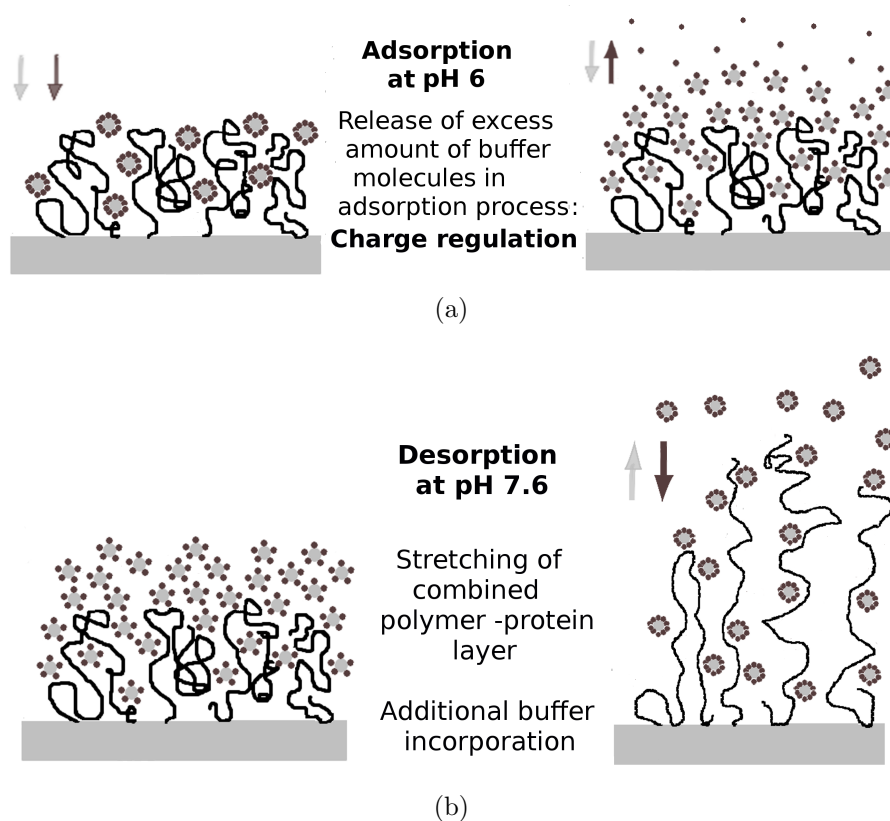


Figure 8.18.: Schemes of protein (light gray) and buffer (dark gray) incorporation into and release from the combined polymer-protein layer in adsorption at the "wrong side" of the $IEP_{protein}$ (a) and desorption at elevated pH (b).

For BSA adsorption at these PAA Guiselin brushes, the rate of increase of the viscoelastically coupled amount was higher than the increase of amount of protein at the surface for both adsorption experiments at overall electrostatic attractive (pH 5.2) and overall electrostatic repulsive (pH 6) conditions. Thus the incorporation of buffer molecules into the protein-brush layer during the adsorption process was investigated quantitatively, providing further insight into the adsorption process of the model protein BSA at flexible polyelectrolyte surfaces.

For adsorption at pH 6 at the "wrong side" of the IEP of the protein a coupling of an excess amount of buffer components could be observed (Scheme 8.18(a)), which could be explained by charge regulation at the protein molecules during the adsorption process.

At electrostatic attractive conditions at pH 5.2 no desorption of protein could be observed in pure 1mM buffer solution, but the amount viscoelastically coupled to the surface decreased, indicating a dependency of the amount of buffer molecules coupled to the surface on the protein concentration in solution at low salt content.

Desorption at pH 7.6 led to an increase in the polymer-protein combined layer thickness accompanied by a strong increase in the viscoelastically coupled amount at both pH, thus underlining a stretching of the combined brush-protein layer with additional incorporation of buffer molecules in the desorption process before desorption of protein molecules actually takes place (Scheme 8.18(b)).

Finally the shear viscosity of the brush-protein layer was one order of magnitude higher upon electrostatic attractive adsorption than upon adsorption at the "wrong side" of the IEP of the protein.

9. Temperature and pH sensitive PNIPAAm-PAA binary mixed brushes

The combination of pH-sensitive PAA and temperature sensitive PNIPAAm has been studied so far in the form of block copolymers in hydrogels, as blends in membranes or as inter-penetrating polymer networks [8, 51, 53], but also in the form of mixed brushes prepared by "grafting-from" on a biodegradable substrate [247]. Among other aspects, the stimuli sensitive drug release from polymer networks as well as the microfiltration behavior of blend membranes due to their swelling dependent on pH and temperature was investigated [51, 53]. For PNIPAAm and PAA grafted to hydroxyethyl cellulose the micellization behavior was studied [247]. No temperature sensitive changes in the hydrodynamic radius of these micelles could be found below pH 5, which was discussed in terms of an interpolymer hydrogen bonding at low pH whereas PNIPAAm and PAA have a critical complexation pH value of pH 4.6 in the absence of salt [248].

We investigated the combination of the polyanionic PAA with the neutral, water soluble PNIPAAm as a binary mixed brush on a planar surface with expected complex swelling behavior [55, 248], and present results on mixed brushes prepared by the "grafting-to" approach, focusing on the surface morphology and the surface wetting behaviour in Section 9.1 as well as on the pH-, salt-, and temperature sensitive swelling behavior of this system (Section 9.2) [249]. Furthermore examples of protein adsorption experiments are added to show the influence of the complex swelling behavior of the mixed brush on its adsorption affinity in Section 9.3. Finally the pH-sensitive swelling behavior and physico-chemical interface properties of PNIPAAm - PAA-b-PS brushes are presented, focusing on the differences compared to PNIPAAm-PAA binary brushes (Section 9.4).

9.1. Physico-chemical interface properties of dry brushes

The physico-chemical interface properties of PNIPAAm-PAA mixed brushes were investigated after immersion in buffer solutions with different pH and subsequent careful drying under nitrogen flux. AFM images of PNIPAAm-PAA (80:20) (a,b) with a low PAA content, and PNIPAAm-PAA (40:60) (c,d) mixed polymer brushes with a high PAA content after immersion at acidic and basic pH values are shown in Figure 9.1. For a high content of PAA a lateral domain formation with an average diameter of $75 \pm 10 \text{ nm}$ can be deduced from Figures 9.1(c)

and 9.1(d), where the inhomogeneity and root-mean-square roughness (see Figure 9.2) of the surface is considerably increased after immersion in pH 3 solution (9.1(c)) compared to the height image after immersion at pH 8 (9.1(d)). Since the PAA is deswollen at pH 3 most probably the protruding domains are consisting of PNIPAAm collapsed on top of the deswollen PAA. Here a scheme for a possible brush structure is inserted into Figure 9.1(c). No comparable domain formation can be seen for the PNIPAAm - PAA (80:20) mixed brush after immersion at pH 3.

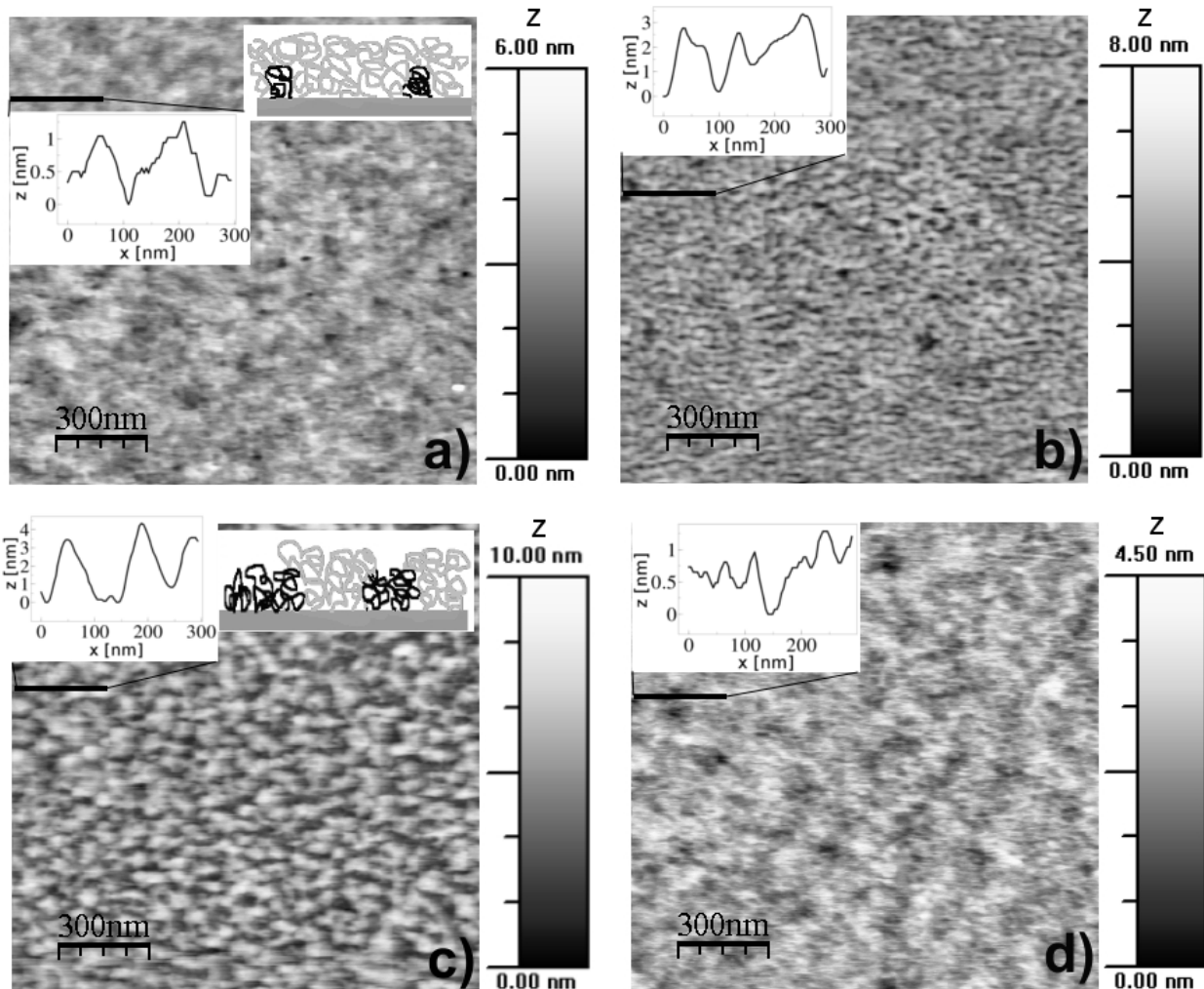


Figure 9.1.: AFM height images of dry brushes after applying the simple flattening procedure, subtracting an offset line by line [148]. Displayed are a PNIPAAm - PAA (80:20) mixed brush after immersion in 0.001M pH 3 NaCl solution (a) and 0.001M pH 8 buffer solution (b) as well as a PNIPAAm - PAA (40:60) mixed brush after immersion in the same solutions at pH 3 (c) and pH 8 (d). Additionally sketches of the assumed dry brush structures after pH 3 treatment (PNIPAAm - gray, PAA - black) are included in (a) and (c).

Furthermore the roughness σ_{rms} of the polymer brush surfaces after pH-treatment was extracted from the AFM height images and analyzed dependent on the composition (Figure 9.2). Here an interesting increase in the surface roughness for mixed brushes with a PAA content

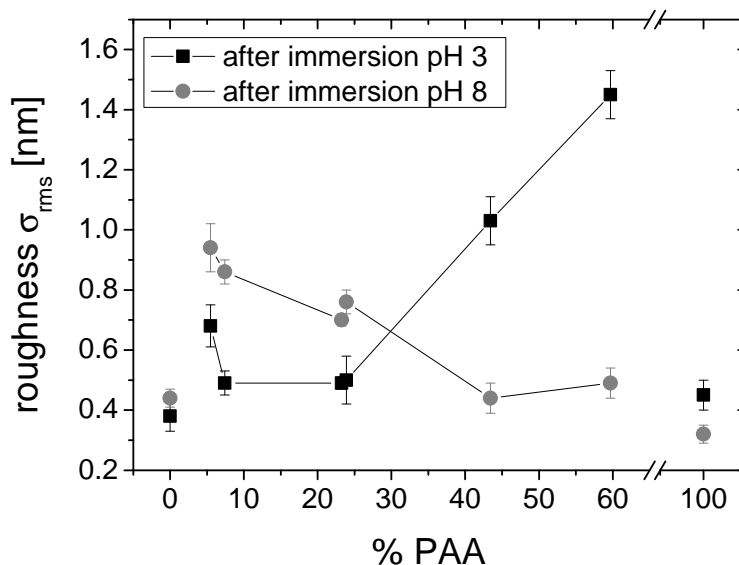


Figure 9.2.: Analysis of the root-mean-square roughness of AFM height images for different PAA contents of the polymer brush samples in dry state after pH-treatment in 0.001 M solutions of pH 3 and pH 8 . Connecting lines between the data points are only a guide for the eye.

higher than 40 % was observed after treatment in pH 3 solution, which matches the structuring results shown in Figure 9.1. After treatment at pH 8 the surface roughness monotonically decreased with decreasing PAA content, leading to a maximum difference in the surface roughness of $0.9 \pm 0.1 \text{ nm}$ for a (40:60) PNIPAAm-PAA mixed brush.

We assume this is due to the formation of lateral domains of PAA / PNIPAAm for high PAA contents as discussed for Figure 9.1. For low PAA contents such a domain formation could not be observed and the surface roughness at both pH values is expected to result basically from the PNIPAAm chains occupying the surface of the dry PNIPAAm - PAA (80:20) brushes. Comparing these findings for the binary brushes with the overall low roughness values for PNIPAAm and PAA monobrushes after pH-treatment, we conclude, that the changes in the roughness after pH-treatment for the binary brushes is unique for this mixed polymer system.

To confirm the presence of PAA on the mixed brush surface after treatment at different pH, dynamic contact angle measurements were performed and advancing water contact angles for the homopolymer brushes and two selected mixed brushes are displayed in Figure 9.3.

The advancing contact angle for the PNIPAAm brushes is independent of the pH, as could be expected since there are no dissociable groups along the chains, and is in good agreement with reported values for similar brush thicknesses [33]. However the advancing contact angle for PAA Guiselin brushes is considerably lower at acidic pH than was reported in the literature for end-grafted PAA brushes [35, 42]. We obtained this results reproducibly and have also controlled the roughness of PAA Guiselin brushes after pH-treatment to be smaller than 1 nm,

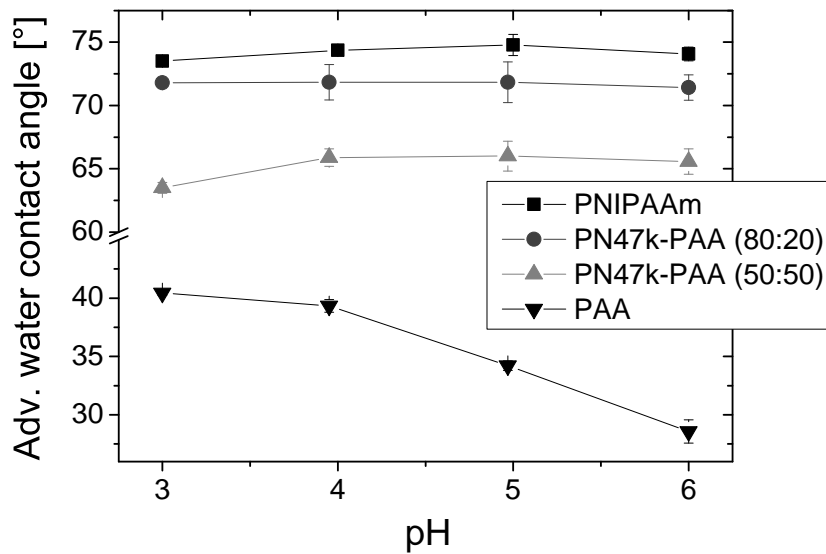


Figure 9.3.: Comparison of the advancing water contact angles of end-grafted PNIPAAm, loop-wise grafted PAA and two selected mixed brushes dependent on the pH in the acidic pH region after pH-treatment and subsequent drying.

thus the contact angle results should not be influenced critically by the surface roughness.

For mixed PNIPAAm-PAA brushes the fraction of each polymer on top of the brushes can be estimated by using the Cassie equation (Equation 4.16). The pH-dependent fraction of PAA (f_{PAA}) at the brush surface was calculated for PNIPAAm PAA (80:20) and (50:50) mixed brushes and is presented in Table 9.1.

Regarding mixed PNIPAAm PAA (80:20) brushes the pH-dependent advancing contact angles closely resemble the independency of the advancing contact angle of PNIPAAm brushes on the pH, whereas a constant fraction $f_{PAA} = 0.07 \pm 0.04$ at the brush surface could be estimated. Thus these results indicate the dominance of PNIPAAm at the polymer brush surface in the dry state after all pH-treatments for this brush with low PAA content. For the PNIPAAm PAA (50:50) brush slight variations in the contact angle dependency can be

Table 9.1.: Estimation of the pH dependent fraction of PAA at the brush surface for PNIPAAm-PAA (80:20) and (50:50) mixed brushes by using the Cassie equation. The error of f_{PAA} was calculated to be below 0.04.

pH	f_{PAA} (80:20)	f_{PAA} (50:50)
3	0.06	0.34
4	0.08	0.28
5	0.09	0.26
6	0.07	0.23

observed. After pH-treatment the advancing contact angle is lower than for PNIPAAm brushes but still considerably higher than for PAA Guiselin brushes and a surface fraction of PAA of $f_{PAA} = 0.34$ after treatment at pH 3 could be calculated, decreasing with pretreatment at increasing pH to $f_{PAA} = 0.23$ after treatment at pH 8. Thus a considerable fraction of PAA constitutes the mixed brush surface of the PNIPAAm-PAA (50:50) mixed brush, consistent with the lateral structuring observed by AFM for mixed brushes with high PAA content.

Furthermore a stick-slip behavior after all pH-treatments was observed for this brush indicating surface inhomogeneity which is most probably due to the lateral domain formation visible in the AFM measurements [166]. However we are aware of the difficulties in interpreting such advancing contact angles at swellable surfaces.

9.2. Environmental sensitive swelling behaviour

9.2.1. Coupled swelling dependent on pH and ionic strength

The pH-dependent swelling of PAA Guiselin brushes, the independence of the PNIPAAm brush parameters on the pH and the swelling behavior of the mixed brushes are displayed in Figure 9.4.

Interestingly the mixed brushes did not behave like a combination of a pH independent brush (PNIPAAm) and the individually swelling pH-sensitive PAA as it would be expected for independent swelling of the two polymers. Instead the mixed brushes expressed a pH-sensitivity similar to the one of PAA brushes but with considerably increased changes in the swollen layer thickness between pH 3 and pH 8. This behavior seems reasonable when the reports on the complexation behavior of these two polymers in solution is taken into account [55]. It is discussed that PNIPAAm and PAA form a rather strong interpolymer complex in solution due to hydrogen bonding, whereas the authors stated the presence of isopropyl groups along the PNIPAAm chains as important, stabilizing the complex formation by hydrophobic interactions. They compared their results obtained with a PNIPAAm-PAA solution with poly(acryl amide) PAAm - PAA solutions, with no isopropyl groups present, where the complex formation was found to be rather weak.

We think the increase in the swollen layer thickness with pH is due to the increase of the degree of deprotonation of COOH-groups of PAA. Deprotonated COO- groups can no longer interact via hydrogen bonding with amide groups of PNIPAAm, thus we assume that at $pH > 6$ most of the COOH groups of PAA are deprotonated, resulting for the mixed brushes in a plateau in the swollen layer thicknesses and the refractive indices as indicated by the swelling measurements (Figure 9.4). For end-grafted PAA brushes Dong et. al. found, that the effective bulk pKa value, the logarithmic value of the acid dissociation constant inside the brush, was at pH 6.5 -

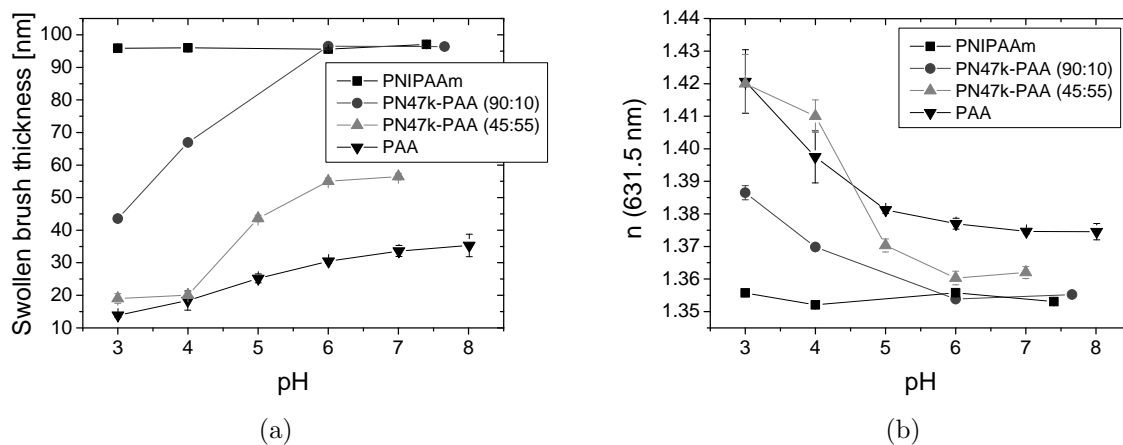


Figure 9.4.: Swollen brush thickness (a) and refractive index at $\lambda = 631.5 \text{ nm}$ (b) of homopolymer and mixed brushes of PNIPAAm and PAA dependent on the pH in 0.01M solutions at 22 °C.

6.6, whereas a pKa at pH 4.4 was found at the brush-solution interface different from the bulk value and almost identical with the pKa value for PAA in solution [42,237]. Thus they proved the presence of a dissociation gradient inside an end-grafted PAA brush.

We assume, that for the decoupling of the polymer complex in the PNIPAAm-PAA mixed brushes by pH, the PAA chains have a different dissociation behavior compared to that reported for PAA chains in homopolymer brushes [238] and more closely resemble the behavior of PAA chains in solution because a plateau in the mixed brush thickness is already reached between pH 6 and 7. Furthermore in comparing the results for the swollen layer thickness of PNIPAAm - PAA (90:10) and (45:55) brushes an increased hindrance of the swelling of the mixed brush with higher PAA content could be found.

Since the deprotonation of COOH-groups is also influenced by the ionic strength of the solution and can be suppressed at low ionic strength [29,238], we also investigated the influence of the salt concentration on the swelling behavior. An example for the salt dependent swelling at pH 8 of a PNIPAAm-PAA (55:45) mixed brush can be seen in Figure 9.5.

The sensitivity of the PAA Guiselin brushes follows again the tendencies known from the literature, showing increased swelling with increased ionic strength in the osmotic regime due to the increase of deprotonated COO- groups and counter ion condensation inside the brush [29,238]. The maximum of swollen layer thickness can be found around 0.1 M ionic strength, at higher salt concentrations PAA enters the salted regime and deswells again. The layer parameters n and d of PNIPAAm brushes on the other hand again are independent of the salt concentration as expected. Similar to the pH-dependent behavior a dependency of the swollen layer parameters on the ionic strength can be observed for the mixed brush, also pointing at a coupled swelling of the two polymers due to interactions between the chains. Furthermore we assume that the decrease in swollen thickness of the mixed brush at 0.3 M salt concentration

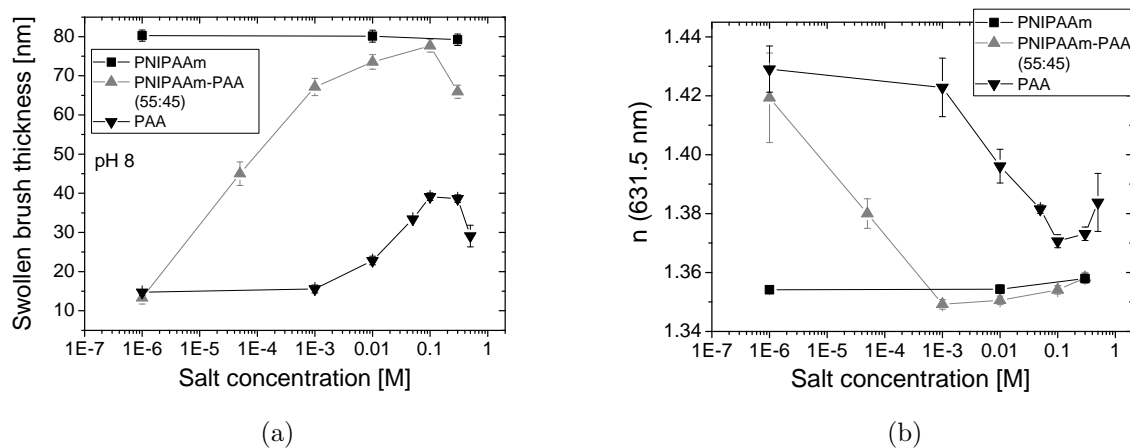


Figure 9.5.: Swollen brush thickness (a) and refractive index at $\lambda = 631.5 \text{ nm}$ (b) of homopolymer brushes and a PNIPAAm - PAA (55:45) mixed brush dependent on the ionic strength of the solution at pH 8 and 22 °C.

could point to a different type of interaction than the hydrogen bonding between PNIPAAm and PAA chains. Since charges along the PAA chains are strongly screened with increasing salt concentration and the PAA chains become more and more neutral [238], one possible explanation could be the presence of hydrophobic interactions between PAA and the isobutyl groups of PNIPAAm leading to deswelling of the mixed brush because of the collapse of PAA chains in the salted regime. However an assignment of the PAA brush behavior to the PAA chains in the mixed brush has to be regarded critically and further investigations with different methods, e.g. interaction measurements with optical tweezers [250], are necessary to achieve more reliable conclusions on interaction forces between PNIPAAm and PAA in a mixed brush conformation.

9.2.2. Temperature sensitivity

To complete the swelling experiments the results of temperature dependent swelling measurements in buffer solutions with fixed pH are displayed in Figure 9.6 for a PNIPAAm-PAA (45:55) mixed brush.

Here two major observations were made. Firstly the temperature sensitivity of the mixed brush, indicated by the magnitude of change in the swollen layer thickness and refractive index below and above the transition temperature, is clearly pH sensitive, with almost no temperature sensitivity at pH 4, remarkably increased sensitivity at pH 5 and again decreased temperature sensitivity at pH 6 and 7. A similar swelling tendency was observed for hydrogels, where hydrogen bonding is discussed to lead to an interpolymer complexation behavior at low pH [7]. Furthermore an univocal increase of the swollen layer thickness below and above the transition temperature can be observed. Comparing this result with the pH-dependent swelling behavior of PAA Guiselin brushes and PNIPAAm-PAA mixed brushes we propose a layered mixed

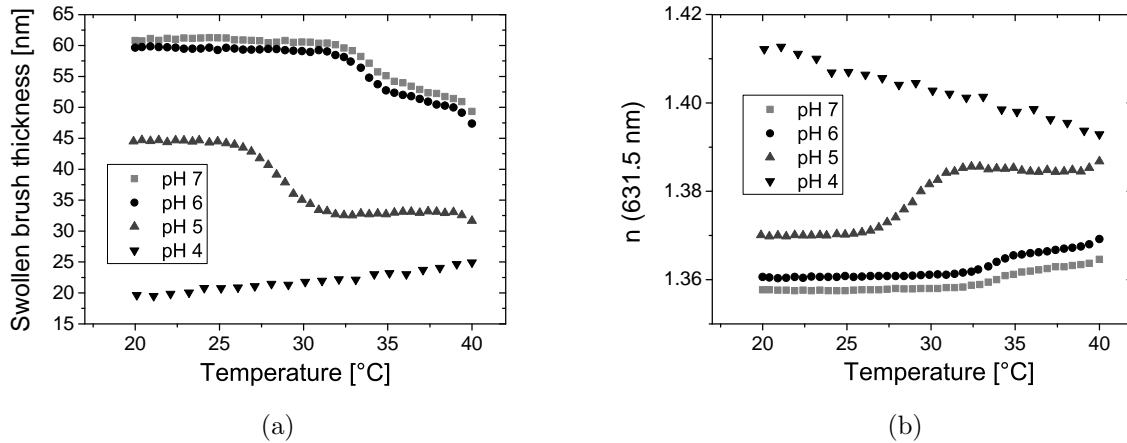


Figure 9.6.: Swollen brush thickness (a) and refractive index at $\lambda = 631.5 \text{ nm}$ (b) of a PNIPAAm-PAA (45:55) mixed brush dependent on pH and temperature in 0.01 M buffer solutions.

brush geometry, with a lower layer of interacting PNIPAAm and PAA chains, thus hindered temperature sensitivity of PNIPAAm and an upper layer with freely swellable PNIPAAm chains. However we are aware of the limits of such a visualization.

Secondly a shift in the transition temperature from $29 \pm 1 \text{ }^\circ\text{C}$ at pH 5 to $33 \text{ }^\circ\text{C}$ at pH 6 ($34 \text{ }^\circ\text{C}$ at pH 7) is visible. These last findings are in agreement with observations of the shift of the LCST for copolymerized PNIPAAm samples, where the increase of the hydrophilicity of the copolymer leads to an increase in the LCST [46].

We also analyzed the dependency of the temperature sensitive change of the layer parameters n and d on the composition of the mixed brush for pH 7 (Figure 9.7). Here we found a decrease in temperature sensitivity with increasing PAA content as it could be expected from our swelling results described above (Figures 9.4 and 9.6) .

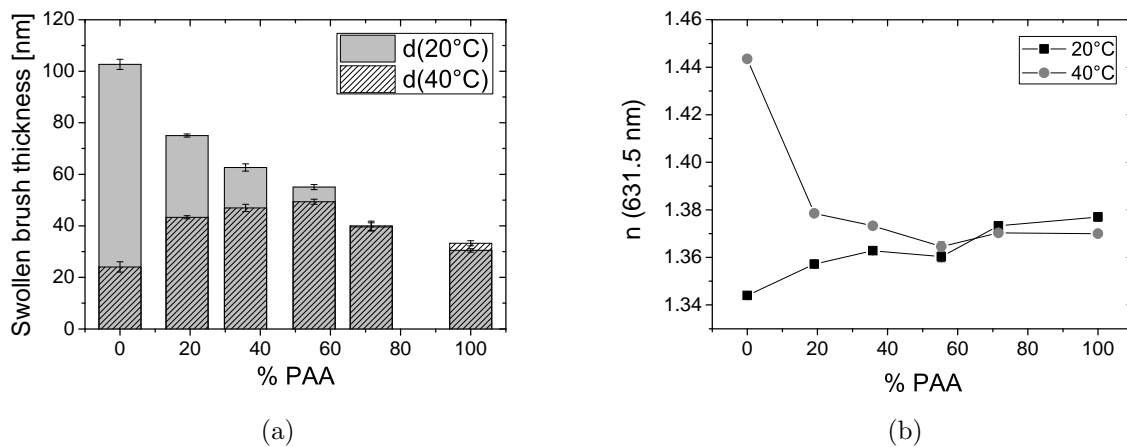


Figure 9.7.: Swollen brush thickness (a) and refractive index at $\lambda = 631.5 \text{ nm}$ (b) at $40 \text{ }^\circ\text{C}$ compared to $20 \text{ }^\circ\text{C}$ dependent of the composition of the mixed brush. Measurements were done in 0.01 M phosphate buffer solution at pH 7.

For pure PNIPAAm brushes the difference in the magnitude of the brush layer parameters at low and high temperature was about 80% and decreased to about 15% for mixed brushes with 55% PAA content. Finally for mixed brushes with 72% PAA content we did not observe any temperature sensitivity. In comparing this decrease in the temperature sensitivity with findings for PNIPAAm homopolymer brushes with different grafting density, displayed in Figure 7.4, we conclude that this decrease in temperature sensitivity in the mixed brush is due to the increase of PAA content and is not an effect caused by the decrease of amount of PNIPAAm at the surface and thus the decreasing grafting density of the PNIPAAm.

9.3. Protein adsorption and release

Having investigated the protein adsorption affinity for PNIPAAm and PAA monobrushes it is now desired to combine the protein repelling properties of PNIPAAm with protein adsorption at PAA into a mixed brush with protein resistant and adsorbing properties assigned to selected environmental conditions as depicted in Figure 9.8. Thus in the following section the pH-sensitive adsorption of HSA (Section 9.3.1), as well as the temperature sensitive adsorption of HSA and α -chymotrypsin (Section 9.3.2) are investigated. We also compare pH-sensitive adsorption and desorption kinetics of HSA with PAA Guiselin brushes and monitor the pH-sensitive release of protein over up to 5 cycles in Section 9.3.3.

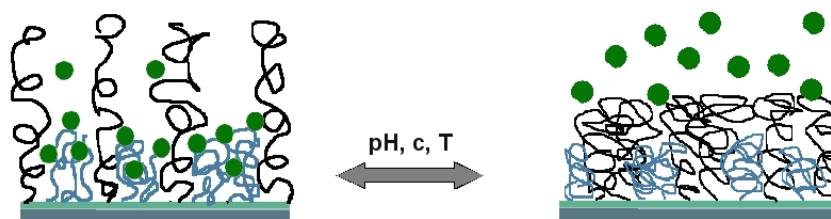


Figure 9.8.: Scheme of the desired switching between protein adsorption and protein repelling state of a mixed polymer brush due to the swelling / deswelling of PNIPAAm (black).

9.3.1. Adsorption of HSA dependent on pH

Due to the unique swelling properties of PNIPAAm-PAA binary brushes with a coupled deswelling at low pH, HSA adsorption was also carried out pH-sensitive and results are presented in Figure 9.9 for a mixed brush with 20 % PAA content.

Here the maximum adsorbed amount was similarly found around the IEP of the protein at pH 5.7 as for PAA Guiselin brushes (Figure 9.9(a)), whereas with 16 ± 1 % the protein volume fraction was much smaller than the HSA fraction of 45 % at the maximum of adsorption at PAA mono brushes (Figure 9.9(d)).

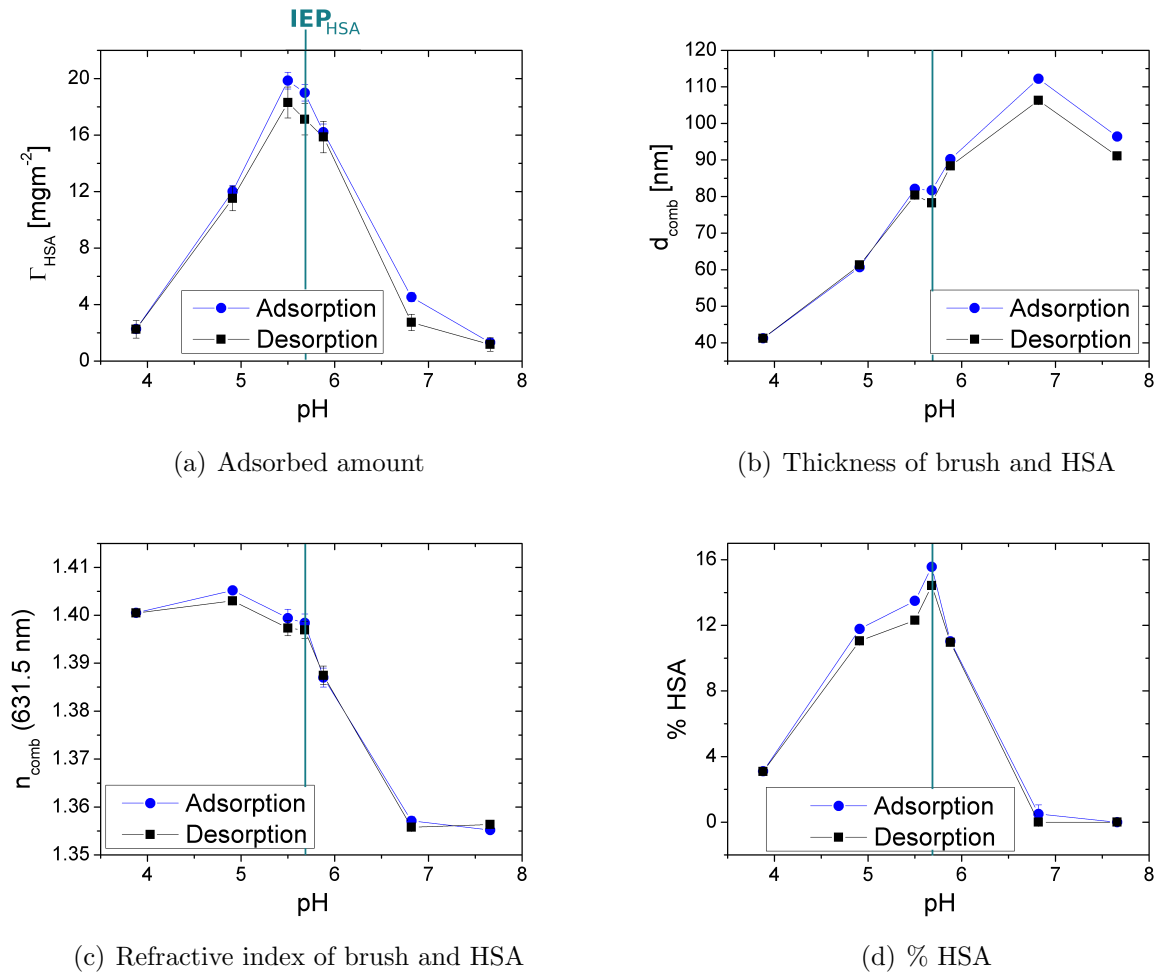


Figure 9.9.: pH-dependent adsorption of HSA to PNIPAAm-PAA (80:20) mixed brushes at 23 °C.

Contrary to the adsorption at PAA Guiselin brushes the adsorbed amount at pH 3.9 was with $\Gamma_{HSA} = 2.3 \frac{mg}{m^2}$ very small. We contribute this effect to the coupled deswelling of PAA and PNIPAAm at low pH and low salt content as it was discussed in Section 9.2.1. Thus when the PAA chains are deswollen and interact via hydrogen-bonding with the PNIPAAm chains, the latter are pinned to the surface as well, forming a relatively dense PNIPAAm layer on top of the PAA layer. Furthermore the charge density on the PAA chains is still low at this pH and the immobilization of protein molecules at the PNIPAAm surface by secondary adsorption are less likely.

The combined polymer-protein layer thickness increases between pH 3.8 and pH 6.8, whereas protein adsorption takes place for the investigated pH values between pH 5 and 6.8. At pH 7.7 no protein adsorption was observed due to the electrostatic repulsion between negatively charged PAA and protein. It is interesting that, similar to the adsorption at PAA-b-PS Guiselin brushes, relatively low differences between Γ_{HSA} after adsorption and desorption in the corresponding buffer solution can be found. Here more informations on the influence of PNIPAAm on the adsorption process will be discussed in Sections 9.3.3 and 9.3.2.

The refractive index of the combined-polymer protein layer is considerably lower than for PAA Guiselin brushes due to the relatively low amount of PAA and thus low adsorbed amount of protein in the mixed brush. Here changes in n_{comb} (631.5nm) proceed in the same way as for PAA Guiselin brushes with a maximum decrease between pH 6 and pH 7.

9.3.2. Temperature sensitive adsorption

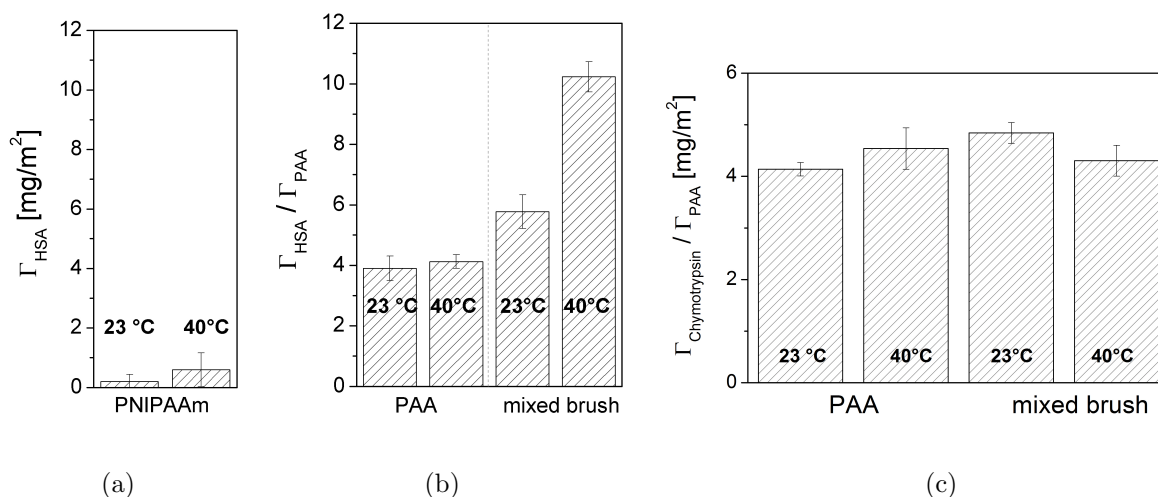


Figure 9.10.: Temperature sensitive adsorption below and above the LCST of PNIPAAm. (a) Adsorption of HSA at pH 6 to PNIPAAm brushes. (b) Adsorption of HSA at pH 6 to PAA Guiselin and (80:20) PN47k-PAA brushes and (c) adsorption of α -chymotrypsin at pH 7.8 to PAA Guiselin and (80:20) PN47k-PAA brushes. All adsorption experiments were carried out in 10 mM buffer solutions.

In this section we present selected results on the temperature sensitive adsorption of HSA and α -chymotrypsin onto binary PN47k-PAA brushes, to illustrate the effect of interaction forces between the deprotonated PAA and the PNIPAAm chains. The adsorption of HSA was performed at pH 6 at overall electrostatic repulsive conditions, whereas α -chymotrypsin was adsorbed at pH 7.8 at attractive conditions. We chose pH 6 for the adsorption of HSA, since it was shown, that the maximum of pH-dependent HSA adsorption (defatted protein) on the PAA Guiselin brushes was at the isoelectric point of the protein at pH 5.7 with a decrease of adsorption affinity of about 93 % when increasing the pH to pH 6.2 (Section 8.5(b)), thus we assume that the system, consisting of protein and sorbate brush surface, should be highly sensitive to any changes in the system itself and in environmental conditions within this pH region.

In Figure 9.10 the total adsorbed amount of HSA at PNIPAAm brushes (a) and the amount of HSA (b) as well as α -chymotrypsin (c), referenced to the amount of PAA on PAA Guiselin brushes as well as on PNIPAAm-PAA (80:20) mixed brushes for 20 °C (below the LCST of PNIPAAm) and 40 °C (above the LCST) are displayed. Here the relative adsorbed amount of

protein with respect to the amount of PAA at the surface was plotted, to compare homopolymer and mixed brushes with different PAA content (see Section 8.2.2).

PNIPAAm brushes are virtually resistant to protein adsorption and we could demonstrate a very good resistance for physiological conditions (PBS buffer) just recently (Section 7.2, [193]).

When comparing the results of HSA adsorption on the homopolymer and the mixed brushes, an increased specific adsorbed amount $\left(\frac{\Gamma_{HSA}}{\Gamma_{PAA}}\right)$ at 23 °C at the PNIPAAm PAA (80:20) mixed brush ($\Gamma_{PAA} = 2 \frac{mg}{m^2}$) compared to the PAA Guiselin brushes ($\Gamma_{PAA} = 8 \frac{mg}{m^2}$) can be found, and an additional significant increase in $\frac{\Gamma_{HSA}}{\Gamma_{PAA}}$ can be observed for the mixed brush when switching the temperature above the LCST of PNIPAAm. Since a large fraction of the COOH-groups along the PAA chains should be dissociated at pH 6, hydrogen bonding between PAA and PNIPAAm chains should not influence the protein adsorption behavior significantly. Nevertheless the protein adsorption affinity of the mixed brush at 23 °C is increased, which points at a strong influence of the small PAA fraction of 20 % on the adsorption process, disturbing the protein repelling behavior of pure PNIPAAm brushes considerably. Together with the further increase in $\left(\frac{\Gamma_{HSA}}{\Gamma_{PAA}}\right)$ above the LCST of PNIPAAm, where PNIPAAm chains collapse and become more hydrophobic, this increased adsorption affinity leads to the conclusion of an increased hydrophobic effect in the adsorption process at these mixed brushes compared to the HSA adsorption on the corresponding homopolymer brushes.

Most interestingly this increase in adsorption affinity cannot be found below and above the LCST of PNIPAAm for the adsorption of α -chymotrypsin, compared to the specific amount adsorbed on PAA Guiselin brushes in Figure 9.10(c), indicating no additional interaction forces besides electrostatic attraction between protein and PAA chains. Since the specific adsorbed amount for HSA is also higher at PN47k-PAA mixed brushes compared to PAA Guiselin brushes at electrostatic attractive conditions (pH 4.8 : $\frac{\Gamma_{HSA}}{\Gamma_{PAA}}(mix) = 5.3$, $\frac{\Gamma_{HSA}}{\Gamma_{PAA}}(mono) = 3.9$), we think a comparison of both experiments for HSA and α -chymotrypsin is possible, with respect to additional effects on the adsorption process by the presence of PNIPAAm.

9.3.3. Adsorption kinetics and protein release

Protein release and reversibility of switching the adsorbed amount

Following the last section firstly pH- and temperature sensitive release experiments of HSA are presented, monitoring the specific adsorbed amount $\frac{\Gamma_{HSA}}{\Gamma_{PAA}}$ 30 min after starting adsorption and desorption respectively.

pH-sensitive desorption was performed at pH 7.9 after protein adsorption at pH 5 and the adsorption-desorption process repeated 3-5 times. As can be seen for PAA Guiselin brushes in Figure 9.11 the remaining adsorbed amount after 30 min desorption increases from the first experiment $\left(\frac{\Gamma_{HSA}}{\Gamma_{PAA}} = 0.25\right)$ to the fifth $\left(\frac{\Gamma_{HSA}}{\Gamma_{PAA}} = 0.5\right)$. Thus twice the amount of HSA remains at

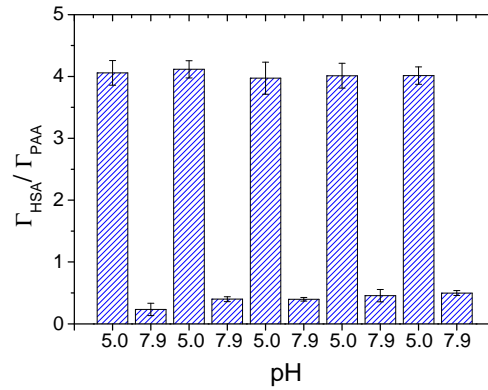


Figure 9.11.: Release experiments and reversibility of switching of the adsorbed amount of HSA dependent on pH at PAA Gueiselin brushes.

the brush surface after the last desorption experiment, whereas the adsorbed amount of HSA at pH 5 is not affected by the altered initial conditions of the brush surface at each adsorption step.

For (60:40) PNIPAAm-PAA mixed brushes pH-sensitive adsorption-desorption cycles were performed at 23 °C as well as 40 °C and are displayed in Figure 9.12(a) and Figure 9.12(b) respectively. Here $\frac{\Gamma_{HSA}}{\Gamma_{PAA}}$ after desorption is in good agreement with remaining specific amounts at the PAA Gueiselin brush, showing the same increase in $\frac{\Gamma_{HSA}}{\Gamma_{PAA}}$ after ongoing adsorption-desorption cycles as observed for PAA with virtually the same total values. This is interesting, since the specific adsorbed amount in the adsorption process at pH 5 is increased compared to adsorption at PAA Gueiselin brushes, thus indicating, that although adsorption is different for the PAA mono brush and binary mixed brushes, desorption is very similar at least on the time scale investigated.

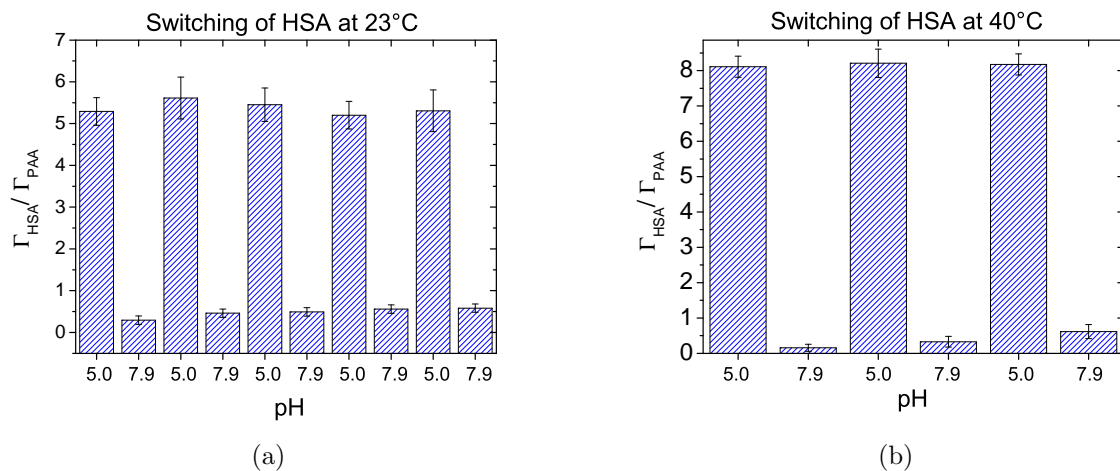


Figure 9.12.: Release experiments and reversibility of switching of the adsorbed amount of HSA dependent on pH at 23 °C and 40 °C for PN47k-PAA (60:40) binary brushes.

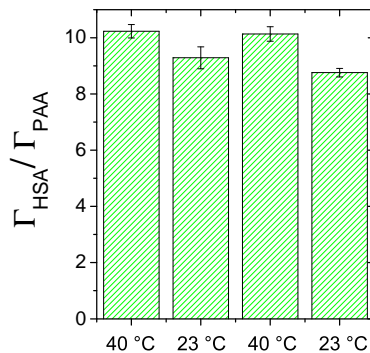


Figure 9.13.: Release experiments and reversibility of switching of the adsorbed amount of HSA dependent the temperature on binary (80:20) PN47k-PAA mixed brushes at pH 6.

To conclude this subsection temperature sensitive release experiments are presented in Figure 9.13. HSA was adsorbed at pH 6 at 40 °C for 30 min and the temperature decreased to 23 °C to monitor desorption. Here a decrease in the specific adsorbed amount about $\frac{\Gamma_{HSA}}{\Gamma_{PAA}} = 1.0 \pm 0.3$ could be observed when decreasing the temperature to 23 °C. The pH value was chosen at pH 6 to compare results of the temperature sensitive switching of the adsorbed amount with individual adsorption experiments at 23 °C and 40 °C as presented in Figure 9.10(b). In individual adsorption experiments $\Gamma_{HSA} = 10 \cdot \Gamma_{PAA}$ could be adsorbed at 40 °C compared to $\Gamma_{HSA} = 5.8 \cdot \Gamma_{PAA}$ at 23 °C. Thus we conclude from both, the switching and the individual experiments, that at 40 °C an additional amount of $\Gamma_{HSA} \approx 3 \cdot \Gamma_{PAA}$ is permanently immobilized at the mixed brush due to the temperature sensitive deswelling of the PNIPAAm chains.

Adsorption kinetics

Adsorption kinetics were monitored at pH 5 in 10 mM salted buffer solution and a comparison between kinetics of HSA adsorption at a PAA and a PAA-b-PS Guiselin brush as well as at a PNIPAAm-PAA (85:15) mixed brush are presented in Figure 9.14.

A distinct difference between the kinetics for the adsorption at the binary brush and the Guiselin brushes can be observed, whereas the relative protein uptake of the mixed brush is found to proceed slower with respect to the maximum specific amount than observed for both Guiselin brushes. We think a good explanation for this behavior would be a hindered diffusion of the protein molecules through the PNIPAAm chains upon electrostatic attractive adsorption conditions for an adsorption of HSA on PAA chains.

Thus this findings could be taken as an indication pointing at a penetration of protein molecules into the mixed brush layer. It is also important to note, that the relative amount of HSA adsorbed at the PNIPAAm-PAA binary brush exceeds the amount adsorbed at both

Guiselin brushes after 2 min of adsorption reflecting the increased adsorption affinity on the binary brush as it was discussed in Section 9.3.2.

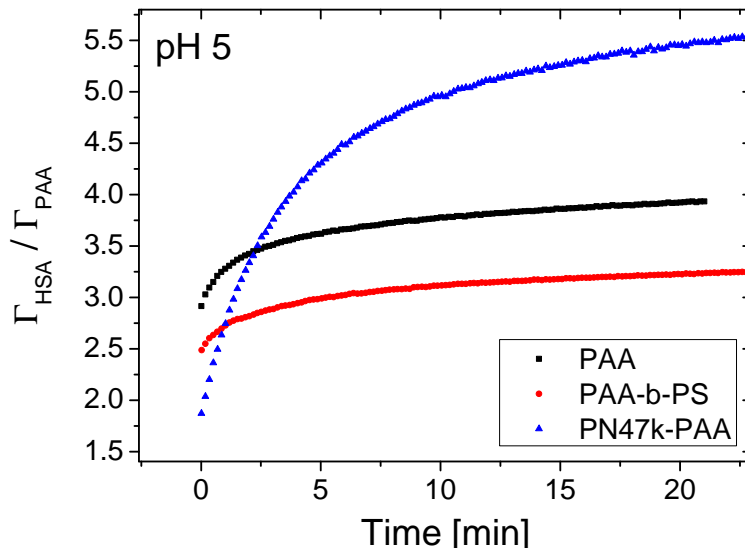


Figure 9.14.: Comparison of the adsorption kinetics of the relative amount of HSA upon adsorption at pH 5 in 10 mM buffer solution at a PAA ($\Gamma_{PAA} = 7.6 \frac{mg}{m^2}$) and a PAA-b-PS ($\Gamma = 8 \frac{mg}{m^2}$) Guiselin brush as well as a (85:15) PN47k-PAA binary brush with $\Gamma_{PAA} = 2.2 \frac{mg}{m^2}$.

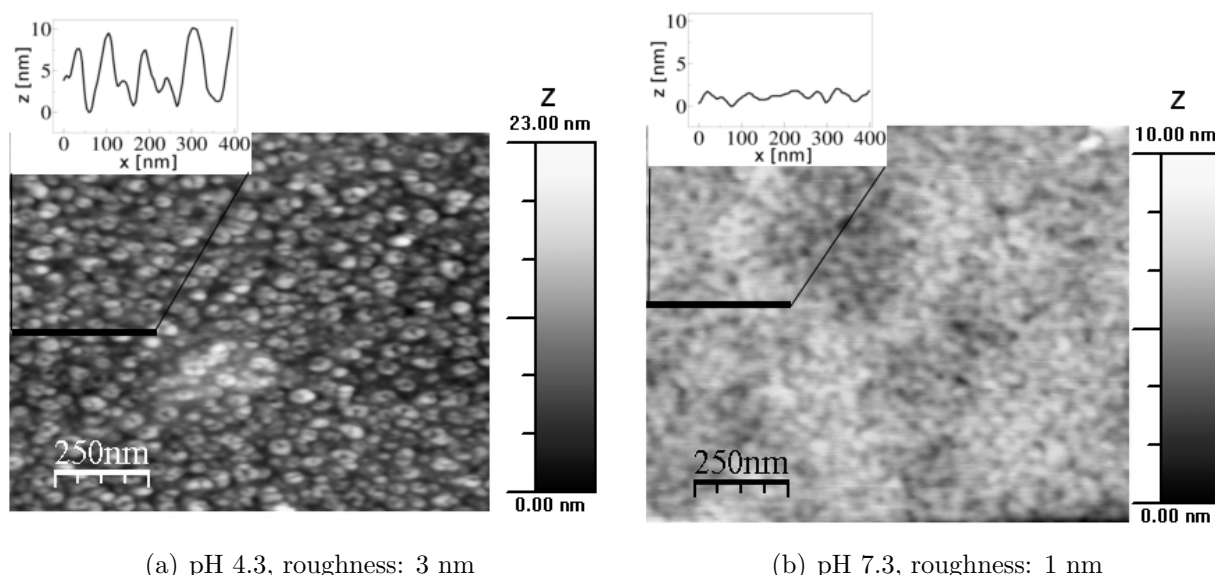
9.4. Comparison to ternary PNIPAAm - PAA-b-PS brushes

We also started to investigate the ternary PNIPAAm-PAA-b-PS brush system, motivated by model considerations. In such a ternary system it is desired firstly to graft a pH-insensitive polymer brush (here PNIPAAm) followed by the grafting of a pH-sensitive polymer (PAA), which is meant to provide a stimuli-responsive lift to expose or hide a hydrophobic model moiety (the PS block) at the brush-solution interface or inside the PNIPAAm brush respectively. For the block-copolymer used here with molecular weights of PAA-b-PS of $27,000 \frac{g}{mol}$ -b- $1,000 \frac{g}{mol}$ no significant changes in the adsorption behavior towards HSA could be monitored, whereas slight changes in surface properties and swelling behavior will be presented in the following.

Other ratios of PNIPAAm and PAA / PS were studied systematically within a diploma thesis, where cell adhesion studies have been performed, showing differences between binary and ternary brushes composed of PN28k chains and a block copolymer with $M_n^{PAA} = 19,500 \frac{g}{mol}$ and $M_n^{PS} = 4,300 \frac{g}{mol}$ [150].

Surface properties and swelling behavior of PN47k-PAA-b-PS brushes

An even increased structuring behavior of ternary PNIPAAm - PAA-b-PS brushes after pH-treatment could be found compared to the binary PNIPAAm-PAA brushes. Here AFM height images after treatment at pH 4 and pH 7.3 are displayed in Figure 9.15.



(a) pH 4.3, roughness: 3 nm

(b) pH 7.3, roughness: 1 nm

Figure 9.15.: AFM height images of a dry PNIPAAm - PAA-b-PS (50:50) brush after pH-treatment.

The surface roughness after treatment at pH 4 was 3 nm, and decreased to 1 nm after immersion of the sample at pH 7.3, whereas for binary PN47k-PAA brushes the maximum change in surface roughness was about 1 nm. Here it has to be noted, that pretreatment was done in 10 mM buffer solutions, thus dissociation of PAA is not complete at this environmental conditions and results for roughness after pH-sensitive pretreatment are changeable by increasing the salt content of the solution. Regarding the pH we would have expected a decrease in the change in roughness upon increasing the pH from pH 3 (binary brushes) to pH 4.3 (ternary brushes) since a larger fraction of COOH-groups along the PAA chains should be dissociated leading to a higher swelling of the mixed brushes as indicated for binary brushes in Figure 9.1. Contrarily here the surface roughness is higher for the ternary brush pretreated at pH 4.3 than for a similar PN47k-PAA binary brush pretreated at pH 3 (Figure 9.2).

When comparing the advancing contact angle of (80:20) and (50:50) ternary brushes in Figure 9.16 with the corresponding contact angle values for binary brushes (Figure 9.3) also a significant difference in the pH-dependent contact angle values for ternary (50:50) brushes can be found. Here the decrease in the advancing contact angle with pH is more pronounced than for the binary system, and at pH 3 $\theta_{adv} = 54.5 \pm 2.0^\circ$ is achieved, very close to the advancing contact angle of PAA-b-PS of $52 \pm 2^\circ$ at this pH. The surface fraction of the PAA-

b-PS copolymer decreased with increasing pH from 0.89 ± 0.05 after treatment at pH 3 to 0.18 ± 0.05 after treatment at pH 6. Compared to the fraction of 0.34 of PAA at the surface of the binary brush after treatment at pH 3, the nominal fraction of PAA-b-PS is remarkably increased after the same treatment, which is also reflected in a difference in the advancing contact angles of $10 \pm 2^\circ$. For the (80:20) PN47k-PAA-b-PS ternary brush θ_{adv} is close to the values for PNIPAAm mono brushes as well when comparing the results to values for the advancing contact angle for the corresponding binary brushes, and the fraction of PAA-b-PS of 0.05 is similar to the fraction of PAA in the (80:20) PNIPAAm-PAA binary brush.

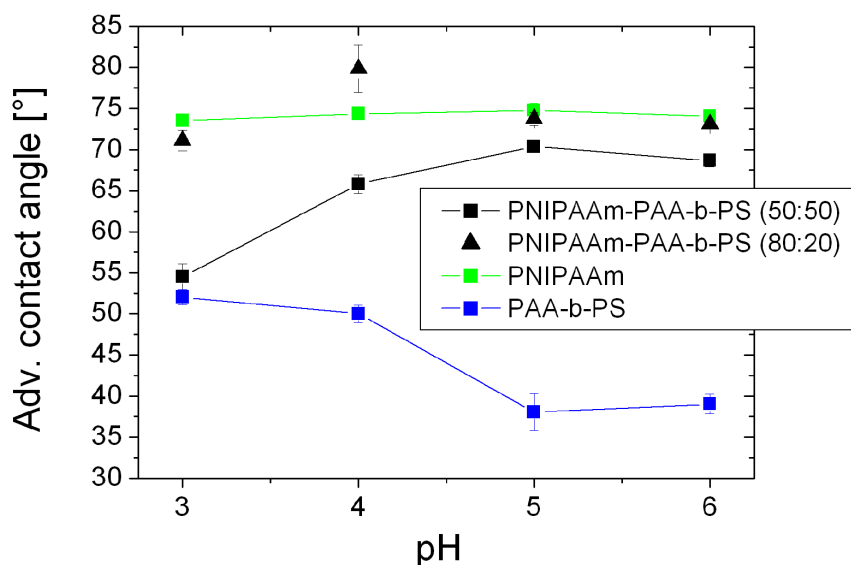


Figure 9.16.: Comparison of the advancing water contact angles of end-grafted PNIPAAm, loopwise-grafted PAA and two selected mixed brushes dependent on the pH in the acidic pH region after pH-treatment and subsequent drying.

Finally the pH sensitive swelling of PN47k-PAA-b-PS brushes with different grafting densities of the PN47k brush, thus different composition, was monitored at pH 4 and pH 9 and compared to the swelling of the corresponding PN47k brushes in water (Figure 9.17). Here the differences between swollen brush thicknesses at pH 4 and pH 9 increase with decreasing grafting density of the PN47k brush, starting with a PN47k homopolymer brush at a grafting density of 0.25 nm^{-2} with only marginal pH sensitivity down to a (50:50) PN47k-PAA-b-PS mixed brush with a PN47k grafting density of 0.08 nm^{-2} . The swollen brush thickness for the latter (50:50) mixed brush changes about $55 \pm 1 \text{ nm}$ between pH 4 and pH 9, comparable to the changes observed for the PN47k-PAA binary brush (Figure 9.4).

It is interesting to note, that the swollen brush thickness observed at pH 9 for the ternary brush is in good agreement with the thickness monitored for the corresponding PN47k homopolymer brushes. Thus we take this results as indication, that PNIPAAm chains in the mixed brush are also deswollen at pH 4 due to the presence of deswollen PAA chains, and are completely swollen at pH 9. The pH-sensitivity of PNIPAAm is considerably less than observed

in the swollen brush thickness for these ternary systems as indicated by the results for a PN47k brush with $\sigma = 0.25 \text{ nm}^{-2}$ plotted also in Figure 9.17. pH-sensitive changes in the swelling behavior of these ternary mixed brushes are reflected in the refractive indices in Figure 9.17(b), whereas for the swelling at pH 9 the refractive index $n(631.5 \text{ nm})$ was found to be slightly higher for brushes with high PAA-b-PS content compared to corresponding PN47k brushes in water, indicating more material at the surface than for the homopolymer brushes.

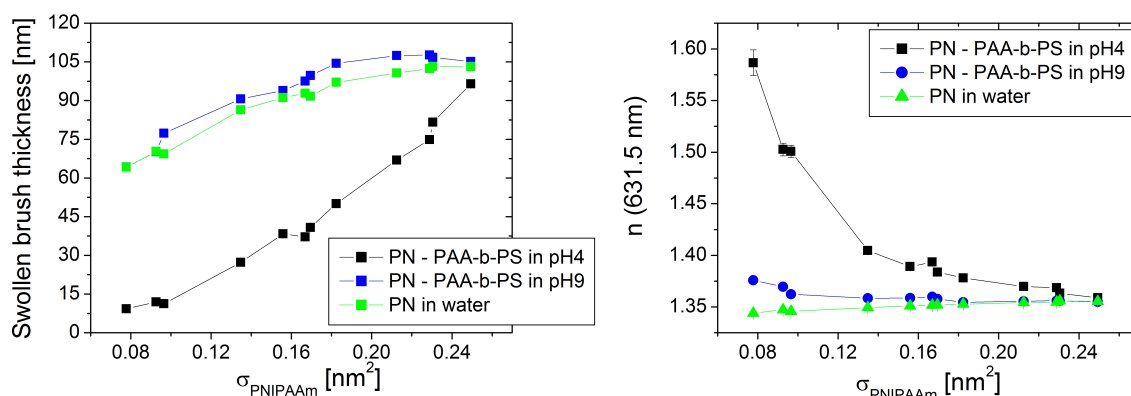


Figure 9.17.: Comparison of the pH-sensitive swelling of a grafting series of PN47k-PAA-b-PS mixed brushes at pH 4 and pH 9 with their corresponding PN47k homopolymer brushes in water.

9.5. Summary

Complex swelling behavior as it is sketched in Scheme 9.18 could be observed for PNIPAAm-PAA mixed brushes with different compositions. Here a coupled deswelling of PNIPAAm and PAA chains was evident at $pH < 5$, whereas above pH 5 the pH and salt sensitivity of PAA Guiselin brushes was enlarged by the presence of PNIPAAm in the mixed brushes. The temperature sensitivity of PNIPAAm-PAA mixed brushes is considerably decreased compared to PNIPAAm homopolymer brushes and even no temperature sensitivity was observed at pH 4 and for mixed brushes with a high PAA content. Here a two layer mixed brush geometry was pro-

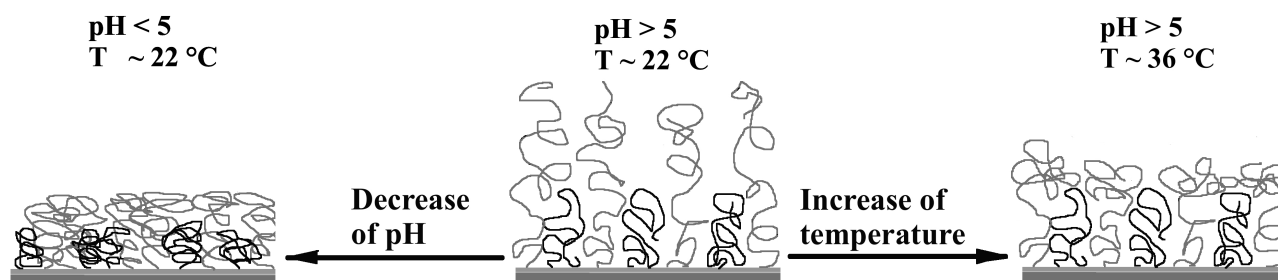


Figure 9.18.: Scheme of the coupled swelling of PNIPAAm (gray) and PAA (black) chains in binary mixed brushes dependent on pH and temperature.

posed, with a lower layer of interacting PNIPAAm and PAA chains, thus hindered temperature sensitivity of PNIPAAm and an upper layer with freely swellable PNIPAAm chains. An univocal dependency of the temperature sensitivity at pH 7 on the brush composition was found, with decreasing sensitivity for increasing PAA content. Coupled deswelling of PNIPAAm-PAA mixed brushes with a high PAA content at low pH was accompanied by a domain formation, observed in AFM height images, and the estimation of a significant fraction of PAA at the surface, derived from advancing contact angle measurements. According to additional roughness evaluations the domain size is assumed to decrease until finally the brush surface in the dry state is constituted almost only of PNIPAAm as indicated by the contact angle results of a PNIPAAm - PAA (80:20) brush.

An increased adsorption affinity of this mixed brush towards HSA was found compared to the adsorption at the corresponding homopolymer brushes, and also an additional temperature sensitive increase in the adsorption affinity, due to the collapse of PNIPAAm chains, could be shown. Thus an increased importance of the hydrophobic effect in the HSA adsorption process at this mixed brush system above but also below the LCST of PNIPAAm is concluded, whereas for the adsorption of α -chymotrypsin no hydrophobic effect could be observed. HSA could be released from the mixed brush surface below the LCST of PNIPAAm as well as above the LCST by increasing the pH, but no significant temperature sensitive release took place. Adsorption of HSA to the binary brush was found to proceed slower than adsorption to PAA Guiselin brushes, indicating a delaying effect of the PNIPAAm chains in reaching the maximum of the adsorbed amount. Possibly this behavior could be due to a hindered diffusion of the protein molecules through the PNIPAAm chains to adsorb electrostatically attractive onto the PAA chains.

A switching of HSA adsorption could be achieved pH- but not temperature sensitive so far. Here it would be highly interesting to investigate if immobilized functional macromolecules, e.g. enzymes, could be hindered in their activity above the LCST of PNIPAAm due to a deswelling of PNIPAAm chains and thus changes in the environmental conditions of these enzymes.

For PNIPAAm-PAA-b-PS brushes changes in physico-chemical interface properties due to coupled deswelling were more pronounced than in binary brushes, indicating an even more complex swelling behavior of these ternary brush system.

10. Mixed brushes containing Poly(ethylene glycol) (PEG)

PNIPAAm as the protein repelling not pH-sensitive component of binary and ternary brushes with PAA and PAA-b-PS respectively, was exchanged in this chapter to poly(ethylene glycol) (PEG). Here PEG chains with a molecular weight of $M_n = 5,000 \frac{g}{mol}$ (PEG-5k) were used, acknowledging the literature about ternary protein adsorption at PEG brushes with considerable higher M_n [48, 147]. The protein repelling behavior of PEG-5k brushes was already proven in Section 7.2, where $0.1 \frac{mg}{m^2}$ of HSA could be adsorbed in PBS solution.

In the literature a complexation of PEG and PAA is discussed due to hydrogen bonding, dependent on the molecular weight of PEG and PAA, whereas complexation could be found below pH 4 for a molecular weight of PEG higher than $5000 \frac{g}{mol}$ [251, 252]. Compared to the binary and ternary brushes consisting of PNIPAAm and PAA or PAA-b-PS, which were discussed in the last Section, it is now interesting how the introduction of PAA and PAA-b-PS chains into a protein repelling PEG brush affects the swelling behavior as well as the protein adsorption affinity of this mixed brush systems.

Basic swelling and adsorption experiments will be presented in this chapter based on cooperative research¹ on ternary polymer brushes, where driving forces for protein adsorption are tuned due to exposition / hiding of small hydrophobic PS-blocks at a overall hydrophilic PEG-PAA-b-PS ternary brush-solution interface [253].

In Section 10.1 PEG-PAA brushes with different PAA content are presented regarding their pH-sensitive swelling behavior and adsorption of HSA onto these mixed brush surfaces. In advance to activity measurements of enzymes immobilized at brush surfaces, also the adsorption of Glucose oxidase is included in the discussion.

Finally the salt sensitive swelling of (50:50) PEG-PAA-b-PS brushes is discussed shortly in Section 10.3 with respect to the effect of the block-copolymer on the swelling behavior.

¹DFG-NSF cooperation project in collaboration with Dr. Karsten Hinrichs, ISAS Berlin, Germany; Prof. Sergiy Minko, Clarkson University, USA; Prof. Igor Luzinov, Clemson University, USA and Prof. Marcus Müller, Universität Göttingen, Germany in the frame of "Materials World Network"

10.1. PEG-PAA brushes

Since the protein repellent behavior of PNIPAAm brushes was exceedingly disturbed by grafting of a small amount of PAA (Section 9.3), we were furthermore interested in how PAA affects the protein resistance of a PEG brush in a PEG-PAA binary system.

Therefore we investigated the swelling and adsorption behavior of PEG-PAA brushes with different PAA contents as listed in Table 10.1. Here the same PAA with $M_n = 26,500 \frac{g}{mol}$ as in previous studies was employed for PEG-PAA mixed brushes to monitor the effect of a PEG brush reference surface on the adsorption affinity of protruding PAA chains with increasing amount of PAA at the surface.

Table 10.1.: Brush parameters of PEG-PAA binary brushes for swelling and adsorption experiments.

Γ_{PEG} [mgm^{-2}]	wt% of PAA solution spin-coated	Γ_{PAA} [mgm^{-2}]	% (PAA)	$\frac{\Gamma_{HSA}}{\Gamma_{PAA}}$	$\frac{\Gamma_{GOx}}{\Gamma_{PAA}}$
5.31	—	—	—	—	—
5.36	0.01	0.86	14	1.1	1.9
5.04	0.1	1.03	17	3.3	2.5
4.36	1	1.55	26	3.3	2.3

The preparation of these PEG-PAA brushes was performed as follows: After grafting the PGMA anchoring layer a PEG brush was grafted from the melt as described by Zdyrko et al. [72]. Furthermore the amount of PAA at the surface was varied according to the concentration of PAA solution spin-coated on top of the PEG brush, whereas both Γ_{PEG} and Γ_{PAA} were calculated from the layer thickness obtained by spectroscopic ellipsometry with a fixed refractive index at $n=1.46$, determined for 8 nm thick PEG brushes beforehand.

Swelling measurements for pH values between pH 3 and pH 8 were performed in 10 mM buffer solutions and are displayed in Figure 10.1.

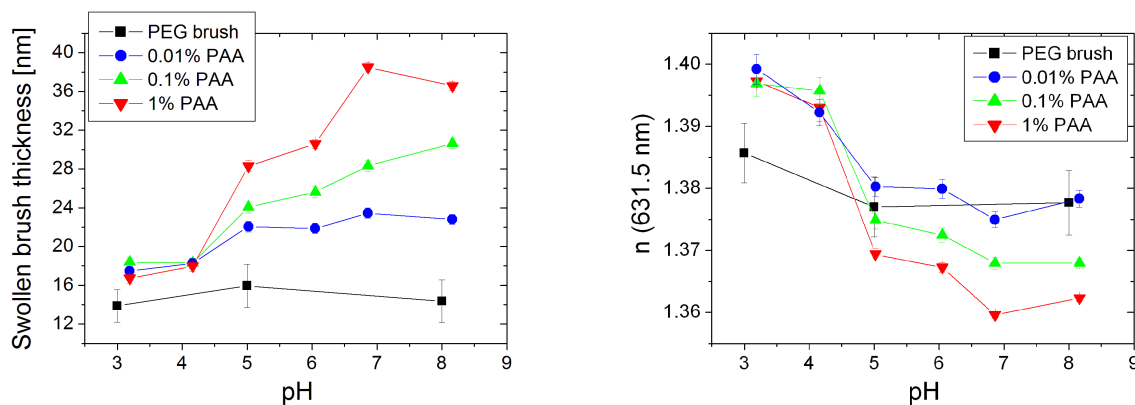


Figure 10.1.: pH dependent swelling of PEG-PAA brushes with different PAA content.

pH-sensitivity of binary brushes could be found for all PAA contents investigated. The sensitivity increased with increasing PAA content starting with a change in the swollen brush thickness of $5 \pm 1 \text{ nm}$ for 14 % PAA to $21 \pm 1 \text{ nm}$ for 26 % PAA in the binary brush, which was also reflected in the pH-sensitive refractive indices that are higher than reference refractive indices of a pure PEG brush at low pH due to the deswelling of PAA. Here the PEG brush was insensitive to changes in the pH with a constant swollen brush thickness of $14 \pm 2 \text{ nm}$ in the range between pH 3 and pH 8. Thus in comparing the swollen brush thickness for pure PEG brushes and PEG-PAA binary brushes it can be concluded, that PAA chains extend above the PEG-brush surface, which was not the case for the PN47k-PAA binary brushes.

Having investigated the swelling behavior, protein adsorption experiments of HSA and the enzyme glucose oxidase at pH 4 in 10 mM buffer solution were performed. The isoelectric point of glucose oxidase is at pH 4.2 thus both proteins adsorb at electrostatic attractive conditions onto the PAA chains, whereas the enzyme has a 2.4 times higher molecular weight of 160 kDa than HSA and with dimensions of $7 \times 5.5 \times 8 \text{ nm}^3$ a 1.6 times larger size [186,187].

In Figure 10.2 total adsorbed amounts of HSA and glucose oxidase are displayed for different amounts of PAA at the surface.

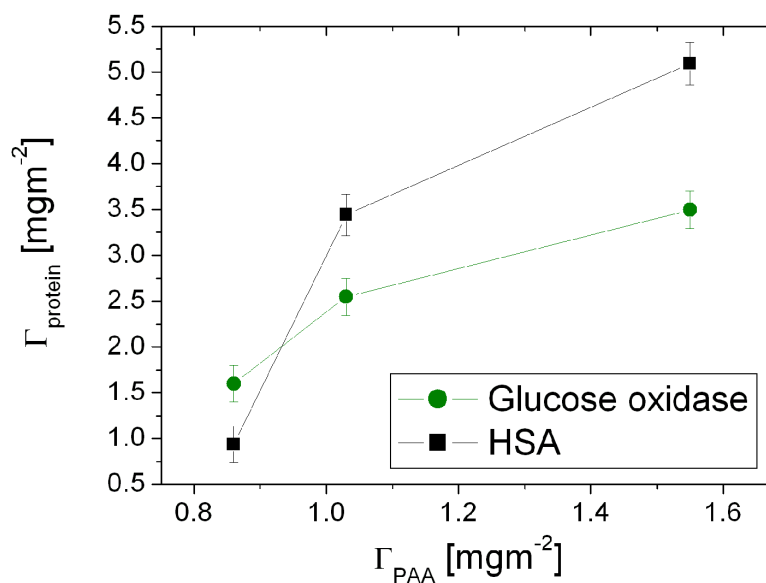


Figure 10.2.: Adsorbed amount of HSA and glucose oxidase on PEG-PAA brushes with different PAA content at pH 4.

Here the total adsorbed amount of protein was monitored for all compositions of binary brushes presented in Table 10.1. For the pure PEG brush an amount of $0.9 \pm 0.2 \frac{\text{mg}}{\text{m}^2}$ of HSA was adsorbed at this environmental conditions (pH 4). Thus an increase of the adsorbed amount of HSA compared to the pure PEG brush could be observed starting at a PAA content of $1.03 \frac{\text{mg}}{\text{m}^2}$ (17 % PAA), whereas for this PEG-PAA brush the specific adsorbed amount of HSA

was $\frac{\Gamma_{HSA}}{\Gamma_{PAA}} = 3.3$ which is in very good agreement with the specific adsorbed amount observed for pure PAA Guiselin brushes at this pH, regarding the results in Figure 8.5(b):

$$\frac{\Gamma_{HSA}}{\Gamma_{PAA}} = \frac{25.0 \text{ } mgm^{-2}}{7.6 \text{ } mgm^{-2}} = 3.3$$

This is another indication that PAA chains protrude above the PEG reference brush, but also that they are not interacting with PEG chains at pH 4. It is also expected, regarding the discussion of complexation of PEG and PAA [251,252], that no interaction between these two types of polymer chains occurs at higher pH. Thus the adsorption of HSA onto this binary brush should be solely influenced by the amount of PAA chains on the surface with no effect of an interaction of PEG and PAA chains on the adsorption, contrary to the PNIPAAm-PAA binary system.

The amount of glucose oxidase adsorbed at these PEG-PAA binary brushes was smaller than observed for HSA. This could be due to differences in the protein size but also due to a different density of positive charges at the protein molecules because of their IEP at pH 5.7 (defatted HSA) and pH 4.2 (glucose oxidase).

For adsorption of glucose oxidase onto PAA Guiselin brushes an amount of

$$\Gamma_{GOx} = 27 \pm 1 \frac{mg}{m^2}$$

was observed at pH 4 in 10 mM buffer solution, corresponding to a specific adsorbed amount of $\frac{\Gamma_{GOx}}{\Gamma_{PAA}} = 3.6$. Thus comparing the adsorption onto PAA Guiselin brushes and PEG-PAA binary brushes $\left(\frac{\Gamma_{GOx}}{\Gamma_{PAA}} \leq 2.5\right)$ a reduction of the adsorption onto the latter brush system due to the presence of PEG can be concluded.

10.2. Salt dependent swelling of PEG-PAA-b-PS

To complete this chapter, salt dependent swelling of a PEG-PAA-b-PS mixed brush is presented in Figure 10.3. A similar sensitivity of the swollen brush thickness to pH for low salt concentrations compared to PAA-b-PS Guiselin brushes (Section 8.1) could be found. Here the layer thickness increased about 10 nm when changing the pH from pH 3 to pH 8, which is in the range of the change in layer thickness of $8.0 \pm 2.5 \text{ } nm$ for PAA-b-PS Guiselin brushes. A maximum of swollen brush thickness was found for both pH at 0.2 M salt concentration. It is important to note, that the total swollen brush thickness of the ternary brush is higher than the swollen brush thickness of a PEG reference brush for all investigated salt concentrations at both pH. Thus it can be assumed that the PAA-b-PS copolymer is present at the brush-solution interface in all cases, as observed similarly for the binary PEG-PAA brushes.

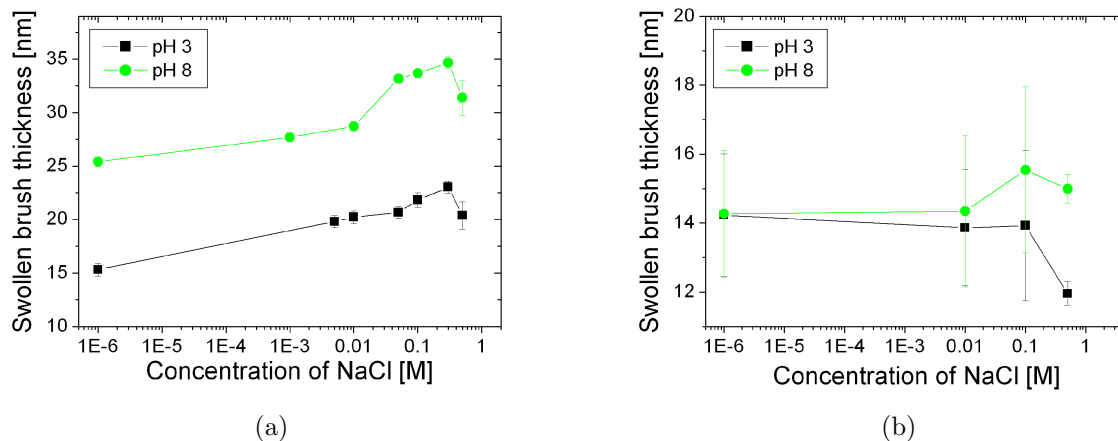


Figure 10.3.: Salt dependent swelling at two different pH of PEG-PAA-b-PS (a) compared to PEG brushes (b). Corresponding refractive indices can be found in the appendix (Figure A.8).

10.3. Summary

In this chapter we aimed at the investigation of PEG brushes with protruding PAA chains to determine the influence of a pH-insensitive PEG reference brush on the adsorption behavior of PAA chains.

Swelling of the binary brush was found to be pH-sensitive due to the presence of PAA chains, whereas the total swollen brush thickness was higher than evaluated for pure PEG brushes, indicating that PAA swells above the PEG brush surface. For the ternary PEG-PAA-b-PS brush a similar pH-sensitive swelling in non-salted solution as for pure PAA-b-PS Guiselin brushes was observed.

Protein adsorption was monitored for HSA and for the larger enzyme glucose oxidase at pH 4, for both proteins upon electrostatic attractive conditions. The specific adsorbed amount of HSA was in very good agreement to the specific amount adsorbed at PAA Guiselin brushes, thus no influence of the PEG content in the mixed brush on the adsorption of this protein was found. When comparing the adsorption of glucose oxidase on the binary and the Guiselin brush, a reduction of the specific adsorbed amount was found for the PEG-PAA brush, indicating an influence of PEG on the adsorption behavior of the mixed brush system. Here possible reasons for the different adsorption affinity of HSA and glucose oxidase could be the different positive charge density on both proteins due to their individual isoelectric points, but also a size effect, thus an increased repellent effect of PEG on the adsorption of the larger glucose oxidase.

11. Activity of glucose oxidase immobilized at mono and mixed brushes

Based on the pH sensitivity of PAA and poly(2-vinyl pyridine) (P2VP) as well as the temperature sensitivity of PNIPAAm, binary polymer brushes with complex swelling behavior are to be utilized in switching enzyme activities at brush surfaces. Here it is desired to switch between an active state of the enzyme at temperatures below the LCST of PNIPAAm to an inactive state above the LCST, where the enzyme is to be covered by the deswollen PNIPAAm in the latter case (Figure 11.1).

For first experiments with immobilized enzymes, glucose oxidase was selected (IEP: pH 4.2, Table 5.2), and immobilized at overall electrostatic attractive conditions at PAA Guiselin brushes, at the "wrong side" of its IEP at P2VP end-grafted brushes as well as at PNIPAAm-PAA and PNIPAAm-P2VP binary brushes.

The immobilization of glucose oxidase has been studied for the development of enzyme biosensors in the literature [186,254]. The enzyme can function as biochemical transducer in an optical sensing device [254], using the depletion of oxygen in the enzymatic reaction and its effect on the quenching of fluorescence signals of organic ruthenium complexes. As another example it can be used to design glucose electrodes, where an electrode is covered by an enzyme membrane and the production of H_2O_2 measured amperometrically [186].

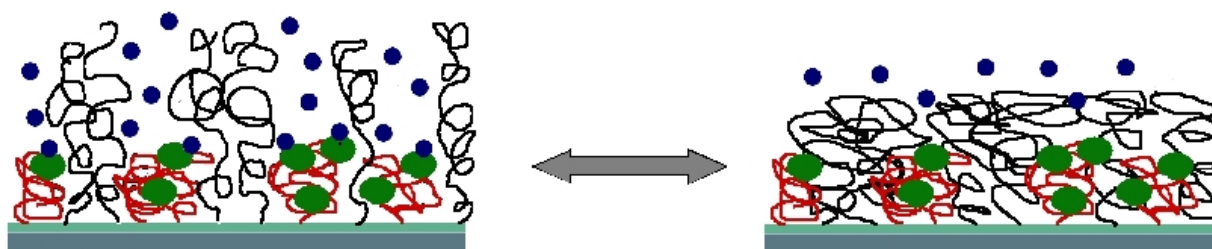


Figure 11.1.: Scheme of the desired switching of the activity of enzymes immobilized at a mixed brush surface.

11.1. Enzyme reaction and quantification of resulting H_2O_2

The oxidation of β -D-glucose by O_2 is catalyzed by glucose oxidase, leading to the products glucono delta-lactone and H_2O_2 (Scheme 11.2), whereas the increase of the H_2O_2 concentration leads to a decrease of the pH in non-buffered solutions. The optimum pH for the catalytic function of the enzyme in solution is at pH 5.5 and oxidation was observed in the range of pH 4 - 7 [187]. The corresponding optimum temperature is 40 °C [255].

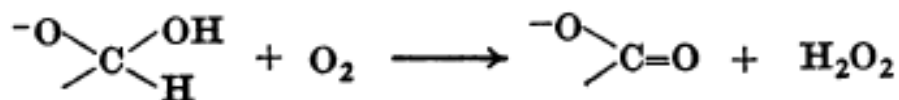


Figure 11.2.: Scheme of the oxidation of glucose catalyzed by glucose oxidase.

In this work glucose oxidase was adsorbed at mono and mixed brushes at pH 4 in 10 mM acetate buffer solution with $0.25 \frac{\text{mg}}{\text{ml}}$ enzyme concentration for 2h, and the enzyme-brush surface equilibrated in the pure buffer solution for 1 h. For the modeling of the amount of glucose oxidase according to the modified de Feijter approach (Section 6.3.4) a refractive index increment for the enzyme of $0.177 \frac{\text{cm}^3}{\text{g}}$ was used, measured by Forzani et. al for glucose oxidase dissolved in water [212], which is lower than dn/dc for the model proteins HSA or chymotrypsin due to the fraction of 16 % carbohydrates in this glyco-protein [186]. For P2VP $dn/dc = 0.254 \frac{\text{cm}^3}{\text{g}}$ was taken [211].

After adsorption the surface was immersed in $1 \frac{\text{mg}}{\text{ml}}$ glucose solution, buffered again with acetate buffer at pH 4 to prevent changes in the activity of the immobilized enzyme during the oxidation of glucose. The concentration of the reaction product H_2O_2 of the oxidation of glucose was measured after 15 min reaction time.

For the quantification of H_2O_2 a colorimetric assay, based on the oxidation of Fe^{2+} to Fe^{3+} and subsequent reaction of Fe^{3+} ions with xylenol orange to complexes, was used [256–258]. In aqueous solution first sorbitol is converted to a peroxy radical by H_2O_2 , and this radical initiates the oxidation of Fe^{2+} to Fe^{3+} . The absorbance of the colored adduct (xylenol orange, 3,3'-bis[N,N-bis(carboxymethyl)aminoethyl]-*o*-cresolsulfonephthaleine, sodium salt) is observed at 560 nm. The assay is linear in the range of 1-7 nmol/ml of H_2O_2 , whereas for higher concentrations the absorbance at 590 nm can also be evaluated.

11.2. Homopolymer brushes

For PAA Guiselin brushes, P2VP end-grafted brushes and PNIPAAm end-grafted brushes the amount of immobilized glucose oxidase as evaluated from in-situ ellipsometry measurements as well as the concentration of H_2O_2 after 15 min in glucose solution are presented in Figure 11.3.

As expected the amount of enzyme immobilized at the polyelectrolyte brushes is relatively high due to adsorption at pH 4 close to the IEP of pH 4.2 of the enzyme, whereas at PNIPAAm brushes with a molecular weight of $47,600 \frac{g}{mol}$ a very low adsorbed amount of glucose oxidase of $0.5 \frac{mg}{m^2}$ could be observed (Figure 11.3(a)).

Regarding the adsorption results, it is most interesting, that the amount of H_2O_2 produced by enzyme molecules immobilized at P2VP brushes is almost twice as high as the amount measured for glucose oxidase immobilized at PAA Guiselin brushes (Figure 11.3(b)). This leads to the conclusion that for the adsorption at the "wrong side" of the IEP at P2VP brushes the active center of a considerable higher amount of enzymes is less disturbed at this overall electrostatic repulsive conditions compared to enzymes adsorbed at overall electrostatic attractive conditions at PAA Guiselin brushes.

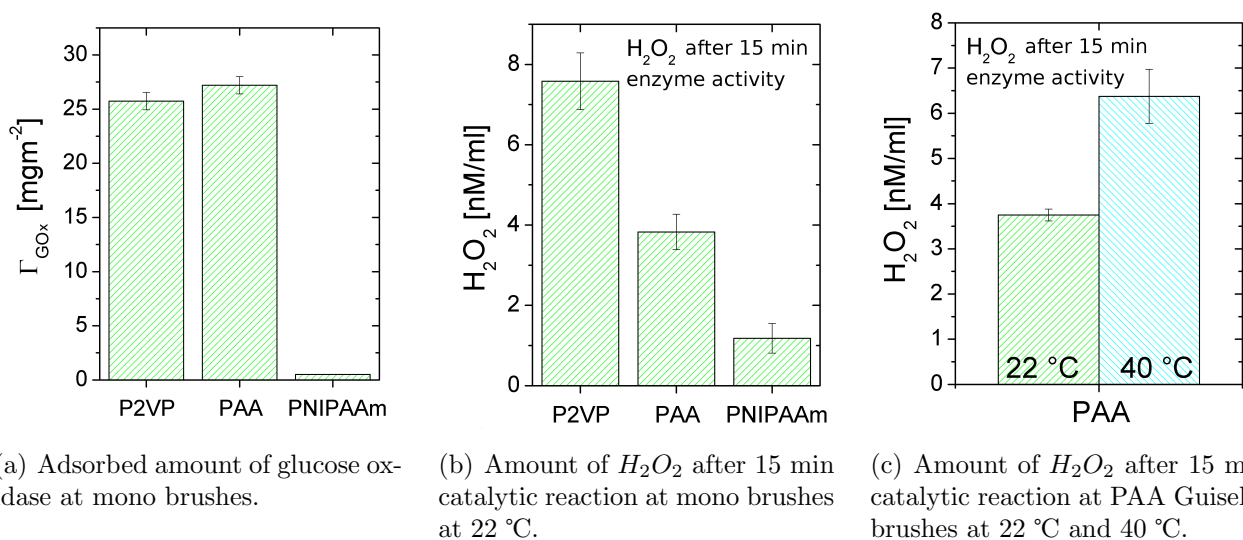


Figure 11.3.: Adsorbed amount of glucose oxidase (a) and analysis of enzyme activity (b), (c) for P2VP and PNIPAAm end-grafted brushes as well as PAA Guiselin brushes.

Together with theoretical studies on charge regulation at weak amino acid side chains upon repulsive adsorption conditions [143], investigation of the activity of enzymes immobilized at polyelectrolyte surface layers offers a very sensitive approach to study adsorption mechanisms. For the brushes presented here, more detailed studies on the influence of the IEP of enzyme and surface would be necessary to conclude trends of the activity of this enzyme immobilized at polyelectrolyte brush surfaces.

Regarding PNIPAAm end-grafted brushes a significant amount of H_2O_2 could be detected after immersion of the brush surface in glucose solution, although the adsorbed amount of enzyme is very small, thus relatively few enzyme molecules would have to be still very active when immobilized at these brushes. This indicates a considerable influence of the enzyme environment on its activity, whereas the total adsorbed amount is of less importance. Since we expect the proteins to adsorb via ternary adsorption at the PNIPAAm chains in analogy to the adsorption behavior at PEG brushes with increasing ternary adsorption for longer chains

[48,147], a discussion of the activity of enzymes immobilized at end-grafted PNIPAAm brushes dependent on the molecular weight of PNIPAAm, would be of high interest.

11.3. Mixed brushes

In a first attempt glucose oxidase was also adsorbed at PNIPAAm-PAA and PNIPAAm-P2VP binary mixed brushes at the same environmental conditions at pH 4 and 22 °C used for the experiments with mono brushes. Parameters of the binary brushes investigated in this section are presented in Table 11.1.

Table 11.1.: Typical parameters thickness d and refractive index n of dry polymer brushes as well as the volume fraction of polymer 2 in the mixed brushes calculated from the ellipsometric thickness data [198]. *Refractive index fixed.

Polymers	d [nm]	n (631.5 nm)	% Polymer 2
PN47k - PAA	6.7 ± 0.2	*1.47	29
PN47k - P2VP	15.1 ± 0.3	1.469	10

As discussed in Section 9.2.2 and displayed in Figure 11.4(a) the binary PNIPAAm-PAA brush is not deswelling temperature sensitively due to the interaction between PAA and PNIPAAm chains. In contrast to this binary brush PNIPAAm is deswelling when grafted in combination with P2VP (Figure 11.4(b)).

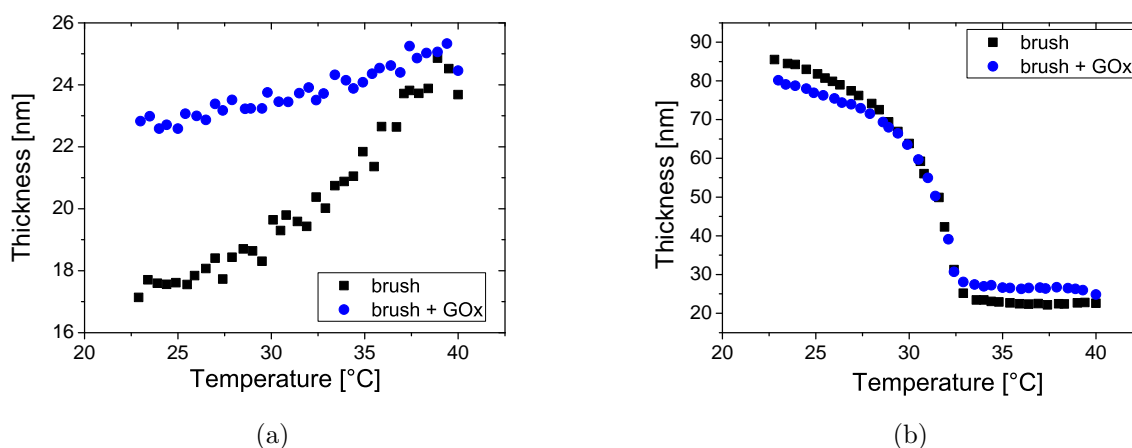


Figure 11.4.: Temperature sensitive swelling of PNIPAAm-PAA (a) and PNIPAAm-P2VP (b) binary brushes before adsorption and after adsorption of glucose oxidase (GOx). Corresponding refractive indices can be found in the appendix in Figure A.9.

Due to the small amount of polyelectrolytes in the mixed brush only a small amount of glucose oxidase is immobilized in both cases (Figure 11.5(a)), and the swelling tendencies do not change significantly after the adsorption of the enzyme. A decrease in temperature sensitivity

of the PNIPAAm-P2VP mixed brush is expected when increasing the amount of enzyme at the surface, whereas the finding of an optimum of brush composition / enzyme loading and environmental parameters pH / salt for switching of enzyme activity within these two binary brush systems will be subject of future research.

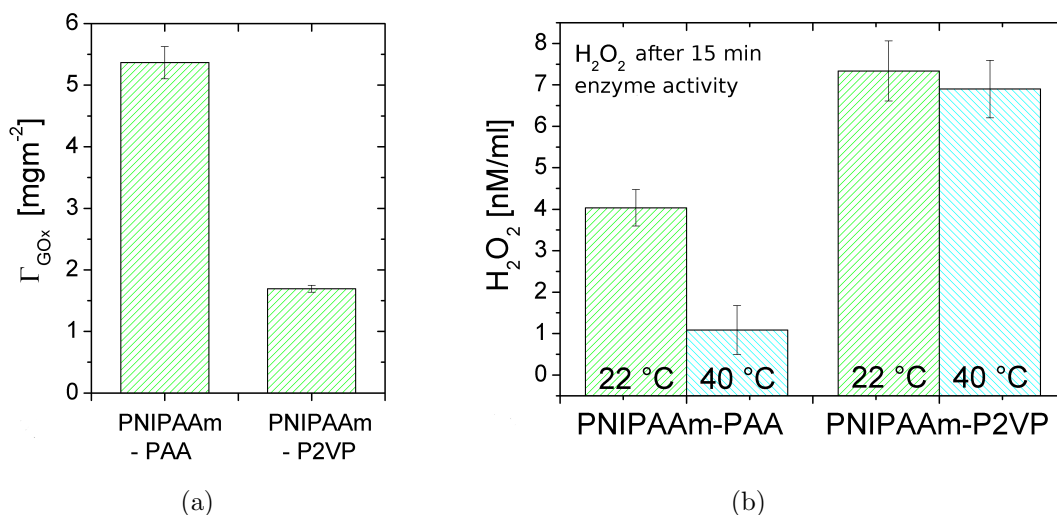


Figure 11.5.: Adsorbed amount of glucose oxidase (a) and analysis of enzyme activity (b) for PNIPAAm-PAA and PNIPAAm-P2VP binary brushes at 22 °C and 40 °C.

As can be seen in Figure 11.5(b) within this first attempt switching of enzyme activity between an active state at 22 °C and a less active state at 40 °C could be achieved for PNIPAAm-PAA binary brushes, whereas for PNIPAAm-P2VP binary brushes the enzyme activity was preserved at the higher temperature. Comparing these results for the PNIPAAm-PAA brush with the temperature dependent activity of glucose oxidase immobilized at PAA Guiselin brushes, the trend for the dependency of the activity on the temperature is reversed for this binary brush. Thus a switching effect due to the presence of PNIPAAm can be concluded.

When regarding the temperature sensitive swelling behavior of the binary brushes in Figure 11.4, these findings are promising to lead to new insights into the effect of the micro-environment of these immobilized enzymes on their activity. Since no temperature sensitive deswelling was measurable for PNIPAAm-PAA brushes, whereas PNIPAAm-P2VP brush deswelled highly sensitive, collective conformational changes of the PNIPAAm chains can be excluded as reason for this switching behavior. It is more likely, that changes in the activity occur due to changes in local degrees of hydrogen bonding as well as local changes in charge densities. Here different methods like, e.g. ATR-FTIR, could provide further experimental data to explain these changes in the enzyme activity.

In the case of the catalysis of glucose by glucose oxidase the substrate molecules (glucose) are rather small, thus the function of the deswollen PNIPAAm chains as a diffusion barrier, preventing the substrate molecules from reaching the immobilized enzymes, is not likely and the absence of activity changes for PNIPAAm-P2VP can be understood. For different enzyme-substrate combinations with substrate molecules with increased sizes the temperature sensitive

deswelling of PNIPAAm chains is expected to lead to a more pronounced switching effect in the enzyme activity.

11.4. Summary

Activity of the immobilized enzyme glucose oxidase was investigated for adsorption at homopolymer and binary mixed brushes by detecting the amount of H_2O_2 after 15 min of enzyme driven catalysis of glucose at constant environmental conditions.

For P2VP brushes the enzyme glucose oxidase was highly active, when immobilized at the "wrong side" of its IEP, whereas upon adsorption at electrostatic attractive conditions at PAA Guiselin brushes the activity was considerably smaller. Most interestingly at PNIPAAm brushes, where only a small amount of glucose oxidase could be detected by null-ellipsometry, a significant enzyme activity could be monitored, thus a small but highly active amount of glucose oxidase has to be immobilized at these PNIPAAm brushes.

Regarding PNIPAAm-PAA and PNIPAAm-P2VP mixed brushes a switching of the enzyme activity to a less active state at 40 °C could be achieved for PNIPAAm-PAA but not for PNIPAAm-P2VP, whereas temperature sensitive deswelling of the binary brushes was evident for the latter case but not for the first one. Thus investigation of the activity of immobilized functional biomolecules leads to new insights on environmental sensitive changes in their physico-chemical nano-environment embedded in mixed polymer brushes.

12. Summary and outlook

Detailed investigation of the stimuli-responsive phase transition of binary and ternary brushes as well as their corresponding homopolymer brushes in aqueous solution was presented, focusing on pH and temperature sensitivity. Beyond the switching of the conformation of mixed brushes by treatment in different organic solvents, as reported in the literature, stimuli-responsiveness of binary and ternary brushes in aqueous solution is desirable, when aiming at a control of the interaction between brush surface and biological macromolecules like proteins, especially enzymes. Here a switching of protein adsorption affinity as well as activity of immobilized enzymes was achieved at binary brushes with pH and temperature respectively. The driving forces for protein adsorption at homopolymer and binary brushes could be further elucidated.

PNIPAAm-brushes

A decrease of the degree of hydrogen-bonding above the LCST was proven by ATR-FTIR measurements in monitoring the temperature sensitive shift of amide vibration bands, whereas the brushes were still considerably hydrated compared to the position of vibration bands in the dry state. No dependency of the band position at 24 °C and 50 °C on molecular weight and grafting density could be observed, indicating a similar state of hydration of the individual polymer chains in the brush for all three investigated PNIPAAm brushes (PN28k: $\sigma = 0.11 \text{ nm}^{-2}$, PN45k: $\sigma = 0.10 \text{ nm}^{-2}$, PN132k: $\sigma = 0.06 \text{ nm}^{-2}$) for each temperature respectively.

The surface hydrophobicity was found to increase with increasing temperature, whereas a dependency of the advancing contact angle on the amount of polymer on the surface was observed.

The phase transition temperature, evaluated from spectroscopic ellipsometry measurements, increased with increasing grafting density, starting for the lowest grafting density at $\vartheta_{half}(d/2) = 26.4 \text{ °C}$, close to the LCST observed for PNIPAAm chains in PBS buffer solution in the literature. Thus inter-chain interactions between polymers were found to increase with increasing grafting density, reducing the salting out effect in PBS buffer solution.

PNIPAAm brushes were found to be highly protein repellent in PBS buffer solution below and above the LCST for molecular weights of PNIPAAm in the range of 28,500 $\frac{\text{g}}{\text{mol}}$ to 132,000 $\frac{\text{g}}{\text{mol}}$ with grafting densities around 0.1 nm^{-2} . Only for the shortest PN28k brushes marginal HSA adsorption could be found above the LCST. The total swollen brush thickness was concluded to be more important for the protein repelling behavior than the buffer volume fraction inside

the brushes, pointing at secondary adsorption at the brush-solution interface for the adsorption observed at PN28k brushes.

PAA and PAA-b-PS Guiselin brushes

pH- and salt sensitive swelling of Guiselin brushes with multiple grafting points could be proven to be comparable to the swelling behavior of end-grafted brushes, thus a similar interaction of these more easily prepared Guiselin brushes with macromolecules from solution is expected. Additionally the small PS block with a molecular weight of $1000 \frac{g}{mol}$ in PAA-b-PS Guiselin brushes was found to increase the pH-sensitivity at very low salt concentrations.

Very high adsorbed amounts of the proteins HSA and α -chymotrypsin were examined quantitatively, with a maximum adsorbed amount centered around the IEP of the protein for HSA and at pH 6 for α -chymotrypsin, thus different adsorption mechanism could be concluded for both proteins. Here the fraction of protein in the combined polymer-protein layer as well as its thickness can be derived from spectroscopic ellipsometry measurements, providing novel informations about changes in surface properties upon loading and release processes. The protein-brush systems were highly sensitive to changes in pH and salt concentration, whereas the density of the combined layer can be controlled due to the amount of protein at the surface alongside with the overall electrostatic conditions. Thus these layers are suitable for a precise control of diffusion processes or for sensor applications.

Furthermore for PAA-b-PS Guiselin brushes the critical pH until adsorption at the "wrong side" takes places was shifted to pH 7, compared to pH 6.2 observed for PAA Guiselin brushes at 10 mM salt concentration.

In coupled ellipsometry and quartz crystal microbalance measurements a considerable increase of the amount of buffer molecules viscoelastically coupled on top of the Guiselin brushes was found upon swelling the brushes in electrolyte solutions.

Changes in the coupled amount of buffer upon adsorption of the protein BSA could be monitored, and thus the incorporation of water molecules (and ions) into the polymer-protein layer during the adsorption process investigated quantitatively. For adsorption at pH 6 at the "wrong side" of the IEP of the protein a coupling of an excess amount of buffer components was observed, which could possibly be explained by charge regulation at the protein molecules during the adsorption process. Desorption at pH 7.6 led to an increase in the polymer-protein combined layer thickness accompanied by a strong increase in the viscoelastically coupled amount, thus underlining a stretching of the combined brush-protein layer with additional incorporation of buffer molecules in the desorption process. Additionally the shear viscosity of the combined polymer-protein layer was evaluated, leading to higher internal friction of the combined layer upon electrostatic attractive adsorption than upon adsorption at the "wrong side" of the IEP of the protein, due to the higher total amount of the protein adsorbed.

Binary and ternary mixed brushes

Complex swelling behavior was observed for PNIPAAm-PAA mixed brushes due to a complexation between these polymers supposedly by hydrogen bonding at low pH. Here a coupled deswelling of PNIPAAm and PAA chains was evident at $pH < 5$, whereas above pH 5 the pH and salt sensitivity of PAA Gueiselin brushes was enlarged, with higher changes in the brush layer thickness and refractive index, when PNIPAAm was present in the mixed brushes. The temperature sensitivity of PNIPAAm-PAA mixed brushes is considerably decreased compared to PNIPAAm homopolymer brushes and no temperature sensitivity could be observed at pH 4 and for mixed brushes with a very high PAA content.

The relative amount of HSA $\left(\frac{\Gamma_{HSA}}{\Gamma_{PAA}}\right)$ was increased upon adsorption at PNIPAAm-PAA binary brushes compared to the adsorption at the corresponding homopolymer brushes. Additionally, above the LCST of PNIPAAm, when the PNIPAAm chains are collapsed and more hydrophobic, $\left(\frac{\Gamma_{HSA}}{\Gamma_{PAA}}\right)$ was further increased. Thus PNIPAAm in this mixed brush conformation was not resistant to HSA adsorption even at very low PAA contents of 20 %, but further increased the adsorption affinity of the system. A disturbance of the PNIPAAm brush structure due to interactions with the PAA chains is concluded, and next to polyelectrolyte mediated HSA adsorption (charge regulation at protein, counter ion release) the importance of the hydrophobic effect in the HSA adsorption process at these binary brushes was discussed.

No increased adsorption affinity and thus no additional effect of the PNIPAAm chains on the adsorption behavior could be observed for α -chymotrypsin, possibly due to a higher structural stability of this protein.

Switching the adsorbed amount of HSA could be achieved similarly to the switching at PAA Gueiselin brushes, in adsorbing the protein at electrostatic attractive conditions at low pH and switching to electrostatic repulsive conditions at high pH. Here the specific amount in the release process decreased on the same timescale. Also temperature sensitive release was observed, though less pronounced. Adsorption kinetics were found to differ considerably between Gueiselin brushes and PNIPAAm-PAA mixed brushes pointing at a delayed adsorption onto the mixed brushes, possibly due to a diffusion barrier introduced by the PNIPAAm chains.

In changing PNIPAAm for the more hydrophilic and well known protein resistant PEG, the adsorption affinity of the PEG-PAA binary brush was found to be in good agreement with the adsorption affinity of PAA Gueiselin brushes. Hence no influence of the grafted PEG chains on the adsorption of HSA onto PAA chains was observed. From this findings it is concluded that PEG and PAA chains do not form a complex due to H-bonding at pH 4 and thus swell independently. For the enzyme glucose oxidase a reduction of the specific adsorbed amount at PEG-PAA brushes was found compared to PAA Gueiselin brushes, indicating an repelling influence of PEG in the mixed brush system on the adsorption behavior of this comparatively large enzyme.

Outlook to enzyme activity on brush surfaces

All polymer chains grafted into polymer brushes within this thesis are hydrophilic and thus it is expected that immobilized biomacromolecules like proteins and especially enzymes can be immobilized highly reversibly at the brush surfaces, whereas environmental conditions can be found where the biomacromolecules maintain their shape and a considerable part of their activity.

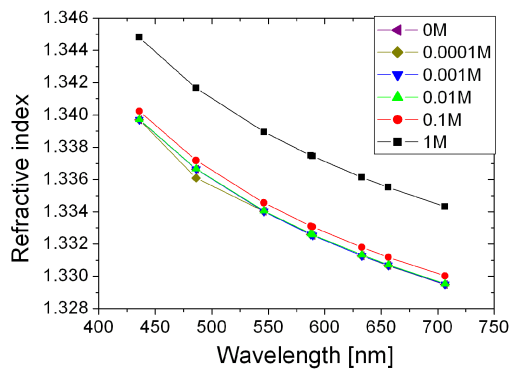
For P2VP brushes the enzyme glucose oxidase was highly active, when immobilized at the "wrong side" of its IEP, whereas upon adsorption at electrostatic attractive conditions at PAA Guiselin brushes the activity was considerably smaller. Most interestingly even at PNIPAAm brushes where no adsorption of glucose oxidase could be detected with null-ellipsometry a considerable enzyme activity could be monitored.

It is now of high interest both from the applicational and scientific point of view whether the activity of the enzyme can be reduced by changing the brush conformation, thus whether the active center of the enzyme can be blocked due to interaction, e.g. by hydrogen-bonding with the polymer chains or due to a hindered diffusion of substrate molecules. Here in first experiments a switching of the enzyme activity to a less active state at 40 °C could be achieved for PNIPAAm-PAA but not for PNIPAAm-P2VP binary brushes, whereas temperature sensitive deswelling was evident for the latter brush system but not for the first one.

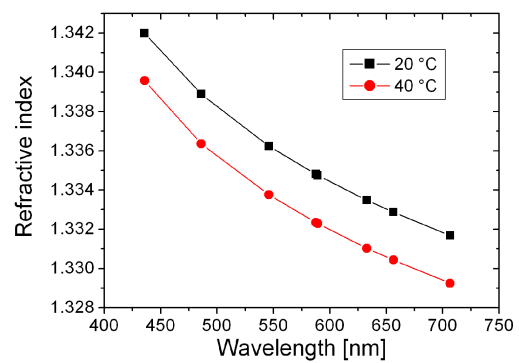
This approach to functional surface coatings can be refined by introducing biocompatible temperature sensitive polymer chains, as well as by tuning the phase transition temperature to human body temperature. In perspective this research could lead to controllable activity of functional drug molecules due to changes in the body temperature or molecule and ion concentration in biological fluids, but also smart sensing devices in biotechnological fields are realizable.

A. Appendix

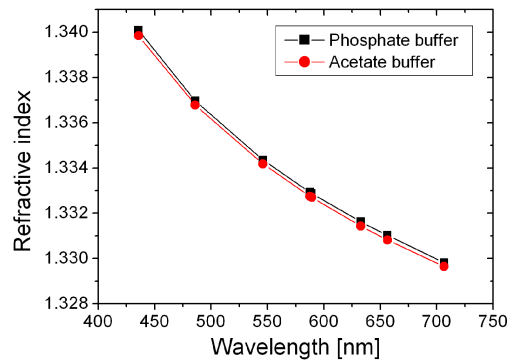
A.1. Dispersion relations for buffer and salted solutions



(a) Dispersion of the refractive index for NaCl solutions with different concentration.



(b) Dispersion of the refractive index for phosphate buffered saline buffer solutions at 20 °C and 40 °C.



(c) Dispersion of the refractive index for 10 mM phosphate and acetate buffer solutions.

Figure A.1.: Dispersion of the refractive index for different ambient solutions. The wavelength-dependent refractive index $n(\lambda)$ is also influenced by temperature and salt concentration, but only marginal by pH.

A.2. Comparison of different models for protein adsorption

In Section 6.3.4 a modified de Feijter approach was presented to calculate the adsorbed amount of protein from the refractive index n and the layer thickness d of a combined protein-polymer

layer. This approach of a uniform composite layer of protein and polymer brush was considered to describe the surface layer after protein adsorption in the best possible way. Here considerations of a penetration of the protein into the brush are based on X-ray reflection experiments of BSA adsorption on PAA end-grafted spherical brushes, where a penetration of the protein into the brush was observed [136].

Within this Section other possible models to derive the adsorbed amount Γ of protein according to the de Feijter equation (Equation 6.4) are presented. Since only the product of refractive index and layer thickness is important for the evaluation of Γ , different models of the protein and the brush layer can in principle lead to the same adsorbed amount of protein.

In Figure A.2 four different models are displayed. Here Model A in Figure A.2(a) refers to the situation we think describes the real adsorption conditions best and the protein amount is derived by the modified de Feijter approach. In Model B (Figure A.2(b)) the swelling of the brush layer is reflected and the protein layer is modeled as top-layer, modeling a lack of penetration of protein into the brush. For the models C and D in Figure A.2(c) the swollen state of the brush is neglected and the refractive index of the dry polymer is used to model the layer thickness of a nominal dry brush. For the adsorption of protein, in Model C fitting of the refractive index of the protein is allowed, whereas in Model D the refractive index of $n = 1.375$ was used, derived from adsorption experiments at uncharged surfaces and so far commonly used to describe adsorbed protein layers.

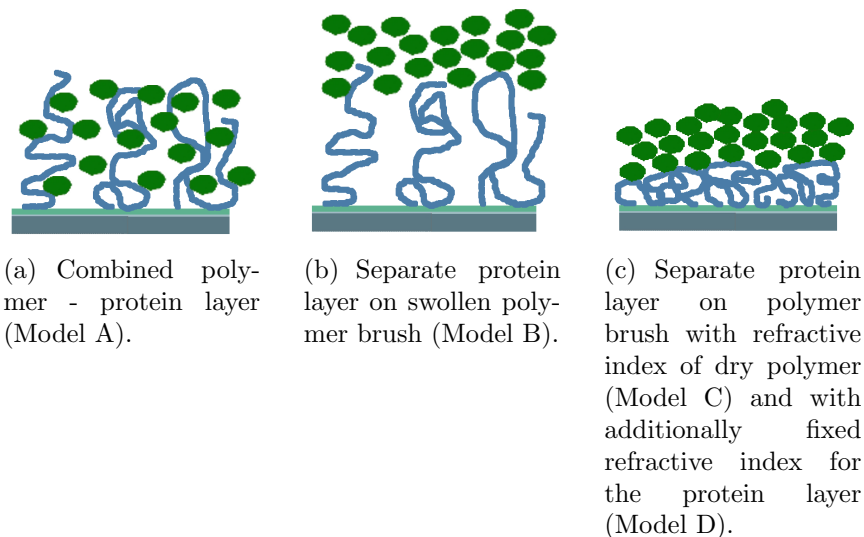


Figure A.2.: Different models to describe protein adsorption at polymer brushes.

In Table A.1 the results for the adsorbed amount of HSA upon adsorption at a PAA Guiselin brush at electrostatic attractive conditions at pH 4.8 and at the "wrong side" of the IEP of the protein at pH 6 are presented. For both adsorption conditions the models A and C lead to a similar adsorbed amount Γ , whereas for the models B and D the values for Γ deviate considerably and the fit quality is not acceptable for valid reproducible results.

Thus for protein adsorption at charged polyelectrolyte brushes the protein refractive index

Table A.1.: Comparison of the adsorbed amount Γ of HSA on PAA Guiselin brushes for four different models. Additionally refractive index n and thickness d of the separate protein layer as well as the mean-square fitting error (MSE) of the modeling is displayed to compare the fit quality. Adsorption was carried out in 10 mM buffer solutions at pH 4.8 (overall electrostatic attractive) and pH 6 ("wrong side" of IEP_{HSA}).

pH	model	MSE	Γ [$\frac{mg}{m^2}$]	d_{HSA} [nm]	$n_{HSA}(631.5 \text{ nm})$
4.8	A: combined layer	1.846	30 ± 0.5	—	—
	B: HSA on top of swollen brush	76.27	20.9 ± 4	27 ± 3	1.475 ± 0.03
	C: HSA on brush with $n_{dry}^{PAA} = 1.522$	1.837	29.4 ± 0.1	39.3 ± 0.1	1.473 ± 0.001
	D: $n_{HSA} = 1.375$ and $n_{dry}^{PAA} = 1.522$	100.4	20.6 ± 0.9	92 ± 4	1.375
6	A: combined layer	1.118	28.7 ± 0.6	—	—
	B: HSA on top of swollen brush	28.98	41.5 ± 5	18.5 ± 1.6	1.751 ± 0.07
	C: HSA on brush with $n_{dry}^{PAA} = 1.522$	1.191	27.5 ± 0.1	60.3 ± 0.2	1.418 ± 0.002
	D: $n_{HSA} = 1.375$ and $n_{dry}^{PAA} = 1.522$	58.86	20.6 ± 0.2	92 ± 10	1.375

should be modeled in all cases, whereas these first comparisons of Model A and C indicate that neglecting of the swollen state of the brush could in principle lead to valid results for Γ of the protein for these special PAA brushes.

The modeling of the adsorbed amount of HSA upon adsorption at binary PNIPAAm-PAA brushes was tested in the same way and the same trends in the validity of the models A to D could be found.

We think, that Model A of a combined polymer-protein layer is the best description of the surface after adsorption of the protein, and the application of the models B, C or D should be considered in each special adsorption case. In our opinion poor applicability is given, when the artificially introduced contrast in the refractive index between the two separately modeled layers is too high. Here in Model B the swollen brush has a refractive index of $n(631.5 \text{ nm}) = 1.36...1.38$, and the protein refractive index is high, whereas in Model D the contrast in n is introduced vice versa ($n_{PAA} = 1.5222$ and $n_{prot} = 1.375$). Thus the good results obtained by Model C can be also an effect of matching refractive indices and the applicability of this model is not necessarily given for all adsorption conditions.

Two-layer modeling of HSA adsorption onto PNIPAAm brushes

For the evaluation of the protein adsorption experiments and the determination of the adsorbed layer thicknesses on the brushes, a layer model similar to that mentioned for swollen samples was applied, adding one more box layer for the protein. The refractive index of the aqueous protein layer was set to $n_{prot} = 1.375$, whereas n of the swollen brush was taken from spectroscopic ellipsometry. The refractive index for the protein was fixed because a modeling of n from the

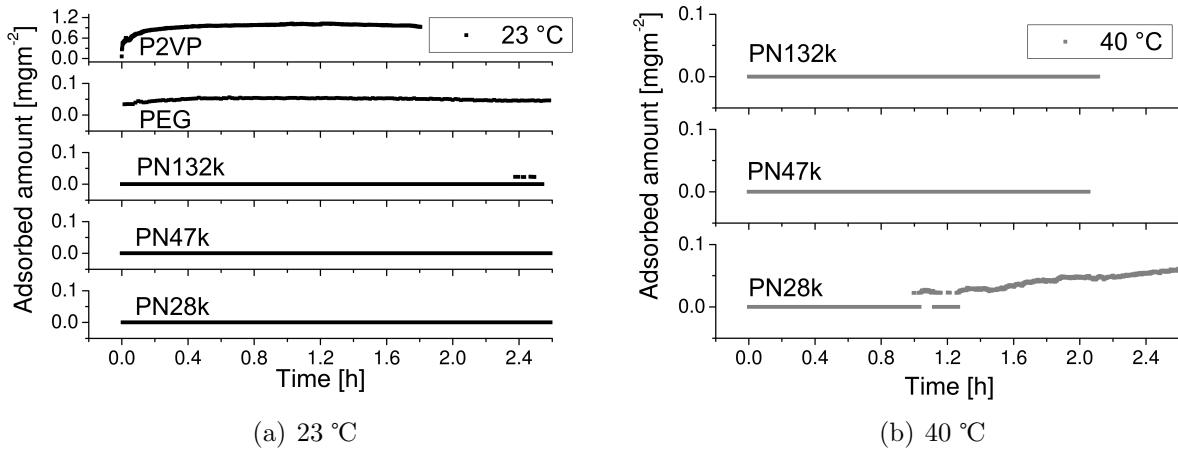


Figure A.3.: Adsorbed amount of HSA with time at PN28k, PN47k, and PN132k brushes at 23 °C (a) and 40 °C (b) compared to the adsorbed amount at a P2VP and a PEG brush in 0.01 M PBS buffer solution at pH 7.4 with a protein concentration of $1 \frac{\text{mg}}{\text{ml}}$. The error of the adsorbed amount was calculated to be maximal 5 % of the absolute value. Only for PN28k brushes at 40 °C an adsorbed amount of HSA could be calculated.

single wavelength null-ellipsometry data was not successful. The adsorbed amount of HSA was calculated using the de Feijter equation 6.4, with d_{prot} the layer thickness, n_{prot} the refractive index of the protein and n_{amb} the refractive index of the ambient solution, as well as the refractive index increment $\frac{dn}{dc}$ of the protein layer.

A.3. Refractive indices of swollen polymer brushes

Dispersion $n(\lambda)$ of dry PNIPAAm brushes

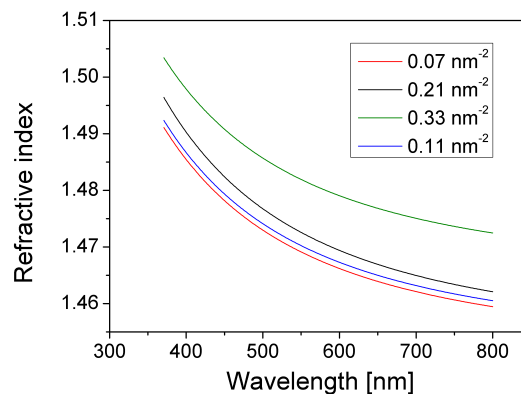
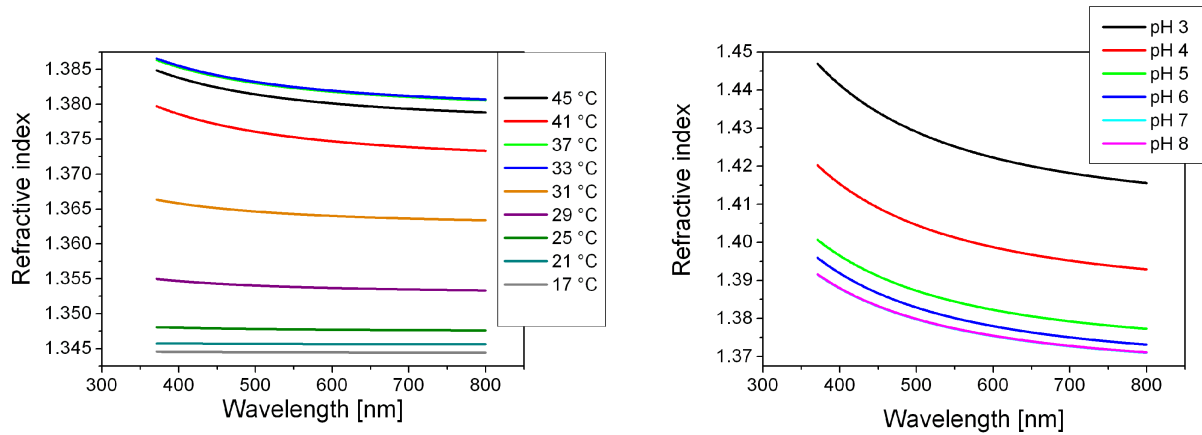


Figure A.4.: Dispersions of the refractive index $n(\lambda)$ of dry PN47k brushes with different grafting density.

Selected dispersions $n(\lambda)$ for environmental sensitive swelling



(a) $n(\lambda)$ of a PNIPAAm brush with a grafting density of 0.07 nm^{-2} dependent on temperature, reflecting the phase transition from a swollen brush state at low temperatures to a collapsed state at high temperatures.

(b) $n(\lambda)$ of PAA Guiselin brushes dependent on the pH, reflecting the increase in swollen brush thickness with increasing pH.

Figure A.5.: Dispersions of the refractive index $n(\lambda)$ for two environmental sensitive swelling / deswelling brush systems.

Temperature sensitive PNIPAAm brushes

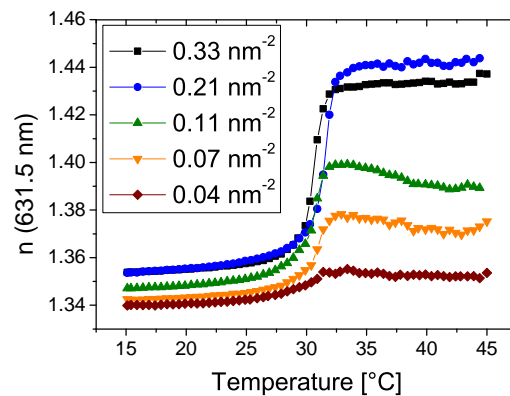


Figure A.6.: Refractive indices of the temperature sensitive cooling of PNIPAAm brushes with a molecular weight of $47,600 \frac{\text{g}}{\text{mol}}$.

PAA and PAA-b-PS Guiselin brushes

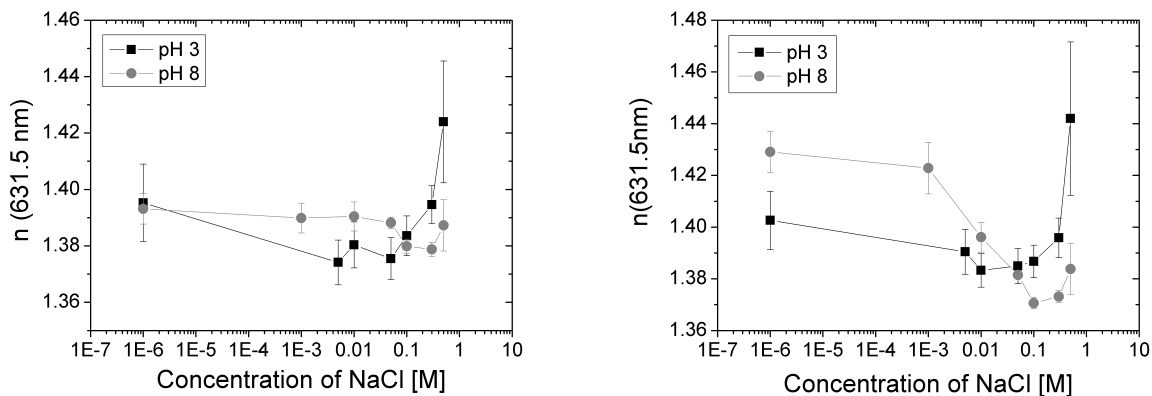


Figure A.7.: Refractive indices of PAA and PAA-b-PS Guiselin brushes upon salt dependent swelling at pH 3 and pH 8.

PEG-PAA-b-PS brushes

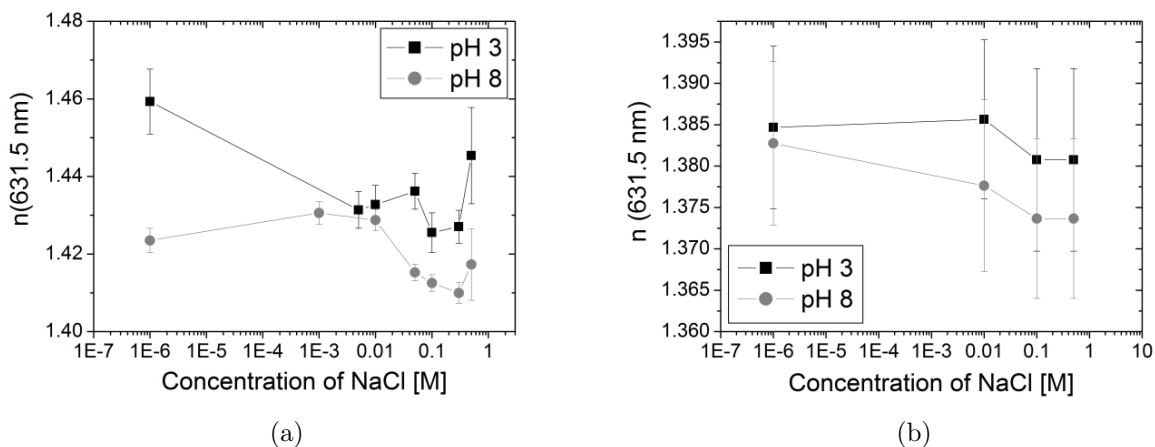


Figure A.8.: Refractive indices of PEG-PAA-b-PS brushes (a) and the corresponding PEG homopolymer brushes (b) dependent on the salt concentration.

Mixed brushes with adsorbed enzyme

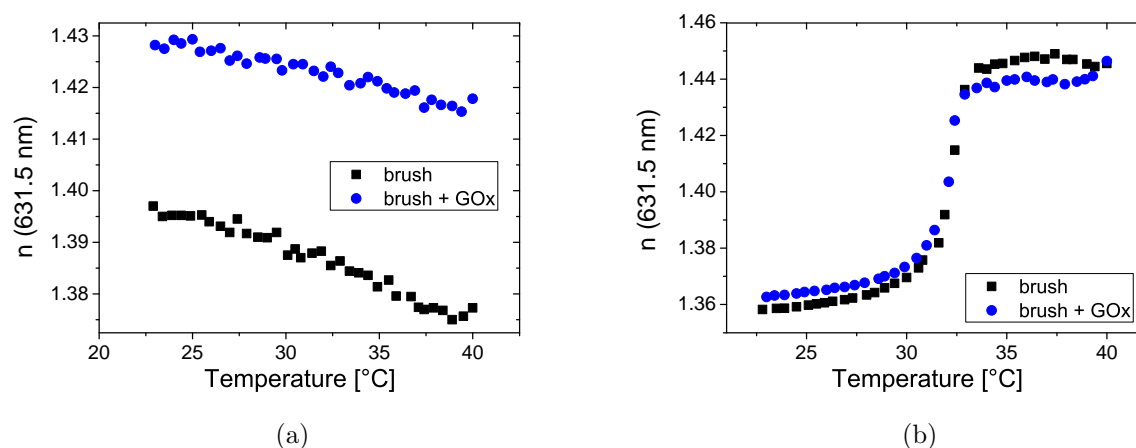


Figure A.9.: Refractive indices of a PNIPAAm-PAA brush and adsorbed enzyme (a) as well as a PNIPAAm-P2VP brush and enzyme (b) dependent on the temperature.

A.4. QCM-D data upon protein adsorption

The raw-data of QCM-D measurements upon BSA adsorption at overall electrostatic attractive (pH 5.2) and overall electrostatic repulsive (pH 6) conditions are presented in Figure A.10 and A.11. All experiments were started with the brush in water, switching to the salted solution, to the protein solution (I) and back to the salted solution (II). Finally the protein was desorbed at pH 7.6 (III) and the experiment ended with the brush immersed in water again. The evaluation of the viscoelastically coupled amount of protein and solvent molecules for Fields I to III are displayed in the Figures 8.12 and 8.14, whereas they are referenced to the brush already in salted solution and the time scale shifted to start with $t=0$ for the insertion of protein solution.

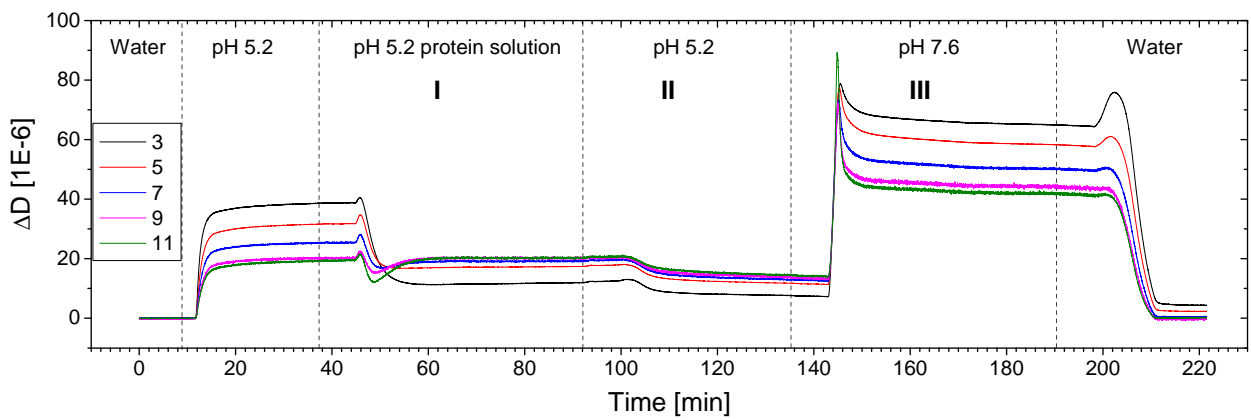
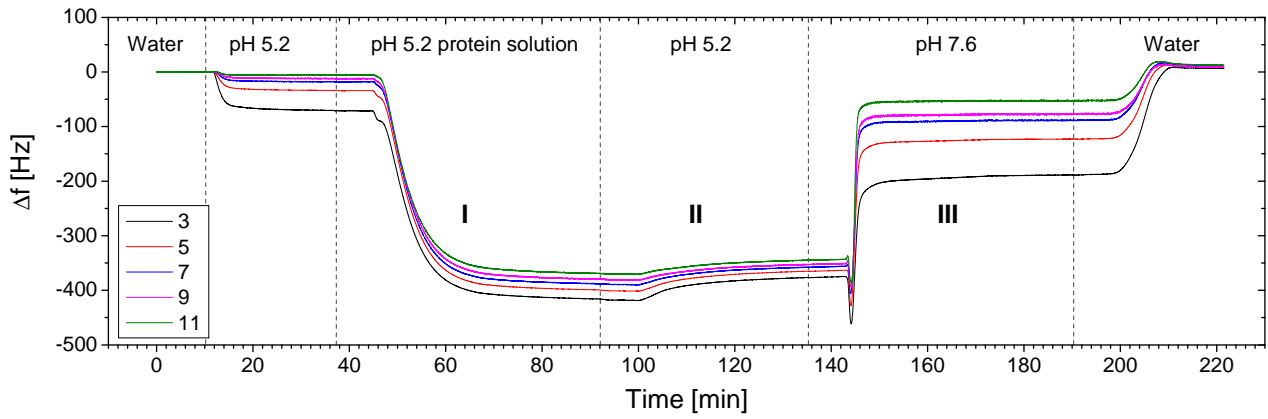
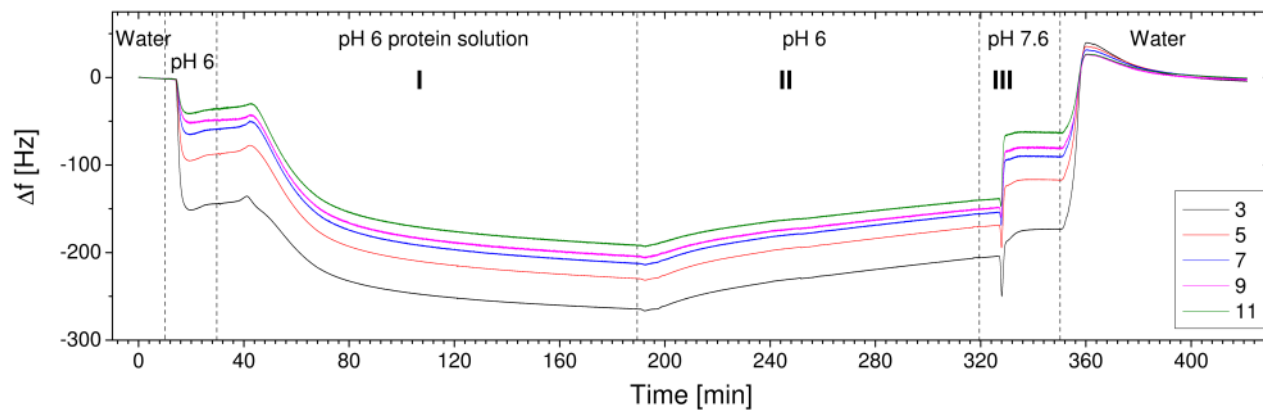
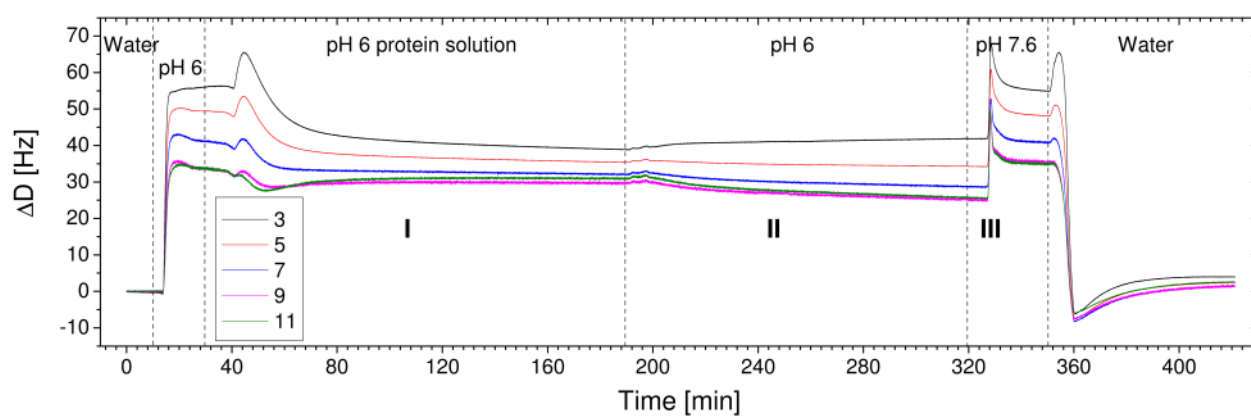


Figure A.10.: Total frequency (a) and dissipation shifts (b) for an adsorption experiment of BSA at a PAA Guiselin brush at pH 5.2.



(a)



(b)

Figure A.11.: Total frequency (a) and dissipation shifts (b) for an adsorption experiment of BSA at a PAA Guiselin brush at p 6.

List of abbreviations

AFM	Atomic force microscopy
ATR-FTIR	Attenuated total reflexion Fourier-transform infrared spectroscopy
BSA	Bovine serum albumin
EKA	ElektroKinetic Analyzer
EMA	Effective medium approach
GOx	Glucose oxidase
GPS	(3-glycidoxypropyl) trimethoxysilane
HSA	Human serum albumin
IEP	Isoelectric point
LCST	Lower critical solution temperature
MSE	Mean square error
P2VP	Poly(2-vinylpyridine)
PAA	Poly(acrylic acid)
PBS	Phosphate buffered saline
PDI	Polydispersity index
PEG	Poly (ethylene glycol)
PGMA	Poly(glycidyl methacrylate)
PNIPAAm	Poly(N-isopropyl acrylamide)
PS	Polystyrene
PN28k	PNIPAAm with $M_n = 28,500 \text{ g/mol}$
PN45k	PNIPAAm with $M_n = 45,000 \text{ g/mol}$
PN47k	PNIPAAm with $M_n = 47,600 \text{ g/mol}$
PN132k	PNIPAAm with $M_n = 132,000 \text{ g/mol}$
QCM-D	Quartz crystal microbalance with dissipation mode
SE	Spectroscopic ellipsometry
THF	Tetrahydrofuran

List of Figures

2.1.	Reaction scheme of the polymer brush formation by "grafting-to".	8
2.2.	Dissociation scheme of PAA.	11
2.3.	Scheme of a Guiselin brush.	13
2.4.	Switching of a PAA-P2VP mixed polyelectrolyte brush.	15
3.1.	Built up of proteins from primary to ternary structure.	18
3.2.	Scheme of the electrical double layer.	22
3.3.	Adsorption isotherm of $\Gamma(c_{eq})$	23
3.4.	Modes of adsorption of particles or proteins on polymer brushes.	26
3.5.	Penetration of albumin molecules into spherical polyelectrolyte brush.	27
3.6.	Total force per unit area acting on a neutral particle approaching a neutral brush	28
4.1.	Scheme of a cell for streaming potential determination.	33
4.2.	ATR-FTIR setup.	34
4.3.	Scheme of the reflection of the electric field vector at a specular surface.	35
4.4.	Reflection in the case of one layer at the substrate surface.	36
4.5.	General ellipsometric setups.	38
4.6.	Balance of interface tensions.	39
4.7.	SE - QCM-D setup.	43
5.1.	Structural formulas of the polymers used in this thesis.	47
5.2.	Variation of the annealing temperature in the preparation of PAA Guiselin brushes.	51
5.3.	AFM images after preparation and extraction in the corresponding solvents. . .	52
5.4.	Zeta-potential measurements for homopolymer and mixed brushes.	54
5.5.	Monitoring of the stability of swollen brushes.	54
6.1.	Box models for the modeling of dry brushes, swelling and protein adsorption. . .	56
6.2.	Grafting series for PN47k-PAA mixed brushes.	57
6.3.	PNIPAAm brush profile at three different temperatures.	58
6.4.	Comparison of optical box models with roughness and graded layer.	59
6.5.	Scheme of the evaluation method applied for the adsorbed amount of protein. .	63
6.6.	Commercial colorimetric assay for the determination of protein concentrations. .	65
7.1.	ATR-FTIR spectra of PNIPAAm brushes for three different molecular weights. .	70

7.2. Temperature dependent advancing water contact angles on PNIPAAm brushes.	72
7.3. Heating and cooling cycles of temperature dependent swelling of PN47k brushes.	74
7.4. Temperature transition dependent on the grafting density for PN47k brushes.	75
7.5. Percentage of dry PNIPAAm in the swollen brush dependent on temperature.	77
7.6. Evaluation of the phase transition temperature.	77
7.7. Molecular weight dependent swelling of PNIPAAm brushes.	79
7.8. Adsorbed amount of HSA at PNIPAAm brushes at 23 °C and 40 °C.	80
7.9. Changes in the ellipsometric angles upon adsorption of HSA.	82
8.1. pH-sensitive swelling of PAA and PAA-b-PS Guiselin brushes.	86
8.2. Salt dependent swelling of PAA (a) and PAA-b-PS (b) Guiselin brushes.	87
8.3. Advancing water contact angles after pH treatment of Guiselin brushes.	89
8.4. Scheme of electrostatic attractive and repulsive protein adsorption.	90
8.5. pH-sensitive adsorption of α -chymotrypsin and HSA.	92
8.6. Protein volume fractions of α -chymotrypsin and HSA.	93
8.7. HSA adsorption at PAA-b-PS Guiselin brushes.	95
8.8. Adsorbed amount of HSA dependent on the PAA amount grafted to the surface.	96
8.9. Example of a combined in-situ swelling experiment of salt dependent swelling.	100
8.10. Schemes of possible states of the swollen PAA brush surface.	101
8.11. Changes in $\Delta\Gamma_{QCMD}^b$ and $\Delta\Gamma_{SE}^b$ upon swelling of a PAA Guiselin brush.	102
8.12. Adsorbed amount of protein and viscolastically coupled to the surface at pH 5.2.	103
8.13. Refractive index and combined polymer-protein layer thickness at pH 5.2.	104
8.14. Adsorbed amount of protein and viscolastically coupled to the surface at pH 6.	105
8.15. Refractive index and combined polymer-protein layer thickness at pH 6.	106
8.16. Changes in the viscosity $\Delta\eta$ upon BSA adsorption.	107
8.17. Adsorption and desorption of BSA for 1 mM and 100 mM salt content.	108
8.18. Schemes of protein and buffer incorporation and release in PAA Guiselin brushes.	110
9.1. AFM height images of dry PNIPAAm-PAA brushes after pH treatment.	114
9.2. Root-mean-square roughness after pH treatment for different PAA contents.	115
9.3. Advancing water contact angle after pH treatment.	116
9.4. pH-sensitive swelling of PNIPAAm-PAA brushes.	118
9.5. Salt dependent swelling of a PNIPAAm-PAA brush at pH 8.	119
9.6. Temperature sensitive swelling for different pH.	120
9.7. Temperature sensitivity dependent on the composition of the mixed brush.	120
9.8. Scheme of the switching between protein adsorption and protein repelling state.	121
9.9. pH-dependent adsorption of HSA to PNIPAAm-PAA brushes at 23 °C.	122
9.10. Temperature sensitive adsorption of HSA and α -chymotrypsin.	123
9.11. Switching the adsorbed amount of HSA at PAA Guiselin brushes.	125
9.12. Switching the adsorbed amount of HSA at PNIPAAm-PAA brushes.	125

9.13. Temperature sensitive switching of the adsorbed amount of HSA.	126
9.14. Comparison of the adsorption kinetics for PNIPAAm-PAA and Guiselin brushes.	127
9.15. AFM height images of a dry PNIPAAm - PAA-b-PS brush after pH-treatment.	128
9.16. Advancing water contact angles of ternary brushes after pH treatment.	129
9.17. pH-sensitive swelling of a grafting series of PN47k-PAA-b-PS mixed brushes.	130
9.18. Coupled swelling of PNIPAAm and PAA chains in binary mixed brushes.	130
10.1. pH dependent swelling of PEG-PAA brushes with different PAA content.	134
10.2. Adsorbed amount of HSA and glucose oxidase on PEG-PAA brushes.	135
10.3. Salt dependent swelling at two different pH of PEG-PAA-b-PS.	137
11.1. Switching of the enzyme activity at a mixed brush surface.	139
11.2. Scheme of the oxidation of glucose catalyzed by glucose oxidase.	140
11.3. Immobilized glucose oxidase and activity at mono brushes.	141
11.4. Temperature sensitive swelling of binary brush-enzyme surfaces.	142
11.5. Immobilized glucose oxidase and activity at mixed brushes.	143
A.1. Dispersion relations for ambient solutions	149
A.2. Different models to describe protein adsorption at polymer brushes.	150
A.3. Adsorbed amount of HSA at PNIPAAm brushes derived by a two-layer model.	152
A.4. Dispersions of the refractive index $n(\lambda)$ of dry PN47k brushes with different grafting density.	152
A.5. Dispersions of the refractive index $n(\lambda)$ for two environmental sensitive swelling / deswelling brush systems.	153
A.6. Refractive indices of the temperature sensitive cooling of PNIPAAm brushes.	153
A.7. Refractive indices of Guiselin brushes upon salt dependent swelling.	154
A.8. Refractive indices of PEG-PAA-b-PS brushes.	154
A.9. Refractive indices of PNIPAAm-PAA / P2VP brushes and adsorbed enzyme.	155
A.10. Frequency and dissipation shift for BSA adsorption at pH 5.2.	156
A.11. Frequency and dissipation shift for BSA adsorption at pH 6.	157

Bibliography

- [1] T. P. Russel: *Surface-Responsive Materials*, Science **297** (2002) 964–967.
- [2] M. W. Matsen and F. S. Bates: *Unifying Weak- and Strong-Segregation Block Copolymer Theories*, Macromol. **29** (1996) 1091–1098.
- [3] A. Sidorenko, I. Tokarev, S. Minko and S. Stamm: *Ordered Reactive Nanomembranes/Nanotemplates from Thin Films of Block Copolymer Supramolecular Assembly*, J. Am. Chem. Soc. **125** (2003) 12211–12216.
- [4] E. B. Gowd, B. Nandan, M. K. Vyas, N. C. Bigall, A. Eychmüller, H. Schlörb and M. Stamm: *Highly ordered palladium nanodots and nanowires from switchable block copolymer thin films*, Nanotechnol. **20** (2009) 415302.
- [5] S. Reichelt, U. Gohs, F. Simon, S. Fleischmann, K.-J. Eichhorn and B. Voit: *Immobilization of a hyperbranched polyester via grafting-to and electron beam irradiation*, Langmuir **24** (2008) 9392–9400.
- [6] H. Chen and Y.-L. Hsieh: *Ultrafine hydrogel fibers with dual temperature- and pH-responsive swelling behaviors*, J. Polym. Sci. A: Polym. Chem. **42** (2004) 6331–6339.
- [7] B. C. Shin, M. S. Jhon, H. B. Lee and S. H. Yuk: *pH/temperature dependent phase transition of an interpenetrating polymer network: anomalous swelling behavior above lower critical solution temperature*, Eur. Polym. J. **34** (1998) 1675–1681.
- [8] A. Roos, D. Klee, K. Schuermann and H. Höcker: *Development of a temperature sensitive drug release system for polymeric implant devices*, Biomat. **24** (2003) 4417–4423.
- [9] N. A. Peppas and A. R. Khare: *Preparation, structure and diffusional behavior of hydrogels in controlled release*, Adv. Drug Deliv. Rev. **11** (1993) 1–35.
- [10] I. Tokarev and S. Minko: *Stimuli-responsive hydrogel thin films*, Soft Matter **5** (2009) 511–524.
- [11] R. Toomey and M. Tirrell: *Functional Polymer Brushes in Aqueous Media from Self-Assembled and Surface-Initiated Polymers*, Annu. Rev. Phys. Chem. **59** (2008) 493517.
- [12] W. J. Brittain and S. Minko: *A structural definition of polymer brushes*, J. Polym. Sci. A: Polym. Chem. **45** (2007) 35053512.

- [13] F. Zhou and W. T. S. Huck: *Surface grafted polymer brushes as ideal building blocks for 'smart' surfaces*, Phys. Chem. Chem. Phys. **8** (2006) 3815–3823.
- [14] E. P. K. Currie, W. Norde and M. A. Cohen Stuart: *Tethered polymer chains: surface chemistry and their impact on colloidal and surface properties*, Adv. Colloid Interface Sci. **100** (2003) 205–265.
- [15] M. Motornov, R. Sheparovych, E. Katz and S. Minko: *Chemical Gating with Nanostructured Responsive Polymer Brushes: Mixed Brush versus Homopolymer Brush*, ACS Nano **2** (2008) 41–52.
- [16] A. M. Granville and W. J. Brittain: *Stimuli-Responsive Semi-Fluorinated Polymer Brushes on Porous Silica Substrates*, Macromol. Rapid. Commun. **25** (2004) 1298–1302.
- [17] Y. S. Park, Y. Ito and Y. Imanishi: *pH-controlled gating of a porous glass filter by surface grafting of polyelectrolyte brushes*, Chem. Mater. **9** (1997) 2755–2758.
- [18] P. Uhlmann, N. Houbenov, N. Brenner, K. Grundke, S. Burkert and M. Stamm: *In-situ investigation of the adsorption of globular model proteins on stimuli-responsive binary polyelectrolyte brushes*, Langmuir **23** (2007) 57–64.
- [19] B. Zdyrko, V. Klep, X. Li, Q. Kang, S. Minko, X. Wen and I. Luzinov: *Polymer brushes as active nanolayers for tunable bacteria adhesion*, Mat. Sci. Eng. C: Mat. Biolog. Applicat. **29** (2009) 680–684.
- [20] M. D. Miller, G. L. Baker and M. L. Bruening: *Polymer-brush stationary phases for open-tubular capillary electrochromatography*, J. Chromatogr. A **1044** (2004) 323–330.
- [21] A. Feldmann, U. Claunitzer and M. Otto: *Optimization of capillary coating by hydroxyethyl methacrylate for capillary zone electrophoresis of proteins*, J. Chromatogr. B **803** (2004) 149–157.
- [22] S. Gupta, M. Agrawal, P. Uhlmann, U. Oertel and M. Stamm: *Gold nanoparticles immobilized on stimuli responsive polymer brushes as nanosensors*, Macromol. **41** (2008) 8152–8158.
- [23] N. Singh, X. Cui, T. Boland and S. M. Husson: *The Role of Independently Variable Grafting Densities and Layer Thicknesses of Polymer Nanolayers on Peptide Adsorption and Cell Adhesion*, Biomat. **28** (2007) 763771.
- [24] M. Heuberger, T. Drobek and N. D. Spencer: *Interaction Forces and Morphology of a Protein-Resistant Poly(ethylene glycol) Layer*, Biophys. J. **88** (2005) 495504.
- [25] W. T. E. Bosker, P. A. Iakovlev, W. Norde and M. A. Cohen Stuart: *BSA adsorption on bimodal PEO brushes*, J. Colloid Interface Sci. **286** (2005) 496–503.

- [26] W. R. Gombotz, W. Guanghai, T. A. Horbett and A. S. Hoffman: *Protein adsorption to poly(ethylene oxide) surfaces*, J. Biomed. Mater. Res. **25** (1991) 1547–1564.
- [27] A. Gransson, E. Jansson, P. Tengvall and A. Wennerberg: *Bone formation after 4 weeks around blood-plasma-modified titanium implants with varying surface topographies: an in vivo study*, Biomaterials **24** (2003) 197205.
- [28] A. Roosjen, W. Norde, H. C. van der Mei and H. J. Busscher: *The Use of Positively Charged or Low Surface Free Energy Coatings versus Polymer Brushes in Controlling Biofilm Formation*, Progr. Colloid Polym. Sci. **132** (2006) 138–144.
- [29] E. P. K. Currie, A. B. Sieval, G. J. Fleer and M. A. Cohen Stuart: *Polyacrylic Acid Brushes: Surface Pressure and Salt-Induced Swelling*, Langmuir **16** (2000) 8324–8333.
- [30] M. Ballauff and O. Borisov: *Polyelectrolyte Brushes*, Curr. Opin. Colloid Interface Sci. **11** (2006) 316323.
- [31] S. S. Dukhin, R. Zimmermann and C. Werner: *Surface Conductivity Reveals Counterion Condensation within Grafted Polyelectrolyte Layers*, J. Phys. Chem. B **111** (2007) 979–981.
- [32] Y. G. Takei, T. Aoki, K. Sanui, N. Ogata, Y. Sakurai and T. Okano: *Dynamic Contact Angle Measurement of Temperature-Responsive Surface Properties for Poly(*N*-isopropylacrylamide) Grafted Surfaces*, Macromol. **27** (1994) 6163–6166.
- [33] K. N. Plunkett, X. Zhu, J. S. Moore and D. E. Leckband: *PNIPAM Chain Collapse Depends on the Molecular Weight and Grafting Density*, Langmuir **22** (2006) 4259–4266.
- [34] H. Yim, M. S. Kent, S. Mendez, G. P. Lopez, S. Satija and Y. Seo: *Effects of Grafting Density and Molecular Weight on the Temperature-Dependent Conformational Change of Poly(*N*-isopropylacrylamide) Grafted Chains in Water*, Macromol. **39** (2006) 3420–3426.
- [35] N. Houbenov, S. Minko and M. Stamm: *Mixed Polyelectrolyte Brush from Oppositely Charged Polymers for Switching of Surface Charge and Composition in Aqueous Environment*, Macromol. **36** (2003) 5897–5901.
- [36] L. Ionov, M. Stamm, S. Minko, F. Hoffman and T. Wolff: *Switching and structuring of binary reactive polymer brush layers*, Macromol. Symp. **210** (2004) 229–235.
- [37] Y. Mikhaylova, L. Ionov, J. Rappich, M. Gensch, N. Esser, S. Minko, K.-J. Eichhorn, M. Stamm and K. Hinrichs: *In Situ Infrared Ellipsometric Study of Stimuli-Responsive Mixed Polyelectrolyte Brushes*, Anal. Chem. **79** (2007) 7676–7682.
- [38] J. Wang and M. Müller: *Microphase Separation of Mixed Polymer Brushes: Dependence of the Morphology on Grafting Density, Composition, Chain-Length Asymmetry, Solvent Quality, and Selectivity*, J. Phys. Chem. B **113** (2009) 11384–11402.

- [39] X. Guo and M. Ballauff: *Spherical polyelectrolyte brushes: Comparison between annealed and quenched brushes*, Phys. Rev. E **64** (2001) 051406.
- [40] M. Biesalski, D. Johannsmann and J. R uhe: *Synthesis and swelling behavior of a weak polyacid brush*, J. Chem. Phys. **117** (2002) 4988–4993.
- [41] H. Zhang and J. R uhe: *Swelling of Poly(methacrylic acid) Brushes: Influence of Monovalent Salts in the Environment*, Macromol. **38** (2005) 4855–4860.
- [42] R. Dong, M. Lindau and C. K. Ober: *Dissociation Behavior of Weak Polyelectrolyte Brushes on a Planar Surface*, Langmuir **25** (2009) 4774–4779.
- [43] M. Heskins and J. E. Guillet: *Solution Properties of Poly(N-isopropylacrylamide)*, J. Macromol. Sci. Chem. A **2** (1968) 1441–1455.
- [44] L. D. Taylor and L. D. Cerankowski: *Preparation of films exhibiting a balanced temperature dependence to permeation by aqueous solutions - a study of lower consolute behavior*, J. Polym. Sci.: Polym. Chem. Edn. **13** (1975) 2551–2570.
- [45] H. Cheng, L. Shen and C. Wu: *LLS and FTIR Studies on the Hysteresis in Association and Dissociation of Poly(N-isopropylacrylamide) Chains in Water*, Macromol. **39** (2006) 2325–2329.
- [46] M. V. Deshmukh, A. A. Vaidya, M. G. Kulkarni, P. R. Rajamohanan and S. Ganapathy: *LCST in poly(N-isopropylacrylamide) copolymers: high resolution proton NMR investigations*, Polymer **41** (2000) 7951–7960.
- [47] M. Nitschke, S. Gramm, T. G tze, M. Valtink, J. Drichel, B. Voit, K. Engelmann and C. Werner: *Thermo-responsive poly(NiPAAm-co-DEGMA) substrates for gentle harvest of human corneal endothelial cell sheets*, J. Biomed. Mat. Res. A **80** (2007) 1003–1010.
- [48] E. P. K. Currie, J. V. der Gucht, O. V. Borisov and M. A. Cohen Stuart: *Stuffed brushes: theory and experiment*, Pure Appl. Chem. **71** (1999) 1227–1241.
- [49] A. Halperin: *Polymer Brushes that Resist Adsorption of Model Proteins: Design Parameters*, Langmuir **15** (1999) 2525–2533.
- [50] A. S. Hoffman: *Applications of Thermally Reversible Polymers and Hydrogels in Therapeutics and Diagnostics*, J. Controll. Release **6** (1987) 297–305.
- [51] Y. H. Lim, D. Kim and D. S. Lee: *Drug Releasing Characteristics of Thermo- and pH-Sensitive Interpenetrating Polymer Networks Based on Poly (N-isopropylacrylamide)*, Journal Appl. Polym. Sci. **64** (1997) 2647–2655.

- [52] J. P. Bearinger, D. G. Castne, S. L. Golledge, A. Rezania, S. Hubchak and K. E. Healy: *P(AAm-co-EG) Interpenetrating Polymer Networks Grafted to Oxide Surfaces: Surface Characterization, Protein Adsorption, and Cell Detachment Studies*, *Langmuir* **13** (1997) 5175–5183.
- [53] L. Ying, E. Kang and K. Neoh: *Characterization of membranes prepared from blends of poly(acrylic acid)-graft-poly(vinylidene fluoride) with poly(N-isopropylacrylamide) and their temperature and pH-sensitive microfiltration*, *J. Membr. Sci.* **224** (2003) 93106.
- [54] G. Burillo, M. Briones and E. Adem: *IPNs of acrylic acid and N-isopropylacrylamide by gamma and electron beam irradiation*, *Nuclear Instr. Method. Phys. Resear. B* **265** (2007) 104108.
- [55] G. Staikos, G. Bokias and K. Karayanni: *Interpolymer Complexes of Poly(acrylamide) and Poly(Nisopropylacrylamide) with Poly(acrylic acid) : a Comparative Study*, *Polym. Internat.* **41** (1996) 345–350.
- [56] S. T. Milner and T. A. Witten: *Theory of the grafted polymer brush*, *Macromol.* **21** (1988) 2610–2619.
- [57] B. Zhao and W. J. Brittain: *Polymer brushes: surface-immobilized macromolecules*, *Prog. Polym. Sci.* **25** (2000) 677710.
- [58] G. F. Belder, G. ten Brinke and G. Hadziioannou: *Influence of Anchor Block Size and the Thickness of Adsorbed Block Copolymer Layers*, *Langmuir* **13** (1997) 41024105.
- [59] W. M. de Vos, P. M. Biesheuvel, A. de Keizer, J. M. Kleijn and M. A. Cohen Stuart: *Adsorption of the protein bovine serum albumin in a planar poly(acrylic acid) brush layer as measured by optical reflectometry*, *Langmuir* **24** (2008) 6575.
- [60] M. Bialk, O. Prucker and J. R uhe: *Grafting of polymers to solid surfaces by using immobilized methacrylates*, *Colloids Surf. A: Physicochem. Eng. Asp.* **198200** (2002) 543549.
- [61] K. S. Iyer and I. Luzinov: *Effect of Macromolecular Anchoring Layer Thickness and Molecular Weight on Polymer Grafting*, *Macromol.* **37** (2004) 9538–9545.
- [62] B. O’Shaughnessy and D. Vavylonis: *Non-equilibrium in adsorbed polymer layers*, *J. Phys.: Condens. Matter* **17** (2005) R63–R99.
- [63] J. Habicht, M. Schmidt, J. R uhe and J. Johannsmann: *Swelling of Thick Polymer Brushes Investigated with Ellipsometry*, *Langmuir* **15** (1999) 2460–2465.
- [64] O. Prucker and J. R uhe: *Mechanism of Radical Chain Polymerizations Initiated by Azo Compounds Covalently Bound to the Surface of Spherical Particles*, *Macromol.* **592** (1998) 602–613.

- [65] M. Husseman, E. E. Malmström, M. McNamara, M. Mate, D. Mecerreyes, D. G. Benoit, J. L. Hedrick, P. Mansky, E. Huang, T. P. Russell and C. J. Hawker: *Controlled Synthesis of Polymer Brushes by Living Free Radical Polymerization Techniques*, *Macromolecules* **32** (1999) 1424–1431.
- [66] B. Zdyrko, O. Hoy, M. K. Kinnan, G. Chumanov and I. Luzinov: *Nano-patterning with polymer brushes via solvent-assisted polymer grafting*, *Soft Matter* **4** (2008) 22132219.
- [67] J. H. Maas, M. A. Cohen Stuart, A. B. Sieval, H. Zuillhof and E. J. R. Sudhölter: *Preparation of polystyrene brushes by reaction of terminal vinyl groups on silicon and silica surfaces*, *Thin Sol. Film.* **426** (2003) 135–139.
- [68] B. Zdyrko, K. S. Iyer and I. Luzinov: *Macromolecular anchoring layers for polymer grafting: comparative study*, *Polymer* **47** (2006) 272–279.
- [69] K. S. Iyer, B. Zdyrko, H. Malz, J. Pionteck and I. Luzinov: *Polystyrene Layers Grafted to Macromolecular Anchoring Layers*, *Macromol.* **36** (2003) 6519–6526.
- [70] T. Wu, K. Efimenko and J. Genzer: *Multivariant investigation of the mushroom-to-brush transition in surface-anchored poly(acrylamide)*, *J. Am. Chem. Soc.* **124** (2002) 93949395.
- [71] M. S. Kent: *A quantitative study of tethered chains in various solution conditions using langmuir diblock copolymer monolayers.*, *Macromol. Rapid. Commun.* **21** (2000) 243270.
- [72] B. Zdyrko, V. Klep and I. Luzinov.: *Synthesis and surface morphology of high-density poly(ethylene glycol) grafted layers.*, *Langmuir* **19** (2003) 10179–10187.
- [73] K. Viswanathan, T. E. Long and T. C. Ward: *Silicon surface modification with trialkoxysilyl-functionalized star-shaped polymers.*, *J. Polym. Sci. A: Polym. Chem.* **43** (2005) 3655–3666.
- [74] S. Alexander: *Adsorption of chain molecules with a polar head - a scaling description*, *J. Phys. (Paris)* **38** (1977) 983–987.
- [75] P. G. de Gennes: *Conformations of polymers attached to an interface*, *Macromol.* **13** (1980) 1069–1075.
- [76] S. T. Milner: *Polymer Brushes*, *Science* **251** (1991) 905–914.
- [77] E. B. Zhulina, O. V. Borisov, V. A. Pryamitsyn and T. M. Birshtein: *Coil-Globule Type Transition in Polymers. 1. Collapse of Layers of Grafted Polymer Chains*, *Macromol.* **24** (1991) 140–149.
- [78] M. A. Carignano and I. Szleifer: *Statistical Thermodynamic Theory of Grafted Polymeric Layers*, *J. Chem. Phys.* **98** (1993) 5006–5018.

- [79] G.-L. He, H. Merlitz, J.-U. Sommer and C.-X. Wu: *Static and Dynamic Properties of Polymer Brushes at Moderate and High Grafting Densities: A Molecular Dynamics Study*, *Macromol.* **40** (2007) 6721–6730.
- [80] C. Devaux, F. Cousin, E. Beyou and J.-P. Chapel: *Low Swelling Capacity of Highly Stretched Polystyrene Brushes*, *Macromol.* **38** (2005) 4296–4300.
- [81] R. Hoogenboom: *Poly(2-oxazoline)s: A Polymer Class with Numerous Potential Application*, *Angew. Chem. Int. Ed.* **48** (2009) 7978–7994.
- [82] E. E. Dormidontova: *Role of Competitive PEO-Water and Water-Water Hydrogen Bonding in Aqueous Solution PEO Behavior*, *Macromol.* **35** (2002) 987–1001.
- [83] M. K. Yoo, Y. K. Sung, C. S. Cho and Y. M. Lee: *Effect of poly complex formation on the cloud-point of poly(*N*-isopropyl acrylamide) (PNIPAAm) in the poly(NIPAAm-co-acrylic acid): polyelectrolyte complex between poly(acrylic acid) and poly(allylamine)*, *Polymer* **38** (1997) 2759–2765.
- [84] V. P. Gilcreest, W. M. Carroll, Y. A. Rochev, I. Blute, K. A. Dawson and A. V. Gorelov: *Thermoresponsive Poly(*N*-isopropylacrylamide) Copolymers: Contact Angles and Surface Energies of Polymer Films*, *Langmuir* **20** (2004) 10138–10145.
- [85] H. Yim, M. S. Kent, S. Mendez, S. S. Balamurugan, S. Balamurugan, G. P. Lopez and S. Satija: *Temperature-Dependent Conformational Change of PNIPAM Grafted Chains at High Surface Density in Water*, *Macromol.* **34** (2004) 1994–1997.
- [86] H. Yim, M. S. Kent, S. Satija, S. Mendez, S. S. Balamurugan, S. Balamurugan and G. P. Lopez: *Evidence for vertical phase separation in densely grafted, high-molecular-weight poly(*N*-isopropylacrylamide) brushes in water*, *Phys. Rev. E* **72** (2005) 051801.
- [87] S. Balamurugan, S. Mendez, S. S. Balamurugan, M. M. J. O’Brie and G. P. Lopez: *Thermal Response of Poly(*N*-isopropylacrylamide) Brushes Probed by Surface Plasmon Resonance*, *Langmuir* **19** (2003) 2545–2549.
- [88] X. Zhu, C. Yan, F. M. Winnik and D. Leckband: *End-Grafted Low-Molecular-Weight PNIPAM Does Not Collapse above the LCST*, *Langmuir* **23** (2007) 162–169.
- [89] S. Mendez, J. G. Curro, J. D. McCoy and G. P. Lopez: *Computational Modeling of the Temperature-Induced Structural Changes of Tethered Poly(*N*-isopropylacrylamide) with Self-Consistent Field Theory*, *Macromol.* **38** (2005) 174–181.
- [90] F. Garbassi, M. Morra and E. Occhiello: *Polymer surfaces*, John Wiley & Sons Ltd, (1996).

- [91] P. Pincus: *Colloid stabilization with grafted polyelectrolytes*, *Macromol.* **24** (1991) 2912–2919.
- [92] O. V. Borisov, T. M. Birshtein and E. B. Zhulina: *Collapse of grafted polyelectrolyte layer*, *J. Phys. II (France)* **1** (1991) 521–526.
- [93] E. B. Zhulina, T. M. Birshtein and O. V. Borisov: *Theory of ionizable polymer brushes*, *Macromol.* **28** (1995) 1491–1499.
- [94] E. B. Zhulina and O. V. Borisov: *Structure and interactions of weakly charged polyelectrolyte brushes: self-consistent field theory*, *J. Chem. Phys.* **107** (1997) 5952–5967.
- [95] M. Aubouy, O. Guiselin and E. Raphael: *Scaling description of polymer interfaces: Flat layers*, *Macromolecules* **29** (1996) 77261–7268.
- [96] B. O’Shaughnessy and D. Vavylonis: *The slowly formed Guiselin brush*, *Europhys. Lett.* **63** (2003) 895–901.
- [97] J.-F. Joanny and A. N. Semenov: *Structure of Adsorbed Polymer Layers: Loops and Tails*, *Europhys. Lett.* **29** (1995) 279–284.
- [98] S. Minko, D. Usov, E. Goresnik and M. Stamm: *Environment-Adopting Surfaces with Reversibly Switchable Morphology*, *Macromol. Rapid. Commun.* **22** (2001) 206–211.
- [99] M. Müller: *Phase diagram of a mixed polymer brush*, *Phys. Rev. E* **E 65** (2002) 030802.
- [100] J. Wang and M. Müller: *Memory Effects of Diblock Copolymer Brushes and Mixed Brushes*, *Langmuir* **26** (2010) 1291–1303.
- [101] L. Ionov, N. Houbenov, A. Sidorenko, M. Stamm and S. Minko: *Stimuli-responsive command polymer surface for generation of protein gradients*, *Biointerphases* **4** (2009) FA45–FA46.
- [102] C. A. Haynes and W. Norde: *Globular proteins at solid/liquid interfaces*, *Colloid. Surf. B.: Biointerphases* **2** (1994) 517–566.
- [103] L. Vroman: *When Blood Is Touched*, *Materials* **2** (2009) 1547–1557.
- [104] M. Caldorera-Moore and N. A. Peppas: *Micro- and nanotechnologies for intelligent and responsive biomaterial-based medical systems*, *Adv. Drug Deliv. Rev.* **61** (2009) 1391–1401.
- [105] R. J. Russell, M. V. Pishko, C. C. Geffrides, M. J. McShane and G. L. Cot: *A Fluorescence-Based Glucose Biosensor Using Concanavalin A and Dextran Encapsulated in a Poly(ethylene glycol) Hydrogel*, *Anal. Chem.* **71** (1999) 3126–3132.

- [106] *protein*, Encyclopedia Britannica, (2009).
- [107] H. P. Erickson: *Size and Shape of Protein Molecules at the Nanometer Level Determined by Sedimentation, Gel Filtration, and Electron Microscopy*, Biol. Proced. Online **11** (2009) 32–51.
- [108] M. A. Cohen Stuart, W. Norde, M. Kleijn and G. A. van Aken: *Food Colloids*, chap. Formation and Properties of Adsorbed Protein Films: Importance of Conformational Stability, 99–119, The Royal Society of Chemistry, Cambridge, UK, (2004).
- [109] W. Norde: *Physical Chemistry of Biological Interfaces*, chap. Proteins at Solid Surfaces, 115–135, Marcel Dekker, Inc., New York, USA, (2003).
- [110] D. H. Chou and C. V. Morr: *Protein-Water Interactions and Functional Properties*, J. Am. Oil Chemists' Soc. **56** (1979) 53A–62A.
- [111] L. Bachmann, W. W. Schmitt-Fumain, R. Hammel and K. Lederer: *Size and shape of fibrinogen, 1. Electron microscopy of the hydrated molecule*, Die Makromolekulare Chemie **176** (1975) 2603–2618.
- [112] O. Stern: *Zur Theorie der Elektrolytischen Doppelschicht*, Z. Elektrochem. **30** (1924) 508–516.
- [113] J. G. Kirkwood: *Theory of solutions of molecules containing widely separated charges with special application to zwitterions*, J. Chem. Phys. **2** (1934) 351–361.
- [114] H.-J. Jacobasch, F. Simon and P. Weidenhammer: *Adsorption of ions onto polymer surfaces and its influence on zeta potential and adhesion phenomena*, Colloid Polym. Sci. **276** (1998) 434–442.
- [115] W. Norde, F. Galisto-Gonzalez and C. A. Haynes: *Protein adsorption on polystyrene latex particles*, Polym. Adv. Technol. **6** (1995) 518–524.
- [116] J. M. Kleijn, D. Barten and M. A. Cohen Stuart: *Adsorption of Charged Macromolecules at a Gold Electrode*, Langmuir **20** (2004) 9703–9713.
- [117] S. Nir: *Van der Waals interactions between surfaces of biological interest*, Progr. Surf. Sci. **8** (1976) 1–58.
- [118] W. Norde and J. P. Favier: *Structure of adsorbed and desorbed proteins*, Colloids Surf. **64** (1992) 87–93.
- [119] B. Lassen and M. Malmsten: *Competitive Protein Adsorption Studied with TIRF and Ellipsometry*, J. Colloid Interf. Sci. **179** (1996) 470–477.

- [120] C. Werner, K.-J. Eichhorn, K. Grundke, F. Simon, W. Grählert and H.-J. Jacobasch: *Insights on structural variations of protein adsorption layers on hydrophobic fluorohydrocarbon polymers gained by spectroscopic ellipsometry (part I)*, Colloid Surf. A **156** (1999) 3–17.
- [121] J. Benesch, A. Askendal and P. Tengvall: *Quantification of adsorbed human serum albumin at solid interfaces: a comparison between radioimmunoassay (RIA) and simple null ellipsometry*, Colloid Surf. B: Biointerfaces **18** (2000) 71–81.
- [122] M. Poksinski and H. Arwin: *Total internal reflection ellipsometry: ultrahigh sensitivity for protein adsorption on metal surfaces*, Opt. Lett. **32** (2007) 1308–1310.
- [123] F. Evers, K. Shokuie, M. Paulus, C. Sternemann, C. Czeslik and M. Tolan: *Exploring the Interfacial Structure of Protein Adsorbates and the Kinetics of Protein Adsorption: An In Situ High-Energy X-ray Reflectivity Study*, Langmuir **24** (2008) 10216–10221.
- [124] T. Kull, T. Nylander, F. Tiberg and N. M. Wahlgren: *Effect of Surface Properties and Added Electrolyte on the Structure of β -casein Layers Adsorbed at the Solid/Aqueous Interface*, Langmuir **13** (1997) 5141–5147.
- [125] P. Tengvall, A. Askendal and I. Lundström: *Ellipsometric in vitro studies on the activation of complement by human immunoglobulins M and G after adsorption to methylated silicon*, Colloid Surf. B: Biointerph. **20** (2001) 51–62.
- [126] M. Lund, T. Akesson and B. Jönsson: *Enhanced Protein Adsorption Due to Charge Regulation*, Langmuir **21** (2005) 8385–8388.
- [127] M. Malmsten: *Ellipsometry Studies of Protein Layers Adsorbed at Hydrophobic Surfaces*, J. Colloid Interface Sci. **166** (1994) 333 – 342.
- [128] B. Lassen and M. Malmsten: *Structure of Protein Layers during Competitive Adsorption*, J. Colloid Interf. Sci. **180** (1996) 339–349.
- [129] L. Vroman: *Effect of Adsorbed Proteins on the Wettability of Hydrophilic and Hydrophobic Solids*, Nature **196** (1962) 476–477.
- [130] L. Vroman and A. L. Adams: *Adsorption of proteins out of plasma and solutions in narrow spaces*, J. Colloid Interface Sci. **111** (1986) 391–402.
- [131] M. van der Veen, W. Norde and M. A. Cohen Stuart: *Electrostatic interactions in protein adsorption probed by comparing lysozyme and succinylated lysozyme*, Colloids Surf. B: Biointerphas. **35** (2004) 33–40.
- [132] T. Zoungrana, G. H. Findenegg and W. Norde: *Structure, Stability, and Activity of Adsorbed Enzymes*, J. Colloid Interface Sci. **190** (1997) 437–448.

- [133] H. Kawaguchi, K. Fujimoto and Y. Mizuhara: *Hydrogel microspheres III. Temperature-dependent adsorption of proteins on poly-N-isopropylacrylamide hydrogel microspheres*, Colloid Polym. Sci. **270** (1992) 53–57.
- [134] S. M. Russel and G. Carta: *Multicomponent Protein Adsorption in Supported Cationic Polyacrylamide Hydrogels*, AIChE Journal **51** (2005) 2469–2480.
- [135] J. Y. Wu, S.-Q. Liu, P. W.-S. Heng and Y. Y. Yang: *Evaluating proteins release from, and their interactions with, thermosensitive poly (N-isopropylacrylamide) hydrogels*, J. Controll. Release **102** (2005) 361–372.
- [136] S. Rosenfeldt, A. Wittemann, M. Ballauff, E. Breininger, J. Bolze and M. Dingenouts: *Interaction of proteins with spherical polyelectrolyte brushes in solution as studied by small-angle x-ray scattering*, Phys. Rev. E **70** (2004) 061403.
- [137] B. Haupt, T. Neumann, A. Wittemann and M. Ballauff: *Activity of Enzymes Immobilized in Colloidal Spherical Polyelectrolyte Brushes*, Biomacromol. **6** (2005) 948–955.
- [138] A. Wittemann and M. Ballauff: *Interaction of proteins with linear polyelectrolytes and spherical polyelectrolyte brushes in aqueous solution*, Phys. Chem. Chem. Phys. **8** (2006) 5269–5275.
- [139] A. Wittemann, B. Haupt and M. Ballauff: *Polyelectrolyte-mediated Protein Adsorption*, Prog. Colloid. Polym. Sci. **133** (2006) 5864.
- [140] E. L. Cabarcos, J. R. Retama and B. Lopez-Ruiz: *Immobilization of glucose oxidase in cross-linked poly(acrylamide/acrylic acid) microgels*, Progr. Colloid. Polym. Sci. **126** (2004) 194–196.
- [141] P. M. Biesheuvel, F. A. M. Leermakers and M. A. C. Stuart: *Self-consistent field theory of protein adsorption in a non-Gaussian polyelectrolyte brush*, Phys. Rev. E: Stat. Phys. Plasmas Fluids Relat. **73** (2006) 011802.
- [142] O. Hollmann, T. Gutberlet and C. Czeslik: *Structure and Protein Binding Capacity of a Planar PAA Brush*, Langmuir **23** (2007) 1347–1353.
- [143] W. M. de Vos, F. A. M. Leermakers, A. de Keizer, M. A. Cohen Stuart and J. M. Kleijn: *Field Theoretical Analysis of Driving Forces for the Uptake of Proteins by Like-Charged Polyelectrolyte Brushes: Effects of Charge Regulation and Patchiness*, Langmuir **26** (2010) 249–259.
- [144] A. P. Ryle: *Behaviour of Poly Glycol on Dialysis and Gel-filtration*, Nature **206** (1965) 1256.

- [145] W. Norde and D. Gage: *Interaction of Bovine Serum Albumin and Human Blood Plasma with PEO-Tethered Surfaces: Influence of PEO Chain Length, Grafting Density, and Temperature*, Langmuir **20** (2004) 4162–4167.
- [146] R. Michel, S. Pasche, M. Textor and D. G. Castner: *Influence of PEG Architecture on Protein Adsorption and Conformation*, Langmuir **21** (2005) 12327–12332.
- [147] A. Halperin, G. Fragneto, A. Schollier and M. Sferrazza: *Primary versus Ternary Adsorption of Proteins onto PEG Brushes*, Langmuir **23** (2007) 10603–10617.
- [148] I. Horcas, R. Fernández, J. M. Gómez-Rodríguez, J. Colchero, J. Gómez-Herrero and A. M. Baro: *WSXM: A software for scanning probe microscopy and a tool for nanotechnology*, Rev. Sci. Instrum. **78** (2007) 013705.
- [149] V. Ribitsch, C. Jorde, J. Schurz and H. J. Jacobasch: *Zeta-potential measurement of films, fibres, and granules*, Progr. Colloid & Polymer Sci. **77** (1988) 49–54.
- [150] M. Kuntzsch: *Binäre und Ternäre Polymerbürsten zur Gestaltung von Biogrenzflächen*, Master's thesis, Universität Görlitz - Zittau, (2009).
- [151] H.-J. Jacobasch, F. Simon, C. Werner and C. Bellmann: *Elektrokinetische Memethoden: Grundlagen und Anwendungen*, Technisches Messen **63** (1996) 447.
- [152] S. Burkert: *Sensitive Polymeroberflächen zur Steuerung der Adsorption von Biomolekülen*, Ph.D. thesis, Technische Universität Dresden, (2009).
- [153] M. Müller, T. Rieser, K. Lunkwitz and J. Meier-Haack: *Polyelectrolyte complex layers: a promising concept for anti-fouling coatings verified by in-situ ATR-FTIR*, Macromol. Rapid. Commun. **20** (1999) 607–611.
- [154] K. Hinrichs and K.-J. Eichhorn: *Combined infrared and visible spectroscopic ellipsometry study of thin polymer layers*, Spectroscopy Europe **19** (2007) 11–14.
- [155] M. Schubert, C. Bundesmann, G. Jakopic, H. Maresch, H. Arwin, N.-C. Persson, F. Zhang and O. Ingans: *Infrared ellipsometry characterization of conducting thin organic films*, Thin Sol. Film. **455-456** (2004) 295–300.
- [156] J. A. W. Co.: *Tutorial on ellipsometry*, (2010), www.jawoollam.com/tutorial_4.html.
- [157] O. Kahle: *Einsatzmöglichkeiten und Grenzen der temperaturvariablen Ellipsometrie*, Ph.D. thesis, Technische Universität Cottbus, (2002).
- [158] R. M. Azzam and N. M. Bashara: *Ellipsometry and Polarized Light*, North Holland Publication, Amsterdam, (1979).

- [159] H. G. Tompkins and E. A. Irene, eds.: *Handbook of Ellipsometry*, William Andrew Publishing, (2005).
- [160] S. Reichelt: *Herstellung, Charakterisierung und Anwendung von immobilisierten und teilvernetzten HBP-Schichten auf unterschiedlichen Substraten*, Ph.D. thesis, Technische Universität Dresden, (2008).
- [161] T. Nylander, F. Tiberg and N. M. Wahlgren: *Evaluation of the structure of adsorbed layers of β -casein from ellipsometry and surface force measurements*, Internat. Dairy Journal **9** (1999) 313–317.
- [162] J. Benesch, A. Askendal and P. Tengvall: *The Determination of Thickness and Surface Mass Density of Mesothick Immunoprecipitate Layers by Null Ellipsometry and Protein 125 Iodine Labeling*, J. Colloid Interf. Sci. **249** (2002) 84–90.
- [163] H. Arwin: *Spectroscopic ellipsometry and biology: recent developments and challenges*, Thin Sol. Film. **313-314** (1998) 764–774.
- [164] E. H. Korte, U. Schade, W. B. Peatman and A. Röseler: *Infrared ellipsometric view on monolayers: towards resolving structural details*, Anal. Bioanal. Chem. **374** (2002) 665–671.
- [165] P. N. Angelova, K. Hinrichs, I. L. Philipova, K. V. Kostova and D. T. Tsankov: *Monolayer Orientation of ω -Substituted Amide-Bridged Alkanethiols on Gold*, J. Phys. Chem. C **114** (2010) 1253–1259.
- [166] K. Grundke, T. Bogumil, C. Werner, A. Janke, K. Pschel and H.-J. Jacobasch: *Liquid-fluid contact angle measurements on hydrophilic cellulosic materials*, Colloid. Surf. A: Phys. Eng. Asp. **116** (1996) 79–91.
- [167] N. Houbenov: *Adsorption and Grafting of Polyelectrolytes at Solid-Liquid Interfaces*, Ph.D. thesis, Technische Universität Dresden, (2005).
- [168] H. Gao, K. X. Xu, B. Chen, L.-Z. Wu, C.-H. Tung and H.-F. Ji: *Ultrahydrophobicity of Polydimethylsiloxanes-Based Multilayered Thin Films*, J. Nanotechnol. (2009) doi:10.1155/2009/709748.
- [169] A. B. D. Cassie and S. Baxter: *Wettability of porous surfaces*, Trans. Farraday Soc. **40** (1944) 546–551.
- [170] S. Lahooti, O. I. del Rio, P. Cheng and A. W. Neumann: *Applied Surface Thermodynamics*, chap. Axisymmetric drop shape analysis (ADSA), 441–507, Marcel Dekker: New York, (1996).

- [171] L. Renner: *Polymer Supported Lipid Bilayer Membranes for the Integration of Transmembrane Proteins*, Ph.D. thesis, Technische Universität Dresden, (2009).
- [172] D. A. Buttry and M. D. Ward: *Measurement of Interfacial Processes at Electrode Surfaces with the Electrochemical Quartz Crystal Microbalance*, Chem. Rev. **92** (1992) 1355–1379.
- [173] G. Sauerbrey: *Verwendung von Schwingquarzen zur Wägung dünner Schichten und zur Mikrowägung*, Zeitschrift für Physik **155** (1959) 206–222.
- [174] M. Rodahl, F. Höök, A. Krozer, P. Brzezinski and B. Kasemo: *Quartz crystal microbalance setup for frequency and Q -factor measurements in gaseous and liquid environments*, Rev. Sci. Instrum. **66** (1995) 3924–3930.
- [175] M. Rodahl and B. Kasemo: *On the measurement of thin liquid overlayers with the quartz-crystal microbalance*, Sensors and Actuators A **54** (1996) 448–456.
- [176] K. K. Kazanawa and J. G. Gordon II: *Frequency of a Quartz Microbalance in Contact with Liquid*, Anal. Chem. **57** (1985) 1771–1772.
- [177] M. V. Voinova, M. Jonson and B. Kasemo: *Dynamics of viscous amphiphilic films supported by elastic solid substrates*, J. Phys.: Condens. Matter **9** (1997) 7799–7808.
- [178] M. V. Voinova, M. Jonson and B. Kasemo: *"Missing mass" effect in biosensor's QCM applications*, Biosensors and Bioelectronics **17** (2002) 835–841.
- [179] K. R. Rajagopal: *A note on a reappraisal and generalization of the Kelvin-Voigt model*, Mech. Res. Commun. **36** (2009) 232–235.
- [180] F. Höök, B. Kasemo, T. Nylander, C. Fant, K. Scott and H. Elwing: *Variations in Coupled Water, Viscoelastic Properties, and Film Thickness of a Mefp-1 Protein Film during Adsorption and Cross-Linking: A Quartz Crystal Microbalance with Dissipation Monitoring, Ellipsometry, and Surface Plasmon Resonance Study*, Anal. Chem. **73** (2001) 5796–5804.
- [181] *J. A. Woollam Co., Inc. Annual newsletter, Issue 11*, (2010).
- [182] P. Törmälä: *Determination of glass transition temperature of poly(ethylene glycol) by spin probe technique*, Europ. Polym. J. **10** (1974) 519–521.
- [183] E. Gianazza, A. Firgerio, S. Astrua-Testori and P. G. Righetti: *The behavior of serum albumin upon isoelectric focusing on immobilized pH gradients*, Electrophoresis **5** (1984) 310–312.
- [184] J. F. Foster and L. J. Kaplan: *Isoelectric focussing behavior of bovine plasme albumin, mercaptalbumin, and β -lactoglobulins A and B*, Biochem. **10** (1971) 630–636.

- [185] M. Höpfner: *Untersuchungen zur Anwendbarkeit der Quarzmikrowaage fr pharmazeutisch analytische Fragestellungen*, Ph.D. thesis, Martin-Luther-Universität Halle-Wittenberg, (2005).
- [186] H. J. Hecht, D. Schomburg, H. Kalisz and R. D. Schmid: *The 3D structure of glucose oxidase from Aspergillus niger. Implications for the use of GOD as a biosensor enzyme*, *Biosensors and Bioelectronics* **8** (1993) 197–203.
- [187] J. H. Pazur and K. Kleppe: *The Oxidation of Glucose and Related Compounds by Glucose Oxidase from Aspergillus niger*, *Biochemistry* **3** (1964) 578–583.
- [188] S. Muzammil, Y. Kumar and S. Tayyab: *Molten globule-like state of human serum albumin at low pH*, *Eur. J. Biochem.* **266** (1999) 26–32.
- [189] K. Wallevik: *Reversible Denaturation of Human Serum Albumin by pH, Temperature, and Guanidine Hydrochloride Followed by Optical Rotation*, *J. Biol. Chem.* **248** (1973) 2650–2655.
- [190] A.-K. Bordbar, N. Sohrabi and H. Gharibi: *Binding Set Analysis for Interaction of Human Serum Albumin with Cethyl Trimethylammonium Bromide*, *Bull. Korean Chem. Soc.* **25** (2004) 791–795.
- [191] B. Zdyrko: *Thin polymer films for biomedical applications: Synthesis and characterization*, Ph.D. thesis, Graduate School of Clemson University, (2005).
- [192] R. Sheparovych, M. Motornov and S. Minko: *Adapting Low-Adhesive Thin Films from Mixed Polymer Brushes*, *Langmuir* **24** (2008) 13828–13832.
- [193] S. Burkert, E. Bittrich, M. Kuntzsch, M. Müller, K.-J. Eichhorn, C. Bellmann, P. Uhlmann and M. Stamm: *Protein Resistance of PNIPAAm Brushes: Application to Switchable Protein Adsorption*, *Langmuir* **26** (2010) 1786–1795.
- [194] C. Werner, H. Körber, R. Zimmermann, S. Dukhin and H.-J. Jacobasch: *Extended Electrokinetic Characterization of Flat Solid Surfaces*, *J. Colloid Int. Sci.* **208** (1998) 329–346.
- [195] R. Zimmermann, W. Norde, M. A. Cohen Stuart and C. Werner: *Electrokinetic Characterization of Poly(Acrylic Acid) and Poly(Ethylene Oxide) Brushes in Aqueous Electrolyte Solutions*, *Langmuir* **21** (2005) 5108–5114.
- [196] S. Reichelt, K.-J. Eichhorn, D. Aulich, K. Hinrichs, N. Jain, D. Appelhans and B. Voit: *Functionalization of solid surfaces with hyperbranched polyesters to control protein adsorption*, *Colloid. Surf. B: Biointer.* **69** (2009) 169–177.
- [197] B. R. Saunders: *On the Structure of Poly(N-isopropylacrylamide) Microgel Particles*, *Langmuir* **20** (2004) 3925–3932.

- [198] L. Ionov, N. Houbenov, A. Sidorenko, M. Stamm, I. Luzinov and S. Minko: *Inverse and Reversible Switching Gradient Surfaces from Mixed Polyelectrolyte Brushes*, *Langmuir* **20** (2004) 9916–9919.
- [199] J. Huang, I. Ichinose, T. Kunitake and A. Nakao: *Preparation of Nanoporous Titania Films by Surface Sol-Gel Process Accompanied by Low-Temperature Oxygen Plasma Treatment*, *Langmuir* **18** (2002) 9048–9053.
- [200] A. Sidorenko, S. Minko, K. Schenk-Meuser, H. Duschner and M. Stamm: *Switching of Polymer Brushes*, *Langmuir* **15** (1999) 8349–8355.
- [201] S. Kidoaki, S. Ohya, Y. Nakayama and T. Matsuda: *Thermoresponsive Structural Change of a Poly(*N*-isopropylacrylamide) Graft Layer Measured with an Atomic Force Microscope*, *Langmuir* **17** (2001) 2402–2407.
- [202] D. E. Aspnes: *Optical properties of thin films*, *Thin Solid Films* **89** (1982) 249–262.
- [203] J. C. Maxwell-Garnett: *Colours in Metal Glasses and in Metallic Films*, *Phil. Trans. R. Soc. Lond. A* **203** (1904) 385–420.
- [204] D. A. G. Bruggeman: *Berechnung verschiedener physikalischer Konstanten von heterogenen Substanzen*, *Annalen der Physik* **24** (1935) 636–664.
- [205] Y. Mikhaylova, V. Dutschk, M. Müller, K. Grundke, K.-J. Eichhorn and B. Voit: *Study of the solidliquid interface of hydroxyl-terminated hyperbranched aromatic polyesters (HBP-OH) in aqueous media II. Adsorption of model proteins*, *Colloids Surf. A: Physicochem. Eng. Asp.* **297** (2007) 19–29.
- [206] H. Arwin: *Optical Properties of Thin Layers of Bovine Serum Albumin, γ -Globulin, and Hemoglobin*, *Appl. Spectrosc.* **40** (1986) 313.
- [207] J. A. de Feijter, J. Benjamins and F. A. Veer: *Ellipsometry as a Tool to Study the Adsorption Behavior of Synthetic and Biopolymers at the Air-Water Interface*, *Biopolymers* **17** (1978) 1759–1772.
- [208] P. S. Sarfare, G. Kegeles and S. J. Kwon-Rhee: *Relationship between Active Sites and Polymerization Sites in α -Chymotrypsin*, *Biochemistry* **5** (1966) 1389–1393.
- [209] J. M. M. Kop, P. A. Cuypers, T. Lindhout, H. C. Hemker and W. T. Hermens: *The Adsorption of Prothrombin to Phospholipid Monolayers Quantitated by Ellipsometry*, *J. Biol. Chem.* **259** (1984) 13993–13998.
- [210] K. Wannerberger, M. Wahlgren and T. Arnebrant: *Adsorption from lipase-surfactant solutions onto methylated silica surfaces*, *Colloid. Surf. B: Biointer.* **6** (1996) 27–36.

- [211] M. Štěpánek, P. Matějček, J. Humpolíčková, J. Havránková, K. Podhájecká, M. Špírková, Z. Tuzar, C. Tritilianis and K. Procházka: *New insights on the solution behavior and self-assembly of polystyrene/poly(2-vinylpyridine) 'hairy' heteroarm star copolymers with highly asymmetric arms in polar organic and aqueous media*, *Polymer* **46** (2005) 10493–10505.
- [212] E. S. Forzani, M. Otero, M. A. Prez, M. L. Teijelo and E. J. Calvo: *The Structure of Layer-by-Layer Self-Assembled Glucose Oxidase and Os(Bpy)₂ClPyCH₂NH-Poly(allylamine) Multilayers: Ellipsometric and Quartz Crystal Microbalance Studies*, *Langmuir* **18** (2002) 4020–4029.
- [213] M. Bradford: *A rapid and sensitive method for the quantitation of microgram quantities of protein utilizing the principle of protein-dye binding*, *Anal. Biochem.* **72** (1976) 248–254.
- [214] T. Zor and Z. Selinger: *Linearization of the Bradford protein assay increases its sensitivity: theoretical and experimental studies.*, *Anal. Biochem.* **236** (1996) 302–308.
- [215] T. Okano, N. Yamada, M. Okuhara, H. Sakai and Y. Sakurai: *Mechanism of cell detachment from temperature-modulated, hydrophilic-hydrophobic polymer surfaces*, *Biomaterials* **16** (1995) 297–303.
- [216] L. K. Ista, V. H. Pérez-Luna and G. P. López: *Surface-Grafted, Environmentally Sensitive Polymers for Biofilm Release*, *Appl. Environm. Microbiol.* **65** (1999) 1603–1609.
- [217] P. S. Stayton, T. Shimoboji, C. Long, A. Chilkoti, G. Chen, J. M. Harris and A. S. Hoffman: *Control of protein-ligand recognition using a stimuli-responsive polymer*, *Nature* **378** (1995) 472–474.
- [218] Y. S. Park, Y. Ito and Y. Imanishi: *Permeation Control through Porous Membranes Immobilized with Thermosensitive Polymer*, *Langmuir* **14** (1998) 910–914.
- [219] O. Chiantore, M. Guaita and L. Trossarelli: *Solution properties of poly(N-isopropylacrylamide)*, *Macromol. Chem. Phys.* **180** (1979) 969–973.
- [220] Y. Maeda, T. Higuchi and I. Ikeda: *Change in Hydration State during the Coil-Globule Transition of Aqueous Solutions of Poly(N-isopropylacrylamide) as Evidenced by FTIR Spectroscopy*, *Langmuir* **16** (2000) 7503–7509.
- [221] Y. Katsumoto, T. Tanaka, H. Sato and Y. Ozaki: *Conformational Change of Poly(N-isopropylacrylamide) during the Coil-Globule Transition Investigated by Attenuated Total Reflection/Infrared Spectroscopy and Density Functional Theory Calculation*, *J. Phys. Chem. A* **106** (2002) 3429–3435.
- [222] Y. Gu, T. Kar and S. Scheiner: *Fundamental Properties of the CH...O Interaction: Is It a True Hydrogen Bond?*, *J. Am.Chem. Soc.* **121** (1999) 9411–9422.

- [223] H. Tavana, G. Yang, C. M. Yip, D. Appelhans, S. Zschoche, K. Gundke, M. L. Hair and A. W. Neumann: *Stick-Slip of the Three-Phase Line in Measurements of Dynamic Contact Angles*, *Langmuir* **22** (2006) 628–636.
- [224] H. Feil, Y. H. Bae, J. Feijen and S. W. Kim: *Effect of Comonomer Hydrophilicity and Ionization on the Lower Critical Solution Temperature of N-Isopropylacrylamide*, *Macromol.* **26** (1993) 2496–2500.
- [225] M. R. Hobabi, D. Hassanzadeh, S. Azarmi and A. A. Entezami: *Effect of synthesis method and buffer composition on the LCST of a smart copolymer of N-isopropylacrylamide and acrylic acid*, *Polym. Adv. Technol.* **18** (2007) 986–992.
- [226] H. G. Schild and D. A. Tirrell: *Microcalorimetric Detection of Lower Critical Solution Temperatures in Aqueous Polymer Solutions*, *J. Phys. Chem.* **94** (1990) 4352–4356.
- [227] M. Ataman: *Properties of aqueous salt solutions of poly(ethylene oxide) Cloud points, θ temperatures*, *Colloid Polym. Sci.* **265** (1987) 19–25.
- [228] Y. H. Bae, T. Okano and S. W. Kim: *Temperature dependence of swelling of crosslinked poly(N,N-alkyl substituted acrylamides) in water*, *J. Polym. Sci. B: Polym. Phys.* **28** (1990) 923–936.
- [229] F. Klein, W. Bronsveld, W. Norde, L. K. J. van Romunde and J. M. Singer: *A modified latex-fixation test for the detection of rheumatoid factors.*, *J. Clin. Pathol.* **32** (1979) 90–92.
- [230] L. Vroman and E. F. Leonard: *The effect of flow on displacement of proteins at interfaces in plasma*, *Biofoul.* **4** (1991) 81–87.
- [231] G. M. Willems, W. T. Hermans and H. C. Hemker: *Surface exclusion and molecular mobility may explain Vroman effects in protein adsorption.*, *J. Biomater. Sci.* **2** (1991) 217–226.
- [232] M. Quirynen, M. Marechal, D. van Steenberghe, H. J. Busscher and H. C. v. d. Mei: *The bacterial colonization of intra-oral hard surfaces in vivo: Influence of surface free energy and surface roughness*, *Biofoul.* **4** (1991) 187.
- [233] D. J. White: *Processes contributing to the formation of dental calculus*, *Biofoul.* **4** (1991) 209–218.
- [234] D. Schmaljohann, J. Oswald, B. Jorgensen, M. Nitschke, D. Beyerlein and C. Werner: *Thermo-Responsive PNiPAAm-g-PEG Films for Controlled Cell Detachment*, *Biomacromol.* **4** (2003) 1733–1739.

- [235] D. Schmaljohann, D. Beyerlein, M. Nitschke and C. Werner: *Thermo-Reversible Swelling of Thin Hydrogel Films Immobilized by Low-Pressure Plasma*, *Langmuir* **20** (2004) 10107–10114.
- [236] S. Burkert, E. Bittrich, K.-J. Eichhorn, P. Uhlmann and M. Stamm: *Biosurface engineering by polymer brushes*, in: *Nanofair*, (2009).
- [237] D. G. Leaist: *Coupled diffusion of weakly ionized polyelectrolytes. Polyacrylic acids in water*, *J. Solut. Chem.* **18** (1989) 421–435.
- [238] T. Wu, P. Gong, I. Szleifer, P. Vlček, V. Šubr and J. Genzer: *Behavior of Surface-Anchored Poly(acrylic acid) Brushes with Grafting Density Gradients on Solid Substrates: 1. Experiment*, *Macromol.* **40** (2007) 8756–9764.
- [239] D. Aulich, O. Hoy, I. Luzinov, M. Brücher, R. Hergenröder, E. Bittrich, K.-J. Eichhorn, P. Uhlmann, M. Stamm, N. Esser and K. Hinrichs: *In Situ Studies on the Switching Behavior of Ultrathin Poly(acrylic acid) Polyelectrolyte Brushes in Different Aqueous Environments*, *Langmuir* **26** (2010) 12926–12932.
- [240] P. Gong, T. Wu, J. Genzer and I. Szleifer: *Behavior of Surface-Anchored Poly(acrylic acid) Brushes with Grafting Density Gradients on Solid Substrates: 2. Theory*, *Macromolecules* **40** (2007) 8765–8773.
- [241] F. Uhlík, Z. Limpouchová, K. Jelínek and K. Procházka: *Polyelectrolyte shells of copolymer micelles in aqueous solutions: A Monte Carlo study*, *J. Chem. Phys.* **121** (2004) 2367–2375.
- [242] S. Tcholakova, N. D. Denkov, I. B. Ivanov and B. Campbell: *Coalescence stability of emulsions containing globular milk proteins*, *Advances in colloid and interface science* **123-126** (2006) 259–293.
- [243] E. Bittrich, K. B. Rodenhausen, K.-J. Eichhorn, T. Hofmann, M. Schubert, P. Uhlmann and M. Stamm: *Protein Adsorption on and Swelling of Polyelectrolyte Brushes: A Simultaneous Ellipsometry - Quartz Crystal Microbalance Study*, submitted to *Biomacromol.* (2010).
- [244] T. J. Halthur and U. M. Elofsson: *Multilayers of Charged Polypeptides As Studied by in Situ Ellipsometry and Quartz Crystal Microbalance with Dissipation*, *Langmuir* **20** (2004) 1739–1745.
- [245] A. Domack, O. Prucker, J. Rühle and D. Johannsmann: *Swelling of a polymer brush probed with a quartz crystal resonator*, *Phys. Rev. E* **56** (1997) 680–689.

- [246] F. Soetewey, M. Rosseneu-Motreff, R. Lamote and H. Peeters: *Size and Shape Determination of Native and Defatted Bovine Serum Albumin Monomers*, J. Biochem. **71** (1972) 705–710.
- [247] S. Wan, M. Jiang and G. Zhang: *Dual Temperature- and pH-Dependent Self-Assembly of Cellulose-Based Copolymer with a Pair of Complementary Grafts*, Macromol. **40** (2007) 5552–5558.
- [248] V. V. Khutoryanskiy, G. A. Mun, Z. S. Nurkeeva and A. V. Dubolazov: *pH and salt effects on interpolymer complexation via hydrogen bonding in aqueous solutions*, Polym. Int. **53** (2004) 1382–1387.
- [249] E. Bittrich, M. Kuntzsch, K.-J. Eichhorn and P. Uhlmann: *Complex pH- and temperature-sensitive swelling behavior of mixed polymer brushes*, J. Polym. Sci. B: Polym. Phys. **48** (2010) 1606 – 1615.
- [250] G. Dominguez-Espinoza, A. Synytska, A. Drechsler, C. Gutsche, K. Kegler, P. Uhlmann, M. Stamm and F. Kremer: *Optical tweezers to measure the interaction between poly(acrylic acid) brushes*, Polymer **49** (2008) 4802–4807.
- [251] H. T. Oyama, W. T. Tang and C. W. Frank: *Complex Formation between Poly(acrylic acid) and Pyrene-Labeled Poly(ethylene glycol) in Aqueous Solution*, Macromolecules **20** (1987) 474–480.
- [252] V. Baranovsky, S. Shenkov, I. Rashkov and G. Borisov: *Nonspecific interactions in polymer-polymer reactions4. Complex formation between polyacrylic acid and monosubstituted poly(ethylene glycol)s*, Europ. Polym. J. **28** (1992) 475–479.
- [253] O. Hoy, B. Zdyrko, R. Lupitskyy, R. Sheparovych, D. Aulich, J. Wang, E. Bittrich, K.-J. Eichhorn, P. Uhlmann, K. Hinrichs, M. Müller, M. Stamm, S. Minko and I. Luzinov: *Synthetic Hydrophilic Materials with Tunable Strength and a Range of Hydrophobic Interactions*, Adv. Funct. Mat. **20** (2010) 2240–2247.
- [254] P. J. Scully, L. Betancor, J. Bolyo, S. Dzyadevych, J. M. Guisan, R. Fernández-Lafuente, N. Jaffrezic-Renault, G. Kuncová, V. Matejec, B. O’Kennedy, O. Podrazky, K. Rose, L. Sasek and J. S. Young: *Optical fibre biosensors using enzymatic transducers to monitor glucose*, Meas. Sci. Technol. **18** (2007) 3177–3186.
- [255] M. A. Zia, K. Rahman, M. K. Saeed, F. Andaleeb, M. I. Rajoka, M. A. Sheikh, I. A. Khan and A. I. Kahn: *Thermal Characterization of Purified Glucose Oxidase from A Newly Isolated Aspergillus Niger UAF-1*, J. Clin. Biochem. Nutr. **41** (2007) 132–138.
- [256] *PeroxiDetectTM Kit for the determination of aqueous peroxides*, (Sigma Aldrich, Inc., Product Code: PD 1).

-
- [257] B. L. Gupta: *Microdetermination Techniques for H_2O_2 in Irradiated Solutions*, Microchemical Journal **18** (1973) 363–374.
- [258] Z.-Y. Jiang, A. C. S. Woollard and S. P. Wolff: *Lipid Hydroperoxide Measurement by Oxidation of Fe^{2+} in the Presence of Xylenol Orange. Comparison with the TBA Assay and an Iodometric Method*, Lipids **26** (1991) 853–856.

List of publications

- Herold, E.; Uhlmann, P.; Eichhorn, K.-J.; Stamm, M. *PNIPAAm brushes mixed with PAA-b-PS: A versatile tool to control the adsorption of human serum albumin* Polym. Mat.: Sci. Eng., **2008**, *99*, 426-427.
- Uhlmann, P.; Herold, E.; Kempe, F.; Stamm, M. *Switching of protein adsorption on polyelectrolyte brushes* Polym. Mat.: Sci. Eng., **2008**, *99*, 118-119.
- Burkert, S.; Bittrich, E.; Eichhorn, K.-J.; Uhlmann, P.; Stamm, M. *Biosurface engineering by polymer brushes* VDI-Report, **2009**, ISBN: 978-3-00-027076-5.
- Bittrich, E.; Aulich, D.; Eichhorn, K.-J.; Hinrichs, K.; Uhlmann, P.; Luzinov, I.; Stamm, M. *Control of Protein Adsorption and Release by Stimuli-Responsive Polymer Brushes* Polym. Mat.: Sci. Eng., **2009**, *101*, 930-931.
- Burkert, S.; Bittrich, E.; Kuntzsch, M.; Müller, M.; Eichhorn, K.-J.; Bellmann, C.; Uhlmann, P.; Stamm, M. *Protein Resistance of PNIPAAm Brushes: Application to Switchable Protein Adsorption* Langmuir, **2010**, *26*, 1786-1795.
- Hoy, O.; Zdyrko, B.; Lupitsky, R.; Sheparovych, R.; Aulich, D.; Wang, J.; Bittrich, E.; Eichhorn, K.-J.; Uhlmann, P.; Hinrichs, K.; Mueller, M.; Stamm, M.; Minko, S.; Luzinov, I. *Synthetic Hydrophilic Materials with Tunable Strength and a Range of Hydrophobic Interactions* Adv. Func. Mat., **2010**, *20*, 2240-2247.
- Bittrich, E.; Kuntzsch, M.; Eichhorn, K.-J.; Uhlmann, P. *Complex pH- and Temperature Sensitive Swelling Behavior of Mixed Polymer Brushes* J. Polym. Sci. B: Polym. Phys., **2010**, *48*, 1606-1615.
- Aulich, D.; Hoy, O.; Luzinov, I.; Brücher, M.; Hergenröder, R.; Bittrich, E.; Eichhorn, K.-J.; Uhlmann, P.; Stamm, M.; Esser, N.; Hinrichs, K. *In Situ Studies on the Switching Behavior of Ultrathin Poly(acrylic acid) Polyelectrolyte Brushes in Different Aqueous Environments* Langmuir, **2010**, *26*, 12926-12932.
- Bittrich, E.; Rodenhausen, K. B.; Eichhorn, K.-J.; Hofmann, T.; Schubert, M.; Uhlmann, P.; Stamm, M. *Protein Adsorption on and Swelling of Polyelectrolyte Brushes: A Simultaneous Ellipsometry - Quartz Crystal Microbalance Study* submitted to Biointerphases.

Contributions to academic conferences

- Uhlmann, P.; Herold, E.; Burkert, S.; Müller, M.; Stamm, M. *Reversible Temperature Induced Switching of Grafted Poly-N-isopropylacrylamide Brushes* - poster presentation at **DPG spring meeting**, 25th – 29th February, 2008, Berlin, Germany

- Herold, E.; Burkert, S.; Uhlmann, P.; Eichhorn, K.-J.; Müller, M.; Stamm, M. *Temperature sensitive swelling and protein resistance of poly (N-isopropylacrylamide) brushes* - oral presentation at **Second Young Scientists Conference**, 13th – 15th April, 2008, Terni, Italy
- Bittrich, E.; Burkert, S.; Winkler, R.; Uhlmann, P.; Stamm, M. *Switchable protein adsorption at mixed polymer brushes* - poster presentation at **4. Thüringer Grenz- und Oberflächentage**, 16th – 18th September, 2008, Jena, Germany
- Bittrich, E.; Uhlmann, P.; Eichhorn, K.-J.; Stamm, M. *PNIPAAm brushes mixed with PAA-b-PS: A versatile tool to control the adsorption of human serum albumin* - poster presentation at 236th **ACS National Meeting**, 17th – 21th August, 2008, Philadelphia, PA, USA and at 1st **European School on Ellipsometry**, 21th – 25th September, 2008, Ostuni, Italy
- Bittrich, E.; Burkert, S.; Eichhorn, K.-J.; Müller, M.; Uhlmann, P.; Stamm, M. *Temperature induced switching of poly(N-isopropyl acrylamide) brushes* - poster presentation at **8. IPF-Kolloquium: Multifunktionelle Polymermaterialien**, 12th – 13th November, 2008, Dresden
- Bittrich, E.; Aulich, D.; Eichhorn, K.-J.; Hinrichs, K.; Uhlmann, P.; Stamm, M. *Application of in-situ VIS-ellipsometry for the investigation of stimuli-responsive polymer brushes and adsorption processes thereon* - oral presentation at 5th **Workshop Ellipsometry**, 2nd – 4th March, 2009, Zweibrücken, Germany
- Bittrich, E.; Aulich, D.; Eichhorn, K.-J.; Hinrichs, K.; Uhlmann, P.; Stamm, M. *In-situ spectroscopic ellipsometry on stimuli-responsive polymer brushes* - poster presentation at **DPG spring meeting**, 23rd – 27th March, 2009, Dresden, Germany
- Bittrich, E.; Kempe, F.; Eichhorn, K.-J.; Uhlmann, P.; Stamm, M. *Reversible switching of protein adsorption on binary polyelectrolyte brushes* - poster presentation at **Nanofair**, 26th – 27th May, 2009, Dresden, Germany
- Bittrich, E.; Aulich, D.; Eichhorn, K.-J.; Hinrichs, K.; Uhlmann, P.; Luzinov, I.; Stamm, M. *Control of Protein Adsorption and Release by Stimuli-Responsive Polymer Brushes* - oral presentation at **ACS National Meeting Fall 2009**, 16th – 20th August, 2009, Washington ,DC, USA
- Bittrich, E.; Rodenhausen, K. B.; Eichhorn, K.-J.; Hofmann, T.; Uhlmann, P.; Schubert, M.; Stamm, M. *Controlled Swelling of Stimuli-Responsive Polymer Brushes and Protein Adsorption Thereon* - oral presentation at 5th **International Conference on Spectroscopic Ellipsometry**, 23rd – 28th May, 2010, Albany ,NY, USA

Erklärung

Hiermit versichere ich, dass ich die vorliegende Arbeit ohne unzulässige Hilfe Dritter und ohne Benutzung anderer als der angegebenen Hilfsmittel angefertigt habe; die aus fremden Quellen direkt oder indirekt übernommenen Gedanken sind als solche kenntlich gemacht. Die Arbeit wurde bisher weder im Inland noch im Ausland in gleicher oder ähnlicher Form einer anderen Prüfungsbehörde vorgelegt.

Die Dissertation wurde in der Zeit von Februar 2007 bis August 2010 unter der Betreuung von Herrn Prof. Dr. Manfred Stamm am Leibniz-Institut für Polymerforschung Dresden e.V. in der Abteilung Nanostrukturierte Materialien angefertigt. Es haben keine früheren erfolglosen Promotionsverfahren stattgefunden. Ich erkenne die Promotionsordnung der Fakultät Mathematik und Naturwissenschaften an der Technischen Universität Dresden vom 20. März 2000 an.

Dresden, den 13. August 2010

Eva Bittrich